

Online Acoustic Monitoring and Localisation of Partial Discharges within Subsea Umbilicals



Lindsay J. Smith
School of Engineering
Newcastle University

A thesis submitted for the degree of
Doctor of Philosophy
January 2022

I would like to dedicate this work to my dad who sadly passed away before completion of this Thesis. He is the reason I became an engineer and I will forever look up to him.

Acknowledgements

Firstly, I would like to thank my sponsor company, TechnipFMC for giving me the opportunity to perform these studies and for providing ongoing support throughout the research project. This PhD was carried out on a part time basis, therefore I could not have completed this research without their complete backing and encouragement. Particular thanks go to my manager Alan Dobson and supervisor Alan Deighton who helped to manage my workload, allowing me to take time to focus on my PhD studies.

Within the University, my sincere thanks go to my supervisor Jeff Neasham. His support and guidance have enabled me to achieve my research objectives. I could not have completed this thesis without his advice and encouragement and therefore I am very grateful. I also owe huge thanks to the researchers in the SEA Lab team for the knowledge they have shared and invaluable support they have provided during field trials. In addition, I would like to thank the technical staff for their assistance in the production of the hardware required for the practical testing performed throughout.

During the field trials and in-house factory testing, a great deal of assistance was required from TechnipFMC technicians, to which I am very appreciative.

At home, I have received amazing support from my family, particularly with childcare, to allow me time to carry out this research and thesis writing. I am very lucky to have such an encouraging and loving family.

Final thanks go to my husband John, daughter Millicent and son Blake. Thank you for being so understanding regarding the time I have needed to put into this PhD and also for keeping me sane throughout the write up. It has been extremely difficult to manage the work, study and life balance but you have all helped make this possible. I could not have done this without you all.

Abstract

There has been an increasing requirement in the quantity of subsea power cables within both the oil and gas and the energy transmission markets. Both sectors are pushing their current operating boundaries, putting more emphasis on the criticality of the components integrity to ensure they are able to meet their lifetime requirements, or in some cases allow for lifetime extension. Failures within subsea power cables are uncommon, however when they do occur, they lead to excessive production downtime and costs. Having the ability to monitor the condition of the cables for potential failures, whilst the system remains online, would be highly beneficial as these failure costs could be eliminated. The condition of a cables insulating layer is key to its operational lifetime and levels of partial discharge (PD) occurrence can provide an indication of its integrity and of any likely upcoming failures. A system which would allow for detection and localisation of PD occurrence would enable potential failures to be reviewed and an assessment made prior to complete breakdown, thus allowing for changes in operation or planned maintenance to remove the large risks and costs associated with unplanned production downtime.

This thesis examines methods for PD detection and localisation within a subsea power cable, whilst considering the many challenges associated with the environment and application of the technology. State-of-the-art technology is reviewed along with an assessment of the market requirements and current gaps in PD evaluation systems. Existing technologies focus on offline testing techniques whereby testing is only performed once a failure has occurred or on occasions during planned maintenance, however, having a system which can operate whilst the cable remains online is vital in order to have an understanding of the condition of the cables and in turn reduce or remove downtime costs.

When PD occurs, a number of emissions are produced such as electromagnetic, optical, acoustic, thermal, and chemical, meaning a variety of sensing methodologies could be used. Acoustic sensing techniques are the focus of this work as this allows most major challenges to be addressed, with particular emphasis on the ability for online monitoring as well as a retrofit design. Acoustic techniques offer a greater potential for accurate localisation of PD in comparison to electromagnetic techniques due to the low velocity of sound wave propagation. Acoustic methods also enable both through-cable and through-water sensing of the discharges, thus both areas are explored.

Experimental through-cable testing validates the methodology for both detection and localisation of the PD occurrence. Signal characteristics are explored, determining a broadband result, with the main signal energy being below 5kHz and a signal velocity of around 2442m/s. Time difference of arrival (TDoA) techniques are evaluated, with cross correlation methods showing favorable results in low signal to noise ratio (SNR) environments, providing a position estimation within 2m of the PD location. Comparative testing with existing electrical detection technology provides an assessment of the severity

of PD which can be detected acoustically, with average discharges measured at 25.5pC peak PD and an average of 837pC/cycle for PD activity.

Through-water experimental testing confirms the ability for PD localisation in an underwater environment. The acoustic signal characteristics are broadband, spanning the measured 22kHz frequency spectrum and are of short duration. The source level of the PD acoustic emission is established to assess the detectability range in varying subsea environments, with a maximum range of 1000m when considering a low noise spectral density level of 45dB. As the time of PD occurrence is unknown, standard time of arrival techniques cannot be used and thus hyperbolic positioning is implemented within the developed localisation algorithm to estimate the position of the PD source. With consideration of the receiver geometry, a highly accurate PD location can be established enabling planned intervention of the fault region and therefore preventing retrieval and replacement of the complete power cable length.

Contents

Chapter 1	1
Introduction.....	1
1.1 Contributions.....	3
1.2 Publications	4
1.3 Thesis Outline	4
Chapter 2.....	6
Background Information and Motivation	6
2.1 Subsea Umbilicals.....	6
2.1.1 Umbilical Design	6
2.1.2 Categories	11
2.2 Umbilical Evolution	13
2.2.1 Industry Downturn	13
2.2.2 Subsea Processing.....	15
2.2.3 All-Electric Control	17
2.2.4 Heated Pipelines.....	18
2.2.4 Energy Transition.....	19
2.3 Failure Modes of a Subsea Power Cable.....	21
2.3.1 Partial Discharge	22
2.3.2 Water Trees	27
2.3.3 Fatigue.....	28
2.3.4 External Damage.....	29
2.3.5 Connector Failures	29
2.3.6 Failure Mode Review.....	31
2.4 Summary	32
Chapter 3.....	34
Current PD Monitoring Technologies and Localisation Techniques	34
3.1 Partial Discharge Detection.....	34

3.1.1 Electrical Detection.....	35
3.1.2 Visual or Optical Detection	37
3.1.3 Acoustic Detection.....	37
3.1.4 Chemical Detection.....	39
3.2 Detection and Localisation within Subsea Umbilicals.....	39
3.2.1 Challenges and Limitations.....	41
3.2.1.1 Long Distance Detection	41
3.2.1.2 Subsea Environment	42
3.2.1.3 Online Sensing.....	43
3.2.1.4 Bespoke Umbilical Design	45
3.2.1.5 Retro Fit Design.....	45
3.2.2 Sensing Summary	46
3.3 Research Aims and Objectives.....	48
Chapter 4	49
Through-cable Acoustic Propagation	49
4.1 Motivation	49
4.2 Characteristics of Acoustic Emission from PD within Cables.....	49
4.2.1 Experimental Test: Induced PD on Cable Sample.....	50
4.2.2 Results and Discussions	53
4.3 Through-cable Propagation Path.....	58
4.3.1 Wave Types	61
4.3.2 Propagation Mediums	61
4.4 Signal Velocity.....	65
4.4.1 Envelope Analysis	65
4.4.1.1 Calculated Velocity utilising Envelope Analysis Techniques.....	68
4.4.2 Cross Correlation Analysis	69
4.4.2.1 Calculated Velocity utilising Cross Correlation Techniques.....	74
4.5 Effects of Propagation Distance on AE Signal	74
4.5.1 Experimental Test: PD Propagation – Varying Sensor Positions.....	75
4.5.2 Results and Discussions	77
4.6 Comparative Electrical PD Energy	81

4.7 Summary	85
Chapter 5	87
Through-cable Source Localisation	87
5.1 Motivation	87
5.2 Localisation Methods	88
5.2.1 Distributed AE Sensors	88
5.2.2 Combined EM and AE Topside Detection	92
5.3 Evaluation of TDoA Techniques	93
5.3.1 Envelope Detection – Distributed AE Sensing	93
5.3.2 Cross Correlation – Distributed AE Sensing	98
5.3.3 Envelope Detection – Combined EM and AE Detection	100
5.3.4 SNR Analysis	103
5.3.5 System Accuracy	111
5.4 Detectability Range - Attenuation	114
5.5 Practical Implementation	117
5.6 Summary	118
Chapter 6	120
Through-water Acoustic Propagation	120
6.1 Motivation	120
6.2 Underwater Acoustic Channel	121
6.2.1 Speed of Sound in Seawater	121
6.2.2 Transmission Loss	123
6.2.3 Multipath	125
6.2.4 Noise and Interference	126
6.3 Open Water Trial - Detection	128
6.3.1 Controlled Testing	128
6.3.2 Calibration & Detectability	134
6.3.3 Open Water Test Configuration and Initial Findings	136
6.4 Summary	144
Chapter 7	146
Through-water Source Localisation	146

7.1 Motivation	146
7.2 Survey of Localisation Techniques	147
7.3 Open Water Trial – Localisation	149
7.3.1 Hyperbolic Positioning	149
7.3.2 System Evaluation	153
7.3.3 Receiver Positioning	161
7.3.4 Impacts of Additional Receiver	164
7.3.5 Additional Trial.....	167
7.4 Electro-acoustic Combined Method.....	174
7.5 3D Source Localisation	175
7.6 Practical Implementation.....	179
7.7 Summary	180
Chapter 8.....	183
Conclusion	183
8.1 Concluding Remarks	189
8.2 Future Work	189
References	191

List of Figures

Figure 2- 1: Umbilical Applications [2].....	7
Figure 2- 2: Typical Umbilical Cross Section	7
Figure 2- 3: Static and Dynamic Umbilicals [3].....	8
Figure 2- 4: Typical Umbilical Designs.....	11
Figure 2- 5: Changes in Crude Oil Price 2009 to 2019.....	13
Figure 2- 6: Field Layout	15
Figure 2- 7: Statoil Subsea Factory [11]	16
Figure 2- 8: Typical FOW Power Cable - ©TFMC Umbilicals Ltd.	20
Figure 2- 9: Cable Construction.....	21
Figure 2- 10: Types of PD in Power Cables [1].....	23
Figure 2- 11: PD Simplified Equivalent Circuit Model.....	24
Figure 2- 12: Time Evolution of Equivalent Circuit Model [1].....	25
Figure 2- 13: Electrical Treeing [1]	26
Figure 2- 14: Water Treeing	28
Figure 2- 15: Failure Mode Effects and Effects Analysis of MV/HV Cable Failures.....	33
Figure 3- 1: Features of an idealised PD Pulse [49]	35
Figure 3- 2: Detection Methods for PD in Umbilicals.....	40
Figure 4- 1: Fault Region – (a) stripped section c/w tapered insulation & conductor divot, (b) initial insulation reinstatement over conductor, (c) insulation reinstatement (<i>pre-heating</i>), (d) insulation heating, (e) additional insulation taping (f) fully bonded insulation (<i>post heating</i>), (g) reinstated copper screen, (h) reinstated tape oversheath.....	51
Figure 4- 2: MV Cable Sample c/w PD Inducing Fault.....	52
Figure 4- 3: Simplified Block Diagram - PD Acoustic Detection	52
Figure 4- 4: Acoustic Signals Measured at Rx1 (14m from fault) and Rx2 (35m from fault) due to PD within Power Cable Insulation.....	53
Figure 4- 5: Individual Emission Measured at Rx1 (14m from fault) and Rx2 (35m from fault)	54
Figure 4- 6: Individual Acoustic Emission – Rx1.....	54
Figure 4- 7: Evaluation of AE Duration – Rx1 and Rx2 signals compared.....	55
Figure 4- 8: Frequency Spectrum of Individual Emission from PD within Power Cable Insulation: (a) EM and AE signal, (b) AE signal only.....	56
Figure 4- 9: Frequency Spectrum of Multiple AE from PD within Power Cable Insulation: (a) 3 individual PD events received on Rx1, (b) 3 individual PD events received on Rx2	57

Figure 4- 10: Spectrogram of Signals Captured from PD within Power Cable Insulation: (a) corresponding 2D time vs frequency plot, (b) corresponding 3D plot including signal magnitude.....	59
Figure 4- 11: Individual Acoustic Emission from PD within Power Cable (a) Power Spectral Density – Rx1 & Rx2 (b) Spectrogram – Rx1 only.....	60
Figure 4- 12: AE Signal, Hilbert Transform and Envelope of Individual Discharge Measured at Rx2 (35m from fault)	67
Figure 4- 13: AE Signal and Envelope of Individual Discharge Measured at Rx1 (14m from fault) and Rx2 (35m from fault).....	67
Figure 4- 14: Signal Envelope of Individual PD Event Detected on Rx1 (14m from fault) and Rx2 (35m from fault)	68
Figure 4- 15: Cross Correlation of Individual PD Event from Rx1 (14m from fault) and Rx2 (35m from fault)	70
Figure 4- 16: Individual PD Event – Comparison of Original Signal against Signal with Added Noise providing a SNR of 3dB (time domain and cross correlation analysis).....	72
Figure 4- 17: Autocorrelation of Individual PD Event (a) Rx1 14m from fault, (b) Rx2 35m from fault	73
Figure 4- 18: Cable Sample Illustration Defining Fault and Sensor Positions	76
Figure 4- 19: Cable Sample Test Setup at TechnipFMC R&D Facility – PD Sensing 5m Increments.....	76
Figure 4- 20: Signal Envelopes – Rx1 35m from Fault, Rx2 5m to 55m from Fault ‘a’ through to ‘k’.	77
Figure 4- 21: Plot of Through-cable Signal Velocity Results, 5m-55m from PD Location, multiple PD events	79
Figure 4- 22: Signal Analysis Rx2 10m and 55m from Fault Location. Individual Discharge (a) time domain, (b) signals envelope, (c) FFT.....	80
Figure 4- 23: Simplified Block Diagram - Comparative Electrical PD Test	81
Figure 4- 24: Comparative Electrical PD Test Setup – Acoustic and Electrical Monitoring	82
Figure 4- 25: Average Peak PD and Average PD Activity at varying Voltage Increments	83
Figure 4- 26: Acoustic Emission from PD occurring at approximately 10kV	84
Figure 4- 27: PRPD Pattern indicative of Internal Void PD utilising HVPD Kronos® ...	85
Figure 5- 1: Through-cable Source Localisation using TDoA	88
Figure 5- 2: Acoustic Signals Measured at Rx1 (35m from fault) and Rx2 (25m from fault) due to PD within Power Cable Insulation, with a detection threshold of 0.2.	89
Figure 5- 3: TDOA between AE signals detected on Rx1 (35m from fault) and Rx2 (25m from fault)	90

Figure 5- 4 Cross Correlation of AE signals detected on Rx1 (35m from fault) and Rx2 (25m from fault)	91
Figure 5- 5: TDOA between EM and AE signals – Rx2 45m trial	92
Figure 5- 6: Signal Envelopes of AE from Multiple PD Events – Rx1 35m from fault, Rx2 15m from fault	94
Figure 5- 7: Signal Envelopes of AE from Multiple PD Events – Rx1 35m from fault, Rx2 25m from fault	94
Figure 5- 8: Signal Envelopes of AE from Multiple PD Events – Rx1 35m from fault, Rx2 45m from fault	95
Figure 5- 9: Through-cable Localisation obtaining TDoA from Rx1 & Rx2 Signal Envelopes, position estimation indicates distance from Rx2 to PD fault	96
Figure 5- 10: Through-cable Localisation obtaining TDoA from Rx1 & Rx2 Cross Correlation, position estimation indicates distance from Rx2 to PD fault	99
Figure 5- 11: Through-cable Localisation obtaining TDoA from EM & Rx2 Signal Envelopes, position estimation indicates distance from Rx2 to PD fault	101
Figure 5- 12: Comparison of Original Signal and those with Varying Levels of added Noise (a) Original Signal, (b) SNR 10dB, (c) SNR 7dB, (d) SNR 3dB, (e) SNR -3dB, (f) SNR -7dB	104
Figure 5- 13: Comparison of Individual Discharge with Varying Levels of added Noise (a) Original Signal, (b) SNR 10dB, (c) SNR 7dB, (d) SNR 3dB, (e) SNR -3dB, (f) SNR -7dB	105
Figure 5- 14: Signal Envelopes of AE from Multiple PD Events including added Noise (a) Original Signal, (b) SNR 10dB, (c) SNR 7dB, (d) SNR 3dB, (e) SNR -3dB, (f) SNR -7dB	108
Figure 5- 15: Cross Correlation of AE from Multiple PD Events including added Noise (a) Original Signal, (b) SNR 10dB, (c) SNR 7dB, (d) SNR 3dB, (e) SNR -3dB, (f) SNR -7dB	110
Figure 5- 16: System accuracy comparison for envelope and cross correlation analysis at an SNR of -3dB and -7dB. Position estimation indicates distance from Rx2 to PD fault	113
Figure 5- 17: Signal Strength Evaluation; (a) Environmental Noise, (b) Acoustic PD Emission – Samples from trial with Rx2 45m from PD	115
Figure 5- 18: Average SNR at Sensor Positions 10m through to 55m	116
Figure 5- 19: Assessment of PD Detectability Range	117
Figure 6- 1: Generic Underwater Sound Speed Profile [127].....	122
Figure 6- 2: Multipath in a shallow water configuration	125
Figure 6- 3: Levels and frequencies of anthropogenic and naturally occurring sound sources in the marine environment. Spectrum Noise Level versus Frequency [130].....	127

Figure 6- 4: Acoustic Signals from PD detected on Rx1 and Rx2 during test in an anechoic water tank.....	129
Figure 6- 5: Individual Acoustic Emission from PD detected on Rx1 and Rx2 during test in an anechoic water tank.....	129
Figure 6- 6: Envelope analysis results for an individual Partial Discharge detected on Rx1 and Rx2 during test in an anechoic water tank.	130
Figure 6- 7: Cross Correlation results for an individual Partial Discharge detected on Rx1 and Rx2 during test in an anechoic water tank.	131
Figure 6- 8: Frequency Spectrum of Individual AE from PD within Power Cable Insulation, detected with Hydrophones via through-water Acoustic Sensing.	132
Figure 6- 9: Spectrogram of AE Signals from PD within Power Cable Insulation detected with Hydrophones via through-water Acoustic Sensing: (a) corresponding 2D time vs frequency plot, (b) corresponding 3D plot including signal magnitude	133
Figure 6- 10: Power Spectral Density of Individual Acoustic Emission from PD within Power Cable Insulation detected with Hydrophones via through-water Sensing.....	134
Figure 6- 11: Anechoic Tank Controlled Experimentation	135
Figure 6- 12: North Shields Marina	137
Figure 6- 13: Open Water Trial – Receiver Positions.....	137
Figure 6- 14: Open Water Trial 1a, PD emission captures on receivers Rx1, Rx2 and Rx3.	138
Figure 6- 15: Transmitter Position – Trial 1a	140
Figure 6- 16: Open Water Trial 1a, Individual Partial Discharge.....	141
Figure 6- 17: Open Water Trial 8a, Individual Partial Discharge.....	142
Figure 6- 18: Transmitter Positions, Trial 8a.....	142
Figure 6- 19: Open Water Trial Pre-test including transmitted signal for ToT Measurements, (a) Individual Partial Discharge in Time Domain, (b) Signal Envelopes	143
Figure 7- 1: Characteristics of a Hyperbola.....	149
Figure 7- 2: Hyperbola with Centre as Origin	150
Figure 7- 3: Distance relationship of Hyperbolic Curves	151
Figure 7- 4: Localisation System Overview	154
Figure 7- 5: Source Localisation utilising Hyperbolic Positioning and Cross Correlation Techniques – Trial 1a.....	155
Figure 7- 6: Open Water Trial 1a – Source Localisation utilising Cross Correlation and Envelope Techniques	156
Figure 7- 7: Open Water Trial 2a – Source Localisation utilising Cross Correlation and Envelope Techniques	156
Figure 7- 8: Open Water Trial 3a – Source Localisation utilising Cross Correlation and Envelope Techniques	157

Figure 7- 9: Open Water Trial 4a – Source Localisation utilising Cross Correlation and Envelope Techniques	157
Figure 7- 10: Open Water Trial 5a – Source Localisation utilising Cross Correlation and Envelope Techniques	158
Figure 7- 11: Open Water Trial 6a – Source Localisation utilising Cross Correlation and Envelope Techniques	158
Figure 7- 12: Open Water Trial 7a – Source Localisation utilising Cross Correlation and Envelope Techniques	159
Figure 7- 13: Open Water Trial 8a – Source Localisation utilising Cross Correlation and Envelope Techniques	159
Figure 7- 14: System Simulation to Identify Influence of Receiver Positions	162
Figure 7- 15: Hyperbolic Positioning Simulation – Transmitter in Red Zone	163
Figure 7- 16: Additional Receiver Simulation – Transmitter in Amber Zone.....	165
Figure 7- 17: Additional Receiver Simulation – Transmitter in Red Zone	166
Figure 7- 18: Open Water Trial Test Setup – Live PD Occurrence through Cable Sample Testing.....	168
Figure 7- 19: Sensing System complete with GPS Synchronisation	169
Figure 7- 20: Open Water Trial – Live PD, Receiver Positions	170
Figure 7- 21: Open Water Trial - Individual Acoustic Discharge detected at Hydrophone Rx2.....	170
Figure 7- 22: Open Water Trial – Rx1 and GPS Signals.....	171
Figure 7- 23:Open Water Trial, Acoustic Discharge and GPS Signal Clock Synchronised on Rx1, Rx2 and Rx3.....	172
Figure 7- 24: Individual Acoustic Discharge Clock Synchronised on Rx1, Rx2 and Rx3	173
Figure 7- 25:Envelopes of Individual Acoustic Discharge Clock Synchronised on Rx1, Rx2 and Rx3	173
Figure 7- 26: Open Water Trial – Source Localisation of Genuine PD AE c/w GPS clock Synchronisation.....	174
Figure 7- 27: Trilateration for Source Localisation	175
Figure 7- 28: Hyperboloid of two-sheets	176
Figure 7- 29: Trial 1b – 3D Localisation utilising Hyperboloid Positioning, (x,y) axis.	177
Figure 7- 30: Trial 1b – 3D Localisation utilising Hyperboloid Positioning, (x,y,z) axis	178

List of Tables

Table 2- 1: PDIV for varying Void Shapes 15kV, 250mm ² Cable	25
Table 4- 1: Cable Cross Section and Material	62
Table 4- 2: Sound Velocity through Cable Materials	64
Table 4- 3: Trial to Evaluate the Effects of Propagation Distance – Sensor Positions.....	75
Table 4- 4: Through-cable Signal Velocity 5m-55m from PD Location.....	78
Table 5- 1: Through-cable Localisation utilising Signal Envelopes from Rx1 and Rx2 – Error Analysis	97
Table 5- 2: Through-cable Localisation utilising Cross Correlation of Rx1 and Rx2 – Error Analysis.....	100
Table 5- 3: Through-cable Localisation utilising Signal Envelopes from EM and Rx2 – Error Analysis	102
Table 5- 4: Comparison of Original Signal and Varying SNR - Error Analysis from Signal Envelopes	107
Table 5- 5: Comparison of Original Signal and Varying SNR - Error Analysis from Cross Correlation	109
Table 5- 6: Comparison of Envelope and Cross Correlation Error Analysis	113
Table 6- 1: Transmitter to Receivers Distances for all Sixteen Trials at Locations 1 through to 8.	139
Table 7- 1: Hyperbolic Positioning System Accuracy Evaluation	160
Table 8- 1: Key Technical Contributions.....	183

Nomenclature

Roman Symbols

<i>A</i>	Amperes
<i>C</i>	Capacitance
<i>c</i>	Speed of Sound
<i>E</i>	Youngs Modulus of Elasticity
<i>f</i>	Frequency
<i>fs</i>	Sampling Frequency
<i>H</i>	Heat Energy
<i>Hz</i>	Hertz
<i>I</i>	Current
<i>j</i>	Imaginary unit
<i>J</i>	Joules
<i>pC</i>	picocoulombs
<i>r</i>	Transmission Range
<i>R</i>	Resistance
<i>SL</i>	Source Level
<i>t</i>	Time
<i>TL</i>	Transmission Loss
<i>U_e</i>	Extinction Voltage
<i>U_i</i>	Inception Voltage
<i>v</i>	Velocity
<i>V</i>	Voltage
<i>V_{pp}</i>	Voltage Peak-to-Peak
<i>V_{rms}</i>	Voltage Route Mean Square

Greek Symbols

α	Absorption Coefficient
β	Bandwidth
λ	Wavelength
ω	Angular Frequency
π	Mathematical Constant ($\approx 3.14\dots$)
ρ	Density
σ	Standard Deviation
τ	Delay

Acronyms

AA	Airborne Acoustic
AC	Alternating Current
AE	Acoustic Emission
AUV	Autonomous Underwater Vehicle
CAPEX	Capital Expenditure
DAS	Distributed Acoustic Sensing
DC	Direct Current
DEH	Direct Electric Heating
DGA	Dissolved Gas Analysis
DNV	Det Norske Veritas
EMF	Electromagnetic Field
EMI	Electromagnetic Interference
ETH-PiP	Electrically Trace Heating Pipe-in-Pipe
FIR	Finite Impulse Response
FLNG	Floating Liquefied Natural Gas Platform
FMEA	Failure Mode Effects Analysis
FPSO	Floating Production Storage and Offloading Platform

FOW	Floating Offshore Wind
GIS	Gas-insulated Systems
GPS	Global Positioning System
HF	High Frequency
HFCT	High Frequency Current Transformers
HV	High Voltage
HVCC	High Voltage Coupling Capacitor
IEC	International Electrotechnical Commission
IR	Insulation Resistance
IWOCS	Intervention Workover Control System
LV	Low Voltage
MAE	Mean Absolute Error
MSE	Mean Squared Error
MV	Medium Voltage
OPEC	Organisation of Petroleum Exporting Countries
OPEX	Operational Expenditure
OTDR	Optical Time Domain Reflectometry
PD	Partial Discharge
PE	Polyethylene
PDEV	Partial Discharge Extinction Voltage
PDIV	Partial Discharge Inception Voltage
PRPD	Phase Resolved Partial Discharge
RMS	Root Mean Square
ROV	Remotely Operated Vehicle
SD	Standard Deviation
SNR	Signal to Noise Ratio
TDE	Time Delay Estimation
TDoA	Time Difference of Arrival
TDR	Time Domain Reflectometry
TFDR	Time Frequency Domain Reflectometry

TLP	Tension-Leg Platform
ToA	Time of Arrival
ToF	Time of Flight
ToT	Time of Transmission
UV	Ultraviolet
VSD	Variable Speed Drives
XLPE	Cross-linked Polyethylene

Glossary of Terms

<i>Brownfield</i>	An existing oil or gas field where production has begun and existing infrastructure is in place. A brownfield project refers to the expansion or extension of an existing facility.
<i>J-Tube</i>	A conduit designed to protect the umbilical/cable between the top and bottom of the sea, where subsea structures are connected to a platform or FPSO. The conduit/tube has the shape of the letter 'J' or alternatively in the case of an I-Tube, the letter 'I'.
<i>Topside</i>	The section of the oil or gas platform or wind turbine structure which is above sea level.
<i>Umbilical</i>	Connection between subsea equipment and platform or FPSO facilities, allowing control and communication from the surface. Umbilicals often contain, hoses, tubes and cables to allow transfer of power, chemicals and communication signals to subsea equipment.
<i>Crosstalk</i>	Unintentional and undesired transmission (leakage) of a signal from one cable pair to another, causing interference or degradation to the other signal.
<i>Joule effect</i>	Joule heating is the physical effect whereby the pass of current through an electrical conductor produces thermal energy leading to a rise in conductor material temperature.
<i>Pigging</i>	A technique of cleaning or inspection of pipelines through insertion of a device known as a 'pig' into process pipelines. Typically used to remove highly viscous fluids and debris from the pipeline, however can be used housed with onboard cameras and ultrasonic equipment for inspection purposes.

Chapter 1

Introduction

Within the oil and gas industry, there is an increasing requirement for more electrical power on the seabed. This is largely due to the current evolution in subsea processing systems whereby many of the separation and pumping operations previously performed topside on the floating production system or platform, are now performed on the seabed. Subsea processing provides many advantages including; reduced capital expenditure (CAPEX) costs of topside processing equipment, improved well productivity, reduced flow assurance problems and a more environmentally friendly solution. This move to the seabed leads to an increased number of medium/high voltage power cables within subsea umbilicals to enable power transfer to the necessary processing equipment.

In addition, the continuous development within the industry to reduce the weight and size of umbilicals denotes a move towards electric control as opposed to hydraulic, which consequently increases the requirement for electrical cables. All-electric control also benefits long distance tieback umbilicals due to the decline in hydraulic power efficiency over long distances.

There is also a large influence on the industry requirements due to the UK governments legally-binding commitment to net zero emissions by 2050. The government forecasts that the oil and gas industry will play an important role in energy transition because of its expertise in supplying technology in harsh environments, established supply chain and transferable specialist engineering skills. To accelerate energy transition, electrification of oil and gas operations is key whereby fossil-based power supplies are replaced with electrical power, either from shore or ideally through renewable energy, such as electricity generated through floating offshore wind farms. Platform electrification provides lower emissions, lower operational expenditure (OPEX), lower CAPEX and is an enabler to further energy transition technologies, which again results in a need for more subsea power cables.

The increased requirement of power cables within the umbilical heightens the criticality of the cable condition, as they are a key element in providing functionality to the overall system. A loss in power, leading to a loss in production is extremely costly, therefore continuous online monitoring of the umbilicals assets is highly beneficial. It would be extremely advantageous to have the ability to detect and locate a fault within a power cable prior to complete cable failure, as this would prevent major unforeseen costs due to unplanned production down time.

Furthermore, due to the recent industry downturn, operators are trying to extend the lifetime of their current fields. The majority of these fields are not setup for continuous integrity monitoring and as a result it is difficult to make an assessment on the remaining lifetime of the umbilical components. Many fields are consequently operating past their initial design life and as a result, a non-intrusive retrofit method for online detection of early faults on power cables would provide reassurance of their operating condition, allowing areas of high insulation deterioration to be localised, which will in turn allow for scheduled maintenance, if required, as opposed to unplanned production down time.

One of the main failure modes of medium and high voltage power cables is due to the occurrence of partial discharges (PD) within the cable. These discharges cause a breakdown in the cable's insulation, which over time leads to complete breakdown and shorting of the cable. All medium voltage (MV) and high voltage (HV) cables are designed and manufactured to try to create an even electrical stress around the conductor and insulating layer in order to minimise the likelihood of PD occurrence. High stress points can stem from the presence of small voids or imperfections, which unfortunately cannot always be avoided, particularly during cable splicing. These small voids or imperfections lead to PD, which can develop into electrical trees and surface tracking, causing insulation breakdown and resulting in cable failure [1]. This then leads to loss of power to the subsea production system causing downtime and excessive unforeseen costs.

When partial discharges occur, sound waves in both the audible and ultrasonic frequency ranges are emitted as well as electromagnetic emissions in the form of light, heat and radio waves and chemical changes occur due to ozone and oxide nitrogen gases. Monitoring of PD within an umbilical whilst the system remains online brings many challenges due to; the subsea environment, long length requirement (>1km), inability to access the far end of the cables, bespoke nature of each umbilical design and the cables remaining operational at voltages between 6kV and 66kV.

In currently installed systems, methods for detecting and locating these cable faults within umbilicals are only available when the cables are offline, hence these methods are typically only used to determine the location of the fault after complete cable failure has occurred, although this is not always possible, even when the system is offline. High frequency current transformers (HFCT's) are relatively non-intrusive and can be used online to detect PD events, however due to the attenuation of the PD signals and the long length requirement of umbilicals, using HFCT's for fault localisation is typically not feasible. A transponder can be used to increase the distance for source localisation, though this is only when access to the far end of the cable is available, which is highly unlikely on an umbilical.

Acoustic emission (AE) sensing has been highlighted as a viable non-intrusive method for online monitoring of PD activity within umbilicals as it is able to overcome many of the challenges associated with umbilical asset integrity monitoring. Acoustic sensing methods are commonly used for PD detection in air insulated switchgear, whereby Airborne Acoustic (AA) sensors are placed on the inner surface of the switchgear housing, or over

external surface air vents, to listen for discharge occurrence. This non-intrusive method allows for online detection, however the position of the AA sensors needs to be in close proximity to the fault location due to high sound attenuation through air. In the case of an umbilical, the cables are surrounded by sea water, which is an excellent sound conductor and as a result the acoustic signal from the discharge will travel long distances with a low attenuation rate. The sound will propagate out from the fault location into the surrounding seawater and also directly through the cable itself, back to the topside facility. Multiple AE sensors can be used to allow for localisation of the fault based on time difference of arrival (TDoA) between sensors and the use of time delay estimation (TDE) algorithms.

Previous research has been performed into suitable localisation methods for known signals where TDoA and cross correlation techniques have been used in estimation algorithms to establish the location of the transmitter. In this scenario, the acoustic signal from each individual discharge is broadband and varies in amplitude in relation to the severity of PD, which consequently increases the complexity of fault localisation as the specific characteristics are dependent on each individual discharge.

This research investigates the use of acoustic emission sensing for the detection of PD within subsea umbilicals, utilising TDoA of received signals in position estimation algorithms to establish the location of the fault prior to complete cable breakdown. Research into both through-cable and through-water propagation of the AE signal has been performed. Practical testing confirms the established system to be a viable solution for PD source localisation in this challenging environment. This thesis discusses potential non-intrusive methods which could be used to monitor the integrity of MV and HV power cables within subsea umbilicals, highlighting recommended techniques for establishing the location of the PD whilst the umbilical system remains operational.

1.1 Contributions

This thesis proposes a viable method for online detection of PD within subsea umbilicals, focusing on novel techniques for fault localisation using non-invasive means. Key areas of novelty can be attributed to; unknown time of AE occurrence, the changing characteristics of the AE signal in relation to each individual discharge, the long length requirements of subsea power cables, the challenging environments in which umbilicals are situated and the bespoke complex nature of both the cables and umbilicals.

The following list summarises the key contributions that have been made within this research:

1. Detailed investigation into the challenges of detecting and locating partial discharges occurring in medium and high voltage power cables within subsea umbilicals, whilst operational.
2. Characteristics of through-cable acoustic propagation of PD along the length of the cable and suitable AE sensing techniques within umbilicals.

-
3. Analysis of through-water acoustic propagation of PD within a saltwater environment.
 4. Development of a time delay estimation algorithm and suitable sensing array capable of detecting and estimating PD fault location, using hyperbolic positioning techniques.
 5. Demonstration of a non-intrusive acoustic sensing system which can be used whilst the umbilical system remains online, to detect and locate PD occurrences within a subsea power umbilical.

1.2 Publications

The following paper has been published based on the work performed during this research, along with a conference presentation.

- L. J. Smith, J. A. Neasham, “Acoustic Emission Methods to Localise Partial Discharge Events in Subsea Umbilicals” *Proc. IEEE Oceans, Aberdeen, United Kingdom, 19-22 June 2017.*

1.3 Thesis Outline

The structure of this thesis is as follows;

Chapter 2 provides a detailed overview of the design requirements for subsea umbilicals and highlights the industry move towards subsea processing, all-electric control and subsea electrification, leading to additional electrical power on the seabed. Potential failure modes of power cables are discussed to establish beneficial areas for online asset monitoring.

Chapter 3 details potential methods for detecting the physical factors accompanying partial discharge in order to assess the condition of the cable. PD propagation paths from within an umbilical are discussed and various sensing methods presented with the aim of overcoming the inherent challenges of integrity monitoring for this particular subsea application. A detailed literature review allows potential sensing methods to be assessed and state-of-the-art technologies evaluated to ensure a suitable approach is taken to allow PD detection & localisation within subsea umbilicals.

Chapter 4 investigates the through-cable propagation of the resultant acoustic emission from a partial discharge event within an MV cable. Results from experimental tests allow the characteristics of the AE signal to be analysed, whilst considering the influence of the propagation channel that is the cable. The varying mediums and potential wave types are discussed to provide an understanding of the complexities due to the cable structure. Further testing provides an overview of the effects on the signal as it travels through the cable length, with particular focus on changes in signal velocity and frequency content. A comparative investigation offers a view of the magnitude of the PD levels being detected

acoustically in relation to existing electrical PD detection technology to allow correlation of the condition of the cable.

Chapter 5 discusses the potential methodologies to be used for through-cable localisation of the discharge, whilst also exploring and comparing envelope and cross correlation TDoA techniques. To understand the accuracy of the localisation system, the SNR is also considered, investigating the effects on both TDoA techniques to establish the most suitable for use in the localisation algorithms. The range of PD detectability is also examined to allow the length capabilities of the through-cable sensing to be estimated, concluding with a summary of how the system could be implemented for use.

Chapter 6 provides a review of the underwater channel and the influence it has on the through-water PD signals, considering; speed of sound, transmission loss, multipath and noise. Testing in an anechoic tank allows for initial signal analysis of the through-water signal properties and recording of the PD acoustic emissions, enabling calibration of the hydrophones along with an understanding of the discharge signals source level and in turn its detectability range. Large scale open water testing is performed to assess the detectability at a greater range, whilst investigating the signals characteristics and velocity.

Chapter 7 focuses on localisation of the PD source in an underwater environment, considering through-water propagation of the emitted acoustic signals. Localisation techniques are reviewed to ensure a suitable methodology is applied within the positioning algorithm. Open water results are analysed and processed to allow for position estimation of the PD source and accuracy of the system to be assessed. Further open water testing confirms feasibility of the system on a larger scale, under more realistic conditions. Combined electro-acoustic sensing is discussed, along with the potential application for the technology.

Chapter 8 summarises the key findings and conclusions from the work performed in this thesis, whilst also considering the initial research aims. Areas of future work are identified to highlight potential ways of taking this research further.

Chapter 2

Background Information and Motivation

This chapter focuses on the use of subsea umbilicals within the Oil and Gas Industry and the complexities of the bespoke nature of the umbilical designs. It goes on to discuss the effects of the increasing requirement for subsea processing, all-electric control systems, heated pipelines, energy transition and the impact this has on the umbilical construction. Potential cable failure modes are reviewed, with a particular focus on the phenomenon of partial discharges. TechnipFMC is the sponsoring company for this research, therefore focus will be on their umbilical designs.

2.1 Subsea Umbilicals

Within the Oil and Gas industry subsea umbilicals are used to form a vital link between subsea production systems and surface facilities such as; floating production storage and offloading platform (FPSO), floating liquefied natural gas platform (FLNG), tension-leg platform (TLP), spars or fixed platforms. The umbilical is able to transport fluid, gas, power and communications to and from the subsea equipment, therefore enabling chemical injection, hydraulic and/or electric production control, communications, asset monitoring, subsea processing, pipeline heating and gas lift injection. Figure 2- 1 [2], illustrates an example of prospective umbilical applications, connecting various topside facilities to seabed architecture in potentially harsh environments.

2.1.1 Umbilical Design

Each umbilical is bespoke in its design as they are engineered specifically for their use and environment. The main factors affecting the umbilical design are; functional requirement, static or dynamic service, length, internal temperatures from joule heating or fluid/gas transfer, along with environmental considerations such as; water depth, external temperatures, sea state and region-specific influences e.g. Arctic conditions or gas inducing environments.

Depending on its purpose, the umbilical can contain steel tubes, thermoplastic hoses, low voltage/signal cables, medium or high voltage power cables, fibre optic cables, strength

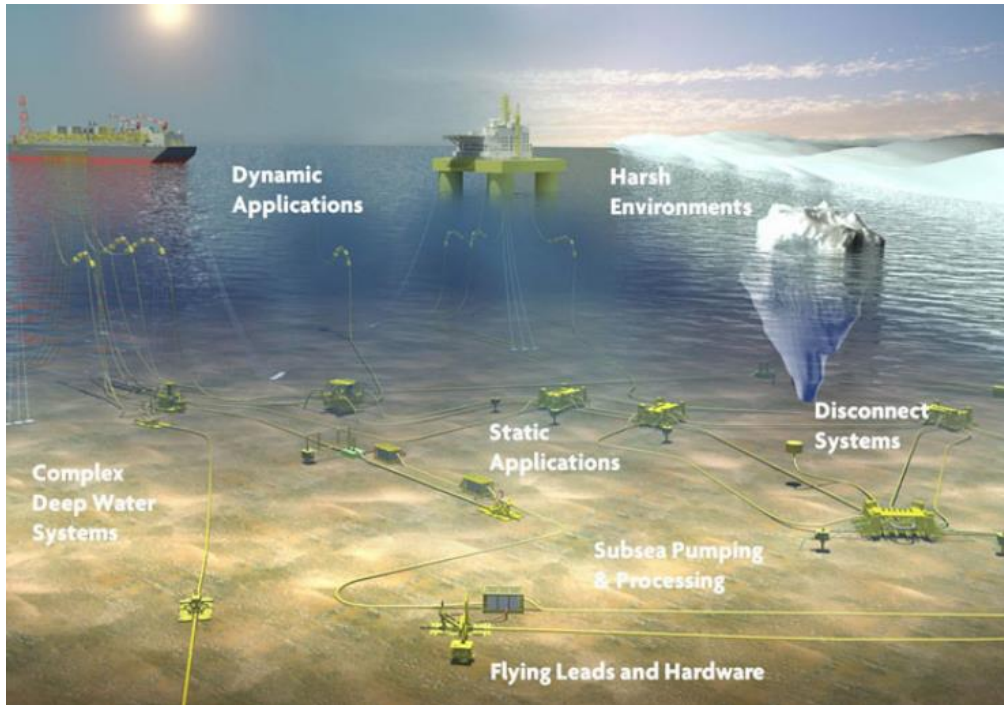


Figure 2- 1: Umbilical Applications [2]

members, armour wires and fillers. Company design rules are followed for the positioning of the umbilical components to ensure they remain fit for purpose throughout the required design life, typically being 30 years. The components are bundled and twisted together in a continuous helix or oscillating helix (S-Z) assembly to allow flexibility. A polymer sheath or rovings provides an outsheath for the bundled assembly enabling visibility and protection. Figure 2- 2 shows a typical cross section of a TechnipFMC umbilical containing electro-hydraulic functionality from low voltage (LV) cables, fibre optic cables and steel tubes.

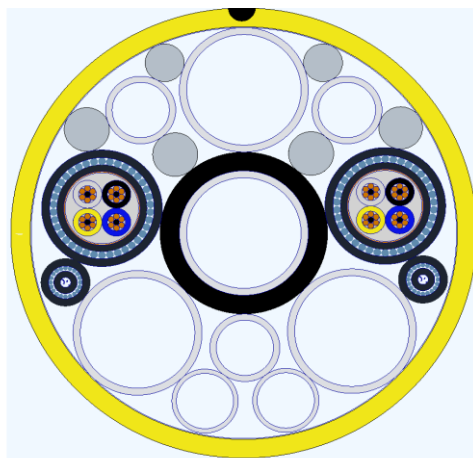


Figure 2- 2: Typical Umbilical Cross Section

Umbilicals are designed to operate in either a static or dynamic environment and the umbilical composition differs between the two applications. A dynamic umbilical connects the topside host facility to the subsea field and is therefore subjected to high tensile loading and fatigue throughout its lifetime. A static umbilical remains on the seabed, or buried, and provides connections between the subsea architecture. Examples of static and dynamic umbilicals can be seen in Figure 2- 3, [3]. Both static and dynamic umbilicals see high tensile loads and fatigue during umbilical installation however, once installed, the static umbilical will no longer be subjected to these extreme fatigue and tensile loadings. Static umbilicals are therefore designed to withstand the tensile and fatigue loads experienced during installation, whereas dynamic umbilicals are designed to ensure they are able to withstand the loads experienced both during installation and throughout its expected lifetime. These loads differ greatly depending on the area in which they are being installed due to changes in sea state within different parts of the world. Consequently, dynamic umbilicals require additional strength in comparison to static and typically include armouring or strength members within this flexible section. Smaller components such as low voltage cables also require armouring within the dynamic section. In some cases, static umbilicals may also be armoured to allow sufficient seabed stability or to provide external protection.

Positioning of the components is key, not only for mechanical strength, fatigue and stability, but also for electromagnetic interaction. When an umbilical contains power cables, it is critical that they are positioned in order to minimise the potential of induced

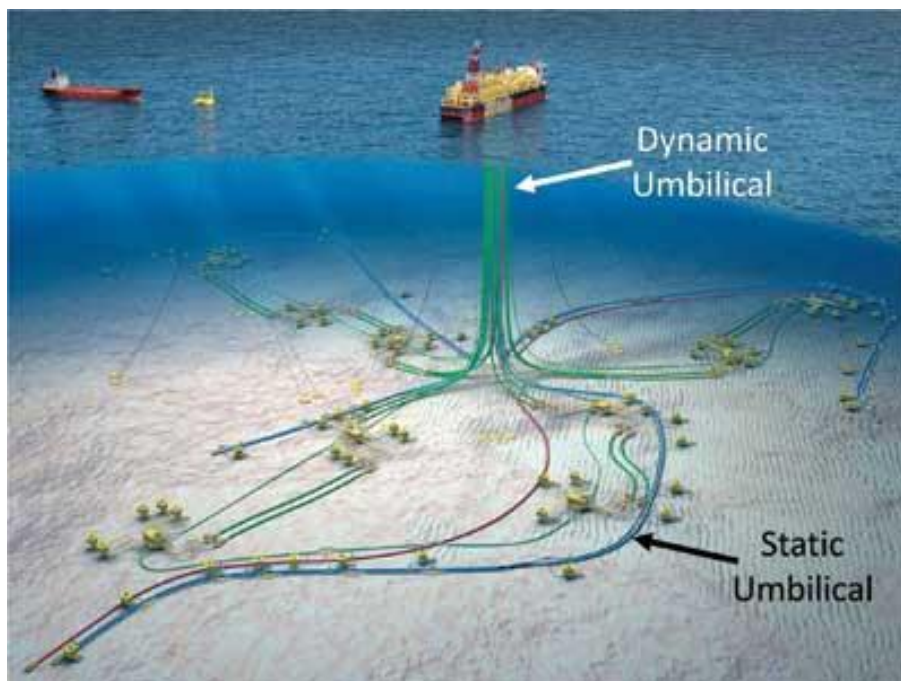


Figure 2- 3: Static and Dynamic Umbilicals [3]

voltages on the surrounding metallic components. The induced voltage, V , in an adjacent component due to the load current, I , in one phase of a power system is defined in (2.1), where M is the mutual inductance between the phase conductor and component and L is the circuit length in parallel with the component in meters.

$$V = j\omega MIL \quad (2.1)$$

When present, induced electromagnetic fields (EMF) can cause interference on surrounding cables, which in turn reduces their efficiency. Induced voltages on nearby steel tubes can lead to a high localised electro-potential and subsequent corrosion. Typically, the 3-phases of a power cable are helically wound together in a tight trefoil formation to create a balanced load through twist rejection between circuits, as the induced voltage picked up from each conductor is equal and therefore cancelled by being 120° out of phase. This, however, is not always the most feasible umbilical layup solution and therefore, should this be the case, the induced voltages will be calculated to confirm they are at a safe and acceptable level.

The required length of the umbilical will also have an effect on the overall design. The operational water depth dictates the length of the dynamic umbilical section and the static section is dependent on the field architecture. The length of the umbilical can have a large impact on the chosen cable designs as it is key to ensure that the system requirements are achievable at the subsea end. LV cables being used for communications have specific electrical characteristics that need to be met and therefore signal attenuation along the length must be taken into account when designing the cable for use in the umbilical. Signal attenuation denotes a reduction in strength of the transmitted signal over distance. This is caused by energy loss from the electromagnetic field created which worsens over long lengths and high frequencies. Another aspect to consider during the cable design is coppers susceptibility to electromagnetic interference (EMI) from surrounding power cables, as discussed previously, and the occurrence of crosstalk between parallel LV pairs. Crosstalk is when a signal from one cable pair leaks to another, causing interference and degradation to the other signal. As a result, the cables are designed and positioned to guarantee the required system characteristics are met and interference is kept to a very minimum. As with LV cables, any medium or high voltage power cables within the umbilical have to be designed to account for any losses along its length. Power cables experience a drop in transmission voltage along the umbilical length due to the impedance. Consequently, power cables are sized to account for the allowable volt drop within the system. Similarly, steel tubes and thermoplastic hoses experience a drop in pressure along the length in order to maintain the required flowrate and are therefore designed to take this into consideration.

Temperature has a large impact on the design of the umbilical as this will dictate the components and materials which can be used. Both the environmental temperature (external influence) and the internal temperature of the operational electrical and hydraulic components have to be considered during the design process. Temperatures external to the

umbilical are typically highest at the surface within the bend stiffener region or within the J-Tube or I-Tube due to solar radiation. The extent of these high temperatures is dependent on the location of the field. This may result in changes in the polymers or components chosen for use within the umbilical, for example; cross-linked polyethylene (XLPE) may be used instead of standard polyethylene (PE) and high temperature hoses may be selected as opposed to regular thermoplastic designs. Umbilicals may also be installed in Arctic environments, therefore extreme operating temperatures down to -40°C also have to be considered as this will greatly impact the design and materials chosen. In addition to these external factors, it is also possible for the components within the umbilical to cause a temperature increase above that of the surrounding environment. MV/HV power cables are an example of this due to the Joules heating effect. The Joule's effect is where electric energy is converted to thermal energy when an electrical current passes through a conductor. The amount of heat generated is dependent upon; the resistance, R of the conductor, the amount of current, I and the time, t for which the current flows. The formula of Joule's law can be expressed by (2.2), where H is the heat generated in Joules J , I is the current in amperes A , R is the resistance in ohms, and t is time in seconds s .

$$H = I^2 R t \quad (2.2)$$

As a result, power cables are often oversized in relation to their current carrying capacity in order to reduce the heat produced and in turn the overall operating temperature of the umbilical. It is also possible for the hydraulic lines, both steel tube and thermoplastic, to cause internal heating of the umbilical, causing a rise above ambient temperature. This is due to the temperatures of the gases or fluids being transported through the umbilical. Again, this will influence the overall design.

At present, umbilicals can be installed in water depths of up to 3000m, however many new technologies are now being qualified for increased water depths of up to 4000m, to allow operation in some previously inaccessible ultra deep-water environments. The collapse resistance of the umbilical structure and its components is a key aspect of the design and is based on the external pressure present at the maximum depth of the field. The deeper the water, the greater the hydrostatic pressure on the umbilical. Approximately every 10m, the pressure increases by 14.5psi (1bar) and the relationship is linear. Each umbilical manufacturer's designs vary, however this research focuses on free flooded umbilicals whereby all components are surrounded with sea water. By free flooding the umbilical, the structure is then pressure balanced, preventing collapse from external water pressure. The flooding occurs by leaving the ends of the umbilical open to allow the sea water to enter through the interstitial gaps and also through vent holes introduced at calculated positions along the length of the umbilical to ensure an adequate flooding rate during installation. Each component within the umbilical will be designed to ensure it is individually able to withstand the pressure equivalent to the field water depth.

Other considerations may be required if the umbilical is being installed in a particularly harsh environment. For example, umbilicals within Arctic regions often require additional quick disconnect ability to allow for passing ice bergs. Another example is that in shallow, warm waters, there have been reported cases of gas build up within umbilicals, where hydrogen gas migrates within the interstices of the cables travelling up to the topside junction box. This could lead to an explosion at the topside platform if not properly managed at design stage.

2.1.2 Categories

Although each umbilical is bespoke in its design, they typically fall into one of the following categories; thermoplastic, steel tube, power transfer, power and control, or hybrid. Typical examples of these designs are shown in Figure 2- 4. The category is dependent on the functionality of the umbilical and therefore the components within the bundle.

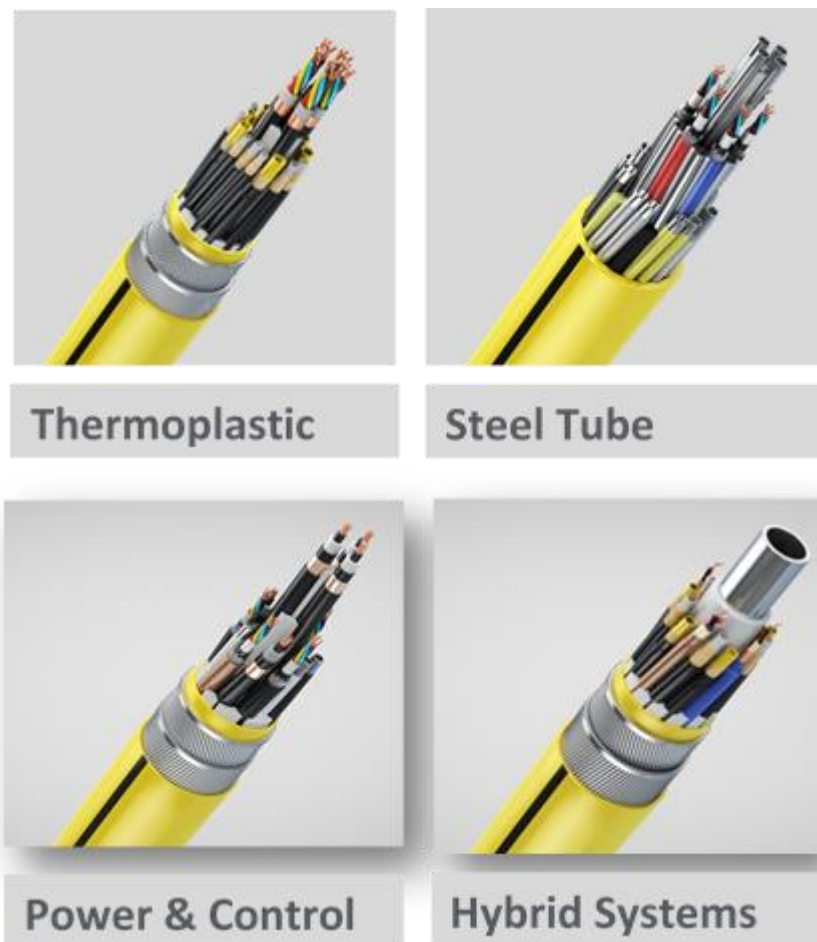


Figure 2- 4: Typical Umbilical Designs

A thermoplastic umbilical contains mainly hoses but may also contain low voltage or fibre optic cables to allow for power transfer and communications. These components are bundled in either a continuous helix or S-Z lay. This bundle is non-load bearing and is therefore armoured for strength and protection. Thermoplastic hoses are suitable for a range of hydraulic control or chemical injection fluids and are able to operate at high working design pressures of up to 10,000psi. When designing the thermoplastic hoses, bore size, design pressure and operating temperature are key.

Along with thermoplastic umbilicals, the primary function of a steel tube umbilical is to provide hydraulic control, chemical injection and gas lift operations. They consist mainly of steel tubes but again may also contain low voltage or fibre optic cables. This construction differs from the thermoplastic umbilicals in that the axial load is shared between the tubes and any additional strength members, therefore, an outer armour layer is typically not required. In certain cases, however, an armour layer may be included to provide additional weight and strength. An umbilical containing steel tubes must be laid up with a continuous helix rather than an S-Z. The main factors to consider for design of the steel tubes are bore size, operational and external pressure, corrosion resistance, operating temperature and tensile strength.

Power umbilicals primarily contain 3-Phase medium voltage cables, which are required for subsea pumping or to transfer power between offshore assets. The MV cables are generally assembled in a trefoil configuration to minimise induced voltages by maintaining a balanced system. A power umbilical may also contain low voltage and fibre optic cables. Power umbilicals are typically non-load bearing and so are generally armoured or contain load bearing strength members to allow for termination to the host vessel or structure.

A power and control umbilical encompasses both power cables and a hydraulic function, through either steel tubes or thermoplastic hoses. If the hydraulic operation comes from steel tubes, then armouring may not be required however, if thermoplastic hoses are used, armouring is most likely needed.

Hybrid umbilicals generally comprise of a combination of thermoplastic and steel tube functional components. A structure containing steel tubes and power cables is typically considered a steel tube umbilical, however, if the proportion of power cables is high to the proportion of steel tubes, the structure may require armour layers; in this case, the structure could also be considered a hybrid umbilical.

In addition, there are also intervention workover control system umbilicals (IWOCS) which differ greatly in their design. IWOCS are flexible, dynamic umbilicals which are on reels on a service vessel and are used for multiple deployments. Due to the highly dynamic and flexible requirements, Kevlar is often used instead of steel armouring. IWOCS are used during installation of subsea systems to ensure everything is working correctly and also for intervention if there are problems during service.

2.2 Umbilical Evolution

Over time the design of subsea umbilicals has continued to evolve to ensure the most efficient solution is provided to meet operational needs in an increasingly challenging subsea environment. In recent years there have been numerous developments within the oil and gas industry which has brought about a transformation in umbilical designs, many of which have led to an increase in the electrical functionality required. The 2016 industry downturn created an essential focus on the reduction of cost within the sector, directing the concentration of any new technologies being produced. Furthermore, the global drive to reduce the carbon and environmental footprint associated with energy production has greatly influenced the operational requirements of the umbilical, again resulting an increased number of power cables subsea.

2.2.1 Industry Downturn

One of the main impacting factor in this step change in umbilical design is due to the industry downturn, where crude oil prices fell from an average of \$110 per barrel between January 2011 and June 2014, to a low of \$29 in January 2016, [4]. Figure 2- 5 illustrates the changing price of Brent Crude oil over the past 10 years. The nominal price has

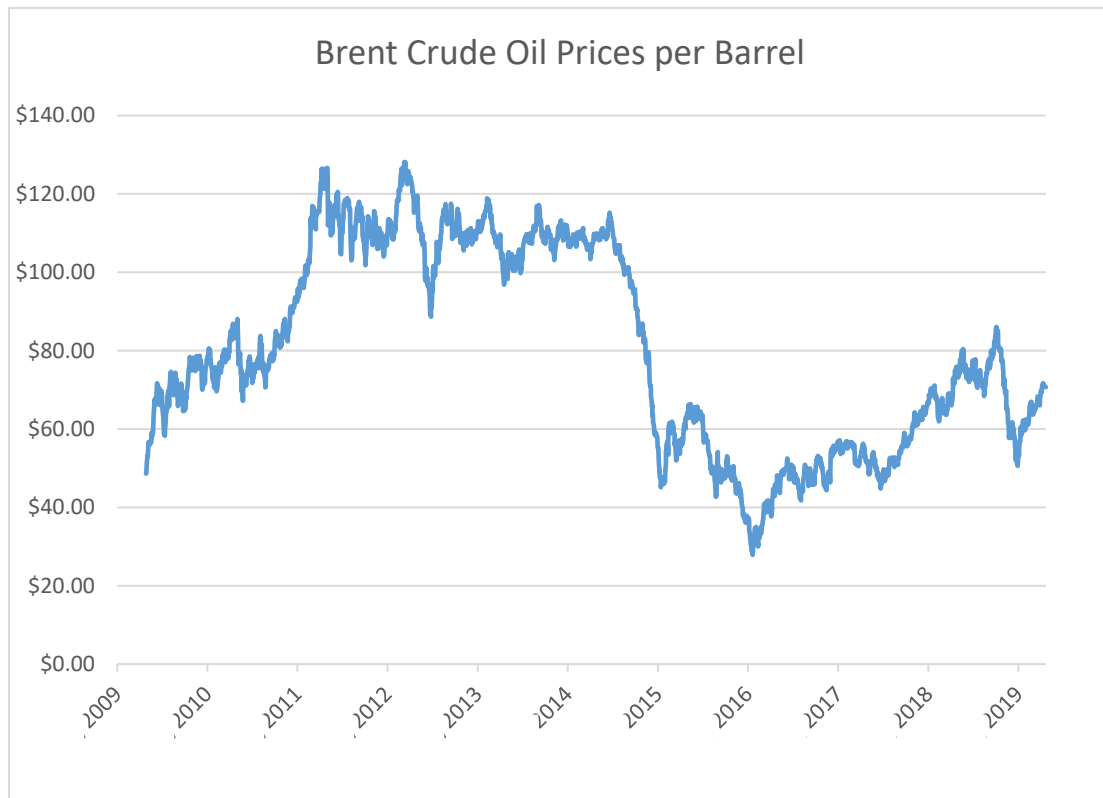


Figure 2- 5: Changes in Crude Oil Price 2009 to 2019

gradually increased and averaged around \$70 per barrel in April 2019. A surge in the production of U.S. shale oil, geopolitical conflict in Africa and the Middle East, a hyper supply environment due to the Organisation of Petroleum Exporting Countries (OPEC) decision in November 2014 to abandon price controls and reductions in consumption growth from previously fast growing economies were some of the many factors believed to contribute towards the dramatic reduction in oil price. Stocker, Baffes and Vorisek discuss each of these issues in detail, highlighting their impact on the price of oil [5]. In summary, U.S shale production was believed to be one of the main drivers as in 2014, U.S, oil production alone exceeded that of global oil demand. Not only were they able to provide lower production costs, they also showed high efficiency gains, which caused the break-even prices to drop almost 30% between 2012 to 2016. During the price drop of 2009, OPEC reduced oil production to stabilise the prices, however in November 2014, OPEC announced that they were not going to do this and instead were aiming to maintain its market share. Following further price decline throughout 2015 into 2016, multiple OPEC members, along with some non-OPEC members including Russia, made an agreement in January 2017 to go ahead with production cuts with the objective of raising the oil price. The market began to stabilise following this agreement, however the rise was less than originally thought indicating that U.S. shale oil has a greater influence on the market than initially predicted. In addition, geopolitical developments have always had an influence on oil production and therefore the price of oil. Prior to the 2014 drop, political tensions in the Middle East and North Africa led to a loss in production, however the increase in U.S. oil production made up for these losses. By the second half of 2014, it became apparent that conflicts in the Middle East and eastern Europe were not having as severe an impact on oil supply as expected. Libya, despite internal conflict, added 500,000 barrels a day of production in the third quarter of 2014, [6]. This contributed to the existing hyper supply environment. Another attributing factor to the price plunge was the decline in the demand for oil from emerging markets and developing economies (EMDE). In 2013 alone, Chinese consumption growth decreased by 54% or 370,000 barrels per day as compared to the demand in 2012, [7].

The discussed industry downturn had a huge impact on the design of subsea fields [8]. Achieving a reduction in CAPEX costs proceeded to be a main driver for field design. Potential for large cost savings were identified with the development of new technologies to treat processed fluids on the seabed, allowing for a reduction in topside facilities [9]. In addition, all-electric control systems would again provide a valuable reduction in costs, whilst also allowing for longer length step-out umbilicals [10]. To coincide with subsea processing and subsea electrification, the use of active heating solutions to mitigate wax deposition or hydrate formation in pipelines could be used to further reduce costs. Similar to subsea processing, the size and weight of the topside facilities would be reduced, as well as the removal of the additional flowline required for pigging. Figure 2- 6 shows a potential field including these new technologies. The introduction of these technologies and changes to field layout has led to an evolution in umbilical design.

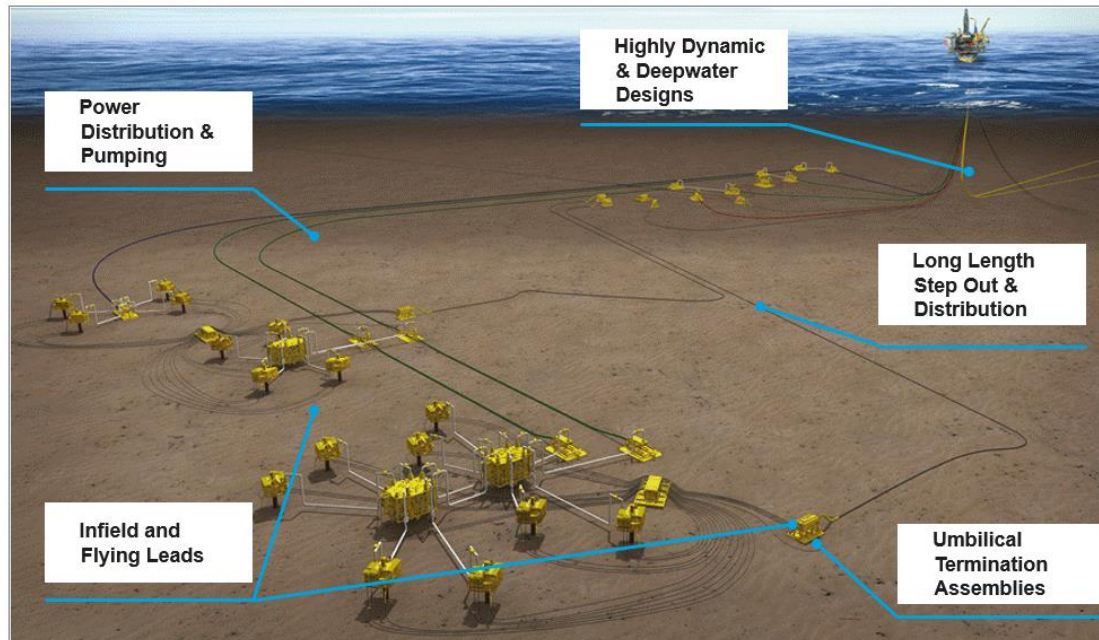


Figure 2- 6: Field Layout

A more detailed overview of each of the suggested cost reduction methods is provided in the following sections to further understand the impact on the umbilical design.

2.2.2 Subsea Processing

Subsea processing relates to the production equipment used for separation, re-injection, boosting and pumping being located on the sea floor as opposed to on a floating production system or fixed platform. The move towards subsea processing has been discussed within the industry over the past few decades, however due to technical issues and challenges, along with the initial uncertainty as to the extent of the potential advantages, the industry did not rush into the deployment of complete subsea processing systems. Initially, subsea processing was thought of as a way to overcome some of the challenges associated with fields in harsh environments or remote deep waters, therefore with production possible in shallower and calmer waters, the risk of deployment of new technology was seen to outweigh the potential benefits. As a result of the ‘lower for longer’ oil price, the industry has again brought subsea processing into focus due to the prospective cost savings these new technologies can offer for future projects.

Many industry leads have fully recognised the need for subsea processing and have been developing technologies to work towards increased processing on the seabed, which in turn leads to a reduced or even fully removed topside facility. Statoil, now known as Equinor, referred to their subsea processing concept as the Statoil Subsea Factory whereby the concept was first launched in June 2012 at the Underwater Technology Conference in

Bergen. Figure 2- 7 illustrates this complete subsea production system [11]. Okland, Davies, Ramberg and Rogno discuss the main drivers for Statoil in working towards this subsea factory, those being; increased hydrocarbon recovery and accelerated production, greater energy efficiency, competitive CAPEX and OPEX, increased lifetime of existing installations, reduction in topside space and weight of new fields, enable marginal field developments, realisation of complex offshore field development including Arctic and deepwater, realisation in sensitive or harsh environments not allowing platform construction and improved flow assurance solutions [11]. Statoil have performed a great deal of research and development within this area, reviewing all aspects of subsea processing including; boosting, raw seawater injection, separation, sand handling, subsea gas compression technology and have provided a step wise approach in the deployment of increasingly complex subsea processing systems in ever more challenging environments [12].

Other major operators including FMC technologies, have also been working towards an ‘All Subsea’ system. McClimans and Fantoft, highlight the past present and future of subsea processing technologies and discuss the building blocks required to perform technically feasible and economically viable field developments. Recognition is made for the requirement of new cost effective technologies to enable the development of future fields, caused by increased step out distance, greater water depths and extreme environments [13]. More recently, Rudd, Idrac, McKenzie and Hoy review the developments made over the past 10 years and go on to discuss how a shared vision and

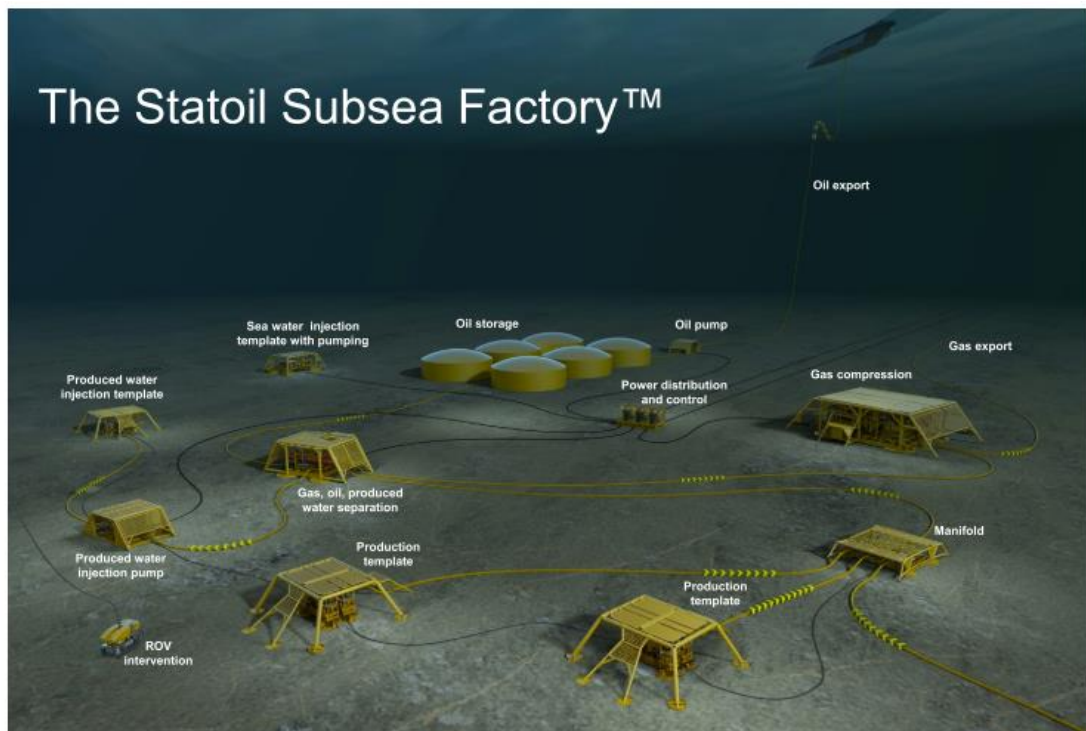


Figure 2- 7: Statoil Subsea Factory [11]

standardisation between all operators is key to the progression of this technology. The authors state that the industry as a whole must agree on technology requirements for subsea processing and where focus in the short, medium and long term should lie to allow resources to be properly applied, highlighting that close collaboration between suppliers and field operators is greatly important if the ‘All Subsea’ vision is to be realised [14]. Following the merger in January 2017, FMC Technologies and Technip, now operating under TechnipFMC, are able to work together to offer the complete ‘All Subsea’ package, including the required bespoke umbilicals.

One Subsea and Petrobras also share a similar vision, recognising the need for development of subsea processing technologies [15], [16].

All of the discussed subsea processing technologies greatly influence the components required within the umbilical structure. The increased processing on the seabed generates a need for additional electrical cables to provide power to subsea equipment to allow for subsea separation, boosting and compression. Subsea separation involves the separation of gas/liquids and/or oil/water on the seabed. Benefits of subsea separation include; debottlenecks of flowlines, risers and topside, minimised hydrate formation, improved pump and compressor reliability and cost savings through reduced topside facility. Subsea boosting is the use of subsea pumps to enhance the pressure in the well stream. This offers multiple advantages including; increased production, low pressure or deepwater field production, long tiebacks and a reduced topside facility. Subsea compression allows for longer step-out distances and improved production rates in low well pressure areas. As with subsea pumping and boosting, subsea compression also profits from a minimised topside facility. These processing systems lead to a requirement for variable speed drives (VSDs), electric motors, switchgear and electric actuators to be located on the seabed, therefore driving the need for additional power cables within the umbilical.

2.2.3 All-Electric Control

All-Electric control has been a focus within the industry as a means of reducing the cost in subsea oil and gas developments. DNV highlight the benefits in terms of both CAPEX and OPEX reduction, along with improved HSE, reliability, flexibility and functionality [17]. This simplification of the control system leads to an umbilical of reduced size and weight, which in turn provides a lower cost umbilical design. In addition, an all-electric system removes the environmental concerns around leakage of control fluids, should the hydraulic line be damaged.

The first all-electric subsea trees began production in September 2008 from the K5F field, situated in the Dutch sector of the North Sea. In 2008 the electric control of the downhole safety valve was not at a suitable technology readiness level, therefore this remained hydraulic operation. Progression in this technology now allows for the use of electric downhole safety valves, therefore further reducing the size and weight of the umbilical as the hydraulic supply and return is no longer needed. Furthermore, the removal of these

hydraulic lines provides a great benefit for long length tieback umbilicals as hydraulic power reduces over longer distances and as a result hydraulic tubes have to be sized to account for this, leading to larger bores and thicker walls for higher operating pressures. Umbilicals will however, continue to include hydraulic lines for service fluids.

At present, alternating current (AC) transmission is used for operation in control umbilicals. The potential savings provided by longer tiebacks will likely impose a move to direct current (DC) transmission due to high reactive losses experienced with long distance AC transmission. As distances increase, it is also likely that required power levels will increase, further influencing the umbilical design.

Deighton and Dobson provide a detailed review of the effects these changes have in relation to the umbilical structure [10]. Diameter, weight and cost savings are discussed, comparing current umbilical structures against future ‘all-electric’ designs. A greater saving is highlighted if subsea chemical storage is used, as this would eliminate the need for hydraulics within the long-distance transmission umbilical, leaving only the infield umbilicals with hydraulic function.

2.2.4 Heated Pipelines

The formation of hydrates within a pipeline is a known issue within the industry. As the hot well stream cools, hydrates may form inside of the pipeline, which in turn reduces or even stops the flow. Depending on the fluid, salt content and pipeline pressure, wax can begin to deposit at temperatures of around 35°C and hydrates can begin to form at temperatures of around 25°C [18]. It is therefore critical that the temperature of the well stream is kept high enough to prevent hydrate blockages and maintain a steady flow.

A commonly used method for hydrate prevention is chemical injection. Typically, this involves the injection of methanol or ethylene glycol into the well stream as this reduces the temperature of hydrate formation. This method comes with many disadvantages including; reduced pipeline capacity, costs of topside process equipment, topside weight and area limitations, environmental limits on overboard discharge, safety considerations and local availability of the inhibitor [19].

Pipeline can be heated using electrical cables in order to maintain a specific temperature, minimising the requirement for chemical injection. A commonly used method for doing so is Direct Electric Heating (DEH). DEH uses a single phase AC power cable piggybacked to the pipeline, with a direct connection to the pipe itself at both ends. The pipe then forms part of the circuit as the current is flowing through the pipe walls to generate heat. Due to the inherent increased risk of AC corrosion, additional anodes are installed at either end of the pipeline.

Another method of electrical heating is the use of 3-Phase electrical trace heated cables wrapped around the length of the pipeline. These cables are wye connected at the far end of the pipe in order to generate heat. An example of this technology is TechnipFMC's Electrically Trace Heating Pipe-in-Pipe (ETH-PiP), where electrical trace heating cables are installed in the annular space between an inner and outer pipe. The cables are in direct contact with the inner pipe underneath a high performance thermal insulation, which provides the technology with a very high heating efficiency [20].

Each of these heating systems require electrical power from the platform or shore to allow for operation and as a result the umbilical will need to include power cables to transfer this. Again, this highlights the growth of cables required within the umbilical structure. Heated pipelines also supports the 'All Subsea' vision, as moving away from chemical injection allows for longer tiebacks due to hydraulic losses over great distances.

2.2.4 Energy Transition

There is a global drive to tackle climate change and reduce greenhouse gas emissions to move to a net zero emissions economy. A number of countries, including the UK, have signed agreements to commit to these targets as a response to climate science showing that carbon emissions have to stop in order to halt climate change [21]. In June 2019, the UK government amended the Climate Change Act [22] to commit the UK to achieving net zero by 2050, instead of its previous target of an 80% reduction from 1990 levels. The agreement outlined that net zero means that any emissions would be balanced by schemes to offset an equivalent amount of greenhouse gases from the atmosphere, such as planting trees or using technology like carbon capture and storage [23]. The oil and gas industry has been identified as having a vital role in the UK energy transition and thus the Oil and Gas Authority (OGA) are working with the government to put net zero considerations at the heart of its business. Having close links between oil and gas and renewables can reduce carbon emissions from oil and gas production to accelerate energy transition through concepts such as; platform electrification, gas-to-wire, carbon capture and storage (CCS) and hydrogen production, storage and transfer [24].

Platform electrification has the largest influence on power umbilicals and has been highlighted as a key enabler to reduce offshore emissions and work towards achieving the longer term goal of net zero [25], [26]. Electricity to oil and gas platforms is generally supplied by gas turbines which emit large amounts of CO₂ and nitrous oxides, thus platform electrification involves the removal of these gas turbines by sourcing the electrical power from shore or from offshore wind farms. In addition to the environmental advantages, platform electrification also provides reduced OPEX, reduced CAPEX and is an enabler to further energy transition technologies, such as CCS.

To enable this electrical power transfer, the construction of the umbilical would typically consist of three MV or HV power cables and one or more fibre optic cables, as shown in Figure 2- 8.



Figure 2- 8: Typical FOW Power Cable - ©TFMC Umbilicals Ltd.

In both floating offshore wind and from-shore platform electrification, the integrity of the power cables is vital to allow operation to take place. A cable failure can lead to a significant cost in both loss of revenue and cost of repair. Warnock et al has performed a review of published cable reliability data and estimates the loss from a typical offshore wind cable failure to be in the region of £5.4 million per month, lasting around 5 to 6 months [27]. It is known that static windfarm cables have a relatively high failure rate which is only expected to increase when moving into the floating offshore wind market, due to the dynamic nature of the power cables [28]–[31]. In addition, an increase in the capacity of future wind turbines to 8-15MW has led to a higher voltage requirement of 66kV for the inter-array cables, as opposed to the previous maximum voltage of 33kV. The higher operating voltage brings benefits from reduced current levels for a given power, thus enabling use of the same cross sectional area of cable for a greater power transfer, which in turn leads to a reduction in cost through reduced quantity and lay operations [32], [33]. Although beneficial to the overall windfarm, the increased voltage does lead to higher stresses within the cable, therefore increasing the chances of cable failure due to PD occurrence. This, along with the track record of failures within static windfarms, has highlighted the importance of IM monitoring capabilities around FOW power cables.

2.3 Failure Modes of a Subsea Power Cable

Failures within umbilicals are uncommon, however they are extremely costly when they do occur. This is caused by; production downtime, support vessel hire, fault localisation equipment and the ability to gain access to the damaged area. In addition, there is also the potential environmental impact to be considered, should a failure occur. As a result of this, it is highly beneficial, where possible, to monitor the condition of the umbilical components throughout their lifetime. As discussed previously, the industry move towards subsea processing, longer tiebacks and heated pipelines has led to an escalating requirement for more power on the seabed and as a result an increased number of MV cables within subsea umbilicals. In addition, the future floating offshore wind market has discussed the need for 66kV HV dynamic power cables for use as array cables between turbines. From this, it is clear that the integrity of these MV/HV power cables is key to the successful operation of future fields in both sectors. Consequently, this research focuses on the integrity of power cables within subsea umbilicals.

Figure 2- 9 shows the structure of a typical power cable which may be used within an umbilical. The cables are designed in line with IEC 60502-2 cable specification [34]. These power cables are of a coaxial structure with a central current carrying conductor of either copper or aluminium. An inner and outer semi-conducting layer are coextruded with the insulation to eliminate any contaminants or moisture between these key layers. XLPE is used for the insulating material as PE has excellent dielectric strength and high insulation resistance and when cross-linked it is able to operate at greater temperatures. The cables

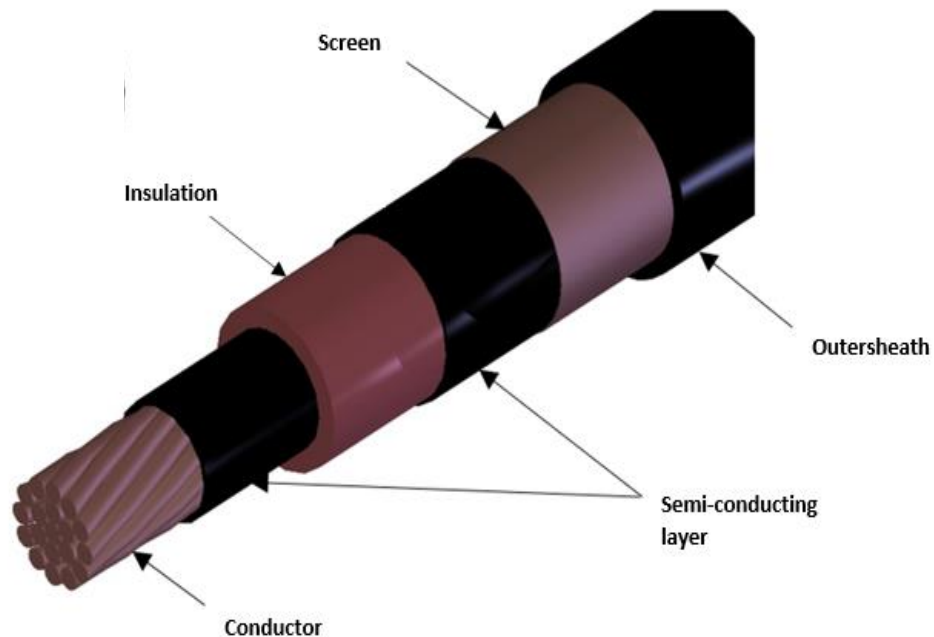


Figure 2- 9: Cable Construction

are designed to be operational up to a maximum conductor temperature of 90°C. The semi-conducting sheaths provide a smooth interface between layers, allowing potential high electrical stress points to be minimised. A copper tape is helically applied on top of the outer semi-conducting layer to provide a screen for the cable. This screen equalises electrical stresses and provides a drain for any leakage or fault currents. The PE outersheath provides protection for the cable within the umbilical bundle. Each cable is designed specifically for its operational function, therefore material choice, thickness and size will be altered to suit the needs of the field. The conductor cross sectional area will be dependent on the required current carrying capacity and the insulation thickness will be chosen based on the voltage rating. There are other varying factors to consider which have influence on the cable design, such as; temperature, short circuit rating, allowable volt drop across the length, relevant international standard and the operational environment.

The following section discusses potential failure modes within these cables to evaluate possible areas where applied condition monitoring can be most beneficial.

2.3.1 Partial Discharge

The international standard for partial discharge (PD) measurements defines PD as a localised electrical discharge that only partially bridges the insulation between conductors, which can or cannot occur adjacent to a conductor [35]. Points of high electrical stress within the insulation, or on the surface of the insulation cause the occurrence of PD. Discharges take place when the stress exceeds the limit of the insulating material. These limits are dependent on; material, temperature, pressure, duration of stress and purity [36]. The types of PD which occur in power cables can be categorised by the origin at which the discharge occurs. Those being; internal discharges, surface discharges and electric trees. Examples of which can be seen in Figure 2- 10 [1].

Internal discharges occur within the insulation layer and stem from gas filled voids/cavities of varying shapes and sizes, as shown in Figure 2- 10a. When a voltage is applied to the cable, the gas within the void will breakdown when the electrical field is greater than that of the gas, which in turn leads to PD. The electric field within the cavity will be higher than the surrounding insulation due to the lower dielectric constant of the gas inside of the cavity, in comparison to the dielectric constant of the insulation material [37].

If a void or cavity is present within the insulation, discharges cause a charge transfer in the circuit by an impulse shape current which can be detected and measured [38]. These discharges occur when the system voltage reaches what is known as the partial discharge inception voltage (PDIV) and will keep occurring until the voltage is lowered past the extinction voltage or until the insulation can no longer withstand the voltage potential causing the dielectric to break down to failure. The inception voltage U_i is the lowest

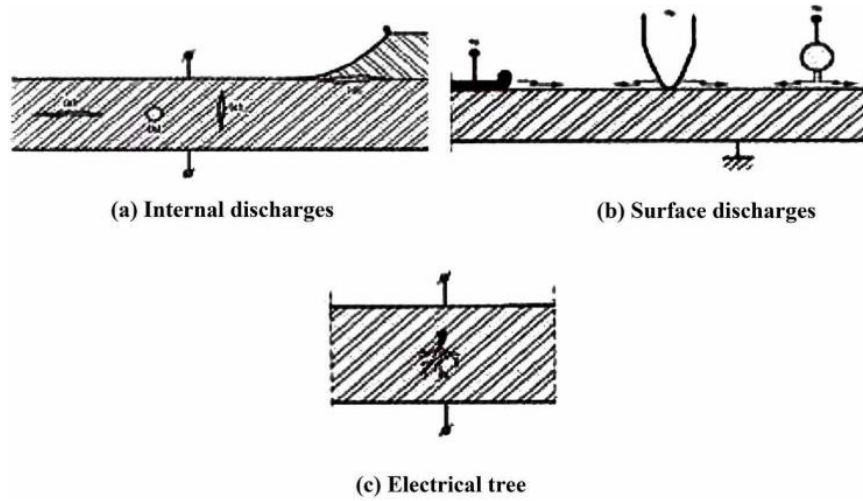


Figure 2- 10: Types of PD in Power Cables [1]

voltage at which partial discharges are first observed when the voltage applied to the object is gradually increased from a lower value at which no such discharges occur. The partial discharge extinction voltage (PDEV) U_e is the lowest voltage at which partial discharges cease to occur in the test object, when the voltage applied to the object is gradually decreased from a higher value at which PD pulses are observed [39]. The inception and extinction voltages do not occur at the same point and are therefore measured individually.

Figure 2- 11 shows a simplified equivalent circuit model used to explain PD in a void or cavity. Partial discharge occurs when voltage V reaches its inception voltage. The spark-gap S represents the discharging defect or void, capacitor C_1 represents the void or cavity, capacitor C_2 represents the insulating material around the void and capacitor C_3 the remaining insulating material. The voltage across capacitor C_1 is given by equation (2.3).

$$V_1 = V \frac{C_1}{C_1 + C_2} \quad (2.3)$$

The discharge of capacitor C_1 leads to capacitor C_2 being stressed with voltage V , causing a change in charges, Q . Prior to breakdown of S , the charge Q_2 of capacitor C_2 is expressed by (2.4).

$$Q_2 = V_2 C_2 = \frac{C_1 C_2}{C_1 + C_2} \quad (2.4)$$

Following breakdown of spark gap S , the charge Q_2^* is expressed by (2.5).

$$Q_2^* = VC_2 \quad (2.5)$$

The difference in charge will be delivered by capacitor C_3 or by the voltage source. Due to the different time constants, the charge will be delivered by capacitor C_3 in a very short pulse, causing a reduction in voltage across the C_2 and C_3 , leading to an increase in voltage to the original value V . The spark gap S then recovers and capacitor C_1 recharges, repeating the process until insulation breakdown occurs. The difference in charge Q can be calculated using equation (2.6).

$$\Delta Q = V \frac{C_1^2}{C_1 + C_2} \quad (2.6)$$

Figure 2- 12 shows the time evolution of the equivalent circuit model. This shows how the voltage and current across the void changes when a sinusoidal alternating voltage is applied. The applied voltage is represented by $V(t)$ and the actual voltage between the discharge gap is represented by $U(t)$. When the voltage $U(t)$ reaches the inception voltage U_{i+} a discharge takes place causing the voltage to collapse and the discharge extinguish. The voltage across the void again begins to increase to U_{i+} until a new discharge takes place and again collapses. It is therefore possible for multiple discharges to take place during the rising part of the sinusoidal alternating voltage. Likewise, during the negative cycle, the void discharges upon reaching U_{i-} .

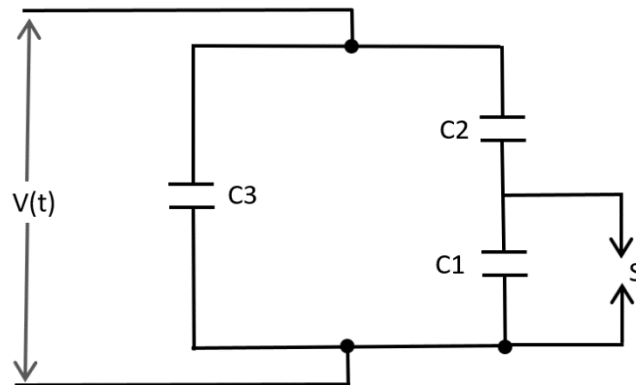


Figure 2- 11: PD Simplified Equivalent Circuit Model

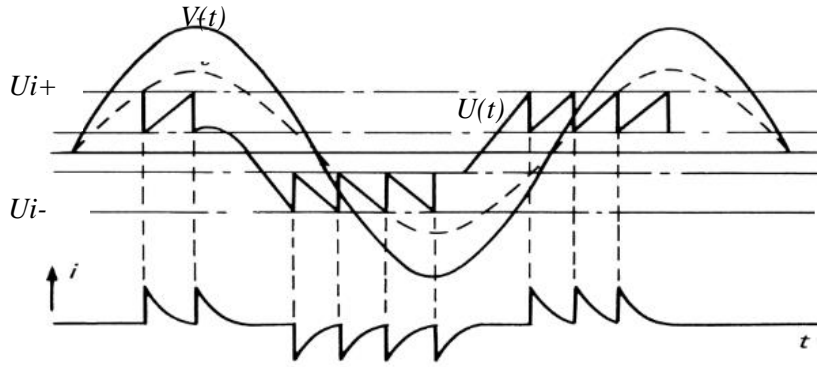


Figure 2- 12: Time Evolution of Equivalent Circuit Model [1]

The PD inception voltage is highly dependent on the shape and size of the void, along with the type of gas and its pressure. Paschen’s Law can be used to calculate this stress at which the discharges take place (2.7) [40]. The critical parameters are the distance between electrodes, d , and the internal pressure, p . Parameters B and χ are constants associated with the gas in the void.

$$V_{PD} = \frac{Bpd}{\chi + \ln(pd)} \quad (2.7)$$

The magnitude of the PDIV is greater for a flat void aligned in the direction of the applied electrical stress, i.e. radially, in comparison to a spherical or flat longitudinal void of similar size. Table 2- 1 shows an example of the effect of similar size voids of varying shapes located within an XLPE insulated power cable . Values are taken from the IEEE standard, Guide to Partial Discharge Testing of Shielded Power Cable Systems [41]. From this it can be seen that the PDIV for the radial void is $\approx 23\%$ greater than that of a spherical void and $\approx 130\%$ greater than that of a flat longitudinal void.

<i>Void Shape</i>	<i>PDIV in kV for 0.5mm (20mil) Void</i>
<i>Spherical</i>	13.8
<i>Flat Longitudinal</i>	7.4
<i>Flat Radial</i>	17.0

Table 2- 1: PDIV for varying Void Shapes 15kV, 250mm² Cable

The magnitude and recurrence of PD increases with the area of the void. The PDIV / PDEV may change during operation due to changes in thermal expansion/contraction or as the conductivity of the void increases. PD within voids leads to erosion of the surfaces, pitting and the formation of electrical trees, which in turn leads to cable failure.

Surface Discharges often occur between the insulating interfaces and cable accessories. These discharges take place when there is a high stress in parallel with the insulation and are frequently caused by the removal of the semi-con layer at the accessory location. Surface discharges can also be in the form of tracking due to insufficient termination of cable ends, poor contacts or the presence of a conductive substance. The PDIV of this type of discharges is typically lower in comparison to that of void discharges.

Electrical treeing is a rapid degradation phenomenon that initiates at an imperfection in the cables insulation causing a point of high electrical stress. Potential causes are protrusion of the conductor or screen, however most often they stem from a void. Voids within the cables insulation often lead to electrical trees prior to complete failure. Once initiated, electrical trees grown rapidly during PD occurrence over a period of seconds or minutes until they progress through the insulation and create a line-to-ground fault [42]. The electrical deterioration of the insulation grows radially in a tree-like path, an example of which is shown in Figure 2- 13. In addition, overvoltage, switching surge or field testing can cause electrical trees to grow from existing water trees within the insulation.

During cable manufacture, procedures are in place in order to minimise the likelihood of irregularities or voids within the insulation. In addition, industry standards such as IEC 60502-2 [34] specify a requirement for partial discharge testing to be performed as part of



Figure 2- 13: Electrical Treeing [1]

cable manufacture to confirm the quality of the insulation and ensure suitability for its required lifetime. The test details are specified in IEC 60270 [35] whereby a coupling capacitor is used to measure the magnitude of PD in picocoulombs (pC). The acceptable maximum value is dependent on the insulating material and the relevant specification. For use within umbilicals, this is typically a maximum value of 10pC, based on a lifetime of 30 years continuous operation. Cable manufacturers are able to achieve this 10pC requirement without great difficulty therefore, assuming planned operating conditions are maintained, there is a low probability of failure due to PD. The chance of failure, however, dramatically increases should a cable joint/splice be required. A joint may be required to obtain the necessary length or if the cable has been damaged to avoid remake of the complete length. By performing the splice operation to join the cable sections, there is an increase in the likelihood of voids or irregularities within the cables insulation. This is largely due to the human element as a trained splicer performs the operation by hand, as opposed to a machine, therefore repeatability is worsened. Not only does this operation have to be performed by a trained operative, it must be done in a controlled environment to minimise the possibilities of contamination. Within umbilicals, splices are often required in order to achieve the required length. The maximum cable length obtainable without splices is dependent on its weight and diameter of the cable as the limiting factor is the cable reels used during manufacture. With the industry focusing on longer tiebacks, remote waters and higher levels of power, it is extremely likely that the need for splices will rise, causing a greater chance of failure by reason of partial discharge breakdown.

In addition to the inherent risk of splicing, voids may also occur once the cable is in service as a result of ageing and deterioration, causing chemical bonds to break down due to over stress during operation.

2.3.2 Water Trees

The initiation of water trees within MV/HV power cables is a well-known ageing mechanism which is brought on by presence of moisture. Water tree growth is a highly complex phenomenon affected by numerous physical, chemical and electrical elements. A comprehensive review of the attributing factors for the initiation and growth of these water trees concludes the main influences are; application time of voltage, electric field, power frequency, temperature, concentration of the water solution, electrode type and the material [43].

Water trees consist of strings of micro-voids, of the order of 1-5 μ m diameter, which are filled with water [44]. Typically, water treeing occurs at a much lower electrical stress value when compared to electrical trees, however the progression rate to failure is slower. Unlike electrical trees, water trees do not consist of permanent hollow channels. Instead water tree channels consist of fine filamentary paths between small cavities through which moisture penetrates under the action of a voltage gradient [45].

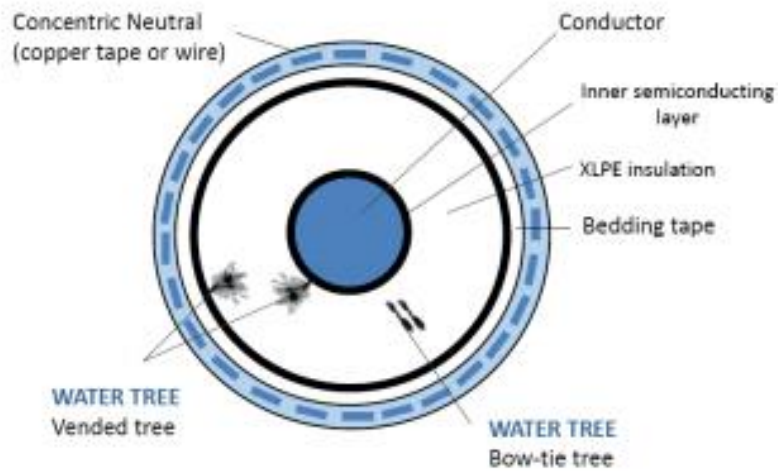


Figure 2- 14: Water Treeing

There are two different types of water trees, those being bow-tie trees and vented trees, examples of which are shown in Figure 2- 14, [46]. Bow-tie trees initiate within the body of the insulation and grow in opposite directions. Their initial growth is quicker than vented trees, however the length is typically restricted by the area of the impurity, therefore bow-tie trees are rarely the cause of failure. Vented trees initiate from the insulating boundary and grow outward to towards the other side of the insulation. They are generally in contact with water, causing the tree to continue to grow until fully bridging the insulating layer. As the vented tree grows, the effective insulation thickness reduces, which in turn may lead to the development of electrical trees due to the increased electrical stress. These electrical trees will then lead to the presence of PD and sequential failure.

2.3.3 Fatigue

As discussed previously, umbilicals are designed to be able to withstand the crushing and tensile loads experienced during handling, installation and service life, whilst ensuring all components remain fully functional. This also includes a large safety factor, therefore a fatigue failure would likely be as a result of unforeseen circumstances such as extreme unexpected weather conditions or issues during installation.

Installing an umbilical can be extremely complex, particularly in challenging environments such as the North Sea. In some cases, there is a very short weather window in which the installation can take place. Any issues during installation may increase the installation time taking it outside of the planned window, therefore exposing the umbilical to unplanned loadings. Installation issues may also result in the umbilical being held over a vessel or chute for a longer period than that included in the initial dynamic analysis performed as

part of the umbilical design process. The dynamic analysis is based on the environment in which the umbilical will be installed and for that reason includes criteria for the specific sea state (wave height and period), wind speed and wave currents. Unexpected severe weather conditions may lead to the umbilical being subjected to excessive loadings above that accounted for in the design. This may also be an issue once the umbilical is in service, as again the additional loadings may exceed the original design parameters. The discussed unforeseen events will likely lead to premature ageing of the umbilical components, which may result in early fatigue failure.

2.3.4 External Damage

All umbilicals have an outer layer which encompasses all of the components and aims to provide protection from external hazards. This is in the form of an extruded thermoplastic material or polypropylene rovings, depending on the application. In certain cases, armour wires may be included underneath the outer sheath to provide additional protection, though they may already be included for mechanical reasonings.

There are multiple external hazards which have the potential to cause damage to the umbilical and its components. Issues experienced during installation may result in damage to the power cables and other components. As the umbilical is not yet in operation, it is likely that the condition of the cables can be checked using existing offline technology, such as a time domain reflectometry (TDR) test. Once the umbilical is installed and in operation, testing following damage is considerably more challenging. Possible causes for external damage once the umbilical is in service are; dredging, penetration from fishing gear in shallower waters, bottom-trawling activities, dropped objects (lost shipment containers or cargo) and icebergs/sea ice ridges. Damages caused by external hazards both during installation and once in service can be considered as unforeseen circumstances.

2.3.5 Connector Failures

Electrical connectors are required at either end of the umbilical, both topside and subsea. There are two types of connector wet-mate and dry-mate. Wet-mate connectors are typically preferred as they allow subsea systems to be assembled on the seafloor using remotely operated vehicles (ROV's) or autonomous underwater vehicles (AUV's), consequently allowing modular installation benefiting from reduced weights. Dry-mate connectors require all connections to be made above sea level, resulting in a more complex installation process.

Failures within electrical connectors lead to a loss in power transfer through the umbilical cable. Brown examines the main causes of connector failures, categorising them as follows [47];

-
- *Corrosion* – Connector corrosion is mainly due to incorrect material selection but can be brought on by operational issues such as; excessive operating temperatures, incorrect connection or poorly designed cathodic protection systems.
 - *De-lamination* – A primer may be used in a connector to bond an elastomer to a metal. Cathodic de-lamination occurs when an electrochemical cell is formed between the connector body and the cathodic protection system. The chemistry of the cell eats away at the primer and adhesive, causing bond failure.
 - *Elastomer Degradation* – Long term exposure to excessive operational temperatures or chemical contamination can cause rapid deterioration of the elastomer.
 - *Damage* – Connector damage can be caused by; incorrect use or fitment, physical damage, excessive use beyond recommended mating cycles, excessive force during installation, excessive temperatures, exposure to pressures beyond its rating and improper selection for the required application.
 - *Premature Unlatching* – Leads to physical isolation of the circuits and is caused by incorrect installation of the connector or by excessive snagging force during operational work.
 - *Seal Failure* – Seal failure can cause water ingress leading to connector degradation. This can be due to physical damage, chemical damage, corrosion or operation in extreme temperatures.
 - *Inadequate Long-Term Protection* – Unmated connectors may not have been designed for long-term operation as a single unit, therefore may be subject to an increased risk of failure. A suitable long term protection cap or dummy connector is required to prevent this.

The specific cause of connector failure would not be known unless it is recovered post failure for examination. With the system remaining connected, it is difficult to identify if the failure is due to the connector itself as measurements include values for both the connectors and the cable terminated between. For example, water ingress within the connector will lead to a low insulation resistance (IR) reading, however the IR measurement takes into account the cable and the connectors at either end, therefore it is unclear if this low reading is as a result of an issue within the cable or within one of the connectors.

2.3.6 Failure Mode Review

The ability to detect and locate partial discharges, whilst the umbilical system remains online, would be highly beneficial as PD is one of the more common modes of failure within power cables, particularly when cable joints/splices are required. As discussed, water trees also lead to PD over time, hence this failure mode would also be captured with a means of PD integrity monitoring. Having the ability to detect and locate PD online would allow the operator to review the existing operating parameters and potentially lower them to extend the life of the cable, or should this not be an option, knowing the position of the fault allows for planned intervention of that particular area. Ideally, location of the PD would be established prior to complete cable failure as this would allow production downtime to be planned and kept to a minimum, significantly reducing unplanned failure costs.

The occurrence of fatigue failure is less likely as the umbilical would be designed for a service life of 30 years based on the environment in which it would be deployed, whether it be dynamic or static service. This would also include a factor of safety, therefore should a fatigue failure occur, this would likely be due to unforeseen circumstances outside of the original design parameters or as a result of poor modelling techniques. As the main cause of fatigue failure is unexpected, its reduction to overall fatigue life cannot be prevented, therefore monitoring will allow an insight into the remaining lifetime, however cannot change the service loading conditions to extend the time to failure. As with fatigue failure, damage from external influences is an unforeseen circumstance which could result in cable failure but could not be prevented with monitoring technology.

Although failure within subsea connectors is a more common failure mode, it is extremely difficult to monitor as it would be unclear if the failure related to the connector, the cable or to the monitoring equipment itself. The ability to provide connector condition monitoring is highly challenging as measurement access is typically topside only, therefore results will also include values for the cable length. There is the potential to include suitable electronics within the connector to monitor certain failure modes, such as water ingress, allowing the individual device to be monitored, however, it is likely the connector would be more reliable than the additional electronics required.

Figure 2- 15 presents a high level Failure Mode Effect Analysis (FMEA) review of the discussed failure modes. The FMEA was performed following the threat assessment methodology specified in Det Norske Veritas (DNV) industry recommended practice DNV-RP-A203 [48]. This document recommends methods and criteria to allow the failure modes to be scored and assessed. The scoring for severity considers safety, environment cost, and time and the scoring for probability is based on industry failure data, engineering judgement by industry experts and any relevant documentation or recognised analysis methods. Any existing techniques can then be assessed to score the detectability, with summarised results showing the risk level of each failure mode as low, medium or high. The results of the performed FMEA highlight both partial discharge and water treeing as

priority high risk considerations for potential cable monitoring technologies in order to minimise the likelihood of power cable failure. As water treeing also leads to PD, having the ability to monitor and locate PD events would cover both potential failure modes. This technology would be highly beneficial as it allows for potential life extension or enables great cost savings through scheduled intervention at a known fault location.

The discussed increase in operating voltage and potential increase in the number of splices for future projects further emphasises the value of developing this technology. It should also be noted that there is currently a knowledge gap for dynamic floating offshore wind projects around the coupled mechanics of the floating host and wind turbine under various environmental loads, and thus higher stresses may be present on the cable which could lead to additional failures, and so, methods to monitor the condition of the cables insulation in these instances is again pertinent.

2.4 Summary

This chapter provides an overview of umbilicals, their evolving design to meet industry needs and the potential benefits brought by condition monitoring of the power cables. A review of the challenges within the industry highlights the main drivers for subsea processing, longer tiebacks and heated pipelines, which in turn leads to a requirement for more power on the seabed. This need for power cables is further enhanced with the desires of the future FOW sector. The impact this requirement has on umbilical design is discussed in detail, concluding in an increased need for MV and HV power cables. The increased requirement for power cables highlights their criticality in the functionality of the overall processing system. By investigating the potential failure modes of the cables, the ability for online monitoring and localisation of partial discharge was shown to be most beneficial as it could be used as a means of preventative cable failure, showing potential to provide large cost savings from unplanned production downtime. The benefits were further emphasised based on the inherent risks of higher operating voltages and more splices due to future industry developments.

Failure Mode	Failure Effect	Severity	Causes	Current Control Prevention	Probability	Current Detection	Detectability	Recommendation	Improved Detection	Priority
<i>Partial Discharge</i>	Degradation of insulation to the point of cable failure	10	Voids or cavities in cable insulation (splices, joints, damage)	PD test performed at cable manufacture only	5	none	0	Online PD Detection	7	High
<i>Water Trees</i>	Degradation of insulation leading to PD to the point of cable failure	10	Moisture presence in cable insulating layer	Material choice for cable manufacture	5	none	0	Online PD Detection	7	High
<i>Fatigue</i>	Failure of armour wire or copper conductor	10	Unplanned installation issues or unexpected severe weather	Dynamic analysis performed & designed to suit environment	1	none	0	Strain Monitoring	7	Medium
<i>External Damage</i>	Component Failure (likely outersheath or armour damage unless in extreme cases)	5	Dredging, fishing operations, dropped objects, icebergs	Armour & outersheath layers	2	none	0	Strain Monitoring	5	Low
<i>Connector Failure</i>	Low IR measurement or complete power transfer/comms failure	7	Corrosion, delamination, degradation, damage, seal failure	minimum of dual water barrier connector design	7	IR Test & TDR (offline)	3	Electronics within connector	5	Medium

Figure 2- 15: Failure Mode Effects and Effects Analysis of MV/HV Cable Failures

Chapter 3

Current PD Monitoring Technologies and Localisation Techniques

This chapter details the physical factors accompanying partial discharge and discusses methods by which these factors can be measured to establish the magnitude, quantity and location of PD, in turn evaluating the condition of the cables insulation. An overview of existing measurement techniques in varying applications and environments is presented, aiding the selection of a suitable method for the proposed condition monitoring system.

Signal propagation paths within the subsea umbilical environment are evaluated, highlighting potential sensing opportunities for the condition monitoring of PD. Previous research presents the advantages and disadvantages of potential detection and localisation techniques aiming to overcome the challenges associated with PD sensing of power cables within subsea umbilicals. An extensive literature review of various monitoring technologies provides an insight into current state of the art methodologies within this area of research.

The chapter concludes with a summary of the discussed technologies, specifying the focus for this research and outlining the authors aims to objectives.

3.1 Partial Discharge Detection

PD pulses are short in duration (approximately 5 nanoseconds), have a fast rise time (1-2 nanoseconds), have a maximum amplitude of around 1V and can have significant frequency components at its source of up to 1GHz [41]. Most types of PD are established by positive and negative current pulses, normally occurring in the ranges of 0° to 90° and 180° to 270° of the AC waveform [49]. The typical parameters describing the shape of an idealised PD pulse are shown in Figure 3- 1, originally by Wu et al [50].

- Pulse rise time, t_r , is the time required to rise from 10% to 90% of the maximum amplitude.
- Pulse decay time, t_d , is the time required to decay from 90% to 10% of the maximum amplitude.
- Pulse width, t_w , is the time interval between 50% on both sides of the maximum amplitude peak

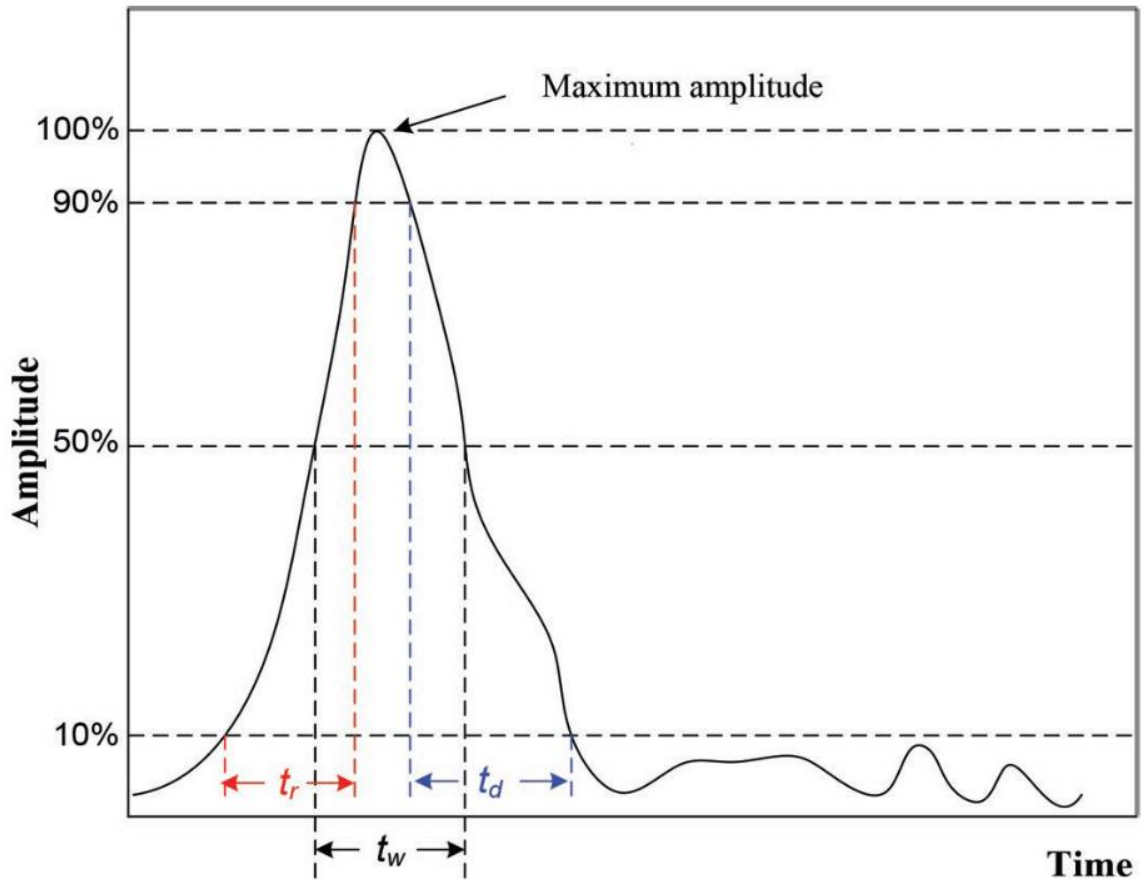


Figure 3- 1: Features of an idealised PD Pulse [49]

When PD takes place, several physical factors also occur including; electromagnetic emission in the form of radio waves, light energy and thermal energy, acoustic emissions both audible and ultrasonic frequencies and chemical reactions due to ozone formation and the release of nitrous oxide gases [51]. These physical factors can be measured as a means of establishing the severity of the PD or as a way of estimating its location.

3.1.1 Electrical Detection

Partial discharges introduce short current pulses onto the conductor which propagate away from the fault location in either direction toward the cable ends. The total current is governed by the transport of a certain number of picocoulombs (pC) of charge. The current flow creates a voltage pulse across the impedance of the insulation [52].

The coupling capacitor is a commonly used method for electrical detection of PD within cables, however the measurement is performed offline as the system is connected to the high voltage terminal and would therefore need to withstand the operating voltages to be able to be used online. When a partial discharge event occurs, the coupling capacitor

provides the cable under test with a displacement current, which is measurable at the coupling device [53]. This capacitive method can be used for both detection and localisation of PD through use of a digital storage oscilloscope alongside the coupling capacitor, to measure TDoA of the initial pulse and following reflected pulses.

PD also creates electromagnetic (EM) signals, therefore allowing online sensing through the use of high frequency current transformers (HFCT's) clamped around the earthing conductor which measure induced high frequency currents caused by PD activity within the power cable. This method is commonly used for PD detection in substations as it is non-intrusive. The HFCT sensor is made with a ferrite core and screened windings. A change in the central current of the HFCT will induce voltage on the output wire, therefore detecting PD. The high frequency components of the PD signal are significantly filtered once it reaches the HFCT sensor and consequently only the frequency spectrum below 10MHz is available when using HFCT detection [54], [55].

In addition, PD excites EM radio waves in the ultra-high frequency (UHF) range of 300MHz to 3000MHz [56], [57]. The RF waves propagate away from the PD source and can be detected using UHF sensors. UHF sensors were first introduced in the late 1980's to detect PD within gas-insulated systems (GIS) and further developments in the 1990's allowed this technology to also be applied to power transformers and cables [58]. Additional research has progressed this technology to allow for localisation of the PD source in certain applications. UHF sensors are commonly used for PD detection and localisation in GIS. The sensors can be mounted both internally and externally to the GIS tank, consequently providing high sensitivity over a wide frequency range and effective noise reduction [59].

Unlike GIS, applying UHF sensing to transformers and power cable applications is much more complex. One of the main issues is the mounting of the sensor itself. Regarding power cables, the UHF sensor cannot be mounted external to the cable as the conductive sheath layer can shield the EM waves, hence minimising the ability to detect PD. The UHF sensors are therefore typically coupled with the cable accessories at the power cable termination, however signals will likely be weak leading to poor sensitivity and accuracy. For power transformers, UHF sensors can be inserted through the oil drain valve, a dielectric window or coupled externally to the transformer tank. Chai et al. discusses the problems with these sensor placement, highlighting the lack of suitable drain valves (typically no more than three), complicated sensor installation process and the low sensitivity when using external sensing [58]. Much work is ongoing to overcome these challenges for UHF sensing in transformers, with aims of improving sensitivity and accuracy for detection and localisation of PD sources [60]–[62].

In addition, research performed by Sarathi et al. discusses the potential use of UHF sensors, positioned close to the PD location, in order to classify the type of electrical tree structure forming within a cables insulation by adopting the Ternary plot method [63].

3.1.2 Visual or Optical Detection

Partial discharges can emit visible and ultraviolet (UV) light. This type of PD is often referred to as corona and it occurs in air at areas of high electrical stress. The optical spectrum of the emitted light is dependent upon the surrounding materials and the magnitude of the discharge. 90% of the total energy of the emitted optical spectrum from PD is in the UV region and is therefore invisible to the human eye [64]. It may be possible to see an emission of around 400nm if conditions allow complete darkness. Depending on the optical spectrum, the following optical sensors can be used for luminary PD detection; night vision, photodiode, photomultiplier or UV-corona cameras. Optical detection of PD is advantageous for certain environments as it is insensitive to electromagnetic and acoustic interferences. Its use is limited when it comes to detection in subsea power cables as the sensors require line-of-sight to the discharge area. A typical application utilising optical detection of corona is the examination of power utilities using UV cameras or sensors.

3.1.3 Acoustic Detection

A partial discharge event can be considered as a small ‘explosion’ which excites a mechanical (acoustic) wave due to molecular collision [65], [66]. The acoustic waves then propagate away from the fault location and can be detected using acoustic sensors which are sensitive to pressure changes occurring in the polymer layers and conductor [67]. Due to the short duration of the PD pulse, the frequency spectrum of the acoustic waves are highly broadband resulting in frequencies spanning from audible to ultrasonic ranges [68] [63], [69]. Harrold discusses how in the early days of electrical engineering design, the human ear served as a valuable PD detector and locator, however microphones and ultrasonic transducers were later used for much improved sensitivity [70]. Research performed by Austen and Hackett determined it possible to hear acoustic emissions from a 40pC air discharge at 1m [68], however Harrold notes that this is most likely in a quiet environment, therefore estimates audible PD values to be around 1,000pC to 10,000pC in a noisy factory environment. Within land based cable systems, the levels of pC are often measured periodically to allow for scheduled maintenance and prevent system failure. The limit values specified for allowable pC through to serious risk pC vary slightly, however values are typically as follows; 0-1000pC normal, 1000-2500pC potential risk – investigate and monitor periodically, >2500pC serious risk [71], [72]. As previously stated, the typical acceptable pC value measured at cable manufacturing stage is 10pC or less, however the purpose of the proposed sensing system is to establish PD location prior to breakdown as opposed to specifying an acceptable level for 30 year operation and consequently the sensitivity of pC detection level can be much lower. The amplitude of the emitted acoustic wave is proportional to the energy released from the discharge and thus a linear relationship between the amplitude of the acoustic signal and the measured discharge in Coulombs is expected [73].

Ultrasonic sensing is a well-established method for detection of AE signals from PD in power transformers. These sensors are typically piezoelectric, measuring in the frequency range of 20 kHz to 500 kHz [74]. Sensors can be mounted to the external wall of the tank and used to detect and locate the source of PD using TDoA techniques. Ultrasonic detection is also commonly used for PD detection in switchgear in the form of an ultrasonic airborne acoustic sensor. The airborne acoustic sensor is able to detect AE signals including corona, surface discharges and tracking, however it needs to be positioned in line-of-sight to the PD source [75].

AE techniques are less commonly used for PD detection in power cables due to limitations with positioning of sensors. Research into AE detection of PD activity with sensors positioned at cable terminations and near splices demonstrates feasibility, however it is dependent upon the surrounding environment and accessibility to these locations [67], [76].

Fibre optic acoustic sensing has been a recent focus for improving AE sensing of PD as it offers the potential for increased sensitivity, whilst maintaining the immunity to EM interference [50]. Czaszejko and Stephens discuss the use of an improved fibre Bragg grating (FBG) photonic AE sensor to detect PD within power cables [77]. An FBG sensor consists of distributed Bragg reflectors embedded in an optical fibre that reflect light of specific wavelengths and transmit others. Initial testing by Czaszejko and Stephens concluded that the FBG sensor would need to be encased in a material with a lower elastic modulus than the optical fibre glass material to allow applied strain to be mechanically amplified in order to improve sensitivity to detect the required levels of PD [77]. This however, would not be feasible within a subsea umbilical as it results in a highly bespoke fibre design and the need to predict the areas where PD occurrence is likely, as FBG sensors are distributed in short segments across the fibre optic length, rather than continuous, thus limiting the sensing region.

Research by Che et al. demonstrates fibre optic distributed acoustic sensing (DAS) using phase sensitive optical time domain reflectometry (OTDR) with an FBG array for PD detection in XLPE cables, though the author highlights the practical challenges in relation to environmental noises and disturbances leading to false alarms [78]. In a DAS system, the back-scattered signal is very low in comparison to the transmitted pulse, which then leads to a poor Signal-to-Noise Ratio (SNR) as it is difficult to differentiate between signals. Furthermore, DAS sensing cannot be used to detect single PD pulses due to the differences in propagation velocity between the optical sensing and acoustic emission. In recent years, fibre optic DAS technologies have been used in different applications such as pipeline leak detection and intrusion alerts, however the sensitivity of fibre optic sensing has often lead to a high false alarm rate. More recent innovations have stated a novel technique whereby machine learning capabilities are applied together with a high data SNR to allow more accurate data, thus minimising false alarms [79]. At the time of this research, this technology has not yet been applied to PD monitoring within subsea or land based cables due to the high sensitivity, low SNR and challenging environmental conditions.

Where possible, AE sensing is often selected as a means for detecting PD as it benefits from being highly sensitive, non-destructive, insensitive to EM noise and can be used to establish the location of the PD source. However, unlike electrical detection methods, the severity of the PD is not as easily understood when reviewing the detected acoustic waveform, as typical methods specify a maximum allowable picocoulomb value which is a unit of electrical charge, rather than a specific acoustic magnitude.

3.1.4 Chemical Detection

The occurrence of PD will likely cause a change/generation of chemical components around the discharge site. The change in chemical components can be measured using a form of chemical detection. This sensing method is primarily applied for PD detection in oil filled components, such as transformers. When a discharge occurs, the components oil decomposes to small molecules such as H₂, CH₄, C₂H₄ and C₂H₆ [80]. In order to detect a presence of these molecules, chemical detection method Dissolved Gas Analysis (DGA) can be used. DGA involves the collection and chemical measurement of dissolved gasses within the components oil. This is the most common and effective chemical detection method used in oil insulated components, however DGA is intrusive, therefore cannot be performed online and also cannot be used to determine the location of the PD.

3.2 Detection and Localisation within Subsea Umbilicals

The focus for this research is the occurrence of partial discharge in power cables within subsea umbilicals. The ability to detect and locate a cable fault prior to complete breakdown brings about many benefits, however the nature of the umbilical and the environment in which its installed makes the method in doing so extremely complex and challenging. It is therefore important to understand both the challenges associated with umbilical monitoring and the propagation paths of the emitted signals from the PD source in order to evaluate the most suitable means for detection and localisation.

As emphasized in previous chapters, a key requirement of the sensing system is the ability to monitor PD whilst the system remains online to allow faults to be detected prior to breakdown. This requirement consequently rules out the use of previously discussed UV and chemical PD detection methods.

Figure 3- 2 illustrates an example of an installed umbilical containing a PD fault within one of its power cables. The energy from the discharge propagates away from the fault location, both through the cable itself and out into the surrounding body of water.

Three potential methods for PD sensing are presented in the figure;

- 1) Electrical/AE topside sensors
- 2) Hydrophones
- 3) Sensing cable within the umbilical

The initial method proposes electrical and/or AE sensors to be positioned above sea level, at the topside of the umbilical, to detect signals propagating through the cable. AE sensors could be coupled to the cables sheath and HFCT's could be clamped around the cables earth to provide a combined electro-acoustic detection system.

The second method illustrates the use of a number of hydrophones positioned in the seawater, in relatively close proximity to the umbilical, to listen for PD occurrence by detecting the acoustic signals propagating away from the fault and through the water.

The third method shows a sensing cable laid within the umbilical, such as a fibre optic DAS cable. This, however, is not a retrofit option as it would have to be included during umbilical manufacture and therefore could not be used on brownfields.

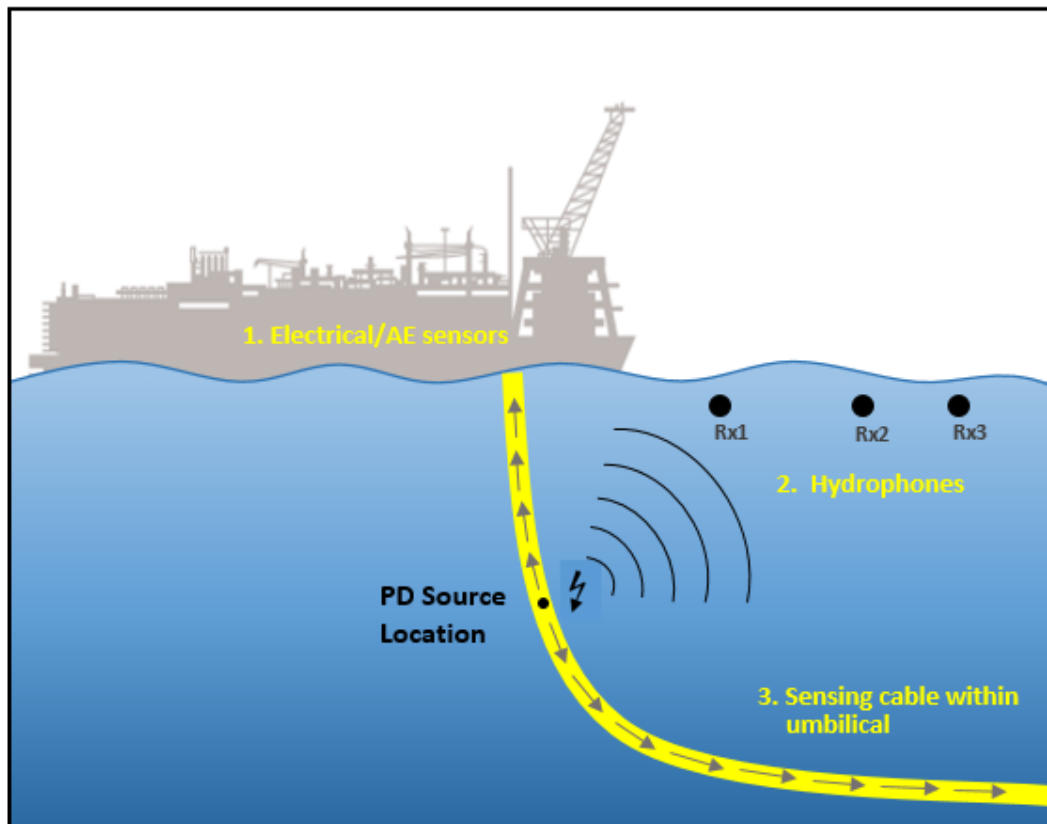


Figure 3- 2: Detection Methods for PD in Umbilicals

3.2.1 Challenges and Limitations

The ability to monitor cables within a subsea umbilical brings about many challenges for the PD detection and localisation system, with the key issues being; the long length requirement, the complexity of the subsea environment, the necessity for online monitoring, the bespoke nature of each umbilical design and the preference for a retrofit system to allow for the monitoring of existing fields. The chosen sensing method must be able to overcome these challenges to allow for suitable detection and localisation of PD faults within the umbilical.

3.2.1.1 Long Distance Detection

The overall length of an umbilical varies depending on the water depth and field layout. A typical power umbilical is around 3km, however subsea processing and long distance tiebacks will lead to much greater lengths of around 40km. This long length requirement generates difficulties with PD monitoring due to a reduction in signal strength along the length, known as signal attenuation. Monitoring from the topside of the umbilical may lead to discharges being missed as a result of the signal attenuating, depending on its amplitude and distance from the monitoring equipment. In addition, the ability to establish the location of the discharge is a key requirement and thus the accuracy of the position estimation must also be taken into account.

When considering a suitable sensing method, the long length requirement of the umbilical is one of the greatest challenges due to the resulting effect this has on the propagating signal. As a PD pulse travels along the length of the cable, the various frequencies within the pulse experience different effects from attenuation and dispersion. The level of attenuation is due to losses in the solid dielectric and propagation through the resistance of the conductor and surrounding polymer layers, where the severity increases along with the frequency [81]–[83]. PD occurrence in solid insulation can generate frequencies up to several hundred MHz which leads to difficulties in pulse detection over long distances, due to signal attenuation. Different frequencies propagating along the cable at different speeds, resulting in frequency dependent phase shifts, is known as dispersion. Both attenuation and dispersion change the resulting PD pulse and the extent of the change is dependent on the distance from the fault location and the cable structure. Cavallini et al. summarise that PD pulses lose frequency content due to attenuation, whilst spreading in the time domain due to dispersion [84]. This leads to a reduced accuracy when locating a pulse in time for PD source localisation due to a reduced SNR and increased pulse width [85].

The most commonly used method for online PD detection is the use of HFCT's as they are non-intrusive and, in some cases, can also be used to establish the location of the discharge site by utilizing TDR techniques, through the detection of an injected trigger pulse. It is not often possible to use this TDR method for localisation as the reflected pulse is often too small and hidden by noise interference as a result of the loss in signal strength along the cable length [86].

Both electrical and acoustic methods will experience detection limitations caused by the systems long length requirement as both types of emitted signals will suffer from attenuation when propagating through the cable, particularly the high frequency components. Wild et al. discusses the practical aspects of PD localisation on long length power cables, emphasising the benefits of double sided measurement with regards to accuracy of the source location and improvement on detectable distance [87]. Dissimilar to land based systems, access at both ends of the umbilical is highly unlikely due to the subsea environment in which they are installed and thus this improvement cannot be applied to the proposed system.

When considering the through water propagation of the emitted signals, there is the likely benefit of a shorter detectability range as the maximum distance will be based upon the water depth of the installed umbilical as opposed to the overall umbilical length, which is often much greater. Acoustic methods are the most commonly chosen technique for communication in subsea environments due to the low attenuation of sound in water, allowing for AE detection and communications over much longer distances [88], [89]. RF sensing suffers from high signal loss in seawater environments due to the conductivity of the seawater causing strong attenuation of the electromagnetic waves, therefore greatly limiting its detection range [90], [91]. Optical waves suffer from high levels of absorption and scattering in water and for that reason are not commonly used in the subsea environment unless improved bandwidth is required over short distance transmissions [92]. The use of through-water acoustic sensing would also allow for localisation of PD as multiple acoustic sensors positioned within the surrounding water could listen and record discharges enabling position estimation through applied TDoA algorithms.

3.2.1.2 Subsea Environment

Umbilicals are installed in a subsea environment in many locations across the world, consequentially, environmental operating conditions for each umbilical vary greatly, which in turn influences the selection of a suitable sensing method for use in the proposed system.

Early research by Steiner and Reynolds presents the fundamental limitations affecting the detectability and localisation accuracy of PD in power cables, highlighting the influence of background noise and propagation characteristics of the cable [93]. Background noise has a significant influence on detectability and accuracy, however the cable characteristics govern the levels of attenuation, therefore causing variation between cable designs. Both background noise and cable design will vary for the proposed system depending on field location and umbilical functionality.

UHF sensors benefit from high detection sensitivity and beneficial resistance to noise, however are limited when it comes to long length cables due to attenuation and shielding effects of the cable [94]. AE through-cable sensing can be seen as preferable in some environments as it can be made immune to electromagnetic interference, should this be an issue.

Through-water sensing of acoustic emissions from PD are also affected by the surrounding environment as the acoustic waves are greatly influenced by the characteristics of the propagating medium. The seawater environment varies depending on its geographical location, time of year, water depth and surrounding activities, which in turn affects the salinity, tides, currents, ambient noise and temperature of the water, therefore changing the characteristics of the propagating medium and thus affecting the acoustic waves. A good understanding of the complex seawater environment would consequently be required to recognise the effects on signal velocity, attenuation, SNR and potential multipath.

3.2.1.3 Online Sensing

One of the major benefits of the proposed PD monitoring system comes from the ability to operate whilst the system remains online, thus causing no interruptions to ongoing production. Online monitoring of power cables brings about many challenges as the cables will remain operational at voltages between 6-66kV. Any monitoring technology connected directly to the cable would have to withstand high currents, voltages and temperatures. As discussed previously, the cables are designed to be operational up to a maximum conductor temperature of 90°C and so the monitoring equipment must also be able to work within these parameters. If the monitoring technology were to sit within the umbilical itself, it would need to be able to withstand the mechanical forces seen during manufacture, installation and in-service operation. A retrofit option which is not in direct contact with the conductor nor fitted within the umbilical bundle would therefore be preferable.

Although beneficial, the requirement for online monitoring greatly adds to the complexity of the proposed PD detection and localisation system. At present, TDR methods are commonly used offline to detect and locate low resistive cable faults by sending a low voltage pulse into the cable conductor and detecting reflections caused by changes in impedance. The location of the fault can be determined by measuring the arrival time of the reflection as the velocity of the pulse is known. One of the potential issues with offline TDR measurements is that the voltage pulse may be lower than the inception voltage of the PD, therefore faults may not be detected. In addition, if the occurrence of PD is at a splice location, the peak of the splice will likely mask the peak of the PD and consequently the location of the occurrence would remain unknown. Lee et al. presents early research of an online method using time-frequency domain reflectometry (TFDR) to locate impedance changes in underground cables, showing promising test results at 2kV on a 58m sample where the reference signal was reflected at a straight joint, as opposed to a PD fault [95]. Similarly, HFCT's can be used online by applying TDR techniques through the injection of a trigger pulse to the cable, but again detectability lengths are limited due to HF attenuation, particularly with one sided access, and the likely occurrence of electrical interference from the umbilical power and control system.

Recently developed technologies such as Wirescan's LIRA (Line Resonance Analysis) offer higher sensitivity as opposed to conventional TDR technologies. LIRA performs

frequency domain analysis, through advanced algorithms, to detect locations of degradation in a cables' insulation due to thermal, electrical or mechanical stress. It is based on transmission line theory to calculate and analyse the complex line impedance as a function of the applied signal for a wide frequency band [96]. Research performed by Fantoni demonstrates that the LIRA technique, using TFDR, offers a higher sensitivity when compared to conventional TDR as LIRA was able to detect additional faults on a length of tested cable which were not identified on the TDR trace [97]. Due to the high sensitivity of the measurement, it is recommended to get an initial trace post cable manufacture and again at major stages, such as umbilical manufacture, installation etc. as this will allow cable degradation to be assessed since any changes in the trace will indicate a potential point of failure. At present, both conventional TDR and LIRA require a physical connection to the cable conductor and for that reason are only operational whilst the system is offline, hence their current uses being a method of condition based maintenance or post incident analysis.

AE sensing, both topside and subsea, offers the significant advantage of not requiring a physical connection to the conductor, therefore allowing it to be used whilst the system remains online. In recent years, fibre optic DAS has become a popular option for online continuous monitoring of leaks within the pipeline industry, however the signal transfer from a leak to a fibre housed within an external cable displays high levels of attenuation, therefore small leaks are often undetectable. Research performed by Stajanca et al. discusses great improvements in detection sensitivity when the fibre is directly applied to the pipe [98], although this is not feasible for the proposed PD monitoring system due to the surrounding components and dynamic nature of the umbilical. Cherukupalli and Andres suggest potential applications where distributed acoustic and strain sensing technology would be beneficial for the monitoring of power cables, focusing on both onshore and offshore uses [99]. There are sensing companies offering systems which use fibre optic DAS, often alongside distributed temperature sensing (DTS), to monitor subsea or buried power cables for short circuit detection, hot spots, third party intervention and accidental or malicious damage [100]–[102]. Hicke and Krebber present the use of fibre optic DAS to continuously monitor offshore windfarm power cables for damage from anchor drops, construction and trawler fishing [103]. Although fibre optic sensing offers a highly sensitive method of acoustic sensing, the signals from a PD event are much smaller in magnitude than the incidents discussed, thus resulting in a very low SNR, therefore, at present, the available 'off-the-shelf' fibre optic sensing cables are unsuitable for use within this umbilical monitoring system. In addition, fibre optic DAS sensing is limited when it comes to monitoring of existing umbilicals as it is not suited for a retrofit design.

Recent research has also been performed into the use of a fibre optic sensor system based on Sagnac interferometry for the monitoring of PD in power cables whereby proof of concept testing has been performed with the sensing fibre was embedded within the cable itself [104]. Results were shown to be promising, however could not be applied to the umbilical application due to the sensor placing and fitment.

As an alternative to fibre optic acoustic sensing, the use of piezoelectric hydrophones would be a favorable online acoustic sensing technology as they are non-intrusive and can be positioned in the surrounding seawater of brownfield environments without disturbance to ongoing production. Piezoelectric hydrophones are specifically designed to monitor underwater noise and work by generating an electrical potential in response to mechanical or pressure changes in the surrounding environment. Hydrophones are often used within marine research to track and monitor underwater marine life. This application is similar to that required for the localisation of the PD source, as the location of the marine life is determined through TDoA methodology, whereby signals are detected at differing times across a number of hydrophones. Hydrophones are ideally suited for underwater acoustic detection and localisation, however, when considering a topside through-cable acoustic sensing method, a different acoustic sensor technology would likely be required as the sensitivity with airborne sounds is much lower due to the acoustic impedance being designed for sound detection in water.

3.2.1.4 Bespoke Umbilical Design

Each umbilical is bespoke as the design is led by the functional requirements, client and industry specifications, mechanical/electrical design considerations and the field environment in which it will be installed. Consequently, each umbilical will contain specifically designed components, causing each umbilical structure to differ. The bespoke nature greatly adds to the complexity relating to the positioning and choice of monitoring technology.

Lubdgaard details the fundamental considerations regarding acoustic PD detection, highlighting the complexities of varying materials and structure in relation to acoustic propagation velocities needed for PD source localisation [65]. The velocity is affected by different wave types and is calculated using the density and elastic properties of the material. The cable structure adds to the complexity as the acoustic wave will propagate from one medium to another, having different density and elasticity properties, resulting in a reduction in signal energy. An additional complexity with long length power cables is attributable to cable splices or joints as they cause significant attenuation of the propagating AE signal [105].

EM sensing methods are less susceptible to variations within the umbilical components, however they are greatly affected by the presence of electrical noise, which will vary depending on the operational field. Changing umbilical length requirements would also impact the ability for EM sensing as it may be suitable for fields requiring shorter umbilical lengths but not viable for longer step-outs.

3.2.1.5 Retro Fit Design

The inclusion of monitoring technology within the umbilical would need to be agreed with the client prior to umbilical manufacture. This may be multiple sensors or sensing cables in order to detect the potential faults, leading to increased CAPEX costs, additional weight

and potential complexity for handling/installation, depending on the mechanical properties of the sensing technology. From the perspective of the client, these added costs and complexity would likely outweigh the benefits of the additional data received during PD monitoring. Failures within umbilicals are extremely costly, however are uncommon as the components are designed to be operational throughout the design life, therefore the monitoring equipment may not be needed if no failure should occur, hence the added costs/complexity of including sensors within the umbilical bundle may not be justified. As a result of this, the ideal method for integrity monitoring would be a retrofit option which could be fitted as and when needed, to any umbilical design.

Furthermore, many operators are now looking to extend the lifetime of existing fields past the typical 25-30 year given life expectancy. Stacey, Birkinshaw and Sharp discuss the life extension issues for ageing offshore installations, highlighting that a significant number of platforms are coming towards the end of their original design life, however there is a continued requirement that they remain operational, either for the original fields or to serve as a base for neighboring subsea completions, and hence they are likely to carry on production for a significant period of time [106]. Life extension requires an understanding of the condition of the components and how they may have depreciated over time. This often involves detailed field extension studies, based on minimal available data from the field and the expertise of specialist engineers. A method to retrofit a monitoring solution to existing umbilical systems for either short or long-term online use, would consequently be highly beneficial when performing a field extension study in order to provide information on the fitness for service of the power cables.

3.2.2 Sensing Summary

To overcome the inherent challenges of this application, various sensing technologies have been evaluated and discussed to allow focus on the most suitable method. Many summary papers exist comparing PD detection techniques for other applications where the challenges and limitations differ from those associated with PD monitoring of a subsea umbilical [50], [105], [107], [108]. Yaacob et al. analyse multiple PD detection techniques for HV equipment discussing the advantages and disadvantages the different sensor types offer in varying applications, highlighting that electrical methods offer higher sensitivity than acoustic, however are vulnerable to noise and electromagnetic interference [51]. Meggs and Daffey review methods commonly applied to HV land based plants in order to assess their suitability for use in a marine HV plant, noting the requirement for online monitoring and discussing the potential use of HFCT's [109]. Different environments and functions have dissimilar constraints therefore not one sensing technique is deemed favorable for all PD detection systems.

When considering the discussed challenges of; long distance detection, subsea environment, online sensing, bespoke umbilical design and retrofit application, the use of acoustic sensing techniques offers great advantages over other technologies in many of the

areas. A key aim of the system is having the ability to operate online, without affecting ongoing operation of the umbilical. Acoustic sensing enables this as there are no physical connections required to the live cable conductor, unlike conventional TDR/FDR techniques. This also facilitates the ability for a retro-fit system, opening the technology up to existing brownfield applications.

Acoustic sensing techniques can be applied to both through-cable and through-water detection and localisation of the AE from the PD event. With regards to long distance, through-water sensing, acoustic methods are preferable in comparison to RF or optical methods due to the strong attenuation of EM and high levels of absorption of optical waves. As discussed earlier, acoustics methods are commonly selected for underwater communications due to their strong performance in water, leading to a much greater detection/communication range. Acoustic waves propagate well within seawater, particularly the lower frequency components within the signal, allowing detection over a very long distance. When considering underwater sensor networks, very-high frequency bands above 50kHz can only be used for short-range communication, whilst 20kHz to 50kHz is often used for moderate range communication, whereas frequencies below 10kHz are used for very long-ranges in the order of tens of kilometers [91]. Concentrating on the detection of the lower frequency waves within the emitted acoustic signal will allow for a greater detectability range. As previously suggested, hydrophones are a preferable option as they are designed for underwater detection of acoustic waves and could be positioned within the body of water surrounding the installed umbilical to listen for PD occurrence. A minimum of three hydrophones would allow for estimation of the PD location by utilising TDoA techniques within position estimation algorithms. Acoustic through-water sensing also minimises the required maximum detectability range, in comparison to through-cable sensing, as this is based on the water depth of the field in which the umbilical is installed, as opposed to the overall umbilical length which is typically greater. Unlike optical techniques, acoustic methods also suffer minimal losses due to the turbidity of the water, therefore making them suitable for varying underwater environments. Fibre optic DAS sensing has also been discussed, however the typical application has focused on larger AE events in comparison to PD detection, therefore the expected low SNR and need for a retrofit design has directed the focus to the use of hydrophones for this specific application.

Regarding through-cable sensing, the use of HFCT's has been discussed as an existing technology which can be used in certain cases, where the overall length permits. This however, is mainly for detection only, as lengths for localisation are further limited. Acoustic sensing may provide a benefit over RF methods as it can be made to be immune to electromagnetic interference, therefore has the potential of providing an improved SNR. The use of HF & UHF sensors does offer greater sensitivity and thus allows for the detection of lower pC discharges, though it is limited in its detectability range due to the vast attenuation of the high frequency components in the emission. Again, TDoA techniques can be applied to the detected AE signals in order to establish the fault location, depending on the distance from the receiving sensor.

Acoustic techniques, whether it be hydrophones for through-water detection or AE sensors for through-cable detection, would allow for both continuous monitoring or a called upon retro-fit option, should it be required. Current online monitoring methods for umbilicals do not allow for localisation of a PD event, however, HFCT's are occasionally used to detect PD occurrence, should the fault fall within the detectable range. In addition, IR measurements are often taken whilst the umbilical is in service, therefore by monitoring these parameters, a retrofit option could be called upon to establish the imminent fault location, should any concerning measurements occur. In some instances, there may be the opportunity to combine electrical and acoustic techniques in order to improve accuracy and minimise false alarms.

3.3 Research Aims and Objectives

The discussed industry developments leading to increased power subsea has stressed the importance of the condition of the cables within the umbilical. The ability to detect and locate PD occurrence whilst the system remains online would provide a valuable insight to the condition of the cable and aid prediction of required intervention or lifetime extension.

At present, existing online technologies are unable to detect and locate PD within subsea umbilicals. Even offline location estimation is difficult due to cable lengths, splices and the required inception voltage. Current state-of-the-art methods focus on offline techniques offering greater sensitivity or methods for online detection of land based systems which benefit from greater accessibility and thus a shorter detection range than umbilicals. This gap in technology therefore highlights the need for a non-intrusive system able to overcome the challenges of long distance online detection and source localisation of PD.

Through exploring the challenges brought by online condition monitoring of the subsea cables, acoustic sensing techniques were considered the most suited option. A retrofit concept was thought to be advantageous as the costs would be kept to a minimum for clients on future projects, yet the system could also be applied to existing fields when looking to assess the potential for life extension. Both through-cable and through-water AE propagation will be explored, with a focus on the lower frequency components of the signal, due to long distance sensing requirement.

The research presented henceforth aims to investigate the characteristics of the emitted acoustic signals, whilst exploring the propagation paths to allow for the development of a suitable sensing system able to both detect and locate PD by utilising acoustic detection methods and TDoA techniques applied to position estimation algorithms.

Chapter 4

Through-cable Acoustic Propagation

As identified in Chapter 3, acoustic sensing methods will be investigated to establish an appropriate system capable of detecting and locating PD within a subsea umbilical. This chapter explores the through-cable propagation path and characteristics of the emitted acoustic signal, considering the various transmission mediums and acoustic wave types.

In order to understand the characteristics of the propagated AE signal, experimental tests were performed on lengths of cable samples containing PD faults, with acoustic sensors coupled to the outersheath. Experimental results allow the complex propagation channel to be further investigated, evaluating changes in the signals' frequency spectrum in relation to distance travelled and establishing the signals' velocity through envelope and cross correlation analysis, thus enabling localisation of the PD source.

4.1 Motivation

Chapter 3 discussed the use of acoustic sensors for PD detection in other applications such as transformers and land based systems, therefore confirming the feasibility of acoustic techniques for the proposed system. A greater understanding of the characteristics of the resulting acoustic signal is required to determine how to suitably detect the emissions amongst the background noise and to develop an algorithm to attain the discharge origin. Consequently, the initial focus of this work is an investigation of the AE signal generated from PD occurrence within an MV cable, followed by experimental testing to further evaluate the effects of acoustic sensing along the overall cable length.

4.2 Characteristics of Acoustic Emission from PD within Cables

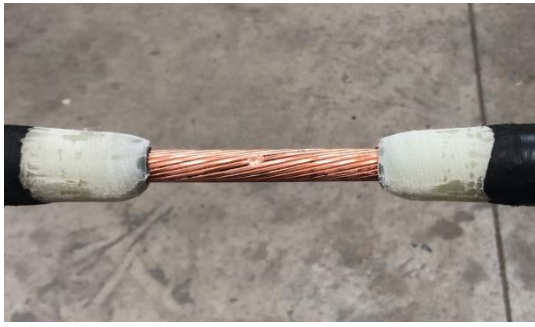
Previous research into AE from PD events shows typical pulse parameters, however this is highly dependent on; the type of PD (corona, surface, treeing or void), the sensor used, environmental noise, the propagating medium and distance from the fault location. An initial trial was therefore performed to ensure focus was on the correct parameters to align with the aims of this research.

4.2.1 Experimental Test: Induced PD on Cable Sample

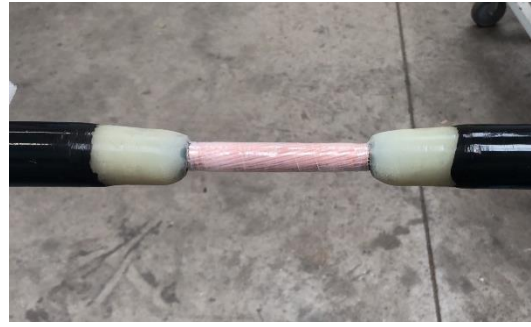
The types of PD which are of interest to this application stem from internal voids and treeing within the cable's insulation. As a result, a cable sample containing this fault type was required for testing and as the presence of voids typically leads to electrical treeing prior to failure, a sample containing a 'poor insulation splice' was constructed. The makeup of this fault region can be seen in Figure 4- 1. The splice involved removal of a small section of the cables outersheath, screen, semi-conducting and insulating layers. To ensure a void remained, a small divot was made in the copper conductor prior to the insulation being reinstated, as shown in Figure 4- 1a. The insulation was tapered at each end of the splice section to allow a suitable bond between the existing insulating material and the reinstated insulation. The reinstated insulation was built up in layers using PE tape with heat applied at multiple stages to melt the insulation and create a bond between the layers, as presented in Figure 4- 1b through to Figure 4- 1f. A dark area can be seen on the images showing the cable prior to screen reinstatement which relates to the void/air pocket introduced to promote the occurrence of PD. The final process was reinstatement of the copper screen followed by a tape layer to create an overall outersheath.

The test was performed at TechnipFMC Umbilicals R&D centre on an 150mm² 18kV cable sample, approximately 50m long, complete with the discussed 'poor insulation splice'. Figure 4- 2 displays the general configuration for this initial test. Although this test was carried out under dry conditions, in reality the umbilical is flooded, hence the interstices surrounding the cable are filled with seawater and thus hydrophones were utilised to detect the AE signals. Acoustic coupling gel was applied as a bonding interface between the hydrophones and the cable sheath to minimise losses through the potential air gap.

Figure 4- 3 shows a block diagram illustrating the architecture of the overall test system. Two hydrophones with a broadband frequency response were used for acoustic sensors Rx1 and Rx2, along with a pre-amplifier providing a fixed gain of 53dB and a data acquisition unit to capture the emitted acoustic signals. The hydrophones were positioned 14m and 35m from the fault location to obtain an initial view of the change in signal attributable to distance travelled. In order to create a discharge, an HVAC 50Hz power supply was connected to the MV conductor, where the voltage was raised incrementally until PDIV was reached. A sampling frequency of 44.1kHz was used to obtain frequencies up to 22kHz, maintaining focus on the lower frequency components due to the necessity for long distance detection. Once PD occurrence could be seen on the data acquisition unit, one minute audio files were recorded, whilst applying a further gain of 5dB. Each recorded file was then post-processed offline using Matlab, where a 100th order Finite Impulse Response (FIR) bandpass filter was applied to suppress noise and 50Hz interference signals.



(a)



(b)



(c)



(d)



(e)



(f)



(g)



(h)

Figure 4- 1: Fault Region – (a) stripped section c/w tapered insulation & conductor divot, (b) initial insulation reinstatement over conductor, (c) insulation reinstatement (*pre-heating*), (d) insulation heating, (e) additional insulation taping (f) fully bonded insulation (*post heating*), (g) reinstated copper screen, (h) reinstated tape overshath.

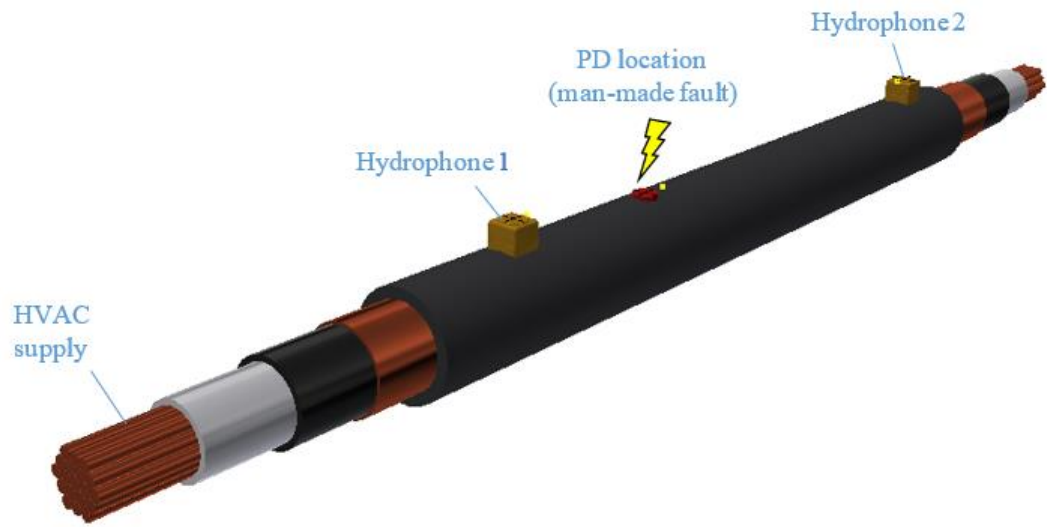


Figure 4- 2: MV Cable Sample c/w PD Inducing Fault

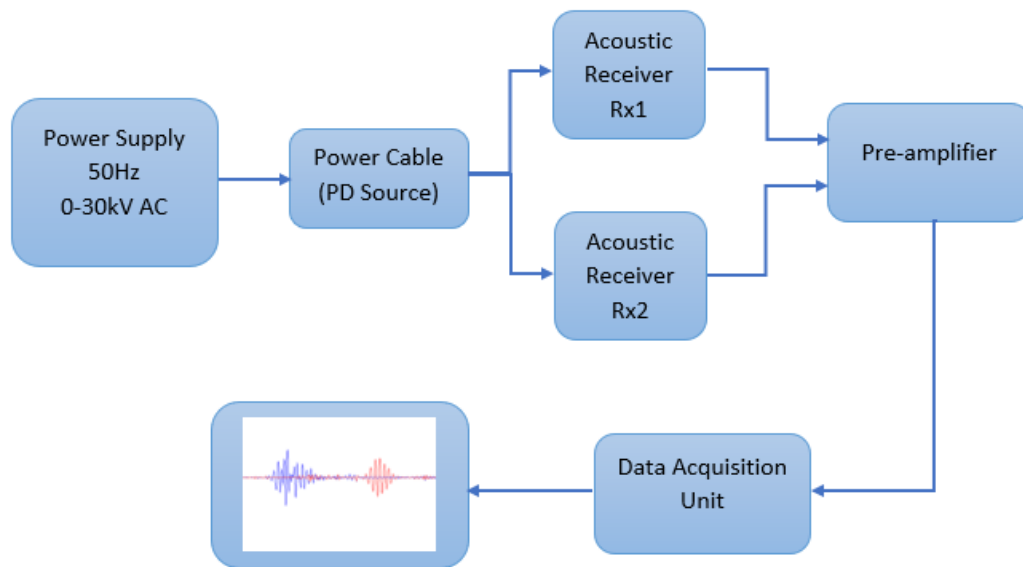


Figure 4- 3: Simplified Block Diagram - PD Acoustic Detection

4.2.2 Results and Discussions

Figure 4- 4 presents a time-domain plot of the signals captured on both Rx1 and Rx2 hydrophones. Multiple discharges with varying amplitudes were detected across the 60 second recording. As expected, the amplitude is greater for the signals obtained on Rx1 in comparison to Rx2 as the sensor is located closer to the PD location.

Figure 4- 5 centers on an individual PD event, revealing that both the EM and AE signals have been detected with this particular test arrangement. The EM signal is detected instantaneously due to the high-speed at which EM waves travel and consequently this could be used as an indicator for time of PD occurrence. As a result of this, the EM signal is detected simultaneously on both sensors. Due to the slower propagation velocity of sound, a delay can be seen before the AE signals reach receivers 1 and 2 respectively, thus confirming the feasibility of employing TDoA localisation methodologies. Figure 4- 6 focuses further on the captured emission from Rx1 positioned closest to the fault, highlighting some key characteristics of the signal. The resultant AE pulses from the PD event are much longer in duration in comparison to the EM signals, with this particular discharge showing an approximate rise time of 1.5ms and duration of around 4.2ms. Upon further examination of the AE pulse, it can be seen that there is slight irregularity in the oscillation of the signal. This is only found on the AE signal detected on receiver Rx1 as

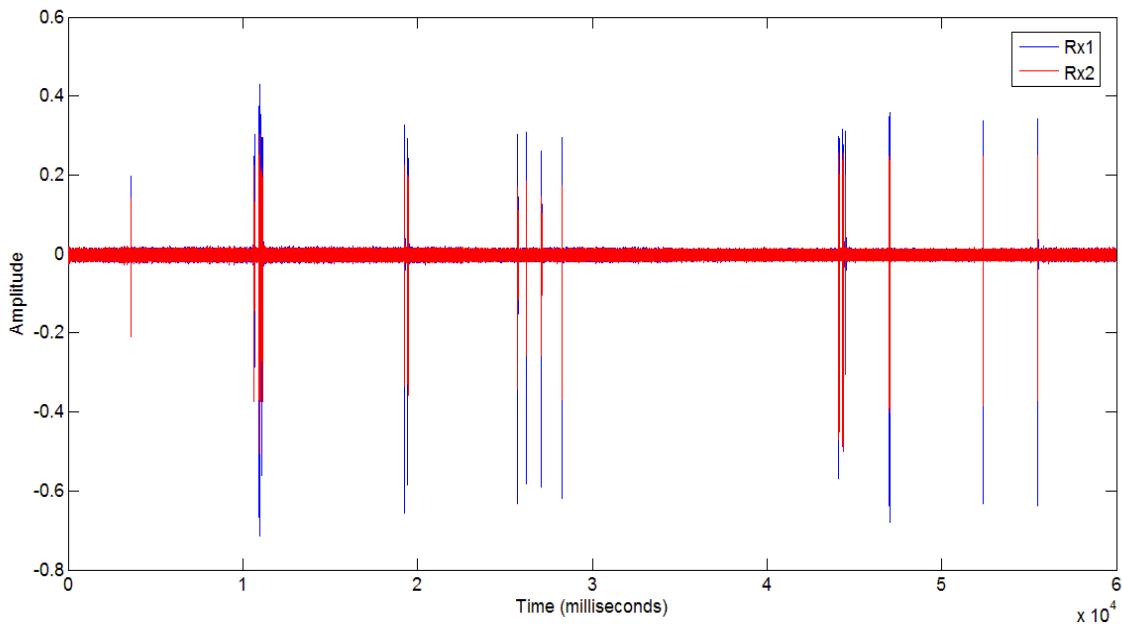


Figure 4- 4: Acoustic Signals Measured at Rx1 (14m from fault) and Rx2 (35m from fault) due to PD within Power Cable Insulation.

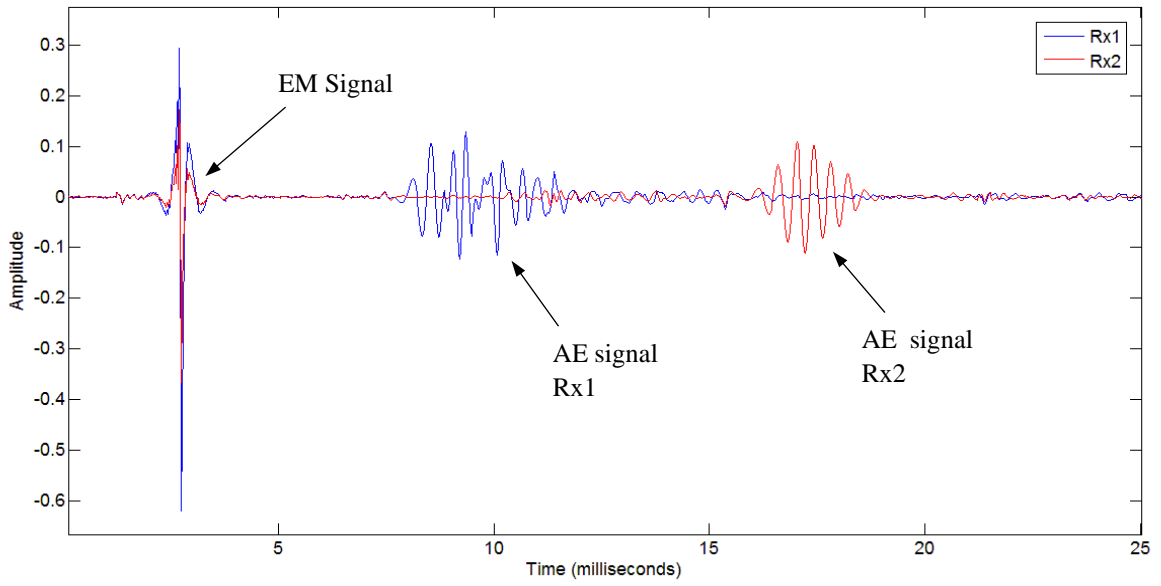


Figure 4- 5: Individual Emission Measured at Rx1 (14m from fault) and Rx2 (35m from fault)

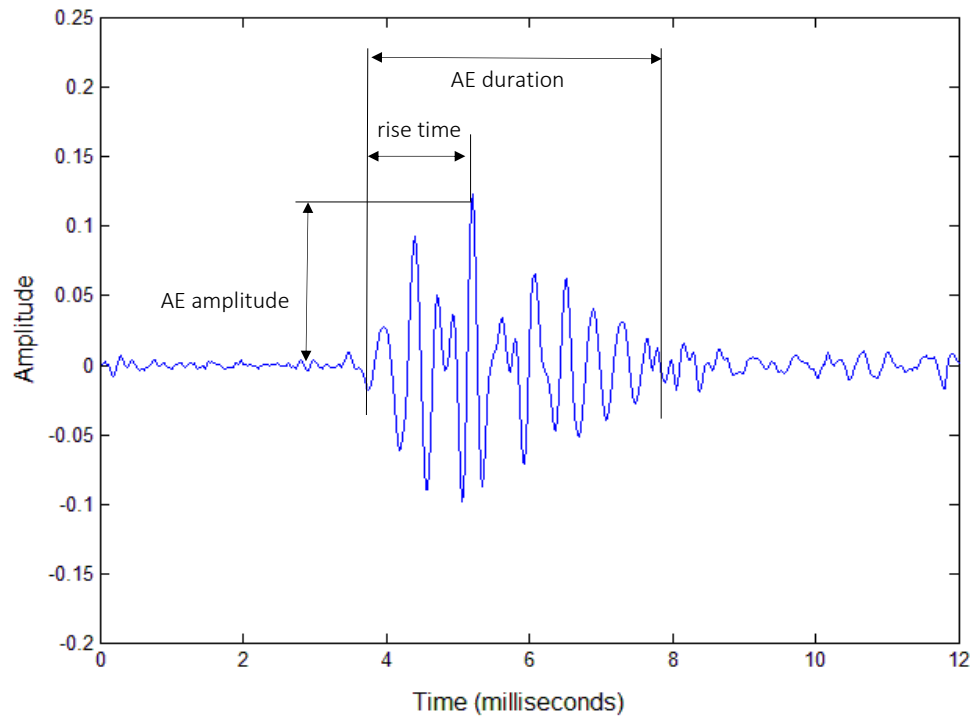


Figure 4- 6: Individual Acoustic Emission – Rx1

the same discharge detected on Rx2 does not display this irregularity, as illustrated in Figure 4- 5. In addition, the duration of the AE pulse is recognisably longer for the signal detected on Rx1, positioned nearest the fault, in comparison to that detected on Rx2, furthest from the fault, however from literature it is known that with distance the AE pulse width increases and signal amplitude decreases. Figure 4- 7 focusses on the two captured emissions making it clearer to see the difference in signal profile. From this it can also be seen that the duration of the signal detected on Rx1 is around 4.2ms whereas the duration of the signal detected on Rx2 is around 3.0ms. The cause of these anomalies is likely due to the effects from multipath propagation. Multipath is due to signals reaching the receiver by two or more paths causing distortion to the amplitude and frequency of the original signal. The multipath signal is an attenuated version of the original, with different phases and different arrival times.

Considering the test performed, the sensor Rx1 was positioned 14m from the fault and approximately 1m from the cable end, whereby the HVAC supply was also connected. When PD occurred, the receiver Rx1 would have firstly detected the direct path signal, travelling 14m, followed promptly by a second signal reflected from the cable end, travelling 16m. Based on the 2m difference between the direct and reflected signals, it is probable that the two signals would overlap in time, thus causing signal distortion. The likelihood of this is further corroborated utilising the velocity of the signal established in

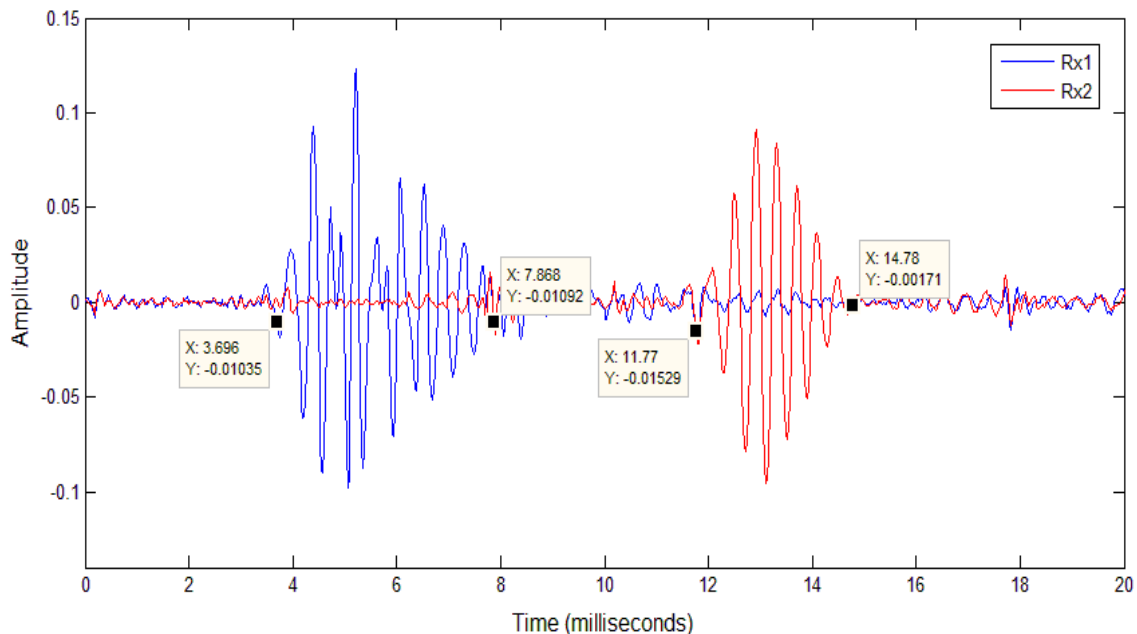


Figure 4- 7: Evaluation of AE Duration – Rx1 and Rx2 signals compared

the forthcoming Section 4.5, as the expected time of arrival of the reflected signal at Rx1 can be calculated to be 0.83ms after the original signal, thus falling within the AE duration. The receiver Rx2 was positioned as close to the cable end as practicably possible with the aim of minimising the effects of multipath. This however, could not be done with Rx1 as the receiver had to maintain a suitable distance from the HVAC supply, whilst maximizing the test sample length and as a result of this suffered from the effects of multipath. Within the discussed PD localisation system, it is unlikely the AE sensors would be positioned as close to the cable ends, however the possibility of multipath remains as signal reflections will also occur at imperfections within the cable length such as splices and repairs.

To further analyse the characteristics of the emitted acoustic waves, Fast Fourier Transform (FFT) algorithms were applied to an individual discharge event to establish the frequency content of the signals. The resulting frequency spectrum can be seen in Figure 4- 8, whereby the FFT of both the electromagnetic and acoustic signals for one individual PD is shown in Figure 4-8a and the FFT of the acoustic emission alone is shown in Figure 4-8b.

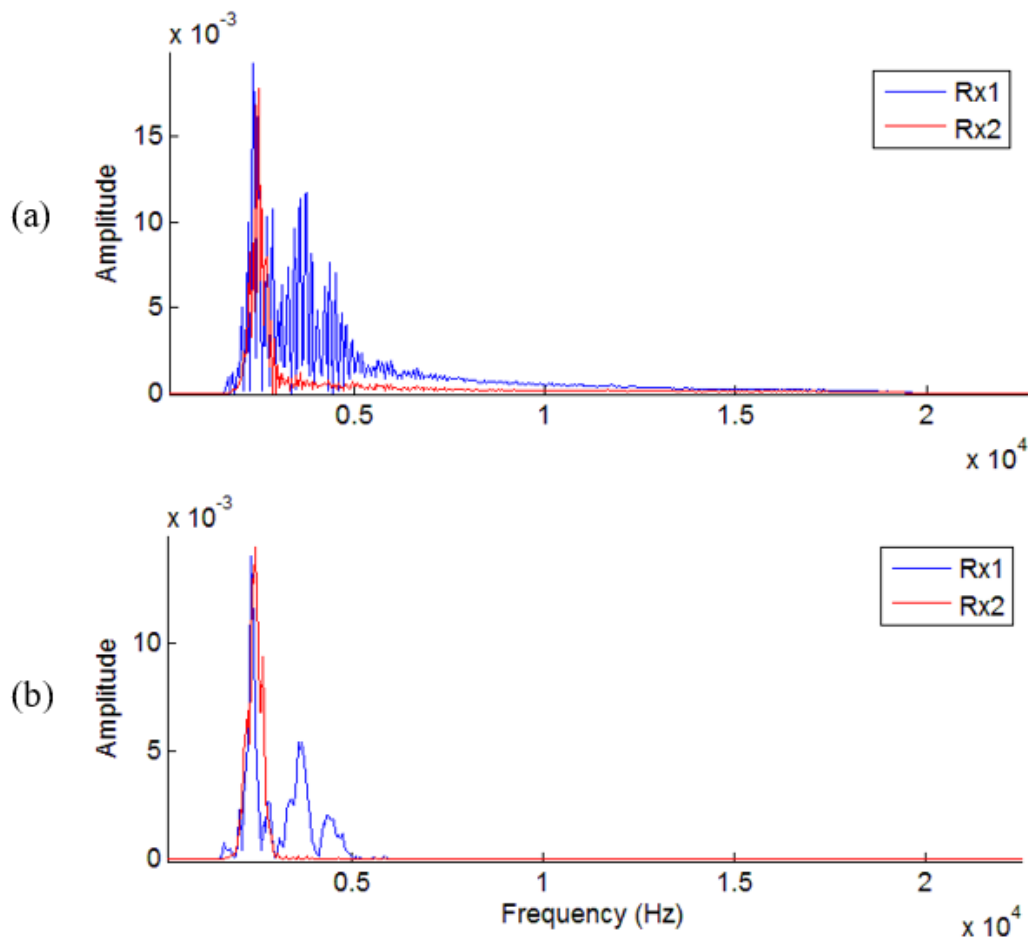


Figure 4- 8: Frequency Spectrum of Individual Emission from PD within Power Cable Insulation: (a) EM and AE signal, (b) AE signal only

In both cases, the bandwidth of the signal detected at the closest receiver, Rx1, displays a greater frequency range, confirming that distance travelled has a large impact on the frequency content of the signal, due to strong attenuation of the higher frequency components. The EM signal shown in Figure 4-8a masks the actual frequency content of the AE signal received at Rx1, however minimal difference can be seen between Figure 4-8a and Figure 4-8b regarding the signal detected on Rx2, therefore highlighting the rapid attenuation of the EM signal.

As the received signal is largely influenced by the distance travelled, it is key to establish the effects due to the frequency response of the channel as well as those relating to the individual discharges. Figure 4-9 presents 3 individual PD events recorded at different time periods on the same channel, with Figure 4-9a displaying those recorded at Rx1, 14m

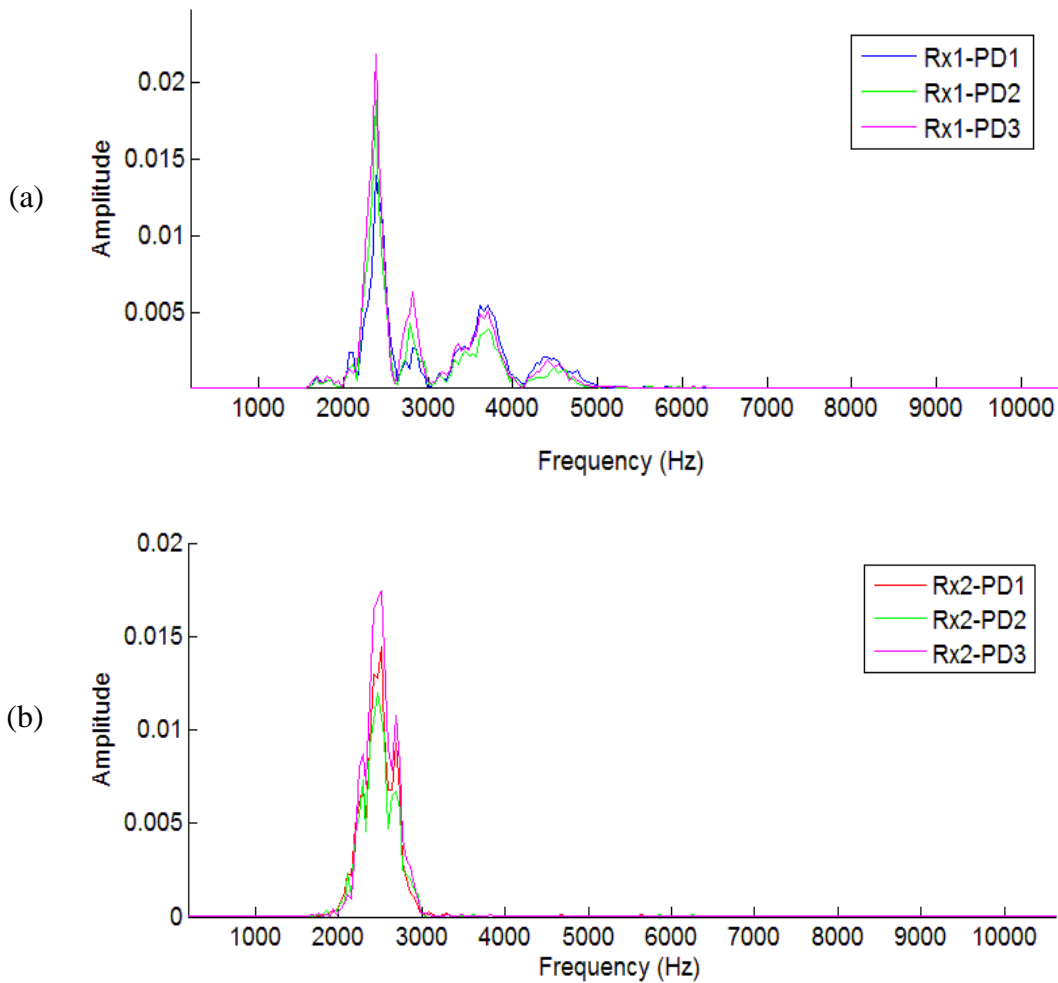


Figure 4- 9: Frequency Spectrum of Multiple AE from PD within Power Cable Insulation: (a) 3 individual PD events received on Rx1, (b) 3 individual PD events received on Rx2

from fault and Figure 4-9b displaying those recorded at Rx2, 35m from the fault. This indicates that the spectrum is dominated by the frequency response of the channel rather than the emission itself as different channels for the same PD event show a different spectrum, whereas different PD events on the same channel display a very similar spectrum. The amplitudes differ slightly between the detected acoustic emissions as this is dependent on the mechanical energy released in each individual discharge.

A visual representation of the signal frequencies over time is shown in Figure 4- 10. The spectrograms represent the 60 second PD capture previously presented in Figure 4- 4, focusing solely on the signals captured on Rx2, located furthest from the fault. As the spectrograms are of the complete capture, they also contain the detected EM signals, however by concentrating on the signals detected on Rx2, the impact is minimised. Figure 4-10a displays the 2D time vs frequency plot, though not all detected discharges can be seen due to the low intensity and short duration of the PD pulses. The 3D spectrogram, Figure 4-10b, provides a clearer view of detected broadband pulses, revealing the main signal energy to be below 5kHz. The higher frequency components shown are thought to be attributable to the EM signal detected, which would not be as visible if the test was performed on a longer sample length. In reality, the fault would likely be at a much greater distance from the receiver and thus the higher frequencies would be greatly attenuated.

To analyse this further, the power spectral density (PSD) of an individual discharge is presented in Figure 4- 11a and the corresponding spectrogram is shown in Figure 4- 11b, highlighting the variations in signal energy as a function of frequency. In both cases, focus is on the acoustic signal only as the EM signal has been removed, therefore confirming that the main signal energy relating to the acoustic emission is around 5kHz and below.

4.3 Through-cable Propagation Path

The cable itself has a large influence on the propagation characteristics of the acoustic signal as the velocity and attenuation are greatly affected by the varying mediums attributable to the multiple cable layers. As emphasized by Lundgaard, assessment of the PD acoustic signal propagation through solids is highly complex, a reduction in signal amplitude can be caused by geometric spreading, multiple transmission paths, absorption and losses due to propagation from one medium to another [73]. Furthermore, there is an added complexity in that the different wave types such as pressure and shear, travel at different velocities. Developing an understanding of the signals potential propagation path and establishing the velocity are key aspects for determining the location of the discharge occurrence and thus these variants are explored further.

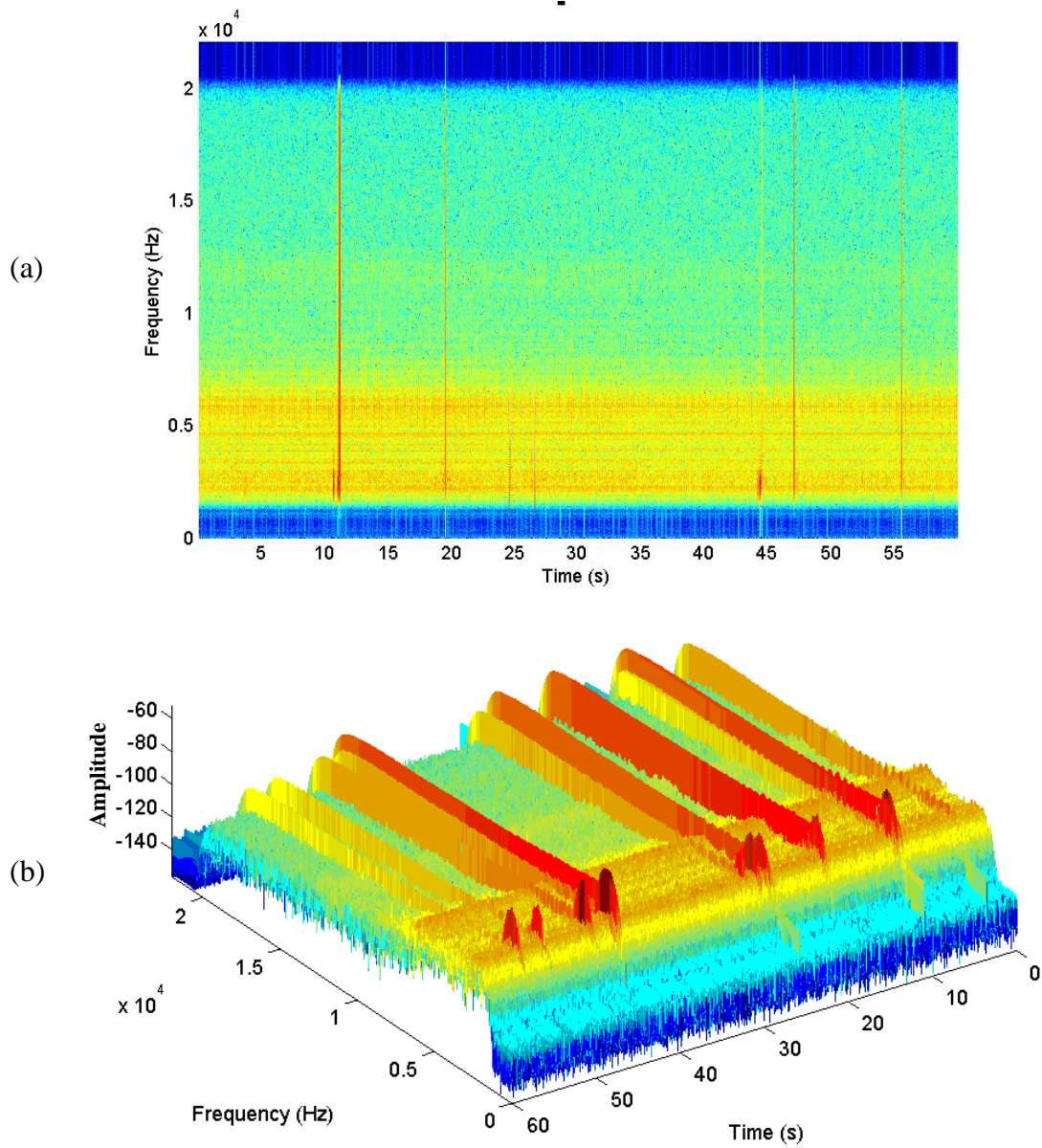


Figure 4- 10: Spectrogram of Signals Captured from PD within Power Cable Insulation: (a) corresponding 2D time vs frequency plot, (b) corresponding 3D plot including signal magnitude

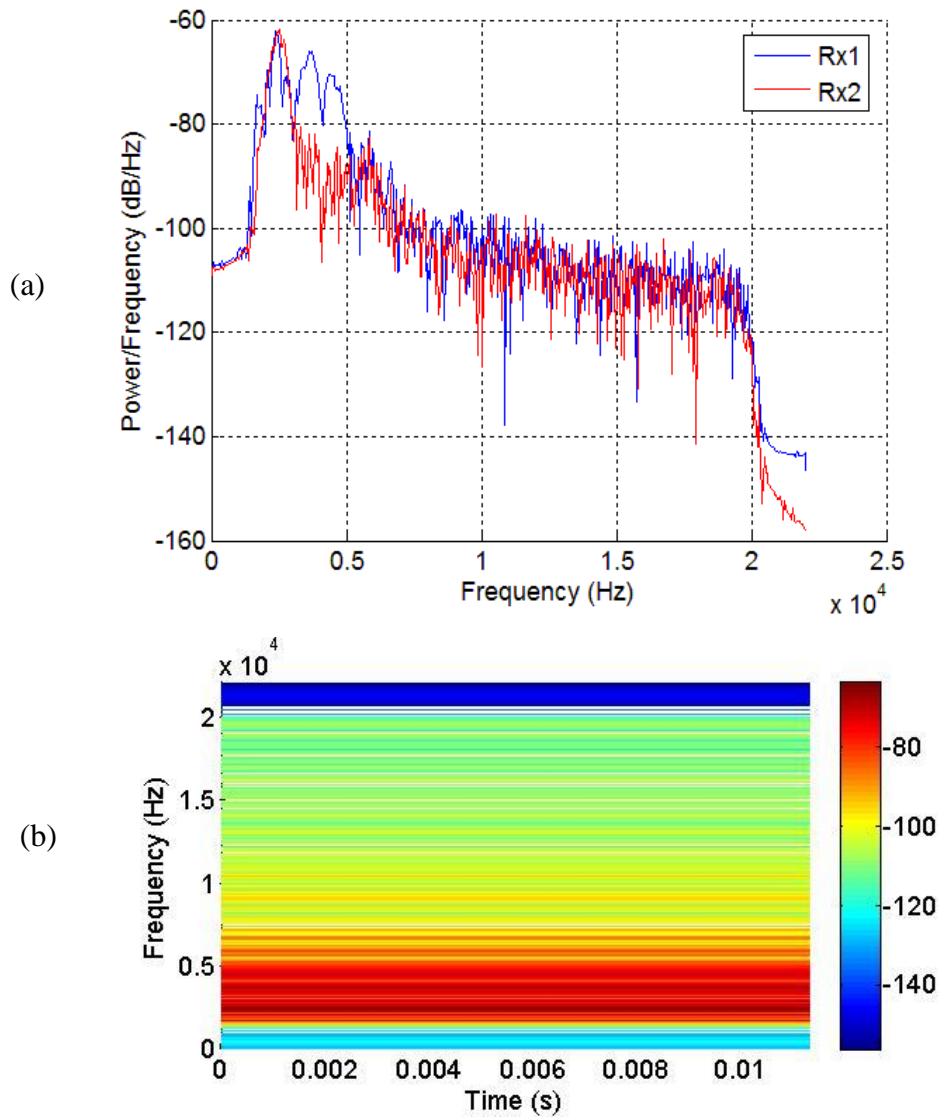


Figure 4- 11: Individual Acoustic Emission from PD within Power Cable
(a) Power Spectral Density – Rx1 & Rx2 (b) Spectrogram – Rx1 only

4.3.1 Wave Types

In a solid material, sound waves can propagate as pressure waves, shear waves, surface waves and, in thin materials, as plate waves. In pressure waves, the particles oscillate in a longitudinal direction, whereas in shear waves, the particles oscillate perpendicular or transverse to the direction of propagation. Shear waves are weak in comparison to pressure waves and are typically generated using energy from the pressure waves. Surface (Rayleigh) waves combine both longitudinal and transverse motion and travel the surface of a material, to a depth of one wavelength. Plate waves are less relevant in this instance due to the construction of the cables.

The relationship between the acoustic signal's velocity, frequency and wavelength is the same for all wave types and can be seen in (4.1), where v is the speed of the wave (velocity), f is the frequency and λ is the wavelength.

$$v = f \lambda \quad (4.1)$$

When PD occurs within a cable, both pressure and shear waves are generally excited simultaneously. The velocity and propagation path of these signals varies with wave type and frequency, making it difficult to estimate the precise discharge location as in most cases the exact propagation paths and attenuation are unpredictable [76]. For the same frequency, shear waves have a slower velocity in comparison to pressure waves and also have a shorter wavelength. Surface waves have a similar velocity and wavelength to shear waves.

Understanding and predicting the resultant acoustic wave types from PD occurrence is extremely difficult, however cross correlation and envelope analysis of the detected signals can be used to establish the signal's velocity through TDoA, therefore providing an indication to the wave type being detected, based on the m/s value.

4.3.2 Propagation Mediums

In addition to the multiple wave types, variations in cable design adds further complication to the signals propagation path as material types (mediums) and thicknesses will vary based on cable supplier, specified voltage and current rating. The signal's velocity and attenuation are greatly affected by the sound waves travelling through one medium to another, due to the construction of the cable having multiple layers and materials. An acoustic signal propagating from one cable layer to the next, where the mediums possess different density and elasticity properties, will experience a reduction in the signal's energy due to reflection and refraction. Furthermore, the elastic properties (Young's modulus) and density of a

material directly influence the velocity of the acoustic wave. Sound travels faster through a medium with higher elasticity and lower density.

The relationship is shown in (2.2), where v is the signals velocity, E is the Young's modulus and ρ is the density.

$$v = \sqrt{\frac{E}{\rho}} \quad (4.2)$$

As previously illustrated in Chapter 2 Figure 2- 9, the MV cables used within the applicable umbilicals comprise of; a metallic conductor, inner semi-conducting layer, insulation, outer semi-conducting layer, copper screen/shield and an outersheath. As highlighted previously, the materials used may vary slightly depending on cable design and supplier, however the focus of this research has been on cables manufactured with the materials shown in Table 4- 1, all of which having different material properties and thus different sound velocities.

The propagation of an acoustic wave in a solid is much more complex than in liquids and gases. Nazarchuk et al. discuss these complexities, noting that solids possess not only the volume elasticity, as with liquids and gases, but also the elasticity of their shape (shear elasticity) and thus introducing the concept of stress [110].


<i>Layer No. (outer to inner)</i>	<i>Cable Layer</i>	<i>Material</i>	<i>Cable Cross Section</i>
1	Outersheath	Polyethylene	
2	Screen/Shield	Copper Tape	
3	Outer semi-con	Ethylene based polymer inc. carbon black or graphite	
4	Insulation	XLPE	
5	Inner semi-con	Ethylene based polymer inc. carbon black or graphite	
6	Conductor	Copper Strand	

Table 4- 1: Cable Cross Section and Material

The wave equation for a solid is derived using Newton's second law of motion, for the displacement of u ; where ρ is density, u is particle shift from an equilibrium state and t is time.

$$\rho \frac{\partial^2 u_x}{\partial t^2} = \frac{\partial \sigma_{xx}}{\partial x} + \frac{\partial \sigma_{xy}}{\partial y} + \frac{\partial \sigma_{xz}}{\partial z} \quad (4.3)$$

From Hooke's law it is known that;

$$\begin{aligned} \sigma_{xx} &= \lambda \Delta + 2\mu e_{xx} \\ \sigma_{xy} &= 2\mu e_{xy} \\ \sigma_{xz} &= 2\mu e_{xz} \end{aligned} \quad (4.4)$$

where, λ and μ are the elastic moduli for the solid and Δ is the fractional change in volume, or dilatation.

Following substitution of the above gives;

$$\rho \frac{\partial^2 u_x}{\partial t^2} = \lambda \frac{\partial \Delta}{\partial x} + 2\mu \frac{\partial e_{xx}}{\partial x} + 2\mu \frac{\partial e_{xy}}{\partial y} + 2\mu \frac{\partial e_{xz}}{\partial z} \quad (4.5)$$

Considering the principle strain components and dilatation Δ the following is obtained;

$$\rho \frac{\partial^2 u_x}{\partial t^2} = (\lambda + \mu) \frac{\partial \Delta}{\partial x} + \mu \nabla^2 u. \quad (4.6)$$

where the Laplace operator is;

$$\nabla^2 = \frac{\partial^2}{\partial x^2} + \frac{\partial^2}{\partial y^2} + \frac{\partial^2}{\partial z^2} \quad (4.7)$$

Definition of the displacement vector $\mathbf{u}:(u,v,w)$ allows all coordinates to be written in one equation;

$$\rho \frac{\partial^2 \mathbf{u}}{\partial t^2} = (\lambda + \mu)\Delta \mathbf{u} + \mu \nabla^2 \mathbf{u}. \quad (4.8)$$

When PD occurs within the cables insulation, the acoustic wave propagates radially from the fault, firstly reaching the semiconducting layer and the conductor, where refraction or reflection occurs causing a reduction in wave energy depending on the medium's acoustic impedance. The longitudinal propagation of the acoustic signal travels far, however the signal will also reach a point of reflection/refraction due to radial propagation through the cable layers prior to reaching the acoustic sensor. The position of sensor is therefore key and where possible, it would be beneficial to couple the acoustic sensors to the semi-con layer, if positioned near the cable termination, in order to minimise the losses. Furthermore, Lundgaard discusses limitations in the detectable PD sensitivity levels in cables due to the sheath and armour layers reducing the acoustic coupling, therefore limiting detection levels of PD events to around 100pC and above [73]. This will differ depending on cable type and potential for air filled cavities between layers, however the relevant umbilical cables are typically unarmoured thus reducing this limitation. As the aim of this research is to establish a method for detecting and locating PD prior to complete breakdown, the discussed pC levels fall well within the sensitivity requirements.

Table 4- 2 shows the typical velocity and density of the materials within the discussed power cables. The velocity of sound in polyethylene varies depending on the material curing degree, therefore values for both high density and low density are shown to provide an indication of the potential speeds through the insulating and outersheath layers. Piche et al. demonstrates that the sound velocity increases linearly with density for PE samples with a density ranging between 0.92 and 0.96g/cm³ [111].

<i>Material</i>	<i>Density (g/cm³)</i>	<i>Longitudinal (m/s)</i>	<i>Shear (m/s)</i>
<i>Polyethylene (high density)</i>	0.957	2430	950
<i>Polyethylene (low density)</i>	0.92	1970	540
<i>Copper, annealed</i>	8.93	4760	2325
<i>Copper, rolled</i>	8.93	5010	2270
<i>Air @ 20°C</i>	0.0012	343	-

Table 4- 2: Sound Velocity through Cable Materials

As with varying wave types, the many cable layers resulting in changing mediums leads to a highly complicated propagation path. Further trials and analysis on detected PD signals will provide insight into the path of the signal, based on the m/s velocity in comparison to the figures shown in Table 4- 2.

4.4 Signal Velocity

In order to establish the through-cable velocity of the resultant AE signals, envelope and cross correlation analysis techniques can be employed. These same techniques are also applied within the localisation system to determine the TDoA between detected signals, therefore allowing the PD position to be calculated.

Envelope and cross correlation signal analysis techniques differ in methodology and consequently experience different effects from the signals spectral characteristics such as SNR, bandwidth and multipath, thus affecting the TDoA results and in turn the accuracy of the localisation system. As a result of this, an initial evaluation of both techniques was performed to develop a greater understanding of how they differ through analysis of the PD signal.

4.4.1 Envelope Analysis

The detected acoustic emissions from PD events result in rapidly oscillating time signals, as shown previously in Figure 4- 5. The signal's envelope relates to the amplitude of these oscillations as they change with time. Envelopes contain important signal information and are a commonly used analysis method for fault detection in rotating machines such as motors and gearbox's [112]–[114]. When considering PD occurrence, the envelopes of the detected signals enable the TDoA to be determined from the envelope peaks.

There are variations on the type of signal envelope such as analytic envelope, pre-envelope and nature envelope, with the analytic envelope based on the Hilbert transform being the most commonly used [115].

The Hilbert transform is used to calculate the analytic signal, whereby it shifts the phases of all frequency components in the original signal by 90°. The Hilbert transform does not affect the signal magnitude, only the signals phase. The positive frequencies are phase shifted by $-\pi/2$, whereas negative frequencies are phase shifted by $\pi/2$.

The Hilbert transform of signal $x_0(t)$ is given by (4.9), where $h(t) = 1/\pi t$.

$$\hat{x}_0(t) = \int_{-\infty}^{\infty} x_0(\tau)h(t - \tau)d\tau \quad (4.9)$$

The analytic signal $x_a(t)$ can then be directly calculated from the new signal $\hat{x}_0(t)$ and original time signals $x_0(t)$ using (4.10), where the magnitude of the signal then forms the signal envelope, as expressed in (4.11).

$$x_a(t) = x_0(t) + j\hat{x}_0(t) \quad (4.10)$$

$$a(t) = |x_a(t)| \quad (4.11)$$

Thrane et al discuss the practical uses and benefits of the Hilbert transform to produce an envelope representation of the signal, highlighting that removal of oscillations allows for a more detailed study of the signal envelope and with the resultant signal being of a positive function, it can be graphically represented on a logarithmic amplitude scale [116].

The discussed methodology was applied to an individual PD event from the previous trial detailed in Section 4.2, in order to obtain the analytic envelope of the AE signal. Figure 4-12 illustrates the original detected AE signal, along with the Hilbert transform and the subsequent envelope.

Within this research, the signal envelope will be used to determine the TDoA and therefore more than one detected emission is required to establish the time difference between peaks. Figure 4-13 displays the original AE signal and the resultant envelope from an individual PD event detected on Rx1 and Rx2, as well as the EM signal detected instantaneously on both sensors with the closest displaying the largest amplitude, as expected. Marker points depict the envelope peaks in relation to the sample number which can then be converted to time utilising (4.12), where n is the sample number and f_s is the sampling frequency.

$$t(s) = \frac{n}{f_s} \quad (4.12)$$

When focusing on the envelope of the signal detected on Rx1, it can be seen that the signal peak is not as clear as that detected on Rx2. The probable cause being multipath propagation from the reflected signal, as discussed previously in Section 4.2. Both multipath and unpredicted noise can lead to a signal with more than one envelope maxima, therefore making it difficult to determine the envelope peak to allow the TDoA to be accurately calculated. A bandpass filter can be used to suppress the noise and smooth the envelope, thus minimising imperfections. Figure 4-14 presents the same PD signal as the previous figure, having applied a 100th order FIR bandpass filter, whereby the passband was set to minimise the effects of environmental noise. Having smoothed the envelope peaks, a more obvious peak can be observed and as a result, a more accurate TDoA can be determined.

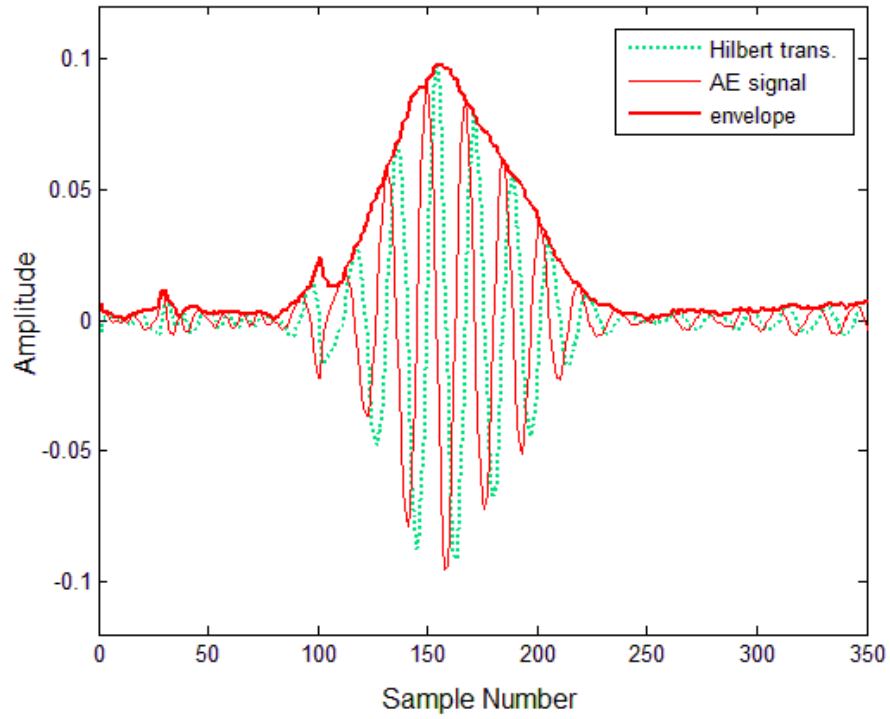


Figure 4- 12: AE Signal, Hilbert Transform and Envelope of Individual Discharge Measured at Rx2 (35m from fault)

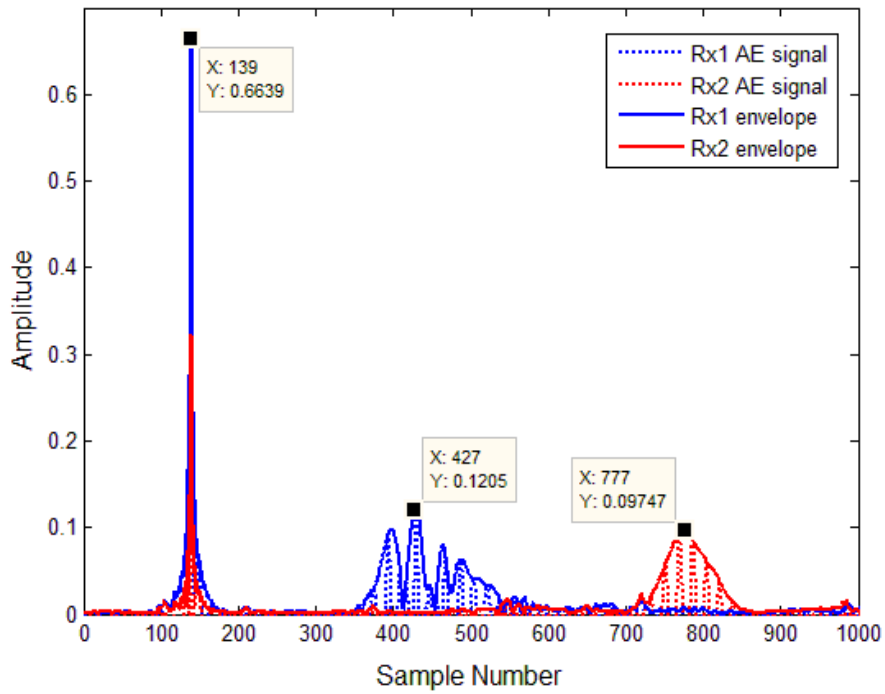


Figure 4- 13: AE Signal and Envelope of Individual Discharge Measured at Rx1 (14m from fault) and Rx2 (35m from fault).

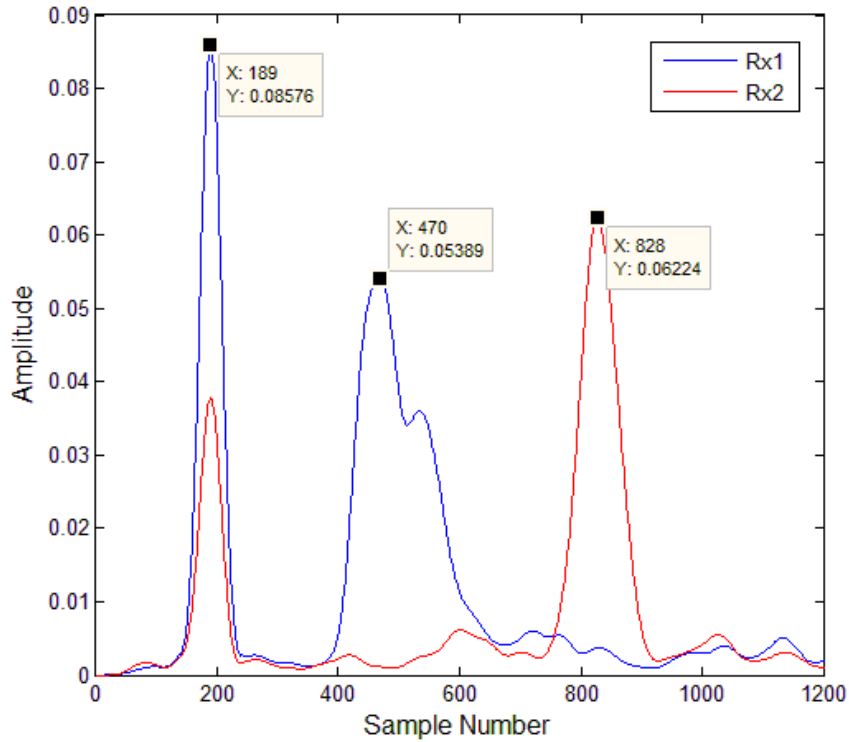


Figure 4- 14: Signal Envelope of Individual PD Event Detected on Rx1 (14m from fault) and Rx2 (35m from fault)

4.4.1.1 Calculated Velocity utilising Envelope Analysis Techniques

The signal velocity can be established from the previous test results as in this case, with results being from a trial, the distance between PD location and AE sensors is known and the TDoA can be determined through analysis of the detected signals.

The signal velocity v can therefore be calculated using (4.13) where d is distance from fault to acoustic sensor and t is TDoA between signals.

$$v = \frac{d}{t} \quad (4.13)$$

When considering the captured PD emissions from the trial, both the EM and AE signals were recorded for each discharge, therefore the EM signal can be considered as the PD time of occurrence and thus the time difference between the envelope peaks from the EM and AE signals can be applied to (4.13) to determine the velocity.

Focusing on Figure 4- 14, there is an offset of 281 samples between the EM signal and the AE signal detected on Rx1, therefore utilizing (4.12) and considering a sampling frequency of 44.1kHz, the time taken for the AE signal to propagate from the discharge location to the receiver Rx1 is 6.37ms. As the distance from PD location to Rx1 is known to be 14m, the velocity is calculated to be 2198m/s. Repeating this process for the AE captured at Rx2 provides an offset of 639 samples and therefore a time delay of 14.49ms from PD occurrence to detection at receiver Rx2. The distance from PD location to Rx2 is known to be 35m and so the velocity is calculated to be 2415m/s. As these calculations are focused on an individual PD event, the method was repeated on the remaining emissions captured from the same trial, each showing very similar values to those calculated with the average velocity at Rx1 being 2202m/s and the average at Rx2 being 2421m/s.

The calculated signal velocity differs slightly between the AE signal detected on sensors Rx1 and Rx2. This is likely caused by the discussed distortion from the reflected signal, along with the changing propagation path of the acoustic emission as the signal propagates along the length of the cable and through the varying layers. The data collected from this initial trial is not sufficient to determine how the velocity changes with length as it is based on only two sensor positions, however it does provide an approximate through-cable propagation velocity of 2202-2421m/s, therefore giving a good indication as to the propagation medium and wave type of the signal. Considering an average velocity of 2312m/s, and based on the values specified in Table 4- 2, the captured signal may have travelled as a shear wave through the copper conductor or a longitudinal wave through the high density polyethylene, with the latter being more likely based on the coupling of the sensors on the cables outersheath.

4.4.2 Cross Correlation Analysis

An alternative method for establishing the TDoA is to analyse the cross correlation of the AE signals detected following the occurrence of PD. Cross correlation is a measurement of similarity between two functions, f and g , where the time series differs. The process involves repeatedly shifting one signal in time against the other, whilst calculating a correlation value for each increment. When a match occurs between functions f and g , the correlation value ($f \star g$) is maximised, resulting in a large peak at this specific point relative to the time delay between the signals. The cross correlation of functions f and g of variable t is defined by (4.14), where \bar{f} denotes the complex conjugate of f .

$$f \star g = \bar{f}(-t) \star g(t) \quad (4.14)$$

Considering the test performed in Section 4.2, the signal detected on Rx2 is for the most part a delayed version of that detected on Rx1, therefore it is expected that there will be a

clear correlation peak due to the strong similarities in signals. Figure 4- 15 presents the cross correlation of the two AE signals from one individual PD event captured at receivers

Rx1 and Rx2. The highest correlation coefficient relates to the best match between the two signals, whereby the lag value at this point divided by the sampling frequency provides the time period by which one signal leads or trails the other. If the signals were detected simultaneously, the highest correlation peak would be central, showing zero lag. Figure 4- 15 presents a clear correlation peak at -376, however a smaller second peak is also visible at around -290. This second peak is likely caused by the presence of multipath within the signal, as identified earlier, in addition to the inherent complexities of the propagation path.

As the resultant AE signals have been identified as broadband, cross correlation is a favorable method for signal detection as signals with higher bandwidth have a narrower autocorrelation peak, therefore principally making them easier to detect, as illustrated by Adrian-Martinez et al. [117]. The width of the correlation peak is inversely proportional to the bandwidth of the signals being analysed, thus making it a highly accurate method for establishing the TDoA of the detected AE signals.

Due to the comparative methodology of cross correlation, the process is exceptionally useful in low SNR situations and over long distances where the signal is weak, which is the expected scenario for the proposed PD localisation system. Figure 4- 16 displays an individual PD event with and without added noise, along with the cross correlation results

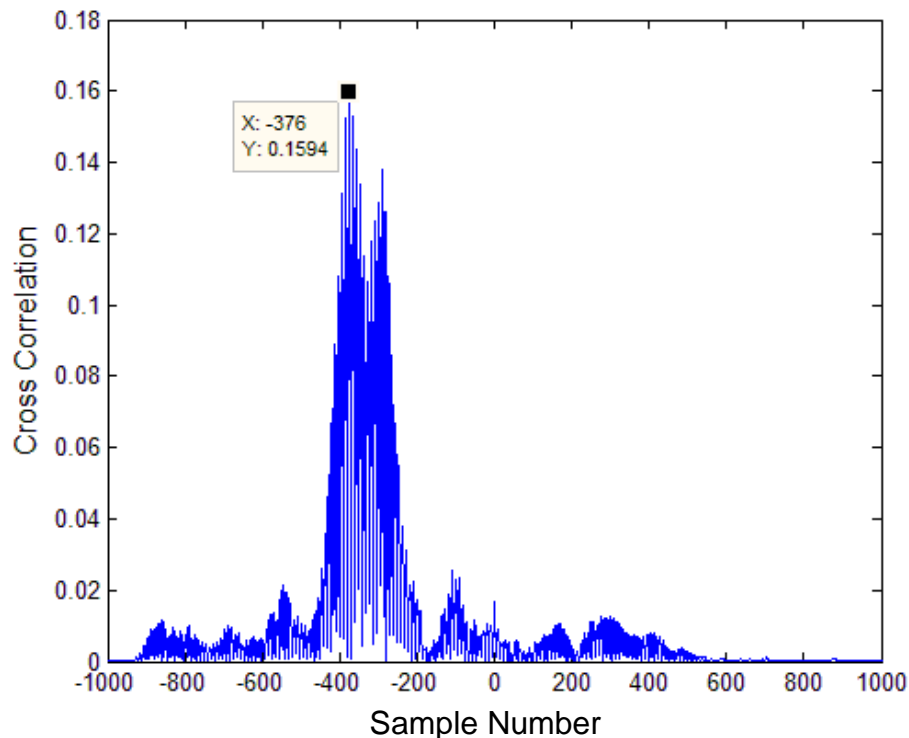


Figure 4- 15: Cross Correlation of Individual PD Event from Rx1 (14m from fault) and Rx2 (35m from fault)

for each case. This demonstrates that the cross correlation in both cases provides the same result for the correlation peak, thus confirming the ability of this analysis technique, even in instances where it is difficult to visibly identify the signal within the background noise. In this example, white gaussian noise was added to the PD signal to provide an SNR of 3dB and although the resultant cross correlation trace is less clear, the correlation peak remains identifiable at the same position as the correlation trace from the original signal with no added noise. More detailed evaluation of the systems allowable SNR follows in Chapter 5, Section 5.3.4.

In addition to cross correlation, the autocorrelation function is often used to provide information about the similarity of a signal in a given time series against a delayed version of itself i.e. a method for measuring the relationship between current and past values. When considering an energy based waveform of finite duration, such as that from PD, (4.15) can be considered where the waveform exists between $t_1 \leq t \leq t_2$;

$$\rho_{ff}(\tau) = \int_{t_1}^{t_2} f(t)f(t + \tau)dt \quad (4.15)$$

Focusing on the recorded AE signals from an individual PD event, Figure 4- 17 presents the autocorrelation for the signal detected on Rx1 (a) and on Rx2 (b). As formerly discussed, the width of the signals spectrum relates to the width of the autocorrelation function, whereby a narrow autocorrelation equates to a broad spectrum, and a broad autocorrelation equates to a narrow spectrum. The figure shows a narrow autocorrelation, thus confirming the broadband nature of the AE signal. It can be seen, however, that the autocorrelations differ and although it has been established that the frequency content and amplitude changes with distance, the main cause of this dissimilarity is likely due to multipath being present in the signal detected on Rx1. Many PD events from the same trial were analysed with all showing similar results as the position of the sensors remained consistent throughout, therefore experiencing effects of multipath in each trace for those signals recorded at Rx1. Evaluation of the changes in the signals characteristics with distance is further assessed in Section 4.5.

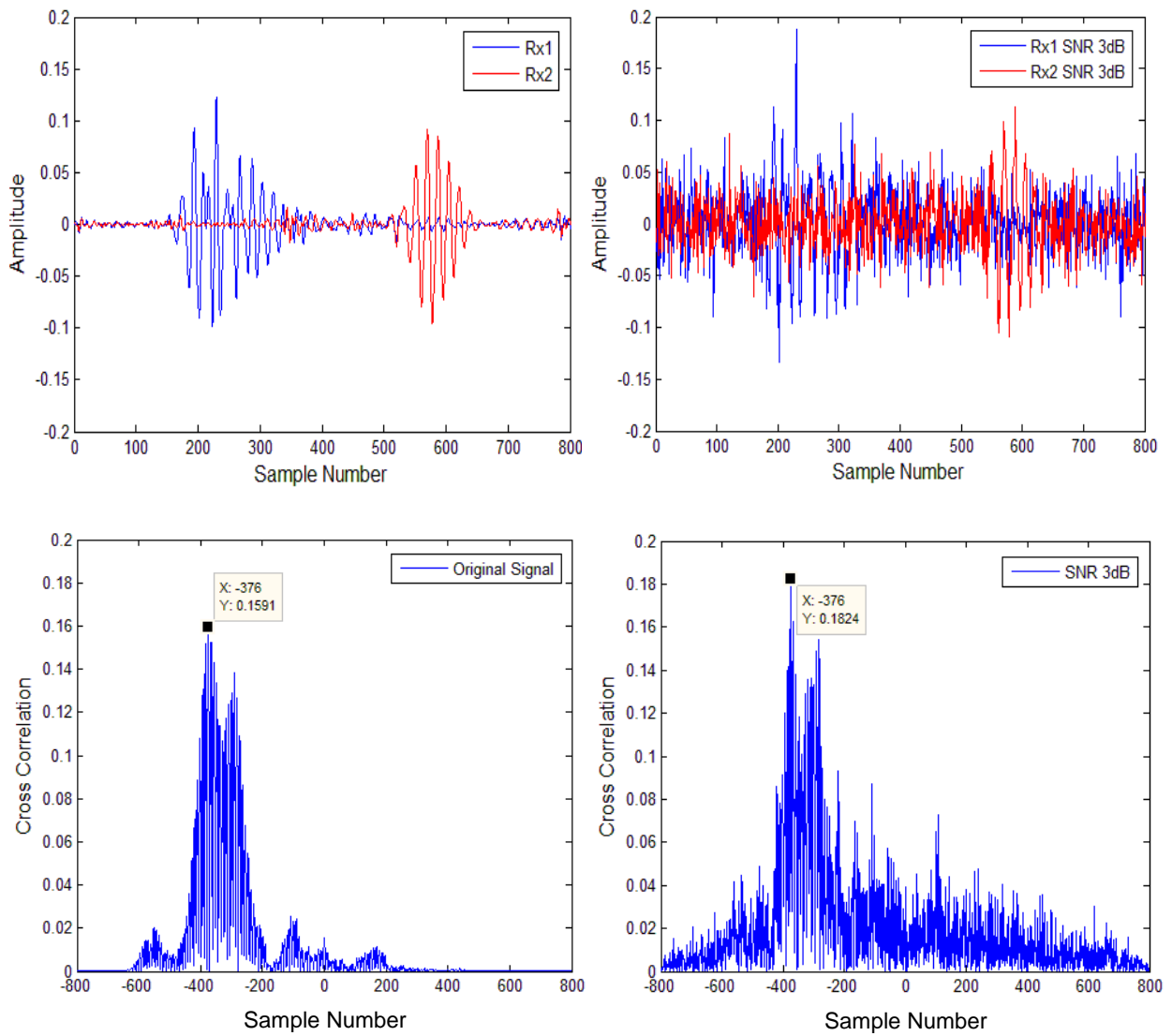


Figure 4- 16: Individual PD Event – Comparison of Original Signal against Signal with Added Noise providing a SNR of 3dB (time domain and cross correlation analysis)

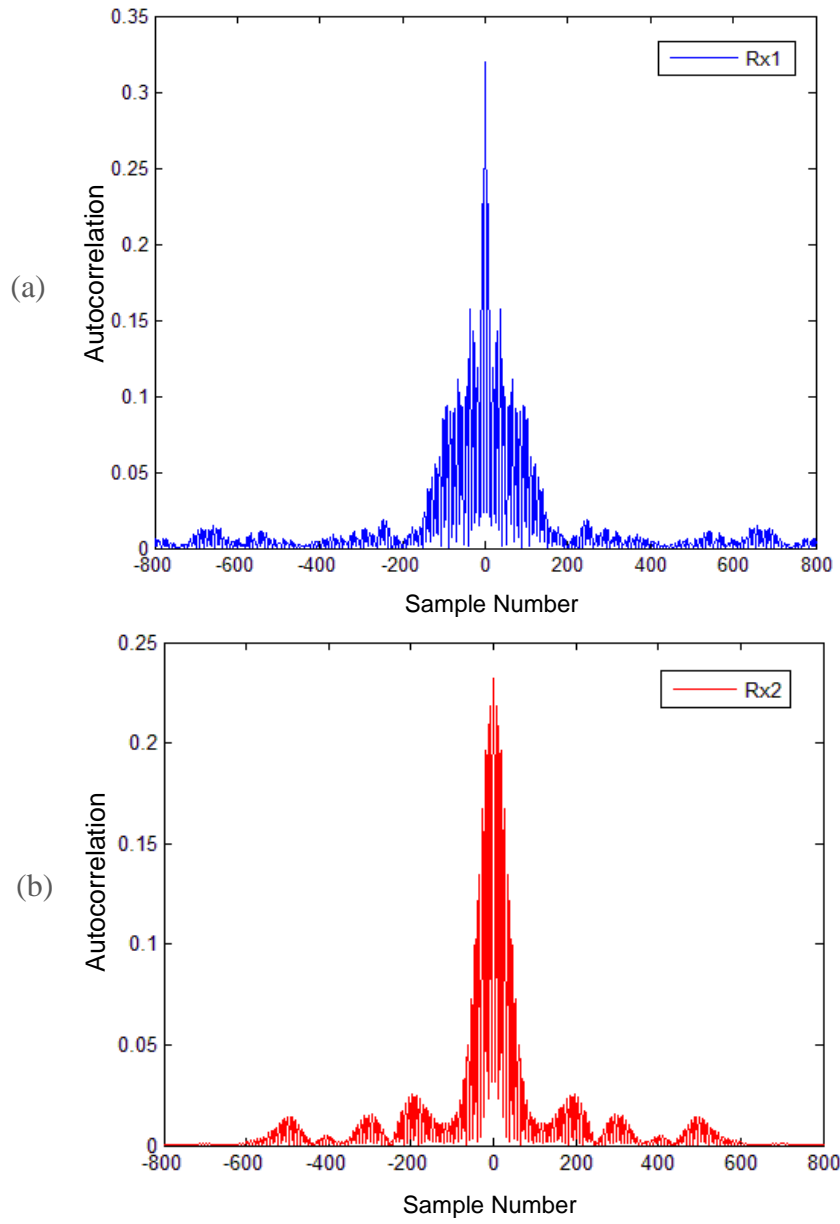


Figure 4- 17: Autocorrelation of Individual PD Event (a) Rx1 14m from fault, (b) Rx2 35m from fault

4.4.2.1 Calculated Velocity utilising Cross Correlation Techniques

As with envelope analysis, cross correlation can in this case be used to establish the velocity of the AE signal. Considering the cross correlation results showed in Figure 4- 15, the correlation peak can be seen at -376, which corresponds to the additional time taken to reach Rx2 over Rx1. The difference in distance between the sensor positions is known to be 21m, therefore by applying the methodology of (4.16) the signal velocity can be calculated to be 2463m/s, where; d relates to the distance between sensors, lag is the position of the correlation peak and f_s the sampling frequency.

$$v = \frac{d_2 - d_1}{\left(\frac{lag}{f_s}\right)} \quad (4.16)$$

Again, multiple discharges were evaluated where cross correlation results showed slightly more variation with velocities ranging from 2405m/s to 2470m/s. The overall results however, were comparable to those calculated from the envelopes of the signals detected on Rx2.

It should be noted that the cross correlation results were calculated using the AE signals only, whereas the envelope velocities were calculated utilising both the EM and AE signals whereby the EM signal was considered as time of PD occurrence. The initial trial has indicated that the velocity changes with distance, however the cross correlation results cannot be used to analyse this effect as the velocity calculated is based on the time delay between sensors Rx1 and Rx2, as opposed to individual results. Further testing and analysis discussed in 4.5 considers the effects of distance travelled on the signals velocity.

4.5 Effects of Propagation Distance on AE Signal

Results from previous tests, along with supporting research, shows that the distance the signal has travelled from the PD location to AE sensor has an effect on many aspects of the detected signal such as, the frequency content of the signal, the pulse width, the signal strength and the propagation velocity. Performing a similar test to that detailed in Section 4.2, but on a longer cable sample with an increased number of sensor positions, would allow these effects to be further investigated to develop a more comprehensive understanding of the changing signal characteristics due to the propagation distance. Having results from multiple sensor positions provides valuable information on the effects of the complex propagation path and allows for more accurate localisation as the changes in velocity will be better understood.

4.5.1 Experimental Test: PD Propagation – Varying Sensor Positions

A cable sample of approximately 100m was used for this test with the cable type being the same as previously tested in Section 4.2. Again, a fault was introduced to the cable sample to ensure PD would take place and both cable ends were prepared for HV testing. As with previous tests, the PD inception voltage was unknown due to the nature of the fault, therefore the HV was applied in gradual increments until PD occurrence began and the discharges were detected through the AE sensors Rx1 and Rx2 coupled to the outersheath of the cable.

As the changes with distance are of significant interest, multiple tests were performed with the position of Rx2 moved in 5m increments. Figure 4- 18 illustrates the key positions of the sensors and fault location. AE sensor Rx1 remained at a fixed position of 35m from the fault throughout all tests, whereas Rx2 was moved away from the fault in 5m increments for each test performed, ranging from 5m to 55m, as shown in Table 4- 3.

<i>Test Number</i>	<i>Rx1 Position (m)</i>	<i>Rx2 Position (m)</i>
<i>1</i>	35	5
<i>2</i>	35	10
<i>3</i>	35	15
<i>4</i>	35	20
<i>5</i>	35	25
<i>6</i>	35	30
<i>7</i>	35	35
<i>8</i>	35	40
<i>9</i>	35	45
<i>10</i>	35	50
<i>11</i>	35	55

Table 4- 3: Trial to Evaluate the Effects of Propagation Distance – Sensor Positions

The methodology and equipment setup was as per previous test detailed in Section 4.2, with the only changes being the cable sample length and receiver positions, as shown on Figure 4- 18. Again, one minute recordings were taken of the PD occurrence at each sensor position. Testing was performed at TechnipFMC R&D Centre, photos of which can be seen in Figure 4- 19.

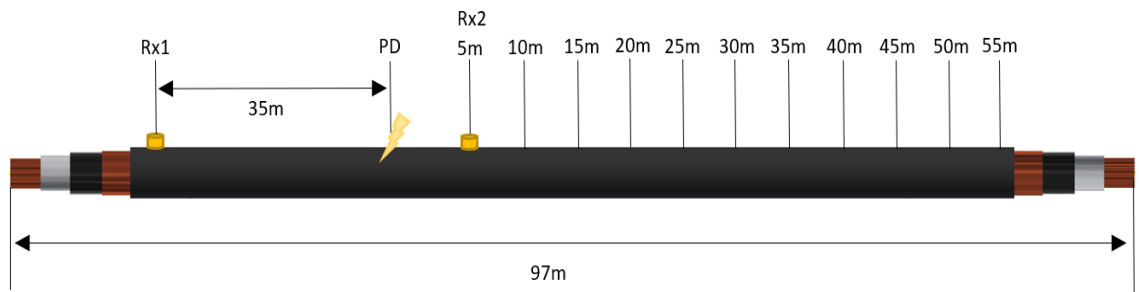


Figure 4- 18: Cable Sample Illustration Defining Fault and Sensor Positions

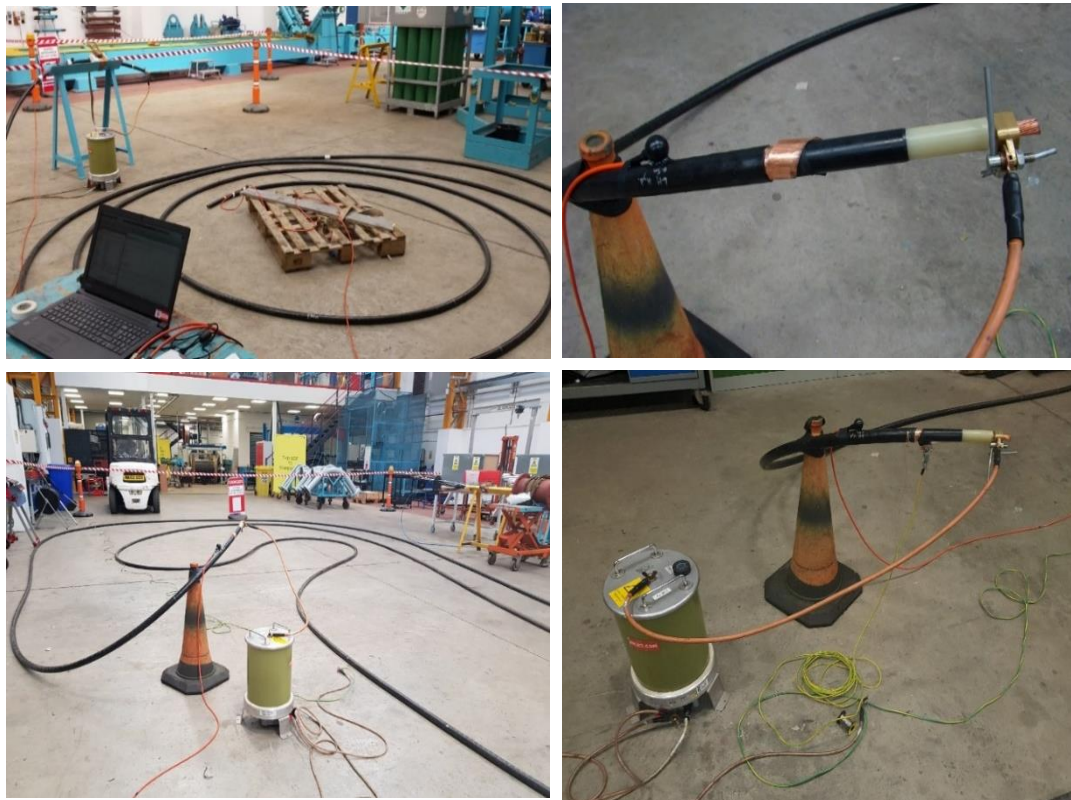


Figure 4- 19: Cable Sample Test Setup at TechnipFMC R&D Facility – PD Sensing 5m Increments

4.5.2 Results and Discussions

One minute recordings were taken for all of the eleven tests performed, therefore multiple PD events were recorded for each Rx2 position. The fault was reinstated numerous times throughout the test due to complete breakdown of the discharge area. Section 4.4 highlighted that cross correlation is not the most suitable method for evaluating the changes in velocity with distance as it relies on two signals from varying sensor locations to provide the one positioning result. Envelope analysis was therefore selected for this evaluation, whereby the TDoA was established between the individual AE signal and the detected EM signal as this requires data from only AE sensor, thus allowing clear evaluation of the effects with distance. Having the data from the fixed sensor position, Rx1, allows for localisation once the velocity has been determined as, in reality, the fault position would not be known therefore two sensors are required to prove the systems methodology.

Results from Figure 4- 20 present the envelope of a single PD event from each test, including the EM signal at the beginning of each trace. Rx1 signal envelope maintains

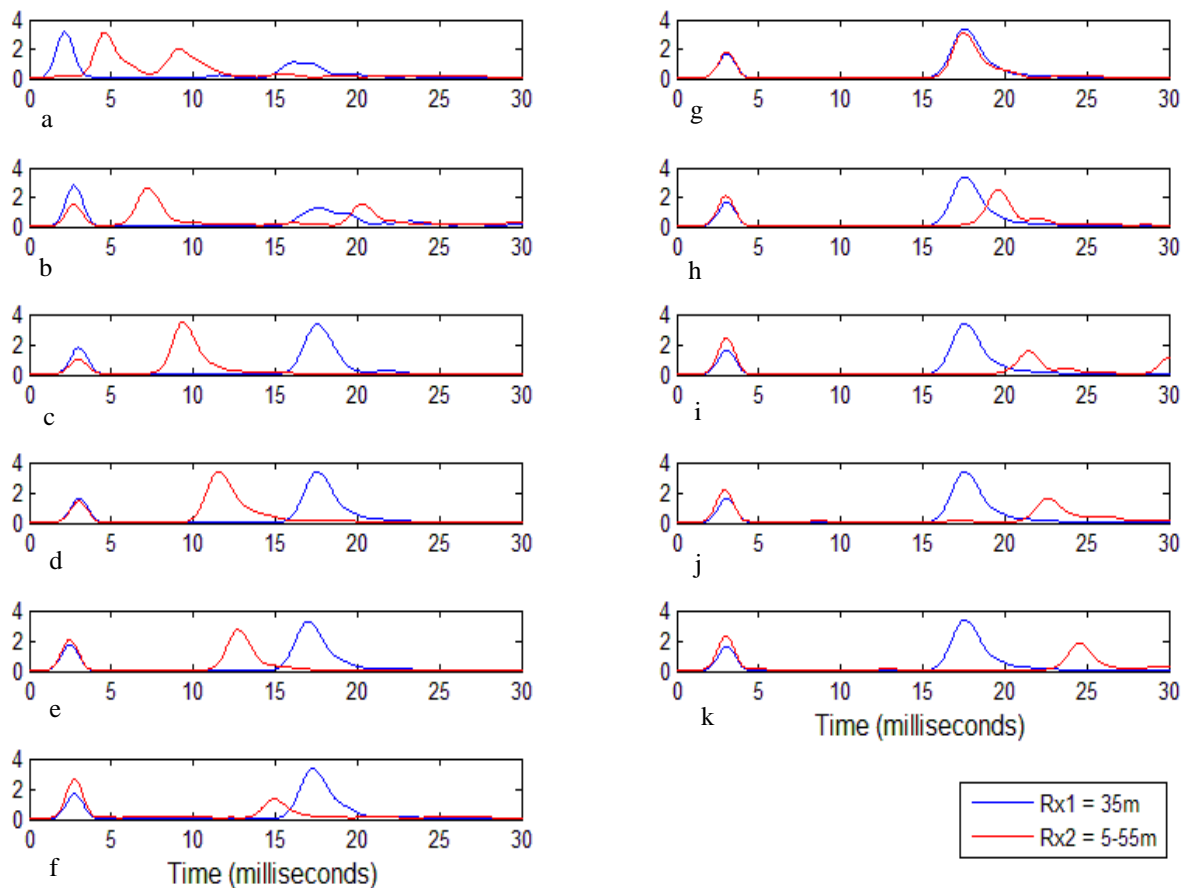


Figure 4- 20: Signal Envelopes – Rx1 35m from Fault, Rx2 5m to 55m from Fault ‘a’ through to ‘k’.

consistency throughout based on the fixed position of the AE sensor. The signals have been normalised to ease comparison as the amplitudes are not key in this evaluation due to each capture being from a separate test and therefore of a separate discharge, thus displaying differing signal energies based on the magnitude of the PD, as opposed to the position of the sensor.

Results from the initial test with Rx2 located 5m from the fault were problematic due to the fault region being in such close proximity to the sensor, causing multiple peaks to be detected and some masked by the initial EM signal. As expected, the time difference between the EM and Rx2 peak increases with distance from the fault location. The peaks of the signals can again be used to calculate the propagation speed based on the TDoA at Rx2, considering the EM signal as the time of PD occurrence.

Table 4- 4 shows the calculated velocities based on 4 discharges from each test, with plotted results displayed in Figure 4- 21. Test results confirm that the propagation speed varies as the signal travels through the length of the cable, showing a gradual increase until around 25m from the fault where the velocity begins to stabilise. Results range between 2427-2457m/s for distances 25-55m, giving an average speed of 2442m/s. This value coincides

<i>Distance of Sensor from Fault (m)</i>	<i>AE Velocity 1 (m/s)</i>	<i>AE Velocity 2 (m/s)</i>	<i>AE Velocity 3 (m/s)</i>	<i>AE Velocity 4 (m/s)</i>	<i>Average Velocity (m/s)</i>
5	2005	2042	2061	2005	2028
10	2216	2216	2216	2239	2222
15	2352	2297	2354	2338	2335
20	2385	2375	2372	2380	2378
25	2450	2445	2445	2434	2444
30	2444	2438	2444	2442	2442
35	2427	2423	2433	2425	2427
40	2422	2428	2431	2427	2427
45	2441	2441	2435	2437	2439
50	2460	2458	2455	2455	2457
55	2458	2460	2455	2452	2456

Table 4- 4: Through-cable Signal Velocity 5m-55m from PD Location

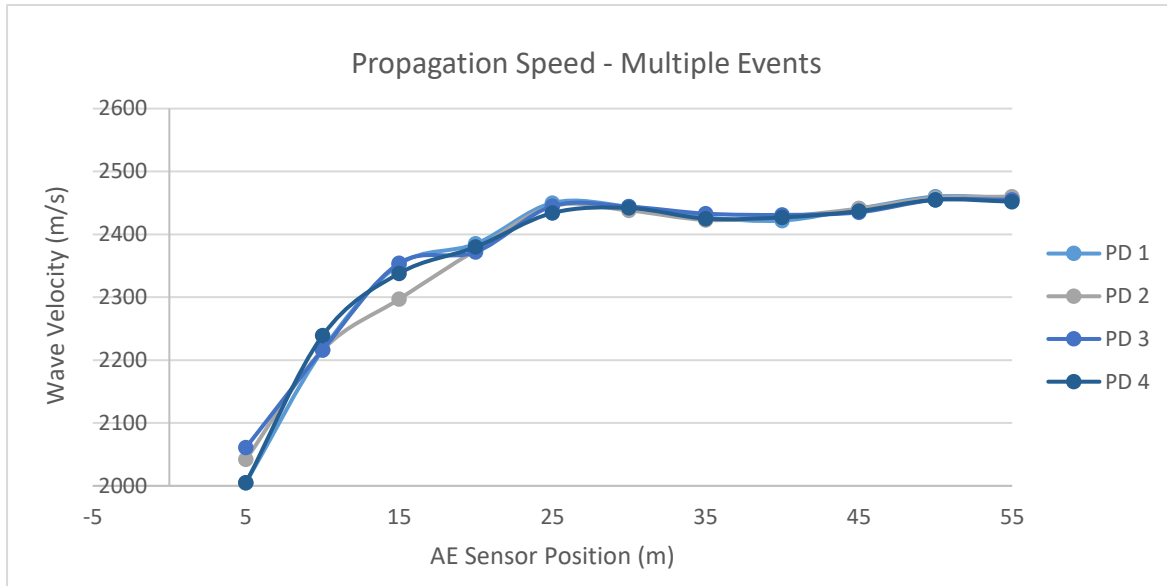


Figure 4- 21: Plot of Through-cable Signal Velocity Results, 5m-55m from PD Location, multiple PD events

with results from Section 4.4 where speeds of approximately 2400m/s were obtained. In addition, it can be seen that there is greater variation in the results below 20m, prior to the signal velocity stabilising. This would lead to a greater tolerance on the estimation of the fault position if the discharge were to occur within this region ($\leq 20\text{m}$).

The overall change in signal speed is predominantly due to the dispersion of the acoustic emission from the discharge location through the varying mediums, where the resultant velocity is in line with that of a longitudinal wave propagating through high density polyethylene, comparable to the outersheath of the cable to which the AE sensor is coupled.

To further evaluate the change in the signals characteristics with distance, results from two tests were analysed, comparing signals from sensors positioned closest and furthest from the fault, thus showing the greatest contrast. Results from the 5m test were unclear, as discussed previously, therefore the 10m test results were utilised for the closest position, along with the 55m results for the furthest position. Figure 4- 22 presents a comparison of the AE signals detected at Rx2 during the 10m and 55m tests. The figure displays a comparison of the captured acoustic emissions, along with the envelope of the signals and the equivalent FFT's. A difficulty arises in that the discharges being compared differ due to the nature of the test. A true comparison would require multiple sensors to be positioned at 5m increments to allow a single PD event to be recorded on each. From literature it is known that with distance the pulse width increases and signal amplitude decreases, however the reduced amplitude shown in Figure 4- 22a and Figure 4- 22b could be due to a smaller discharge energy rather than the propagation distance as differing PD events are being analysed. Nonetheless, multiple discharges were analysed and the amplitude was

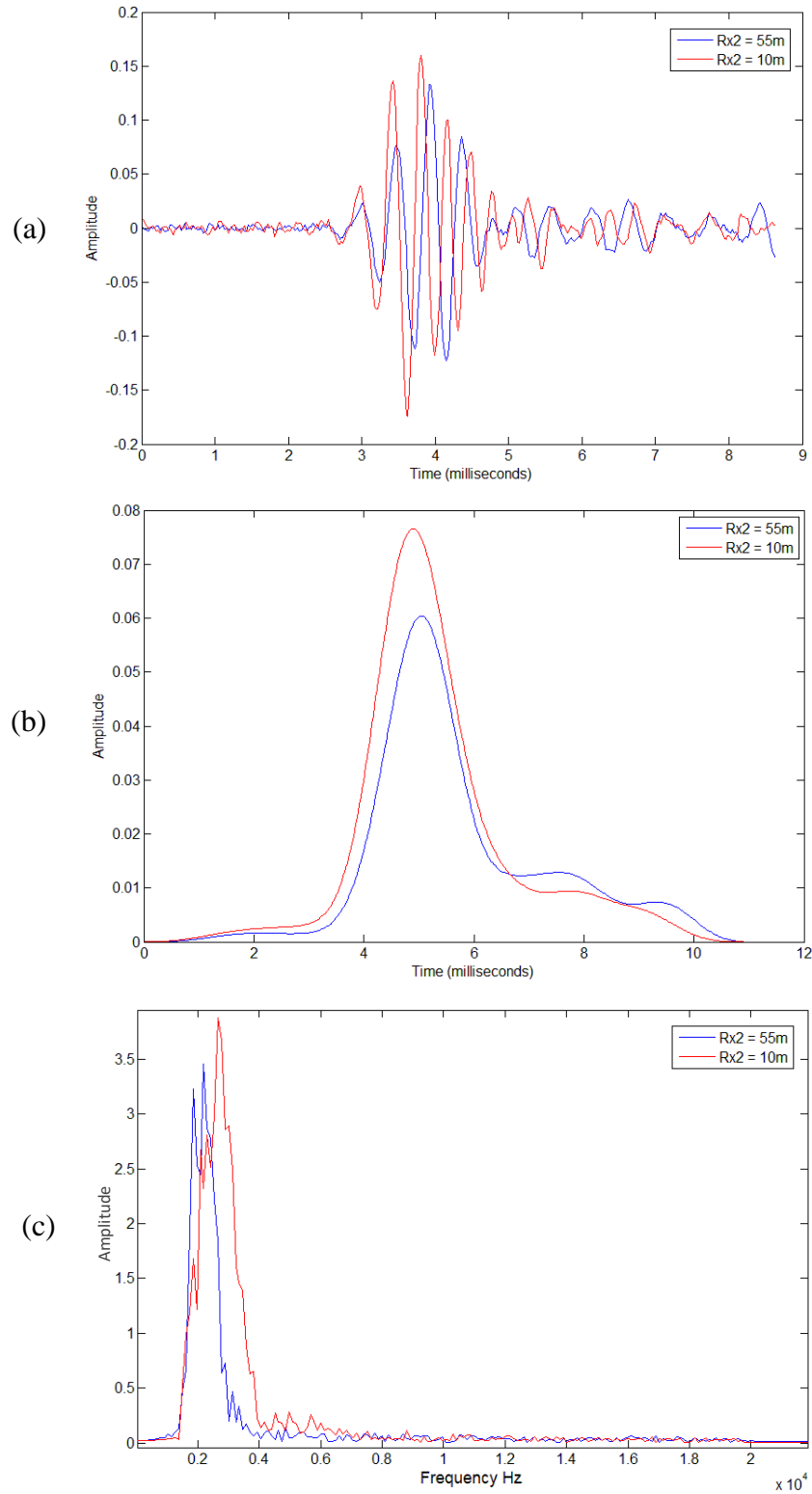


Figure 4- 22: Signal Analysis Rx2 10m and 55m from Fault Location. Individual Discharge (a) time domain, (b) signals envelope, (c) FFT

consistently less at 55m than at 10m from the fault, therefore suggesting that the reduced amplitude is in fact due to the increased propagation distance. Figure 4- 22c displays a clear change in frequency content between the two signals, revealing attenuation of the higher frequency components with distance travelled. Again, this finding was consistent throughout the multiple discharges evaluated and is as expected, confirming the focus on the lower frequency components due to the long distance requirements of the sensing system.

4.6 Comparative Electrical PD Energy

In order to understand the severity of the PD being detected acoustically, an additional trial was performed utilising conventional PD detection methods. This would allow an assessment to be made as to the condition of the insulation and also provide further backing to the feasibility of AE detection. Conventional electrical methods are used for PD detection, rather than localisation, however the focus of this trial was to gain an understanding of the detected AE from PD in relation to the detected electrical charge in coulombs. Typically, the condition of a cable is assessed by the measured pC level, considering both the average peak PD and average PD activity. The average peak value relates to the magnitude of the PD and the average activity relates to the intensity of the PD and is calculated by the magnitude of PD * number of PD pulses per power cycle. A key aim of the test was to have a reliable value for the magnitude of the PD which was able to be detected acoustically to understand the capability of the AE system in relation to the fault severity.

The test was performed on a 30m section of the same MV cable type as previous trials, whereby a fault had again been introduced using the same methodology. Figure 4- 23 shows a simplified block diagram of the test setup, including both electric and acoustic detection methods.

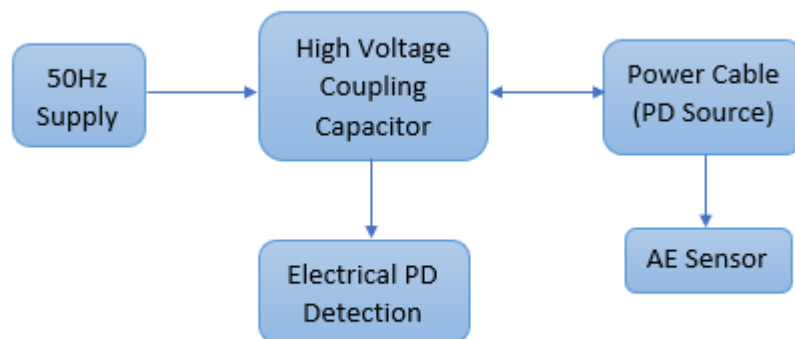


Figure 4- 23: Simplified Block Diagram - Comparative Electrical PD Test

The cable sample was connected to the 50Hz HVAC supply and the electrical PD detection equipment HVPD Kronos®, which was hired from HVPD, a company who specialise in PD monitoring solutions for various sectors. As the purpose of this test was not related to the localisation of the discharge, only one acoustic sensor was required and positioned approximately 10m from the fault location. There was however, a lot of noise present on the detected signal during pre-test calibration and so an additional sensor was used as a reference signal for the noise and was positioned free from the cable undergoing test. The sensor being used for PD detection was bonded to the cable sample to minimise signal losses.

Figure 4- 24 displays images from the test, showing the cable sample, High Voltage Coupling Capacitor (HVCC), HVAC supply equipment and the acoustic monitoring setup. Space was limited in the test container therefore the cable sample was coiled and positioned on tressels to raise the sample off the floor. In addition, insulating material was used at all cable touch points to minimise vibrations from external sources. The AC voltage was applied in incremental stages, with continuous PD monitoring from traditional electrical methods, as discussed.

Figure 4- 25 presents the average peak PD and average PD activity at each voltage increment. The PDIV occurred between 4kV and 4.5kV and complete breakdown occurred after being held at 10kV for a short period of time. Each PD event emits different levels of energy, therefore the rise in magnitude does not directly correlate to the voltage increase as is heavily dependent on the characteristics of the fault, however, it can be seen that the average magnitude of the discharges (average peak PD) typically increases with each voltage increment, with a greater increase when nearing complete breakdown. It can also



Figure 4- 24: Comparative Electrical PD Test Setup – Acoustic and Electrical Monitoring

be seen that the average peak PD activity increases exponentially with the voltage increments, as both the average magnitude and number of PD pulses grows more rapidly when nearing the breakdown voltage.

During the test, at each incremental voltage period, 1minute acoustic samples were recorded and analysed to look for detected PD emissions. It was known through electrical detection that PD was present from around 4.5kV upwards, however acoustically PD could not be detected until around 9-10kV. The voltage levels however are not the main interest as this is highly dependent on the fault itself and can differ in each instance. It is the pC level which is key, hence the need for the electrical detection for comparative assessment.

A number of discharges were identified within the traces recorded at >9kV. Figure 4- 26 presents one of the detected AE events from PD occurrence at around 10kV. The red trace shows the reference signal and allows the noise to be clearly identified as this occurs instantaneously on both traces, whereas Rx1 shows the detected acoustic discharge which was only detectable by the sensor bonded to the cable sample. The characteristics of the detected signal also match those analysed in earlier trials. At the time of detected acoustic emissions from PD, the average pC readings were around 25.5pC peak PD and 837pC/cycle of PD activity. This provides an insight to the magnitude of the PD events which can be detected utilising these acoustic techniques. The conditions during test were more onerous than in real life application, as the stresses were increased rapidly to create a breakdown over a short timeframe. In normal operation, the voltage would be maintained and the pC levels would increase over time as the insulation degraded. If monitored continuously, the corresponding pC activity levels detectable acoustically are just below

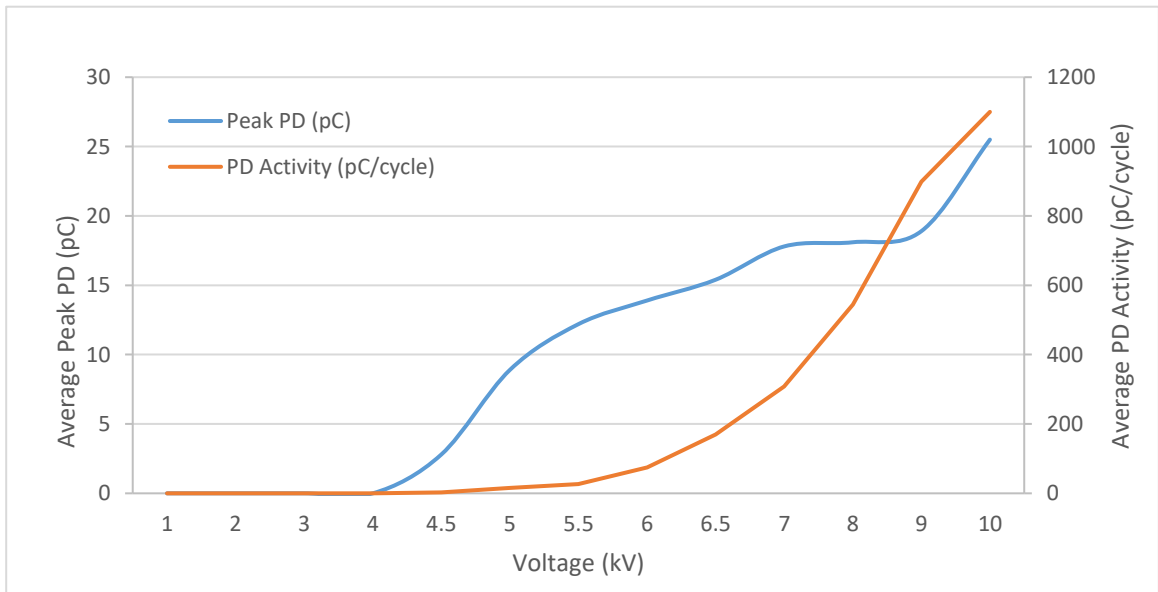


Figure 4- 25: Average Peak PD and Average PD Activity at varying Voltage Increments

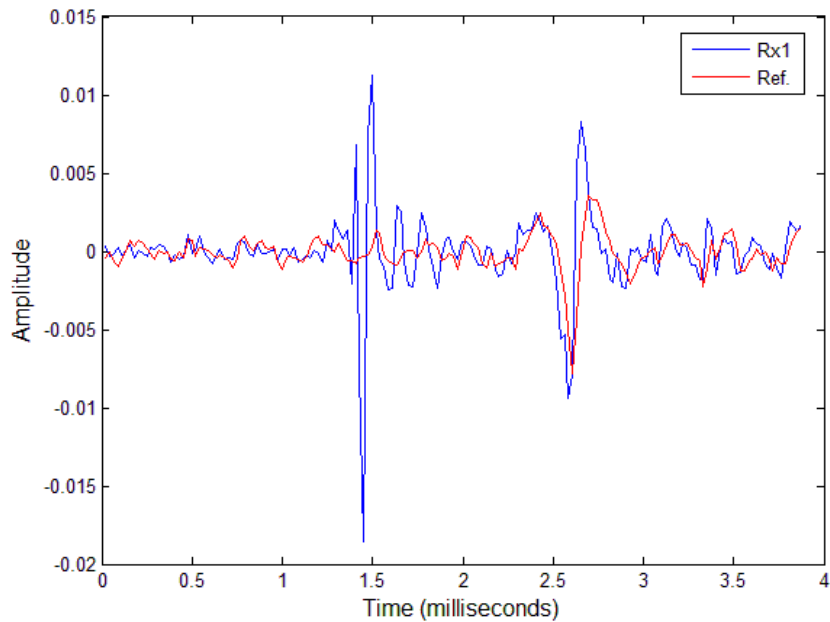


Figure 4- 26: Acoustic Emission from PD occurring at approximately 10kV

those which indicate a potential risk whereby increased monitoring and evaluation be required, as per typical allowable pC levels discussed in Section 3.1.3. This provides confidence in the capability of the system as acoustically detection is achievable at a low enough level to allow intervention or adjustments prior to complete failure of the cable.

In addition to the average peak PD and average PD activity, the HVPD Kronos® electrical test equipment was able to confirm that the PD being detecting was from a void within the insulation, rather than corona at the surface, or cable ends. This was done through their analysis of the Phase Resolved Partial Discharge (PRPD) pattern, which is a representation of the PD apparent charge, Q , versus the phase angle of the applied voltage, ϕ , including information of the count of PD pulses. The pattern shown in Figure 4- 27 is taken from the test and is characteristic to that of an internal void as opposed to surface discharges. The electric field in a void follows the sinusoidal nature of the voltage waveform, therefore resulting in a curved PRPD pattern. Furthermore, the electric field on the surface of the void is symmetrical, therefore the PRPD pattern of the void discharge at both positive and negative cycles of the applied voltage are also symmetrical, unlike the PRPD patterns for surface discharges, which are not symmetrical because the electric field at the material surface during positive and negative cycles is not symmetrical [118].

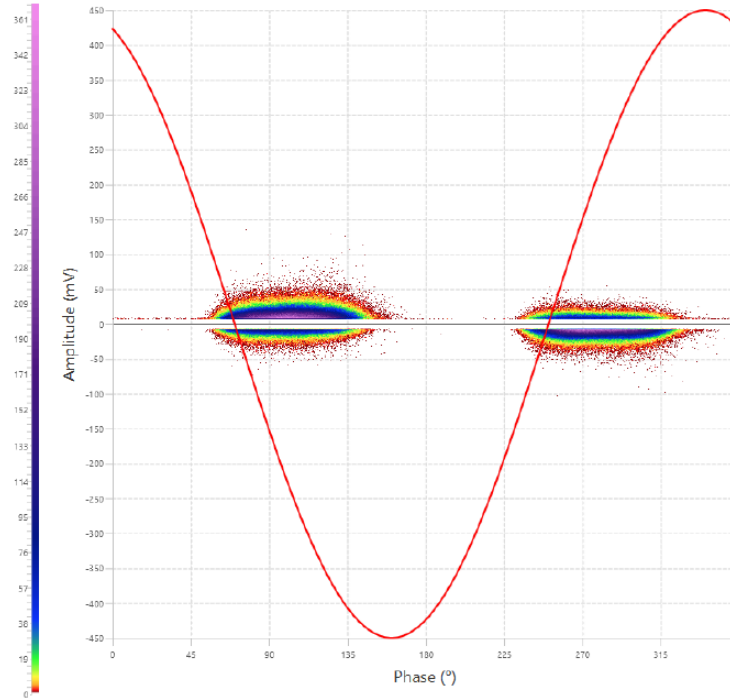


Figure 4- 27: PRPD Pattern indicative of Internal Void PD utilising HVPD Kronos®

4.7 Summary

This chapter has investigated the through-cable propagation of the acoustic signal emitted from partial discharge within a cables insulation. The characteristics of the resultant AE signal have been evaluated and the effects of propagation distance assessed through both literature and experimental testing.

Early testing confirmed that the spectrum is dominated by the frequency response of the channel rather than the emission itself and the signal changes as it propagates along the cable length. Detected signals were broadband with the main signal energy being below 5kHz. Both the AE and EM signals were detected, therefore permitting the EM signal to be considered as time of PD occurrence, thus aiding the evaluation of changes in signal properties with distance.

The complexities of the propagation path have been discussed, highlighting the varying wave types and propagation mediums through which the signal will travel, all having an effect on the characteristics of the signal, in particular the signal velocity.

Envelope and cross correlation analysis methodologies were evaluated with the impacts of multipath and noise being discussed, whereby the benefits of cross correlation in low SNR and long distance situations were emphasised.

Further testing on a longer length cable sample confirmed a clear change in signal velocity due to distance travelled. The propagation speed gradually increased until it reached around 25m from the fault location, whereby it then stabilised at a speed of approximately 2442m/s. This velocity coincides with the speed of sound propagating through high density polyethylene which is the material of the cables outersheath to which the AE sensor is coupled. Through comparative evaluation of results from varying sensor positions, testing also confirmed a reduction in signal amplitude and attenuation of higher frequency components through increased propagation distances.

Comparative testing allowed the average pC levels of the detected acoustic emissions to be evaluated through both electrical and acoustic detection of PD. Acoustic discharges were detected once the voltage was increased past 9kV, where the average peak PD was measured at around 25.5pC and the average activity at around 837pC/cycle. This comparative assessment provides an understanding of the severity of the PD which is able to be detected through acoustic means, thus providing confidence that the through-cable sensing system is able to detect PD prior to critical condition of the insulation.

Chapter 5

Through-cable Source Localisation

This chapter details how captured acoustic signals from partial discharges can be utilised to determine the location of the fault through TDoA and TDE methodologies. Recorded signals from the previous test presented in Chapter 4.5 have been used for this process, whereby envelope and cross correlation analysis have been employed within a localisation algorithm to allow for estimation of the PD position.

Investigation is performed on the accuracy of the localisation system, considering the mean squared error (MSE), mean absolute error (MAE) and percentage error of the estimated PD position, whilst comparing the precision of envelope and cross correlation methodologies. The effect of background noise is also analysed to establish the impact on the systems accuracy through evaluation of varying SNRs.

Furthermore, the attenuation of the signal is significant as this dictates the number and positions of the acoustic sensors required. The detectability range is therefore investigated and potential sensing methods discussed, whilst considering the practical implementation of the proposed PD sensing system on the overall umbilical.

5.1 Motivation

A critical aspect of the proposed system is having the ability to establish the location of the partial discharge within the cable length. This allows the risk to be assessed and if necessary, planned intervention to be carried out on the correct area, consequently greatly reducing failure costs and production downtime.

Existing technologies have shown advancement over the years, however many challenges remain when it comes to localisation of PD [83][119]. One of the main complexities associated with online PD monitoring is due to the attenuation rates of the emitted EM signal, making the required long distance detection difficult to achieve. The use of AE sensors positioned every 'X' meters along the umbilical length would remove this issue, however this would involve more complex implementation. Positioning AE sensors at the topside of the umbilical would be the ideal scenario as is the least invasive option, though is reliant on the low frequency acoustic signals remaining detectable over the required distance.

Both instances will be investigated within this chapter, including evaluation of the system accuracy relating to the calculated PD location, along with the comparison of envelope and cross correlation methodologies.

In addition, captured PD signals are contaminated by environmental noise, thus increasing the complications related to position estimation. Liu et al. discuss the benefits of adaptive filters and wavelet selection schemes for detecting EM signals from PD, particularly when the SNR is low [120]. To understand the allowable SNR at which the PD acoustic signal remains detectable in the proposed system, varying levels of noise are added to the previously detected discharges with results being evaluated within this Chapter.

5.2 Localisation Methods

Detected acoustic signals emitted during PD occurrence can be used to establish the position of a fault within the cable length. Two particular methods have been considered; the first having acoustic sensors positioned periodically along the cable length where TDoA between two AE signals can be used to calculate the fault location, or the second where an acoustic sensor is coupled topside of the umbilical and the TDoA between the EM and AE signal is used, whether the EM signal be detected direct from the acoustic sensor or through the use of an additional HFCT.

5.2.1 Distributed AE Sensors

Firstly, the use of multiple AE sensors is discussed as this is likely the most suitable option for longer length umbilicals. This method requires a minimum of two AE sensors, which are synchronised to the same time stamp to allow for accurate position estimation. Figure 5- 1 illustrates this methodology whereby both x_1 and x_2 distances can be calculated utilising equation (5.1), where x_n is the distance from fault to AE sensor, T_0 is the TDoA

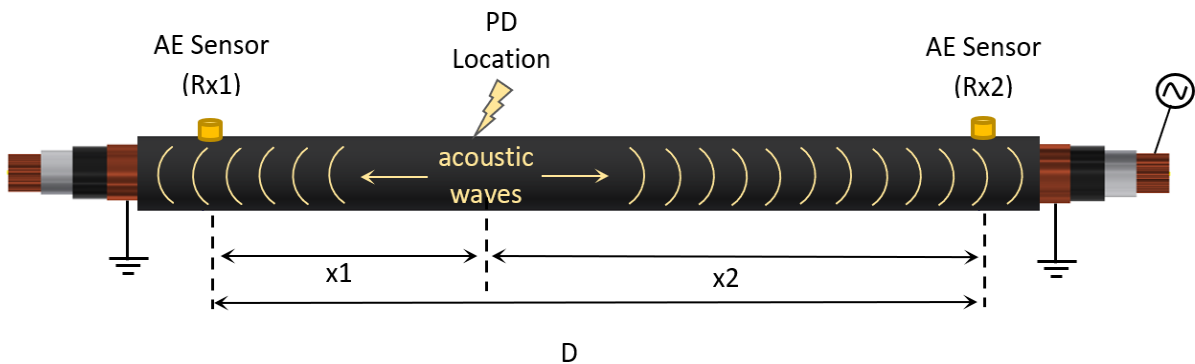


Figure 5- 1: Through-cable Source Localisation using TDoA

between signals detected on Rx1 and Rx2, c is the propagation velocity of the signal and D is the distance between sensors.

$$x_n = \frac{(D - c T_0)}{2} \quad (5.1)$$

The TDoA is obtained from envelope or cross correlation analysis of the signals received at Rx1 and Rx2. Results from the previous test detailed in Chapter 4.5 can be used to aid this investigation into suitable localisation techniques.

Figure 5- 2 shows the one minute capture from the previous test with Rx1 positioned 35m from the PD fault and Rx2 positioned 25m from the fault in the opposing direction. To obtain the TDoA for each detected PD event, a threshold level of 0.2 was chosen based on the amplitude of the signals and the level of noise. Having a threshold allows for continuous monitoring of the system, where a section of the signal following the point at which the threshold is met is processed to allow for localisation i.e. when an emission is detected, the threshold is met and a section of signals from both receivers are analysed,

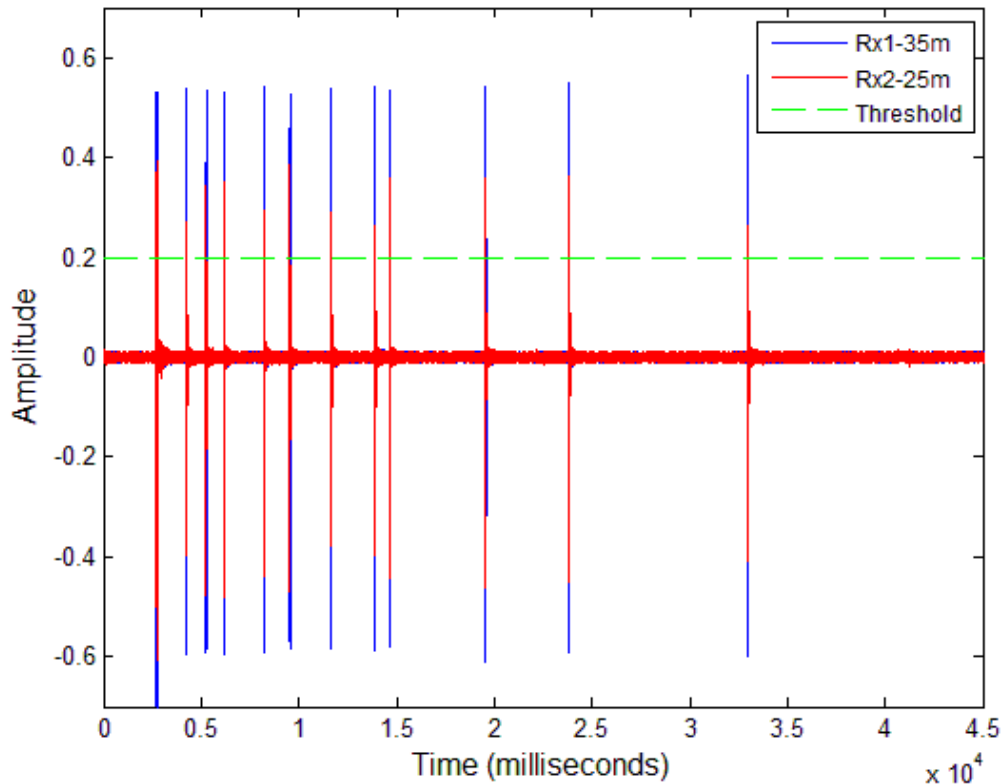


Figure 5- 2: Acoustic Signals Measured at Rx1 (35m from fault) and Rx2 (25m from fault) due to PD within Power Cable Insulation, with a detection threshold of 0.2.

establishing the TDoA between Rx1 and Rx2 through envelope or cross correlation analysis. This is then repeated for each individual PD event, allowing for multiple position estimations and thus improving the accuracy of the localisation system. The ideal level to set the threshold is as low as noise level permits, without too many false alarms.

To confirm this methodology, signals from the test shown in Figure 5- 2 were further evaluated, resulting in a time difference of 4.2 milliseconds between signal envelope peaks, as shown in Figure 5- 3. This time difference can be used within (5.2) to determine how much further the fault is from one sensor to the other, where c is the propagation velocity of the signal, T_0 is the TDoA between signals detected on Rx1 and Rx2, and d is the equivalent distance.

$$c * T_0 = d \tag{5.2}$$

The calculated distance d is approximately 10.2m, thus demonstrating that the fault is $\approx 10.2\text{m}$ further from one AE sensor than the other. To calculate the distance from sensor to fault x_n , (5.1) can be employed, as distance between receivers for this particular test is

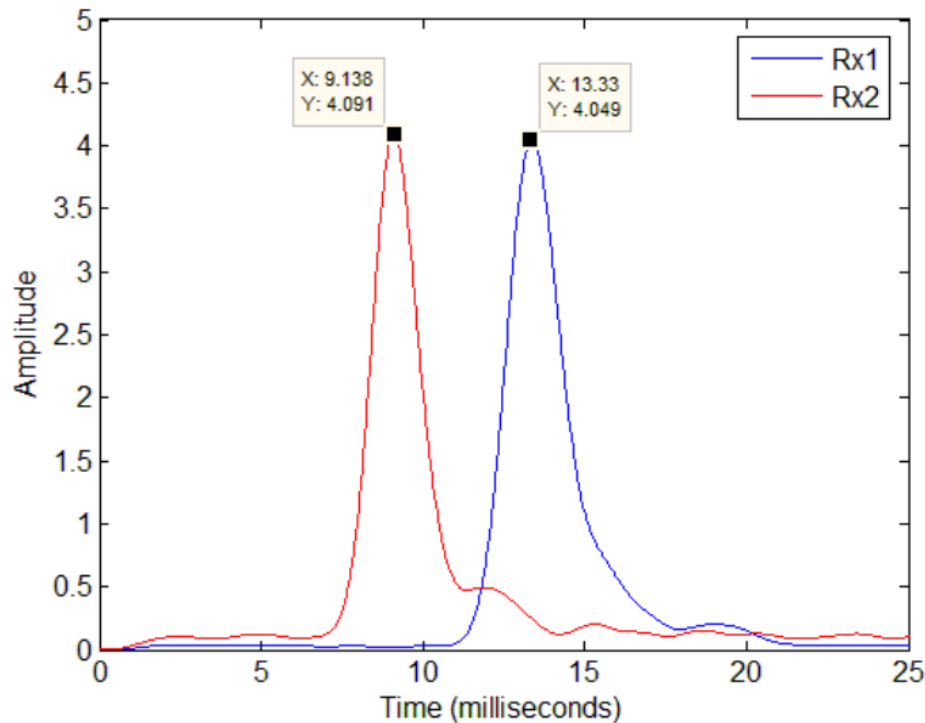


Figure 5- 3: TDOA between AE signals detected on Rx1 (35m from fault) and Rx2 (25m from fault)

known to be 60m and the propagation velocity was found through earlier analysis to be $\approx 2442\text{m/s}$, therefore resulting in distances of 35.1m for x_1 and 24.9m for x_2 . The true distances were known to be 35m and 25m respectively, thus providing a percentage error of less than 1%.

To further confirm the methodology, Figure 5- 4 presents the cross correlation results for the same signals, showing a correlation value of 183, thus equating to a TDoA of 4.1milliseconds when again considering a sampling frequency of 44.1kHz. Determining which receiver is closest to the fault is clear as the signal arrives at one receiver before the other and so the localisation algorithm can account for this. The established TDoA of 4.1milliseconds is very similar to that obtained through envelope analysis, with the cross correlation results showing a very slight improvement in position accuracy, however both results have revealed an extremely low percentage error.

Both the envelope and cross correlation examples discussed have therefore confirmed the feasibility of the proposed localisation method whereby multiple AE sensors are distributed throughout the length of the umbilical in order to detect the occurrence of PD.

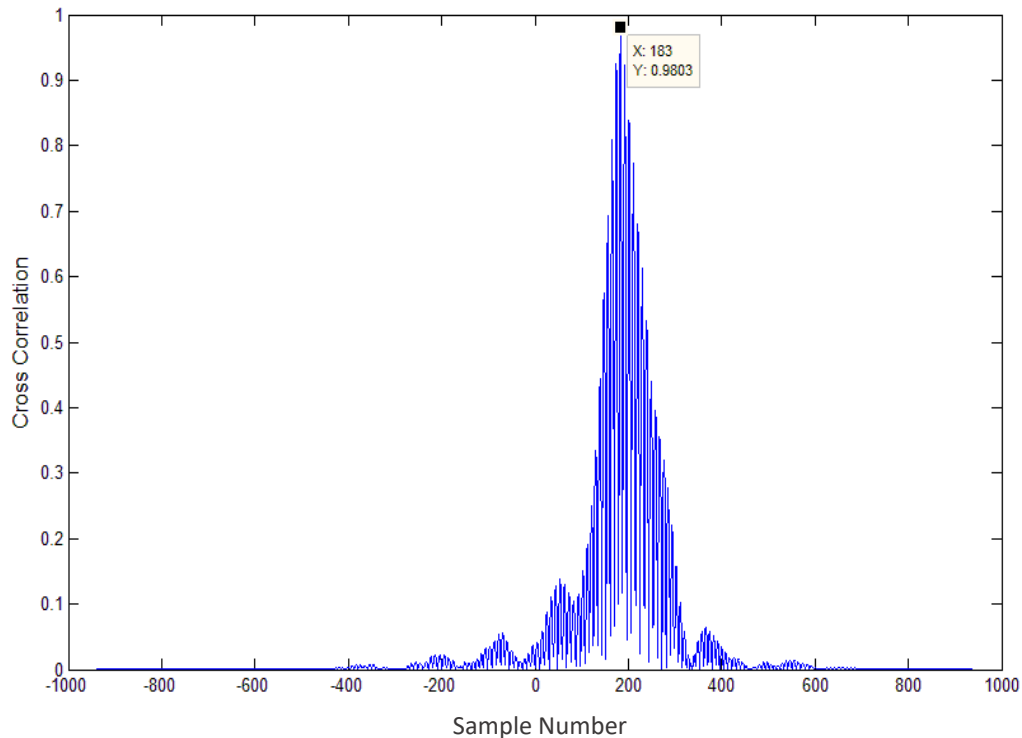


Figure 5- 4 Cross Correlation of AE signals detected on Rx1 (35m from fault) and Rx2 (25m from fault)

5.2.2 Combined EM and AE Topside Detection

As an alternative to distributed AE sensors, a method whereby the EM signal is analysed along with the detected AE signal allows the position of the discharge to be estimated with a single acoustic receiver by considering the EM signal as time of PD occurrence. This method involves an EM and AE sensor being positioned topside of the umbilical, thus allowing for a retrofit option and minimal impact to the umbilical design and manufacturing process. Utilising this approach will likely require the additional use of an HFCT and will be further limited when it comes to detectability lengths, though it has been considered as a potential option as it is the least intrusive of the through-cable detection techniques being investigated.

The practicality of this will be further assessed when considering the detectability range, discussed in the forthcoming Section 5.4, as this method will likely only be suited to detection on shorter umbilical lengths in shallower waters.

To calculate the fault position using this approach, the TDoA between the EM and AE signal is established and multiplied by the signal velocity, as detailed in (5.2). The resultant distance equates to the distance from the AE sensor to the PD location as the EM signal is detected instantaneously when PD takes place, therefore the TDoA relates directly to the time from PD occurrence to detection of the subsequent AE signal.

To make an assessment on the feasibility of this method, the results from the previous test were again analysed in order to maintain consistency. Figure 5- 5 presents the signal

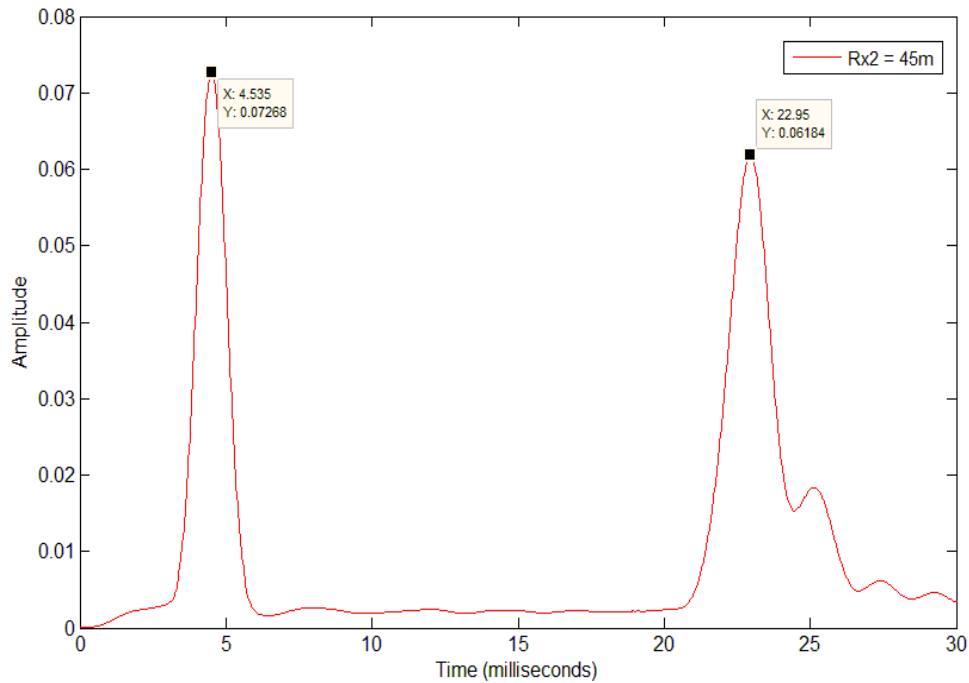


Figure 5- 5: TDOA between EM and AE signals – Rx2 45m trial

envelopes from an individual PD event from this test, whereby the time difference between peaks is determined as 18.42ms. Considering a signal velocity of 2442m/s, the fault position can be calculated as being 44.93m from the AE sensor, therefore providing an error of less than 1% and proving the methodology of this alternative localisation technique.

5.3 Evaluation of TDoA Techniques

Initial analysis demonstrates that both of the discussed sensing methods are able to offer highly accurate localisation of the PD source, with the first being preferable for longer lengths. Considering this method of multiple distributed sensors, both envelope and cross correlation analysis techniques can be utilised to establish the TDoA between detected AE signals, which in turn allows the PD location to be calculated. The following sections therefore focus on evaluation of both envelope and cross correlation techniques to establish the most suitable for use within the PD localisation algorithm.

5.3.1 Envelope Detection – Distributed AE Sensing

Envelope analysis of the received emissions allows the signal's peaks to be clearly identified, which is a crucial part of the localisation algorithm allowing TDoA to be determined. Having discussed two potential methods for through-cable localisation, the initial focus was on the most likely method of distributed AE sensors along the cable length. Again, results from the trial performed in Chapter 4.5 were used for this analysis as they provide multiple results at varying sensor positions.

For each trial performed (i.e. 5m through to 55m) multiple PD emissions were captured during a one minute recording. When the signal amplitude was greater than the set threshold, a section of the following acoustic wave was processed to ascertain the peak values from the signal envelopes, thus establishing the TDoA between receivers Rx1 and Rx2. Having results from numerous discharges within each trial allows the accuracy of the localisation to be greatly improved as the time difference between the majority of peaks should be consistent, with not too many outliers. An example of this is presented in Figures 5-6 to 5-8, showing the normalised signal envelopes from trials with Rx2 positioned 15m, 25m and 45m from the fault. There are outliers present within each of the figures, however it is clear as to which peaks to focus on for the TDoA measurement due to the repetition at specific time periods. Results from only three trials have been presented, however this is evident across results from all eleven trials performed, with Rx2 positioned 5m through to 55m from the fault location.

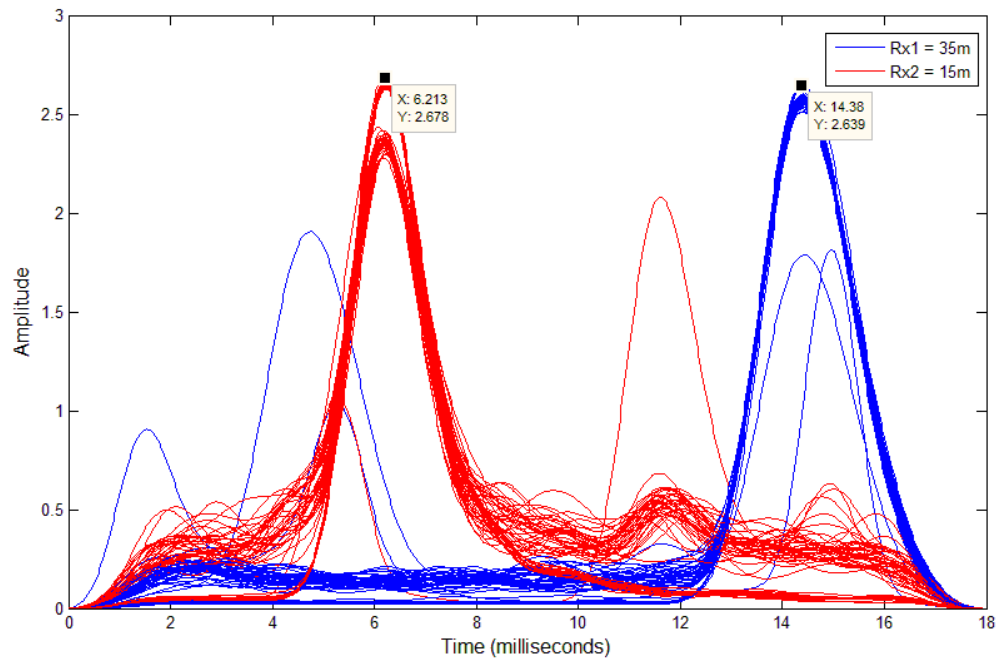


Figure 5- 6: Signal Envelopes of AE from Multiple PD Events – Rx1 35m from fault, Rx2 15m from fault

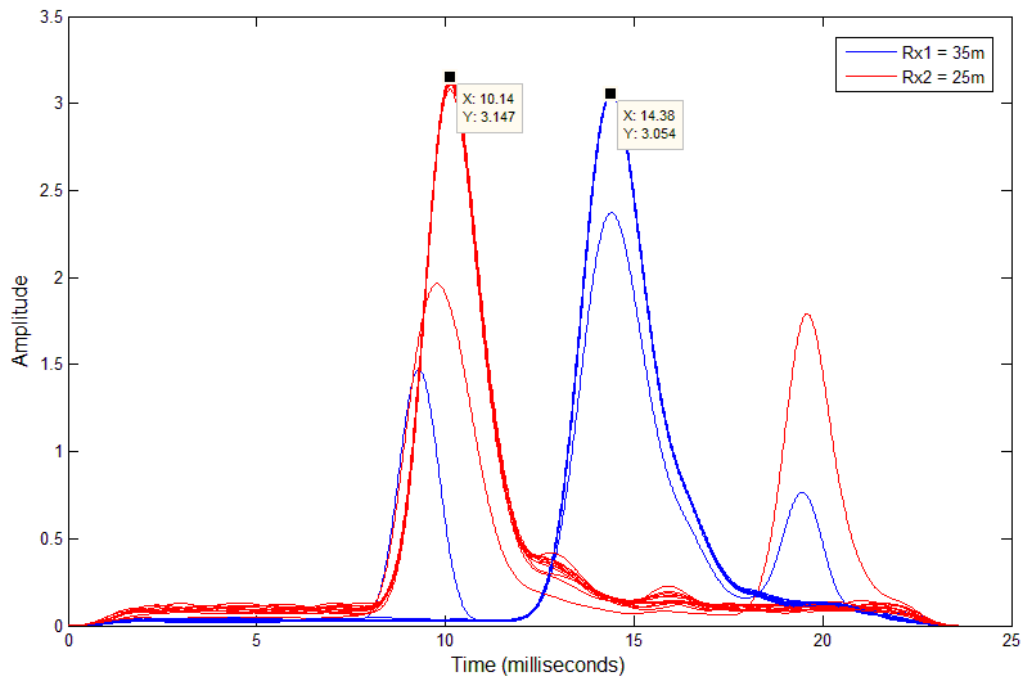


Figure 5- 7: Signal Envelopes of AE from Multiple PD Events – Rx1 35m from fault, Rx2 25m from fault

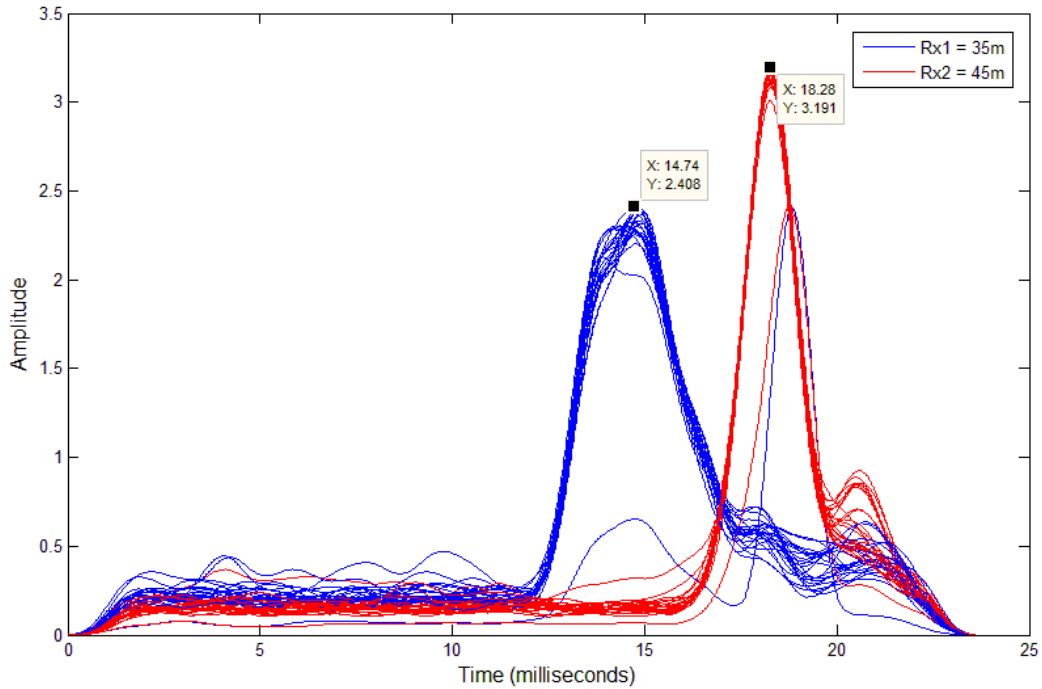


Figure 5- 8: Signal Envelopes of AE from Multiple PD Events – Rx1 35m from fault, Rx2 45m from fault

In order to evaluate the accuracy of the localisation system and to allow comparison between envelope and correlation methods, the mean square error (MSE) was calculated for the estimated fault position at each sensor location . The MSE is an average of the squared difference between the actual fault position and the estimated value, expressed mathematically in (5.3).

$$MSE = \frac{1}{n} \sum_{i=1}^n (y_i - \hat{y}_i)^2 \quad (5.3)$$

As the MSE is calculated by squaring the errors, outliers are emphasised resulting in higher MSE values. The impact of this however was minimal on the results obtained, due to the small number of outliers present in comparison to the number of discharges detected. Figure 5- 9 displays the estimated distance from receiver Rx2 to the fault location in relation to the actual distance, along with the MSE for each position. The MSE values are relatively small, ranging between 0.04 to 2.49, providing an overall value for the system of 1.20. This would be reduced further if all clear outliers were removed from each dataset prior to calculation of the MSE. This could be achieved by applying a standard deviation (SD) from the mean as a cut off in data, thus causing any points above and below mean*SD

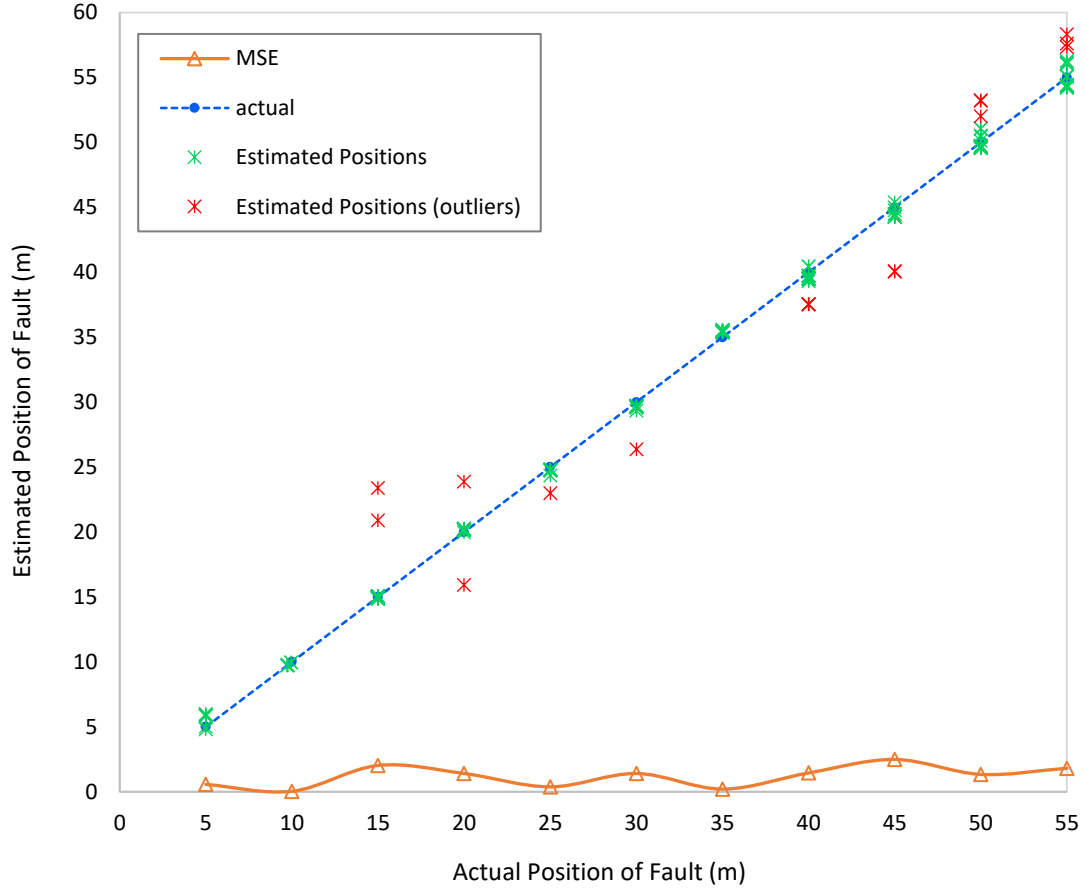


Figure 5- 9: Through-cable Localisation obtaining TDoA from Rx1 & Rx2 Signal Envelopes, position estimation indicates distance from Rx2 to PD fault

to be eliminated from the estimated position plots and highlighted as outliers. These equivalent outlier values are shown in red in Figure 5- 9. Removing the outliers from the dataset reduces the range of the MSE values to between 0.01 and 0.61, providing an overall system average of 0.24. The detection system is iterative and relies on more than one data point to calculate the SD. PD events will be continually logged and plotted periodically at a time period suitable for the severity of the fault, i.e. when PD activity is minimal, plots will be less frequent and when PD activity increases, the frequency of the plots will increase, thus displaying the relevant dataset.

To further evaluate the systems accuracy, the mean absolute error and the percentage error were also calculated using (5.4) and (5.5).

$$MAE = \frac{1}{n} \sum_{i=1}^n |y_i - \hat{y}_i| \quad (5.4)$$

$$\% \text{ Error} = \frac{\text{Absolute Error}}{\text{Actual Value}} * 100 \quad (5.5)$$

Table 5- 1 presents the MSE, MAE and percentage error results for both the complete data set and also the resulting values once the outliers have been removed. This is done so through implementation of a cut off of one standard deviation from the mean, in line with the plotted results presented in Figure 5- 9. As expected, the removal of outliers provides an improved accuracy on the overall PD localisation system, whereby a reduction in MSE, MAE and percentage error can be seen.

<i>Rx2 Position from Fault (m)</i>	<i>Mean Estimated Distance of Rx2 from Fault (m)</i>		<i>Mean Square Error</i>		<i>Mean Absolute Error</i>		<i>% Error</i>	
	<i>all data</i>	<i>outliers removed</i>	<i>all data</i>	<i>outliers removed</i>	<i>all data</i>	<i>outliers removed</i>	<i>all data</i>	<i>outliers removed</i>
5	5.61	5.61	0.58	0.58	0.67	0.67	12.2	12.2
10	9.83	9.83	0.04	0.04	0.17	0.17	1.70	1.70
15	15.24	14.97	2.03	0.01	0.33	0.05	1.60	0.20
20	20.17	20.20	1.41	0.04	0.53	0.20	0.85	1.00
25	24.62	24.80	0.38	0.08	0.38	0.25	1.52	0.80
30	29.34	29.67	1.41	0.11	0.66	0.33	2.20	1.10
35	35.45	35.45	0.21	0.21	0.45	0.33	1.29	1.29
40	39.22	39.67	1.45	0.21	0.87	0.45	1.95	0.83
45	44.01	44.36	2.49	0.51	1.03	0.68	2.21	1.42
50	50.31	49.91	1.34	0.24	0.76	0.43	0.62	0.18
55	55.39	54.92	1.81	0.61	1.05	0.71	0.71	0.15
	<i>average</i>		1.20	0.24	0.63	0.39	2.44	1.90

Table 5- 1: Through-cable Localisation utilising Signal Envelopes from Rx1 and Rx2 – Error Analysis

By using different methods to evaluate the accuracy, a view can be taken on both the variance in data spread and the difference between the estimated average and the actual fault location. When considering the complete data set (including outliers), the MAE results display a much tighter range of between 0.17m and 1.05m in comparison to the MSE results of 0.04 to 2.49, as the individual errors are not squared. With the outliers removed, both the MSE and MAE provide similar results, each displaying a tight range.

Overall, the position estimation results display a high level of accuracy for both the complete data set and the data with outliers removed. This provides confidence in the use of envelope analysis within the localisation algorithm when utilising distributed AE sensors, as this methodology has shown a low error rate, with all average positions falling within 1m of the true fault location.

5.3.2 Cross Correlation – Distributed AE Sensing

When considering the proposed PD localisation system, the process followed for obtaining the TDoA from cross correlation is largely similar to that discussed using envelope analysis. Once the amplitude of the acoustic signal meets the set threshold, a subsequent section is then processed, this time performing cross correlation between signals detected on Rx1 and Rx2, as opposed to envelope analysis. The resultant cross correlated signal displays its largest peak at a position equivalent to the TDoA between signals detected at Rx1 and Rx2. The position of this peak is considered as the lag, as previously discussed in Section 4.4. The lag can then be used to calculate the position of the fault by applying (5.1), where T_0 is lag divided by fs . As with the envelope analysis, this process is repeated each time the threshold is met, thus allowing multiple TDoA values to be obtained for each sensor position.

To further analyse this approach, the estimated location for all PD events detected at each sensor position were plotted in Figure 5- 10, along with the MSE. The mass of the estimated fault positions sit in and around the line relating to the actual PD location, however multiple outliers can be seen resulting in a large increase in the calculated MSE value due to squaring of the errors. Removing the clear outliers would greatly improve the system's accuracy, therefore all values above and below mean*SD are shown in red, thus allowing the MSE to be greatly reduced when these values are removed from the position estimation dataset.

Again, the MAE and percentage error were also calculated to provide a more thorough analysis of the systems accuracy, with results displayed in Table 5- 2. The MSE values for the complete dataset range between 0.04 and 14.74 and the MAE between 0.47m and 2.01m, resulting in an average of 3.55 and 0.93m respectively. When considering the results with the outliers removed, the accuracy is greatly improved with the average MSE being reduced to 0.29 and the MAE to 0.43m. Both the MSE and MAE results again display a much tighter range following exclusion of the outliers.

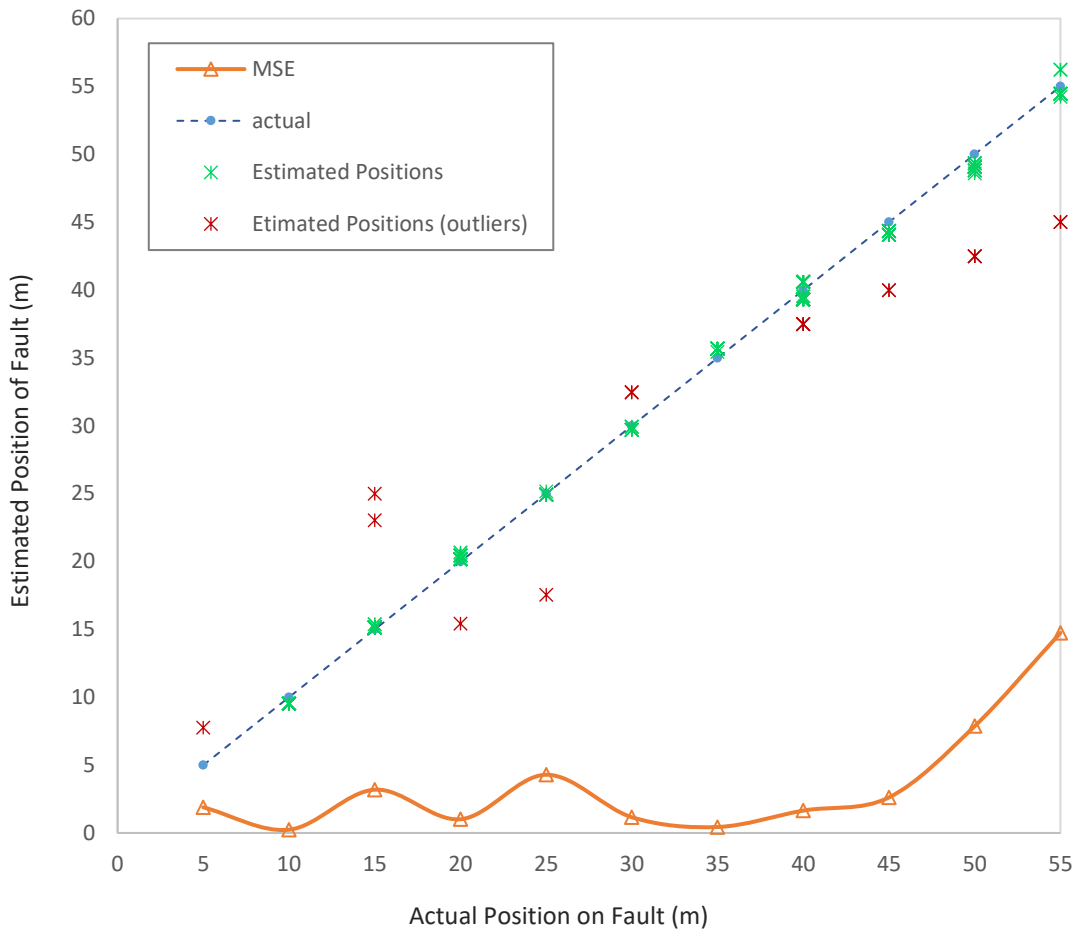


Figure 5- 10: Through-cable Localisation obtaining TDoA from Rx1 & Rx2 Cross Correlation, position estimation indicates distance from Rx2 to PD fault

As with envelope analysis, the use of cross correlation on signals from the distributed AE sensing method has provided accurate PD localisation results with a low percentage of error, thus confirming the suitability of this technique within the PD system. Cross correlation results have shown a percentage error of less than 1%, whereby the estimated discharge location is within 0.5m of the actual PD event.

In both envelope and cross correlation analysis of the received AE signals, the application of a cut-off of one SD from the mean vastly improved the precision of the PD localisation as the estimate is based on the main body of data and not influenced significantly by any outliers, hence this methodology shall be included within the localisation algorithm.

<i>Rx2 Position from Fault (m)</i>	<i>Mean Estimated Distance of Rx2 from Fault (m)</i>		<i>Mean Square Error</i>		<i>Mean Absolute Error</i>		<i>% Error</i>	
	<i>all data</i>	<i>outliers removed</i>	<i>all data</i>	<i>outliers removed</i>	<i>all data</i>	<i>outliers removed</i>	<i>all data</i>	<i>outliers removed</i>
5	5.42	5.03	1.89	0.94	1.22	0.96	8.40	0.60
10	9.52	9.52	0.04	0.04	0.17	0.17	1.70	1.70
15	15.49	15.15	3.19	0.02	0.49	0.15	3.27	1.00
20	20.07	20.29	1.01	0.11	0.47	0.29	0.35	1.45
25	24.38	24.95	4.28	0.01	0.64	0.07	2.48	0.20
30	30.27	29.78	1.16	0.06	0.63	0.22	0.90	0.73
35	35.66	35.45	0.43	0.21	0.66	0.33	1.89	1.29
40	39.20	39.71	1.80	0.43	1.09	0.65	2.00	0.73
45	43.89	44.74	2.62	0.59	1.11	0.76	2.47	1.69
50	48.22	49.91	7.87	0.24	1.78	0.43	3.56	0.18
55	53.35	54.74	14.74	0.53	2.01	0.68	3.00	0.47
		average	3.55	0.29	0.93	0.43	2.73	0.91

Table 5- 2: Through-cable Localisation utilising Cross Correlation of Rx1 and Rx2 – Error Analysis

5.3.3 Envelope Detection – Combined EM and AE Detection

When considering the alternative sensing method whereby an HFCT is used alongside a single topside AE sensor, envelope analysis can again be employed to establish the TDoA. For this methodology, cross correlation cannot be used to obtain the TDoA as a comparison between similar signals is not possible due to the use of only one AE sensor. In this case, the relevant time difference is between the EM signal detected on the HFCT, which is considered as the time of PD occurrence, and the acoustic signal detected at the AE sensor. This time difference can be best obtained through envelope analysis and therefore the approach specified in 5.3.1 was repeated, this time focusing on the time difference between the EM and AE peaks of the detected emissions.

Figure 5- 11 shows the plotted results for each of the estimated fault positions, along with the MSE values. The majority of the plotted results lie on or in close proximity to the actual PD location, with results one SD from the mean highlighted in red as outliers.

The average estimated position, MSE, MAE and percentage error results are all presented in Table 5- 3 with values shown for the complete data set and for that with outliers removed. The MSE values for the complete dataset range between 0.09 and 3.24 and the MAE between 0.12m and 1.20m, resulting in a system average of 1.35 and 0.66m respectively. With outliers removed, the average MSE is reduced to 0.31 and the MAE to 0.43m, along with a significant reduction in data range. The calculated error rates are very low with minimal variation in data spread and the average estimated location of PD is within 1m of the true value.

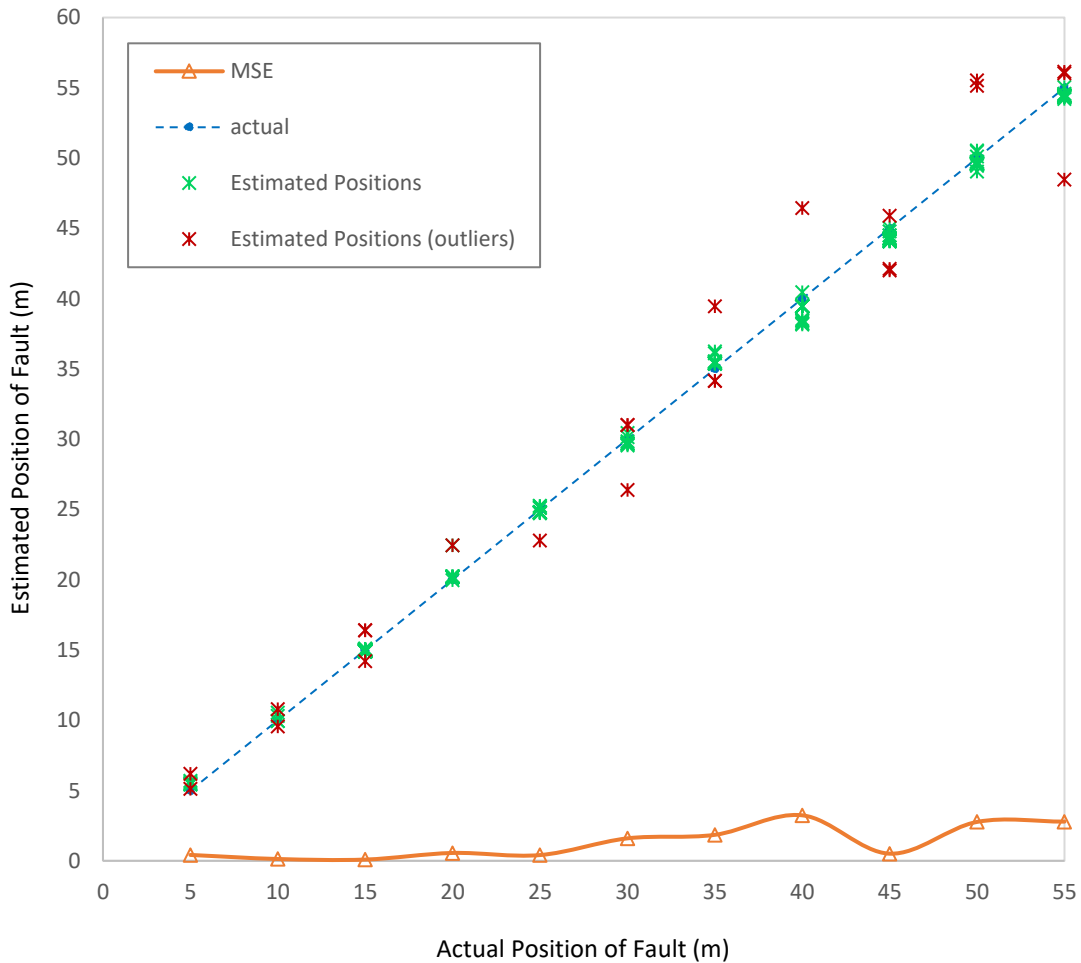


Figure 5- 11: Through-cable Localisation obtaining TDoA from EM & Rx2 Signal Envelopes, position estimation indicates distance from Rx2 to PD fault

<i>Rx2 Position from Fault (m)</i>	<i>Mean Estimated Distance of Rx2 from Fault (m)</i>		<i>Mean Square Error</i>		<i>Mean Absolute Error</i>		<i>% Error</i>	
	<i>all data</i>	<i>outliers removed</i>	<i>all data</i>	<i>outliers removed</i>	<i>all data</i>	<i>outliers removed</i>	<i>all data</i>	<i>outliers removed</i>
5	5.57	5.53	0.42	0.30	0.57	0.53	11.40	10.60
10	10.17	10.19	0.13	0.09	0.29	0.23	1.70	1.90
15	15.01	14.97	0.09	0.01	0.12	0.05	0.07	0.20
20	20.39	20.30	0.56	0.31	0.40	0.30	1.95	1.50
25	24.76	24.92	0.41	0.04	0.35	0.20	0.96	0.32
30	29.74	29.85	1.46	0.10	0.75	0.30	0.87	0.50
35	35.65	35.58	1.85	0.42	0.89	0.58	1.86	1.66
40	39.52	39.14	3.24	1.11	1.20	0.91	1.20	2.15
45	44.17	44.31	1.18	0.52	0.86	0.69	1.84	1.53
50	50.22	49.71	2.77	0.19	0.86	0.41	0.44	0.58
55	54.31	54.46	2.78	0.33	0.94	0.55	1.25	0.98
		<i>average</i>	1.35	0.31	0.66	0.43	2.14	1.99

Table 5- 3: Through-cable Localisation utilising Signal Envelopes from EM and Rx2 – Error Analysis

This analysis method of combined EM and AE detection provides a high level of accuracy for PD source localisation, however its limitations are emphasized on longer lengths due to attenuation of the signals as the sensors are located at the topside of the umbilical. As the detection distance increases, the magnitude of the signal decreases, thus providing a lower SNR, which will lead to undetected PD or increased position estimation errors if the threshold is too close to the noise level. As a result of this, its application would be heavily dependent upon the field in which the umbilical is installed, with the preference being; short lengths, shallow waters, or instances where the fault is believed to be within the dynamic section only.

5.3.4 SNR Analysis

The SNR is a measure of the signal level compared with the background noise. It can be considered as the ratio of meaningful data to unwanted data and is often expressed in dB, as shown in (5.11), where A relates to the amplitude. A ratio greater than 1:1 demonstrates that the signal is more than the noise level i.e. greater than 0dB.

$$SNR_{dB} = 20\log_{10}\left(\frac{A_{signal}}{A_{noise}}\right) \quad (5.11)$$

When considering the localisation system, the SNR needs to be high enough to ensure the PD events are detected above the noise. To investigate the minimum SNR where detection of PD maintains a high level of accuracy for localisation of the discharge, varying levels of white gaussian noise have been added to the recorded audio files from the previous test. Figure 5- 12 presents results from the trial with Rx2 positioned 45m from the fault, showing both the original signal and those with added noise, providing differing SNR levels of; 10dB, 7dB, 3dB, -3dB and -7dB, from (a) through to (f). Results from the 45m trial were selected for detailed analysis as it is at a great enough distance from the fault whereby signal velocity will have stabilised to around 2400m/s and also at a reasonable distance from the cable ends, to minimise the effects of multipath. The calculated SNR levels are based upon the RMS of the detected AE signal as opposed to the EM signal, as it is due to the test conditions that the EM signal is detected on the hydrophone and consequently, in actual service conditions, it may only be the acoustic signal that is detected unless also utilising an HFCT. The detected EM peaks remain clear throughout all captures, however it is difficult to visually see the AE peaks over the noise whilst observing the complete one minute recording.

Figure 5- 13 centers on an individual PD event from each of the traces shown in Figure 5- 12, along with the original signal as a visual aid. Although the trace is not as clear as the original, both the EM and AE signals remain visible on Figures 5-13a through to 5-13d, as the peaks of the emission can be seen above the noise. The EM signal remains identifiable in Figure 5-13e, however the AE signal is less prominent with the peak amplitude being close to that of the noise, thus an increased error rate within the localisation system is likely, particularly for PD events with a lower breakdown strength. Figure 5-13f presents the lowest displayed SNR of -7dB, whereby both the EM and AE signals are almost fully masked by the noise level, making it unlikely that the position of fault could be accurately determined.

To further assess the impact of the SNR value in determining the fault position, noise was added to the localisation algorithm to evaluate the resultant errors. The threshold level remained at 0.2, as per the analysis in Section 5.2, and each time the threshold was met a

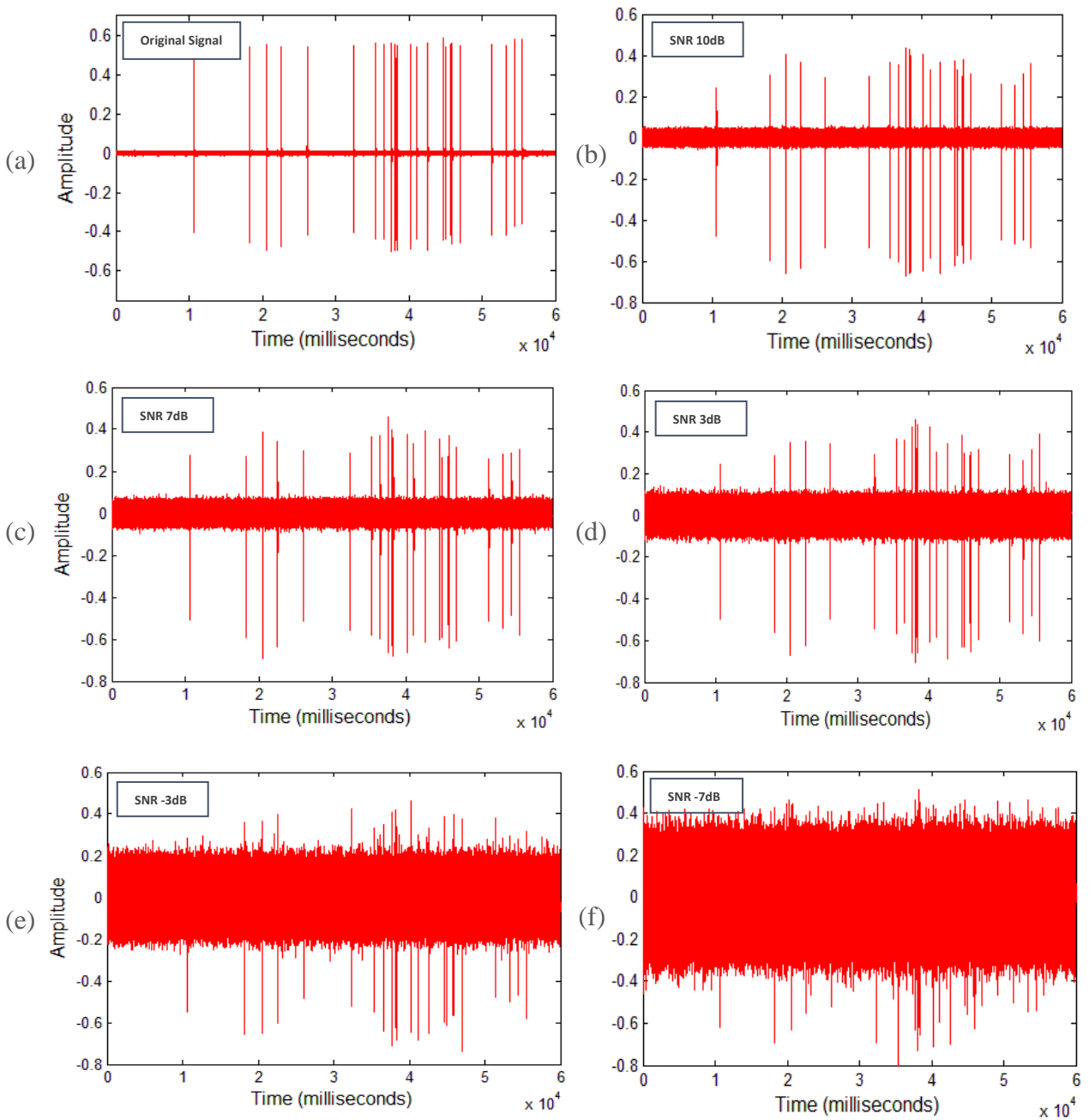


Figure 5- 12: Comparison of Original Signal and those with Varying Levels of added Noise (a) Original Signal, (b) SNR 10dB, (c) SNR 7dB, (d) SNR 3dB, (e) SNR -3dB, (f) SNR -7dB

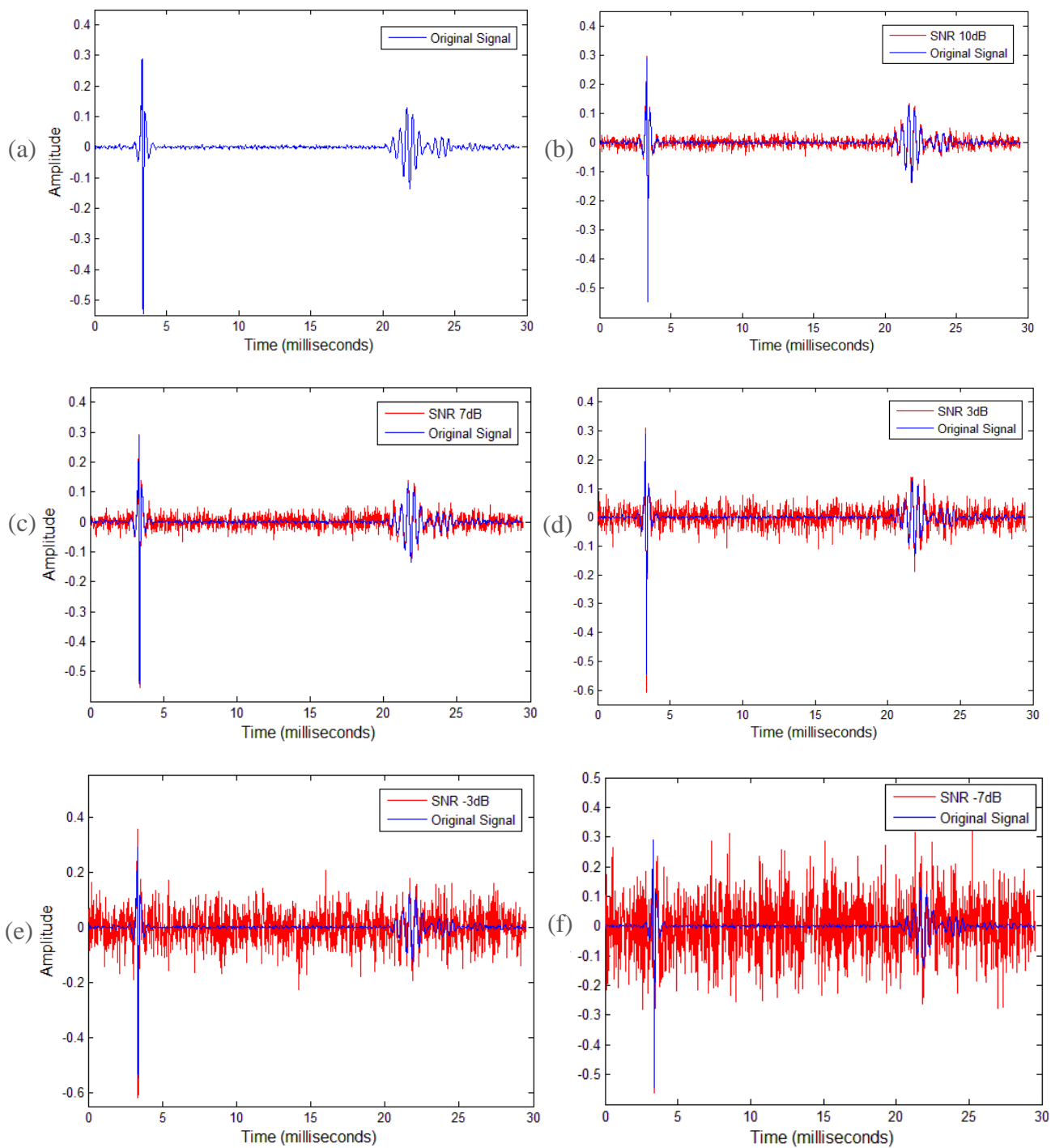


Figure 5- 13: Comparison of Individual Discharge with Varying Levels of added Noise (a) Original Signal, (b) SNR 10dB, (c) SNR 7dB, (d) SNR 3dB, (e) SNR -3dB, (f) SNR -7dB

section of both Rx1 and Rx2 signals were processed to establish the TDoA from the envelope peaks, thus allowing the fault position to be estimated and the accuracy evaluated. The subsequent normalised envelopes are shown in Figure 5- 14, again considering an SNR of 10dB, 7dB, 3dB, -3dB and -7dB. Visually, the envelopes peaks having an SNR of 10dB and 3dB remain relatively clear, showing minimal effect from the added noise. The trace relating to an SNR of -3dB displays a greater impact, with additional noise peaks shown to be close in amplitude to the peaks of the detected AE signal on Rx1. A major effect is found on the signal with an SNR of -7dB, where the signal of lesser amplitude is almost lost within the noise, once more indicating a high error rate for localisation of the fault region. In addition, a large peak remains consistent on each capture at around 20ms, whereby a signal is detected simultaneously on both receivers. The simultaneous nature of the detected signals would suggest detection of an EM signal as opposed to acoustic, as a delay would be expected between received AE signals due to the slower signal velocity and time to reach each sensor position. It is likely that two discharges have occurred within a close period of time, whereby the EM signal of the second discharge was captured within the section of data processed after the initial discharge met the threshold. This would impact the established peak envelope value of this particular capture, consequently leading to an 'outlier' in the position estimation of the fault. This signal was not seen during earlier analysis of the 45m trial as the focus was on an individual event, whereas Figure 5- 14 presents the envelope of multiple PD events from the same trial overlaid upon each other. When considering the 45m trial, many discharges were detected and analysed within the localisation algorithm and the additional presence of the EM signal within the AE capture only occurred once, thus allowing the resultant position estimation to be considered as an anomaly, therefore only having a minor effect on the overall system accuracy when considering all data.

To further analyse the impact of SNR on the overall accuracy of the system, the approximate position of the fault from Rx2 was calculated, along with the MSE and the MAE for each SNR, with results shown in Table 5- 4. The position estimation is performed within the TDE algorithm, whereby the time difference is calculated between the maximum peak of each signal envelope which is determined within Matlab. Results show a negligible change in localisation accuracy between the signals with an SNR of 10dB, 7dB and 3dB, with each providing an MSE of around 8.4 and MAE of around 2.0m. This is an increase from the original signal, however is still considered to be highly accurate. There is a large increase in the average MSE results for signals with an SNR of -3dB, however the average fault position is within 2m of the estimated PD location of the original signal, thus revealing that although outliers are more common, localisation is still achievable with a reasonable level of accuracy with this level of noise. As expected, results show a further decrease in accuracy for signals with an SNR of -7dB, where the MSE value has increased to 42.44 and the MAE to 5.14m. The average PD location was calculated to be at approximately 48m from Rx2, which is within 3m of the actual fault location but almost 4m of the original estimated position. A lesser tolerance would be preferable, however this would still provide a valuable indication of the PD location, particularly if in the region of a cable splice or

<i>SNR</i>	<i>Mean Estimated Distance of Rx2 from Fault (m)</i>	<i>Mean Square Error</i>	<i>Mean Absolute Error</i>
<i>Original Signal</i>	44.01	2.49	1.03
<i>10dB</i>	43.96	8.39	2.04
<i>7dB</i>	43.59	8.38	1.95
<i>3dB</i>	43.55	8.41	2.03
<i>-3dB</i>	45.80	29.59	3.30
<i>-7dB</i>	47.98	42.44	5.14

Table 5- 4: Comparison of Original Signal and Varying SNR - Error Analysis from Signal Envelopes

joint as they are considered to have a higher probability of failure suggesting discharge occurrence at that point.

When considering the localisation system, analysis shows that estimation of the PD position remains achievable for SNR's of -7B and above. Below -3dB, the error rate increases rapidly making the system much less reliable. The system was further evaluated to establish the lowest SNR at which the PD location can still be estimated. It was found that an SNR of -11dB provided an MSE of 54.85 and an estimated position of approximately 5m from the true location. Analysis of SNR's below this value caused errors within the localisation algorithm due to both noise and the AE signal triggering the threshold, consequently preventing the location from being obtained. It should be noted, however, that the localisation algorithm also considers the EM peak being detected which is a greater amplitude than that of the AE signal, and thus, for long distance detection whereby the strength of the EM signal is reduced, a much higher minimum SNR is likely. Revisiting Figure 5- 13, it is likely that for long distance detection, where no additional EM sensing is used, an SNR of 3dB or above would be preferred for more accurate localisation results.

To evaluate the effects of the processing methodology used to determine the TDoA, the above process was repeated, this time considering the effects of the SNR on cross correlation results. Figure 5- 15 presents the cross correlation results for the original signal and those with an SNR's of 10dB, 7dB, 3dB, -3dB and -7dB. The correlation peak remains clear through images Figure 5- 15a to Figure 5- 15d. The impact from noise greatens on the trace showing an SNR of -3dB, however the correlation peak remains consistent at around the same lag position. For Figure 5- 15f, the peak remains identifiable, however it

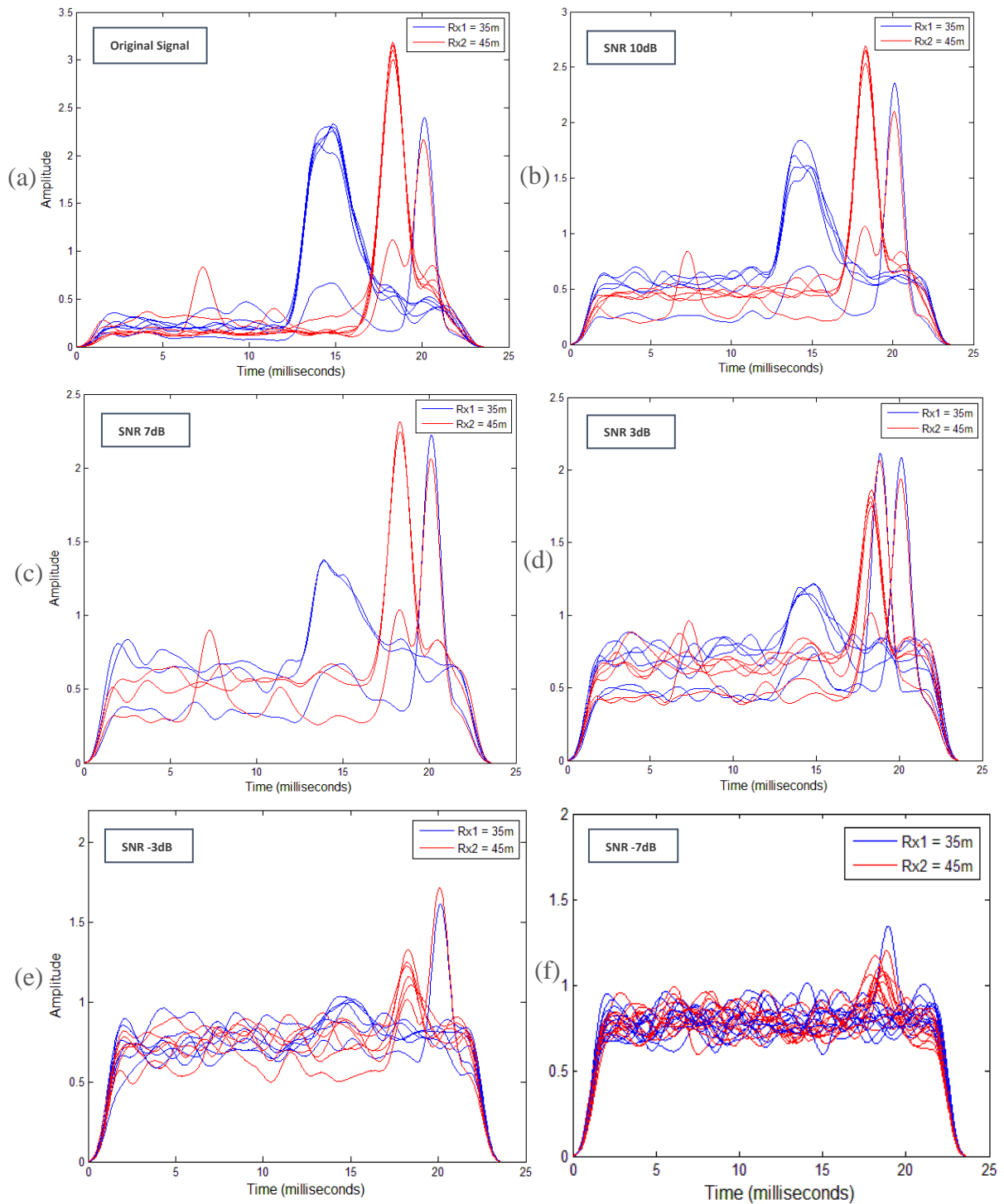


Figure 5- 14: Signal Envelopes of AE from Multiple PD Events including added Noise (a) Original Signal, (b) SNR 10dB, (c) SNR 7dB, (d) SNR 3dB, (e) SNR -3dB, (f) SNR -7dB

does become less distinct, therefore likely leading to an increase in localisation errors.

To further investigate the impact on the system accuracy, the estimated PD location was established from the cross correlation results of AE signals captured within the localisation algorithm. The MSE and MAE values were then calculated and results are shown in Table 5- 5. As with the envelope analysis, the results show minor variation in the calculated errors for SNR's 10dB through to 3dB, however the MSE and MAE values are much lower at around 2.6, and 1.1m respectively. The estimated PD location remains closer to that of the original signal than with the previous envelope results. The error rate does show an increase at -3dB, taking the MSE to 8.0 and MAE to 2.31m. These error rates are still considered low and are comparable to the envelope results from an SNR of 10dB to 3dB. At an SNR of -7dB, results show an increased MSE of 10.51 and MAE of 3.06m, yet the estimated position remains within 1m of the location for the original signal and thus is considered acceptable for the system. Once more, the noise level was further increased to worsen the SNR to -11dB. The resultant MSE only slightly increased to 10.72 and the MAE to 3.26m, with the estimated location staying within 1m of the original signal estimation. Decreasing the SNR past this level again led to issues within the localisation algorithm as the AE signal could not be differentiated. As with the envelope SNR analysis, the cross correlation localisation algorithm is initially triggered off the EM peak and then a section following this is analysed. Long distance detection would again cause attenuation of the EM signal, potentially below the noise level, unless EM sensing methods were used alongside the AE sensing techniques. The use of cross correlation, however, is expected to allow a lower SNR due to the methodology of the process whereby 2 signals are compared in similarity as a function of displacement, as opposed to analysis of the signal peaks, which is more likely to be affected by noise.

<i>SNR</i>	<i>Mean Estimated Distance of Rx2 from Fault (m)</i>	<i>Mean Square Error</i>	<i>Mean Absolute Error</i>
<i>Original Signal</i>	43.89	2.62	1.11
<i>10dB</i>	43.93	2.58	1.08
<i>7dB</i>	43.95	2.61	1.08
<i>3dB</i>	43.89	2.74	1.16
<i>-3dB</i>	43.36	8.04	2.31
<i>-7dB</i>	43.27	10.51	3.06

Table 5- 5: Comparison of Original Signal and Varying SNR - Error Analysis from Cross Correlation

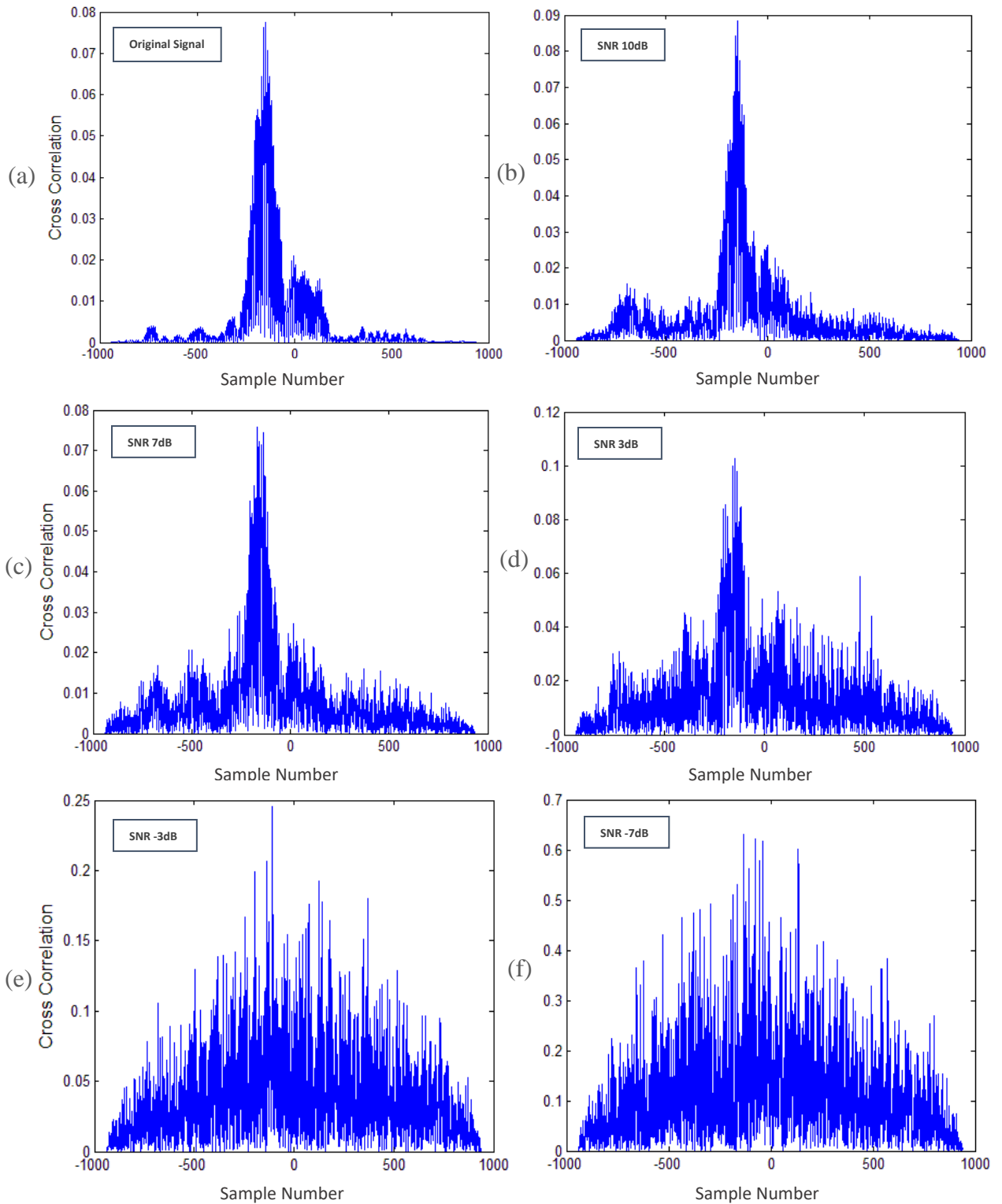


Figure 5- 15: Cross Correlation of AE from Multiple PD Events including added Noise (a) Original Signal, (b) SNR 10dB, (c) SNR 7dB, (d) SNR 3dB, (e) SNR -3dB, (f) SNR -7dB

5.3.5 System Accuracy

Both envelope analysis and cross correlation techniques have provided successful results when utilised within the localisation algorithm to establish the TDoA. Within each method, a small number of outliers were identified therefore increasing the error rate within the system. As the signal propagates through the cable it is affected by distortion and attenuation, therefore resulting in changes to the emitted PD pulse shape, causing a displacement in time reference and thus leading to localisation errors [121]. Focusing on the results presented in Section 5.31 and 5.32, the average accuracy of the system is slightly higher with the use of envelope analysis as opposed to cross correlation, however, once the clear outliers have been removed through a cut-off based on mean*SD, a similar level of accuracy can be found for both methods. In addition to distortion and attenuation, surrounding noise contributes to the error rate, even with applied denoising and filtering techniques, all noise cannot be eliminated. Although initial analysis of the captured signals showed envelope methods to provide favorable results, it is known that cross correlation is highly beneficial in low SNR situations [122][123]. The ratio of signal energy to noise energy has a large impact on the overall system accuracy and therefore a sound understanding of the most suitable analysis techniques to use within the localisation system is highly beneficial. Cross correlation techniques have also proven beneficial in multipath environments when applying a statistical approach based on multiple peaks [124]. This involves focusing on a percentage of peaks with the strongest values from the cross correlation results, as denoted by (5.12) and (5.13), whereby r relates to the AE receivers, t to time, τ to the lag and M to the number of peaks in the resultant cross correlation. The value p specifies the percentage of strongest peaks in which to focus on and thus the number should be chosen to ensure emphasis on the key peaks, whilst not omitting any valuable data.

$$\hat{c}_{r,r'}(t, \tau_1) > \hat{c}_{r,r'}(t, \tau_2) > \dots > \hat{c}_{r,r'}(t, \tau_M) \quad (5.12)$$

$$\hat{t}_{r,r'}(t, n) = |\tau_n|, n \in [1, \dots, \lfloor pM \rfloor] \quad (5.13)$$

This statistical method can be further improved by taking a weighted average of these delays, (5.14), whereby the peaks are weighted based on their amplitude, to differentiate between the main peaks and those of similar amplitude. We consider $N = \lfloor pM \rfloor$ and therefore the weights, $w_{r,r'}$, are applied to each correlation peak based on the ratio between the amplitude of that specific peak over the amplitude of the Nth largest peak (5.15).

$$\hat{t}_{r,r'} = \frac{1}{T \cdot [pM]} \sum_{t=1}^T \sum_{n=1}^{[pM]} w_{r,r'}(t, n) \hat{t}_{r,r'}(t, n) \quad (5.14)$$

$$\hat{w}_{r,r'}(t, n) = \hat{c}_{r,r'}(t, \tau_N) / \hat{c}_{r,r'}(t, \tau_N), n \in [1, N] \quad (5.15)$$

The analysis shown in Section 5.3.4 provided an overview of the effects of varying SNR on the capabilities of the localisation system. The focus of the analysis was on the trial with Rx2 positioned 45m from the fault location as this was considered desirable for signal velocity stabilisation and minimising the likelihood of multipath. The outcome indicated that both envelope and cross correlation techniques could be effectively utilised within the localisation system when considering an SNR of 3dB and above. Below this SNR, cross correlation showed favorable results, with an SNR of -3dB and -7dB both providing high levels of accuracy for PD source localisation.

To further confirm this theory, the overall system performance was evaluated, considering each test performed at varying sensor positions, whilst focusing on signals with an SNR of -3dB and -7dB. The discussed methods were applied within the localisation algorithm to remove outliers and focus on the key data through statistical evaluation, thus improving the accuracy of the position estimation. Multiple PD events were considered at each sensor position, with an average of the system localisation results being shown in Figure 5- 16. The figure shows the estimated PD location in relation to the actual position. It can be seen that the cross correlation are closer to the true position and show a lesser range in results between the two analysed SNR's, thus providing a more accurate system. Improved results are also visible from the adaption of the reviewed analysis techniques, allowing less relevant data to be omitted from the dataset within the algorithm.

Table 5- 6 presents a comparative summary between the two methods, considering the MSE, MAE and percentage error at both SNR's. Again, the results highlight the superior cross correlation performance in low SNR environments and thus this technique should be used within the PD localisation system.

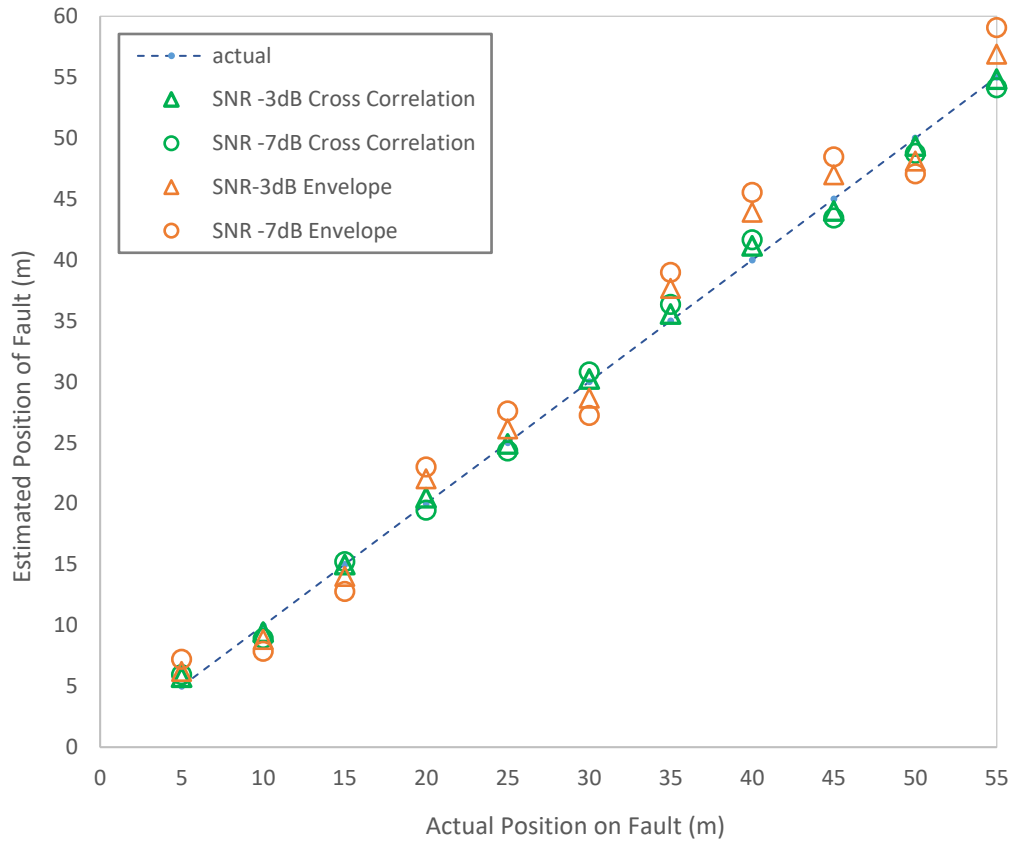


Figure 5- 16: System accuracy comparison for envelope and cross correlation analysis at an SNR of -3dB and -7dB. Position estimation indicates distance from Rx2 to PD fault

<i>Error Analysis</i>	<i>MSE Average</i>	<i>MAE Average</i>	<i>% Error</i>
<i>SNR-3dB Envelope</i>	4.02	1.83	8.24
<i>SNR -3dB Cross Correlation</i>	0.38	0.51	2.93
<i>SNR -7dB Envelope</i>	11.02	3.17	14.63
<i>SNR -7dB Cross Correlation</i>	1.16	0.99	4.98

Table 5- 6: Comparison of Envelope and Cross Correlation Error Analysis

5.4 Detectability Range - Attenuation

To obtain an improved understanding of the detectability range, the change in signal magnitude with distance was investigated. Results from previous tests detailed in Chapter 4.5 were again used for this analysis. As the tests were performed using only two AE sensors, with one sensor being moved in 5m increments for each repetition, results relate to separate discharges and for that reason they can only be used as an indication to the detectability range. To attain a more accurate comprehension of the signals attenuation, multiple sensors would be required throughout the cable length, therefore enabling multiple recordings of the same discharge from varying positions to allow for a true comparison. The complication is due to the varying breakdown strengths of each individual PD event, meaning in certain cases, a larger amplitude may be found further from the sensor if the PD region is close to complete failure. To minimise this issue as much as practicably possible, the following analysis was performed considering an average of all recorded AE discharges at each sensor position.

As the SNR is key in evaluating the detectability range, the strength of the PD emissions and the background noise was considered, an example of which can be seen in Figure 5-17. This figure focuses on an individual PD event from the trial with Rx2 positioned 45m from the discharge location, with Figure 5-17a displaying the envelope of the signal noise and Figure 5-17b displaying the envelope of the acoustic PD emission. The background noise is found to have a strength of around -50dB and the AE signal around -26dB , thus providing an SNR of 24dB .

To investigate the potential detectability range in relation to the SNR, the root mean square (RMS) value of the PD signals captured between 10m and 55m from the PD location is presented in Figure 5-18. It is important to note that the detected EM signals were not included in this evaluation, only the emitted acoustic signals from the PD were considered. It can be seen that although the results are from differing discharges, the signal magnitude does decrease with distance, as expected, starting at around 57dB at 10m and dropping to around 19dB at 55m distance. The SNR at 45m is determined to be around 24dB , aligning with the conclusion of Figure 5-17. Figure 5-18 presents a relatively linear degradation of the SNR with increasing distance from the fault and therefore, a linear trendline was utilised to extrapolate the estimated SNR at distances greater than the recorded 55m.

The estimated signal attenuation based on the extrapolated results is illustrated in Figure 5-19. The outcome of the analysis presented in Section 5.3.4 confirmed that a relatively high level of localisation accuracy could be maintained at an SNR of -7dB and the localisation algorithm could provide a position estimation down to around -11dB , however the accuracy rapidly decreased. Both SNR's are highlighted in the figure to give an estimation of the distance at which each ratio would be reached. This is based on an average of the signal strength whereby the aim is to estimate the SNR of the captured PD signal as the distance increases and, as the maximum allowable SNR within the localisation

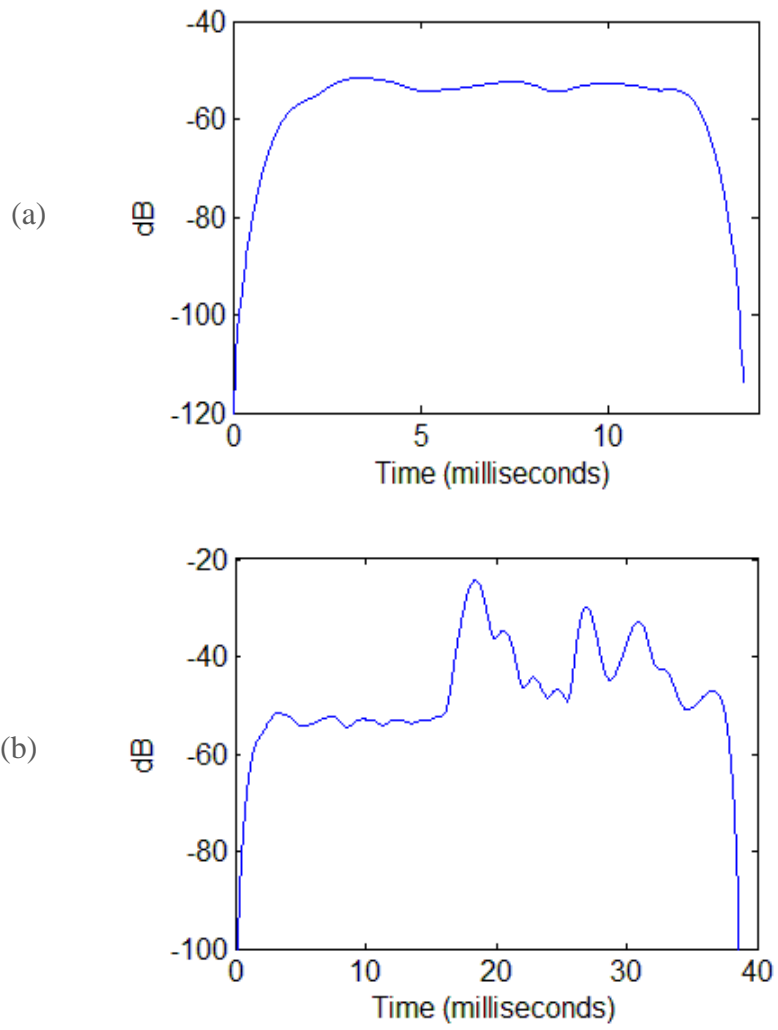


Figure 5- 17: Signal Strength Evaluation; (a) Environmental Noise, (b) Acoustic PD Emission – Samples from trial with Rx2 45m from PD

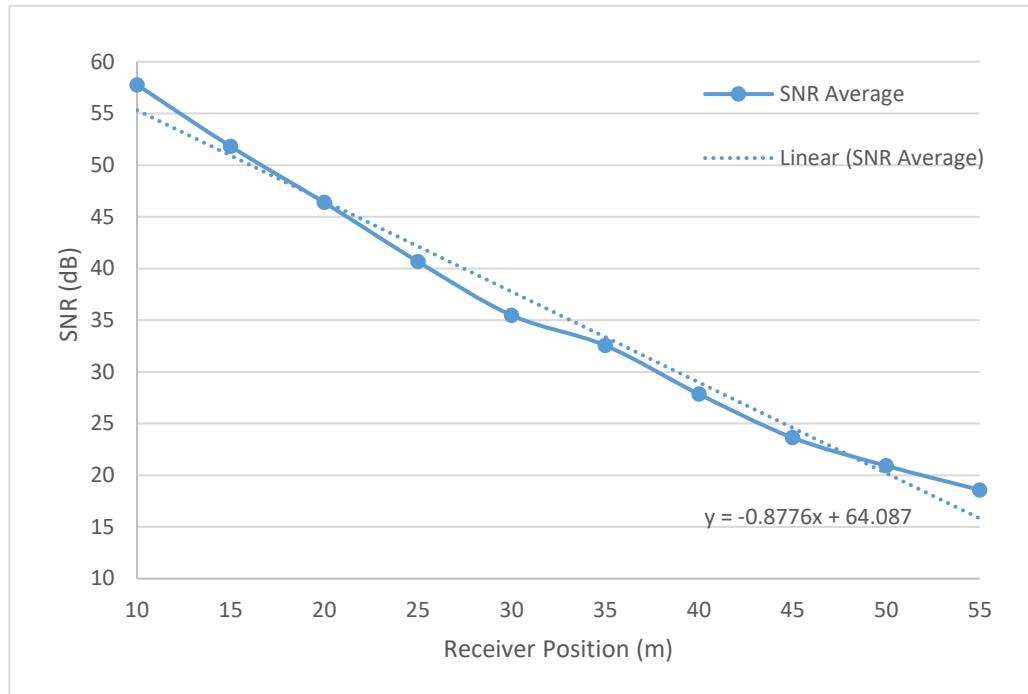


Figure 5- 18: Average SNR at Sensor Positions 10m through to 55m

is known, the maximum detectability range can therefore be estimated. From the figure it can be estimated that an SNR of -7dB will occur at approximately 80m from the discharge location and an SNR of -11dB will occur around 85m from the discharge location. As discussed in Section 5.3.4, the EM signal triggers the system to allow analysis of the captured PD event, therefore a greater SNR of around 3dB should also be considered to account for variation in the system, and so in this instance, a distance of around 70m would be applicable.

It is imperative to note that improvements could be made to increase the detectability range with changes to both the acoustic sensor type and position. As discussed in Chapter 2, existing research considers the benefits of having the sensor placed below the outersheath, coupled directly to the semi-conductive or insulating layers in order to minimise losses of the emitted acoustic signal due to propagation through varying mediums. By doing so, the strength of the detected signal would be improved, consequently providing a higher SNR and greater detectability range. Alternatively, bonded methods for coupling the sensor to the cable could be investigated to provide improved results through reduced air gaps, as the sensors were taped in place with the inclusion of ultrasonic coupling gel during the performed through-cable tests. In addition, this analysis was based on the noise level at the time of the test and therefore can be considered as an indication only based on the available test data.

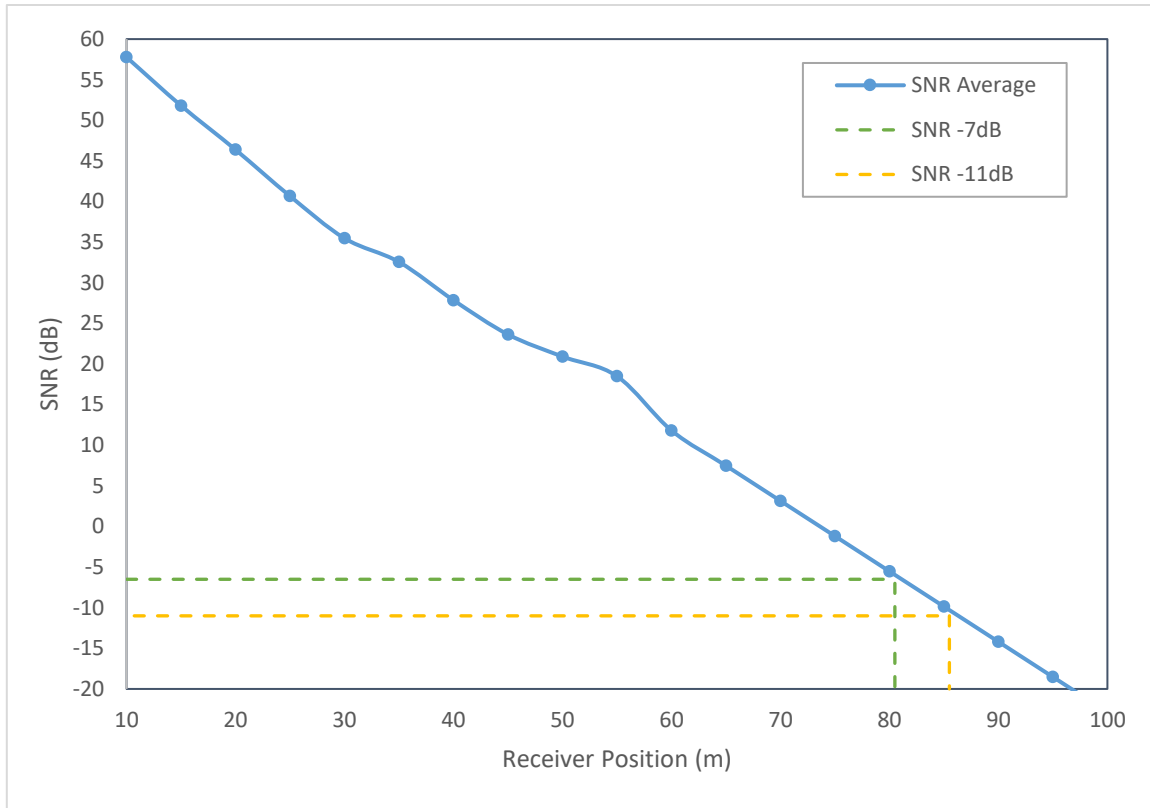


Figure 5- 19: Assessment of PD Detectability Range

5.5 Practical Implementation

When considering through-cable PD detection within the umbilical system, a crucial requirement of the localisation system is that there is zero to minimal impact on the umbilical operation, therefore signifying that the least intrusive option is preferable. Cost is also a key consideration as the operator is less likely to choose to include a method of integrity monitoring if the cost to do so has a large impact on the overall umbilical system.

The least intrusive and lowest cost option would be for the AE sensor to be positioned at the topside of the umbilical, above sea level and ideally coupled to the semi-con or insulating layer of the cable to obtain the greatest detectability range. This method would likely have one sensor only and so would be reliant on TDoA between the EM and AE signals. The use of an HFCT is expected in order to detect the EM signal as it may not be identifiable from the coupled AE sensor when considering greater distances, due to the increased attenuation rate at higher frequencies.

A single AE sensor could be used without the addition of an HFCT by adapting TDR methodology and establishing the TDoA between the direct AE signal and the reflected version of itself. The reflected signal will have travelled to the far end of the cable and

back to the sensor, experiencing greater losses as a result of noise and attenuation. The reflected signal also suffers from distortion due to terminal reflections as well as those associated with propagation through the cable. As the direct and reflected signals travel different lengths through the cable, the shapes and distortion of the signal will differ, resulting in an increased localisation error due to complexities in establishing the peaks of the waves [125]. As a result, this method is only suitable for very short umbilical lengths, however it does offer a minimalist approach.

If the umbilical length is greater than the maximum detectability range, acoustic sensors could be positioned along the cable every ‘X’ number of meters, taking into account the detectability range estimated in Section 5.4. This method does not require an HFCT as the position estimation is calculated based on the TDoA between the discharges detected at two AE sensors synchronised to the same clock. Although this approach is preferred for longer distances, it would be considered intrusive as the sensors would need to be layed within the umbilical bundle and consequently this could not be included as a retrofit option for existing fields looking for life extension. The cost would also be greater than the single topside sensing technique as multiple sensors would be required, along with additional LV power cables and a method for protecting these within the umbilical structure. A similar but less intrusive proposal would be to position the AE sensors on the external sheath of umbilical, piggybacking them to along the length. This could be done at the time of umbilical installation or they could be retrofitted to existing systems using ROV intervention, however this would likely be a costly procedure.

The practicalities of sensor installation and placement would differ for each umbilical depending mainly upon accessibility, environment and umbilical length, along with the operator’s requirements and needs for condition monitoring of the power cable.

When considering the floating offshore wind sector, the water depth will typically be <350m as the focus is for North Sea waters and thus a more minimalistic approach could be considered in comparison to typical umbilicals within the oil and gas sector. In addition, FOW array cables have a typical length of ≈ 2 km and will be connected between turbines, consequently reducing the maximum required detection length due to the ability for topside sensor placement at both umbilical ends.

5.6 Summary

This chapter has discussed potential through-cable acoustic sensing methods to allow for online PD localisation within a subsea umbilical power cable. It has been established that both envelope and cross correlation analysis can be utilised within the localisation algorithm to determine the TDoA between received signals, thus allowing for estimation of the PD location as the propagation velocity and distance between sensors are known.

An initial evaluation of the system accuracy for both cross correlation and envelope analysis showed high levels of accuracy for both methods, with envelope analysis showing

marginally favorable results prior to more detailed post-processing of the recorded AE signals. With outliers removed, localisation results were similar for each technique, however cross correlation provided improved capabilities when at lower SNR's.

Investigation into the effects of the SNR on the overall system confirms that the PD location can be estimated down to an SNR of around -11dB. Lower SNR's leads to system errors whereby a position cannot always be estimated. This was validated for both envelope and cross correlation detection, with cross correlation analysis again displaying preferable results. A high level of accuracy was maintained for both systems down to an SNR of -3dB, as localisation results were found to be within 2m of the PD location. Beyond this, the precision of the envelope analysis results rapidly decreases, whereas cross correlation results present a tight tolerance on accuracy through to an SNR of -7dB, whilst maintaining the average position estimation within 2m of the PD location and 1m of the original signal estimation.

The PD detectability range was explored, providing an indication of the maximum distance at which the location of the PD can be estimated, whilst considering the allowable SNR values for the desired level of accuracy. Analysis showed the maximum detectable distance to be around 85m from the AE sensor, based on a minimum SNR of -11dB. This estimation was established from varying discharges recorded independently at each sensor location and consequently assumptions were made regarding the rate of attenuation through extrapolation of the available data. The potential reduction of the EM signal was also considered, causing a possible reduction in detectable length to around 70m for a higher SNR of 3dB.

The practical implementation of the AE sensors was discussed, whereby the ideal scenario would provide minimal intrusion to umbilical system through only topside sensing, however the length limitations of this approach were highlighted. Alternative techniques were reviewed, requiring multiple sensors to be placed at intervals along the length of the cable or umbilical. The actual positioning and employment of the sensors would be heavily dependent upon the umbilical's application, environment and functionality. Through-cable acoustic detection has shown to be a feasible method for localisation of partial discharges within a subsea power umbilical, however the most suitable method of implementation would be established on case by case basis depending on the umbilical requirements.

Chapter 6

Through-water Acoustic Propagation

The focus of this Chapter is on the through-water detection of the acoustic signal emitted during PD occurrence within the subsea power cable. The influence of the underwater acoustic channel is evaluated as this differs greatly from that previously investigated during the through-cable analysis. Signal velocity, losses, multipath and noise are all considered during this evaluation.

A small scale test was performed in an anechoic tank whereby the acoustic PD signals were recorded to allow simulation of PD through a transmitter during an initial open water trial. The open water trial allowed larger scale testing, under more realistic environmental conditions to provide representative results for evaluation and further analysis of the signals characteristics. The SNR is investigated to estimate the distance at which the signal is detectable within an assumed typical sea state to develop an understanding of the systems capabilities.

6.1 Motivation

Acoustic techniques have been highlighted as a favorable method for underwater sensing due to the low attenuation of sound in water, allowing for AE detection over very long distances, particularly for low frequency signals.

Hydrophones are well suited for underwater acoustic sensing as they are readily used for research within marine environments, where acoustic signals are monitored for tracking of marine life. Acoustic sensing through hydrophones also provides the valuable benefit of a retrofit, non-intrusive system which is highly beneficial for both existing and new field developments.

The use of hydrophones would provide a cost effective, non-intrusive method for online monitoring of PD within the discussed environment, therefore the capabilities are evaluated within this chapter through assessment of the underwater channel and through open water experimental testing.

6.2 Underwater Acoustic Channel

For many years acoustic techniques have been utilised for underwater transmission and detection due to the long range propagation of acoustic waves, which is best supported at low frequencies. Stojanovic provides an overview of the channel properties, highlighting the speed of sound in water, signal attenuation, multipath and external noise as key areas of consideration when designing any underwater acoustic system [126].

6.2.1 Speed of Sound in Seawater

Sound propagates in the ocean at a speed of around 1500m/s. In fluids, the bulk modulus and the density of the medium give the speed of sound. In seawater, these values are dependent on the water temperature, salinity and the surrounding pressure due to the corresponding water depth [90]. The variation in the speed of sound in seawater is minor, though it does have an effect on the positioning algorithm and therefore is considered. Calculating the exact speed is highly complex as changes to the discussed influencing parameters not only vary based on the geographical location, but also due to seasonal variations and time of day, particularly in the upper ocean depth.

Figure 6- 1 presents a typical sound-speed profile, showing greatest variation near the surface [127]. In non-polar regions, the temperature near the surface increases during the warmer parts of the day and consequently the speed of sound increases in this area. The near surface water can also be affected by wind and wave activity, creating a mixed layer of a relatively constant temperature, whereby the depth of the mixed layer is dependent upon the severity of the conditions. The speed of sound within the mixed layer increases with water depth due to the pressure increase. At the base of this mixed layer is the thermocline where there is a rapid decline in temperature causing a decrease in the speed of sound. Below the thermocline is the deep isothermal layer where the temperature is nearly constant at around 2°C, with temperatures fluctuating by less than half a degree per year, hence being considered one of the most thermally stable regions on earth [128]. Although the temperature is low in the deep isothermal layer, the speed of sound increases with depth as the extreme pressure dominates. The minimum sound speed is between the main thermocline and deep isothermal layers and is known as the deep sound channel axis, or the sound fixing and ranging channel, whereby sound waves can travel very long distances. Figure 6- 1 is typical of non-polar regions and considers deeper waters. When considering polar regions, the water is coldest at the surface and there is minor difference between that and the deep water temperature, leading to a lack of a strong thermocline. In shallow waters, only the mixed layer of the sound profile is considered and therefore the environmental temperature and sea state has a large impact on the propagation speed at these depths.

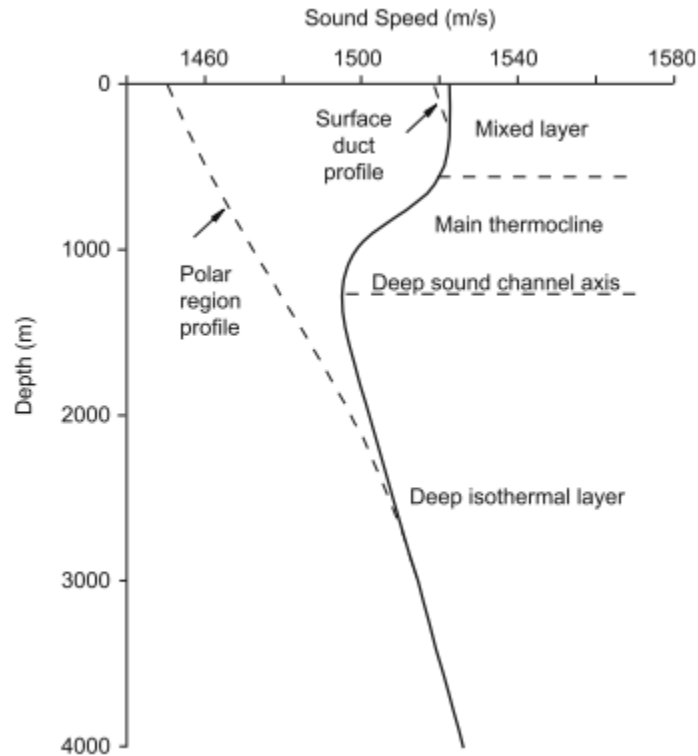


Figure 6- 1: Generic Underwater Sound Speed Profile [127]

The salinity of the ocean is typically recorded by measuring the amount of salt per 1000g of water and is therefore referred to as parts per thousand (ppt). Salinity has less of an influence on the speed of sound in comparison to temperature and pressure. The effect of the salinity on sound speed is minor and generally, the variation in the salinity of the ocean is minor, with most locations falling between 34ppt and 36ppt.

The speed at which the acoustic emission from the PD travels is used within the localisation algorithm to establish the position of the potential fault, therefore it is important to input a value as close as practicably possible to the actual speed in order to improve the accuracy of the system, and for that reason it is key to consider the salinity, temperature and pressure of the surrounding seawater.

Another aspect to consider is the doppler effect as this causes frequency shifting, along with frequency spreading. The doppler effect occurs due to changing distances between the receiver and the object transmitting the sound wave, resulting in variations in signal delay. The proposed sensing system will not be largely influenced by the doppler effect as, unlike autonomous underwater vehicles, the hydrophones are not intentionally in motion, The hydrophones will however, be subject to waves, currents and tides, consequently affecting the accuracy of the localisation system.

6.2.2 Transmission Loss

Sound waves travelling through the water become weaker the further they travel due to spreading and absorption. The total reduction in signal strength is referred to as transmission loss, TL , and is expressed in dB. The transmission loss is defined as the ratio of the sound intensity at a reference point of 1m from the source of the emission, I_s , to the intensity at distance R , given by (6.1).

$$TL = 10 \log \frac{I_s}{I(R)} \quad (6.1)$$

Spreading loss is a measure of how much the signal weakens as it propagates out from the source of the emission. The energy in the sound wave remains the same as it spreads outwards from the source and therefore the energy per unit length reduces, consequently causing a reduction in amplitude of wave. In the ocean, sound waves propagate in all directions, leading to spherical spreading, whereby the intensity will decrease proportionally to the surface area of a sphere. This works on the assumption that there are no boundaries to influence the acoustic energy. The intensity of the energy decreases as the inverse square of the range for spherical spreading. Cylindrical spreading needs to be considered in environments where the sound wave reaches the surface or bottom of the ocean and is reflected back or trapped within these boundaries. With cylindrical spreading, the sound is no longer transmitted spherically, but instead the propagation is considered as a cylinder, whereby the radius equates to the range of the transmission and the height of the cylinder to the width of the channel. The loss of acoustic energy with cylindrical spreading is typically less than with spherical spreading.

Sound absorption is dependent upon the medium the wave is passing through, which in this case relates to the properties of the seawater and considers; viscous absorption, boric acid relaxation process and magnesium sulfate relaxation process. Propagation of the sound wave through seawater changes some of the acoustic energy into heat, resulting in a reduction in the signals strength. The energy from the sound wave causes the molecules within the seawater to vibrate, however, the molecules must be powerful enough to overcome the viscosity of the water and thus some energy from the sound wave is used, causing absorption. The impact of sound absorption on transmission loss is particularly influenced by the frequency of the sound waves. Sound absorption increases with frequency as the vibration of the molecules within the seawater also increases, therefore requiring more energy from the sound wave. Low frequency sound waves vibrate less, requiring less energy and consequently resulting in low frequency sound waves travelling further than high frequency when in a comparable environment. In addition to the discussed absorption loss, chemicals which affect the salinity of the seawater also absorb sound, causing a further loss of acoustic energy through heat.

The formula for transmission loss, considering both spherical spreading and absorption is given by (6.2), where the left side of the equation relates to spherical spreading and the right to the absorption coefficient, α , in dB/m.

$$TL = 20\log_{10}(r) + \alpha(r) \quad (6.2)$$

The transmission loss has a direct impact on the detectability of a system and the SNR. The SNR takes into account whether or not a signal will be detectable amongst the background noise in the surrounding environment. SOund Navigation And Ranging (SONAR) equation is used to estimate the SNR for both active and passive sonar systems. Passive sonar is most relevant to the discussed application as the system is used to listen to sources of underwater sound, as opposed to active system whereby pulses are transmitted and the receiver listens for the corresponding echoes. The SONAR equation for passive systems considers the source level, sound spreading, attenuation, background noise and any gain at the receiver. The source level, SL , can be calculated using (6.3) and is the ratio of the sources signal intensity at 1m distance, I_s , and the reference intensity of the wave having a RMS pressure of $1\mu\text{Pa}$, I_{ref} .

$$SL = 10\log \frac{I_s}{I_{ref}} \quad (6.3)$$

The source level, SL , of the sound is reduced by the transmission loss, TL , between the source of the emission and the signals receiver, resulting in the received signal in dB, as expressed in (6.4).

$$\text{Received signal intensity (dB)} = SL - TL \quad (6.4)$$

The noise level (NL) and array gain (AG) at the receiver can then be considered to calculate the SNR (6.5).

$$SNR (dB) = SL - TL - (NL - AG) \quad (6.5)$$

6.2.3 Multipath

Acoustic signals propagate in an omnidirectional way and therefore the received signal often contains both the direct path signal and multiple reverberations. In certain cases, the direct path signal is distorted with dips or fades in the response due to reflections causing cancellations of certain frequencies and changes in signal amplitude. Reflections occur when the signal hits a channel boundary such as the sea surface, sea floor or another object in its path. The reflections are dependent on the angle of incidence and the boundary mediums as this will determine how much of the signal energy is reflected back and how much is absorbed. Reflections of nearby objects can lead to multipath signals of similar signal energy as the direct signal which can result in deep nulls in the received signal amplitude. Selective fading occurs when multipath fading affects different frequencies varying amounts, resulting in changes to phases and amplitudes across the channel. In certain cases of data transmission, Orthogonal Frequency Division Multiplexing (OFDM) can be used to spread the data over a wide channel so that only a portion of the data is lost by any nulls. The data is then reconstituted using error correction techniques to reduce the negative effects of fading. This however, is not possible for the discussed application.

Multipath is less of an issue in deeper waters as the reflected signals will largely be attenuated by spreading and absorption losses before reaching the receiver, whereas in shallower waters there are many boundaries for the signal to meet. Figure 6- 2 presents the complexities of multipath showing an example of multipath trajectories in a shallow water environment [90]. The direct path of the signal is shown in *A*, and signals *B* to *E* display the potential reflection signals whereby the sound wave has hit a boundary of the surface or the seabed.

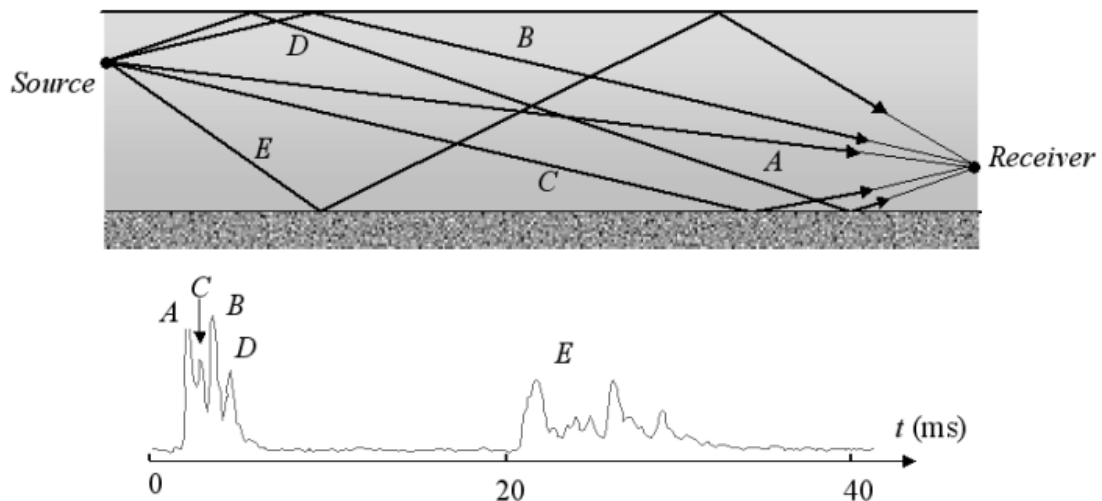


Figure 6- 2: Multipath in a shallow water configuration

The use of directional hydrophone sensing would also minimise the impacts of multipath as the receiver would be focused on the area of interest, increasing the sensitivity in that direction and minimising the omnidirectional reflection signals.

The refraction of a signal occurs due to changes in the temperature, pressure and salinity of the water, which in turn alters the speed of sound. Snell-Descartes law describes how the variation in sound speed across the thermal layers can result in the acoustic signal becoming refracted. The change of sound between two mediums induces reflection of the wave in the first medium and the refraction of the wave in the second medium at an angle given by (6.6), where c_1 and c_2 represent the velocity of the sound within the first and second layers and β_1 and β_2 represent the angle of arrival and refraction from the boundary.

$$\frac{\cos \beta_1}{c_1} = \frac{\cos \beta_2}{c_2} \quad (6.6)$$

The limit angle (low-grazing incidence), β_c , is the critical angle for the interface and is given by (6.7). For angles β smaller than β_c there is total reflection and transmission into the second medium is impossible [129].

$$\beta_c = \arccos\left(\frac{c_1}{c_2}\right) \quad (6.7)$$

Refraction is more of a concern over longer transmission distances due to changes in the sound velocity profile, resulting in bending and refraction of the sound waves, consequently leading to received multipath signals. Shorted ranges have a more consistent sound velocity profile, leading to less refraction of the sound waves.

6.2.4 Noise and Interference

Underwater sounds in the ocean come from a variety of sources, both natural and anthropogenic. Natural sounds include environmental occurrences such as rain, wind, waves and seabed movement, as well as sounds from marine life. Anthropogenic sounds are from human activity and include; shipping, construction of offshore facilities, oil and gas operations, seismic surveys and sonar sources. Underwater noise sources cover a wide range of frequencies at varying noise levels, as shown in Figure 6- 3 [130].

Wind strength, sea state and surface gravity waves are the main mechanisms of natural sounds in the ocean, all of which are heavily dependent on the geographical location. Deeper waters will see less of an effect from breaking waves in comparison to shallower depths. Arctic environments experience different impacts where the ice acts as a protective layer from wind exposure, however additional noise is present from ice cracking or glacial movement. The position of the sensing system will also influence the impact of the natural

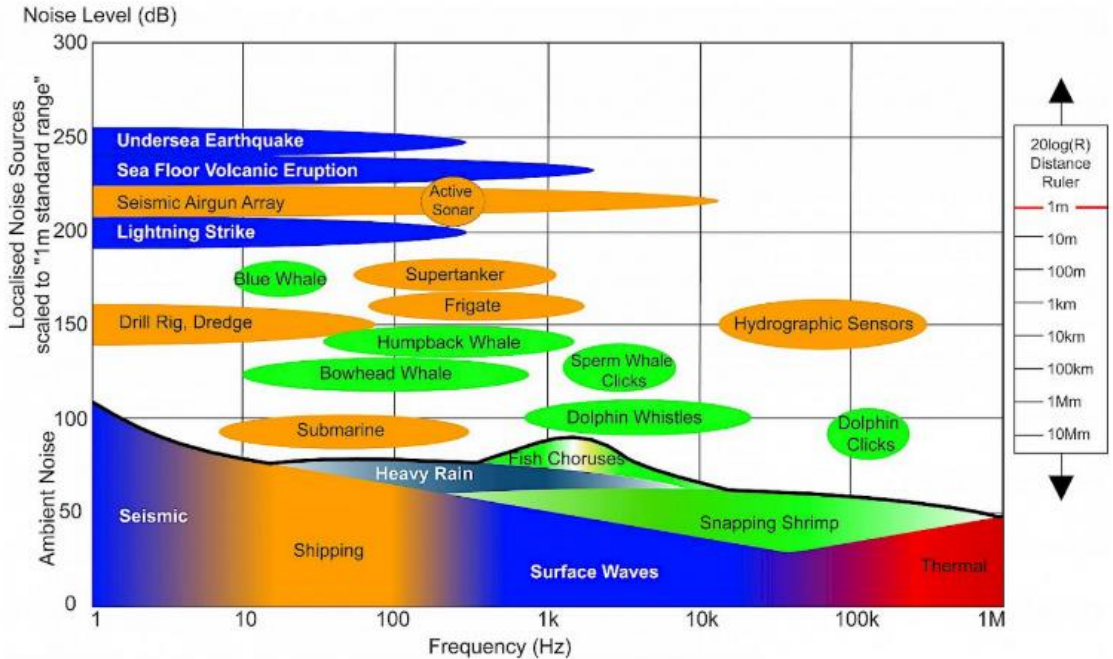


Figure 6- 3: Levels and frequencies of anthropogenic and naturally occurring sound sources in the marine environment. Spectrum Noise Level versus Frequency [130]

noise sources, as hydrophones positioned close the surface will experience the greatest impact from breaking waves, rain fall and wind.

In addition to environmental considerations, marine life also adds to the collection of underwater sounds. Many marine mammals use sound as a way to communicate and sense in an underwater environment, resulting in a variety of tones and noises across the acoustic spectrum.

Anthropogenic sounds can be both impulsive or continuous. Impulsive sounds are of short duration and occur irregularly or repetitively, whereas continuous sounds occur without a pause. A common cause of continuous noise is due to commercial shipping which generates low frequency sound. Hildebrand discusses many sources of anthropogenic sounds in the marine environment, noting the increase in ambient noise over the past 50 years at both low frequencies (less than 1000Hz) and mid-frequencies (1-2KHz) [131].

An additional aspect to consider is the potential interference or noise from the system itself. In the proposed acoustic sensing application, depending upon the connections and setup topside, there is potential for electrical noise on the power supply. The umbilical will also produce its own sounds due to movement and hydraulic flow, as well as the acoustic emissions from PD in which the system is trying to detect.

Some forms of underwater noise can be predicted based on environmental data from the geographical location, time of day and knowledge of anthropogenic activities in the

surrounding area, however some sounds are less predictable and more erratic in nature, potentially impacting the ability of acoustic sensing systems in certain operations.

6.3 Open Water Trial - Detection

An understanding of the through-water propagation of the AE from PD is imperative to the proposed localisation system. Testing in an open water environment allows the system to be trialed in relevant operating conditions to assess the initial feasibility for PD sensing. North Shields Marina was identified as a suitable testing site for an open water trial whereby multiple hydrophones would be positioned at varying distances within the water to listen for PD occurrence. To minimise the complexity of the initial trial, the partial discharge signals were recorded and replayed through a transmitter, thus removing the need for HVAC equipment at the waterside.

6.3.1 Controlled Testing

Prior to testing in a large open water environment, small scale testing was performed in an anechoic water tank filled with fresh water at Newcastle University, allowing evaluation of the through-water acoustic signal characteristics in a controlled environment, along with the recording and calibration of the AE signals to enable simulation of PD through the use of a transmitter.

A short cable sample of approximately 2m was used, again containing a man-made fault. The fault was positioned close to the far end of the cable sample with the fault region and cable end sealed appropriately to prevent water ingress. The area containing the fault was fully submerged and two hydrophones were positioned in each corner of the tank to listen for any PD occurrence. The hydrophones used are Neptune Model D/70 which have an omnidirectional beam pattern, with a broadband frequency response and high sensitivity. The open cable end was connected to an HVAC supply and the voltage increased in incremental stages until PD could be detected.

Figure 6- 4 presents a 1minute capture of the acoustic signals detected during the trial. Numerous PD events were detected, with both hydrophones detecting the emission at similar times due to their positioning at each corner of the anechoic water tank.

Figure 6- 5 focuses on an individual discharge recorded during the trial. From this it can be seen that the signal is detected first on hydrophone Rx2, however the difference in sensor positions is very minor. When concentrating on the detected EM signal, it is noted that the amplitude is much smaller than that detected during through-cable sensing. The EM signal experiences high attenuation due to the conductivity of water, with an even greater impact expected when testing in seawater as the conductivity is around 5 Siemens/meter. This EM

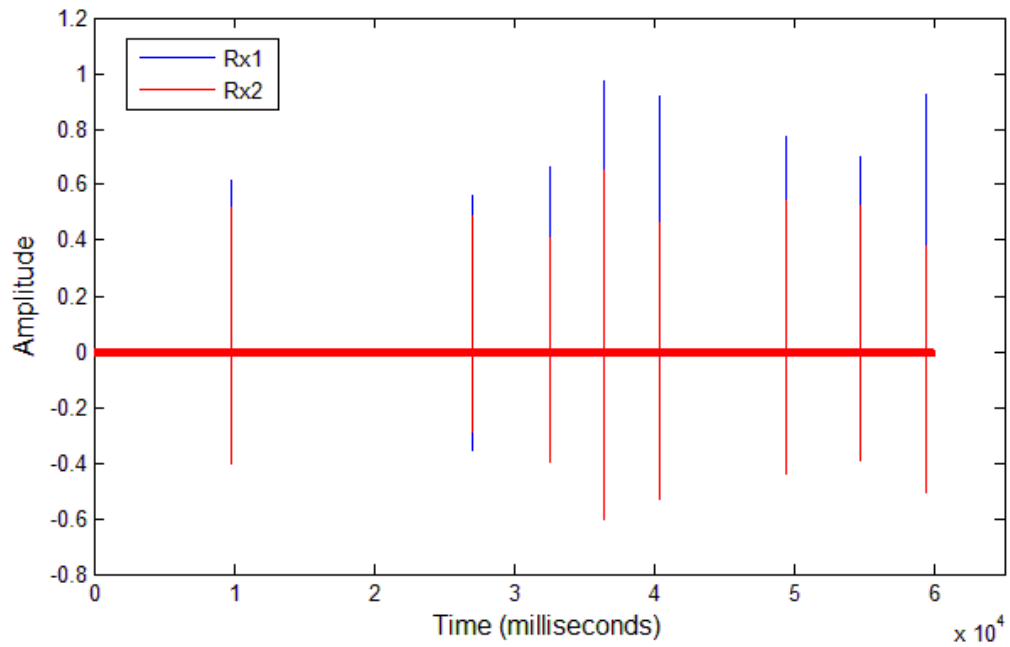


Figure 6- 4: Acoustic Signals from PD detected on Rx1 and Rx2 during test in an anechoic water tank

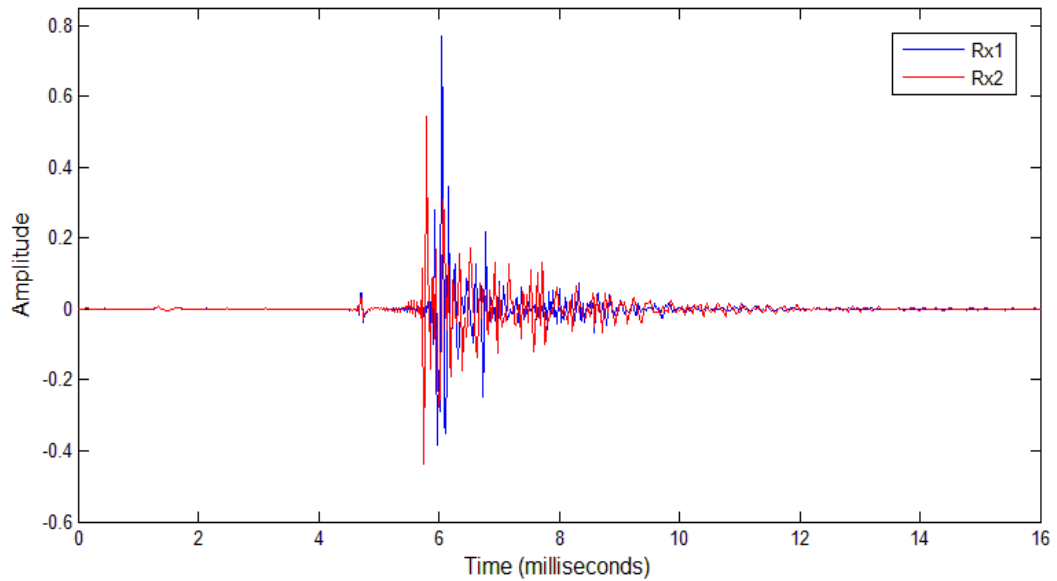


Figure 6- 5: Individual Acoustic Emission from PD detected on Rx1 and Rx2 during test in an anechoic water tank

attenuation is expected therefore the focus of the through-water sensing is on the acoustic signals where TDoA techniques are utilised to allow PD source estimation. Should the EM signal be required to understand time of PD occurrence, other methodologies such as HFCT's can be used, alongside the acoustic sensing system. The shape of the individual pulse differs from that detected during through-cable sensing, however the duration of the pulse is similar at around 4ms in length. Multiple PD events were analysed, each showing similar results.

The envelope and cross-correlation of the signals recorded on each hydrophone were also analysed to ensure the results were showing as expected, with minimal difference in distance between the fault position and the two acoustic sensors. Figure 6- 6 presents an average of the envelope analysis results, showing a difference of 7 samples between the two peaks and Figure 6- 7 presents the cross correlation results, showing a lag of 13. Considering (4.12) and a sampling frequency of 44.1kHz, the time difference between the received signals based on 7 samples and 13 samples is 0.16ms and 0.29ms respectively. To calculate the distance at which one sensor is further from the PD source (4.13) can be applied, where a typical velocity of 1500m/s is considered, resulting in 0.24m from the envelope analysis and 0.44m from the cross correlation. There is a discrepancy between the calculated distance from the two TDoA methods, however this is minor at around 0.2m but would have a slight impact on the systems accuracy. The hydrophones were considered to be approximately 1.5m from the fault region, however in this case the exact distances

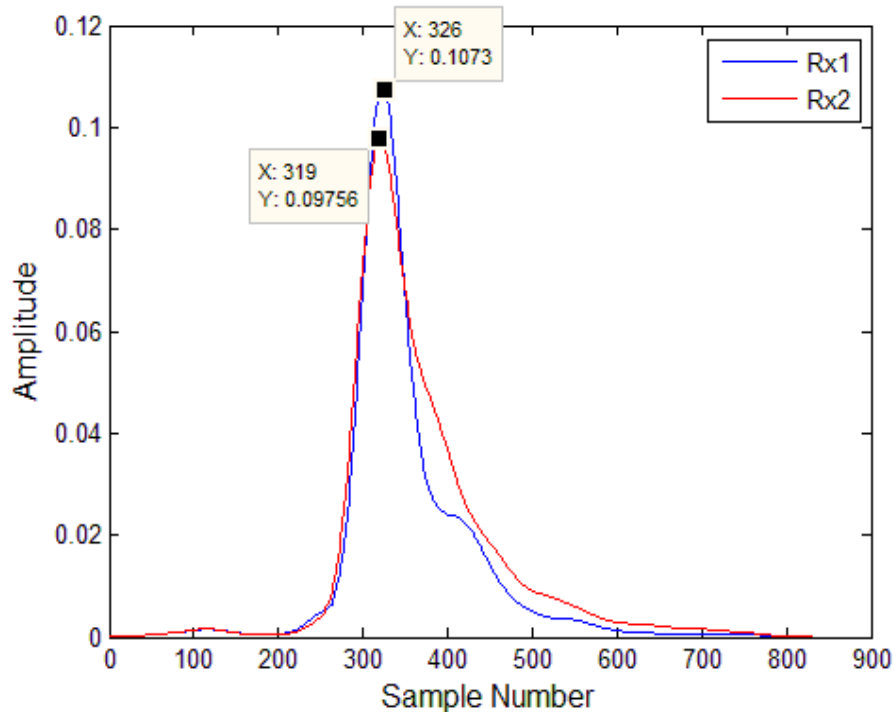


Figure 6- 6: Envelope analysis results for an individual Partial Discharge detected on Rx1 and Rx2 during test in an anechoic water tank.

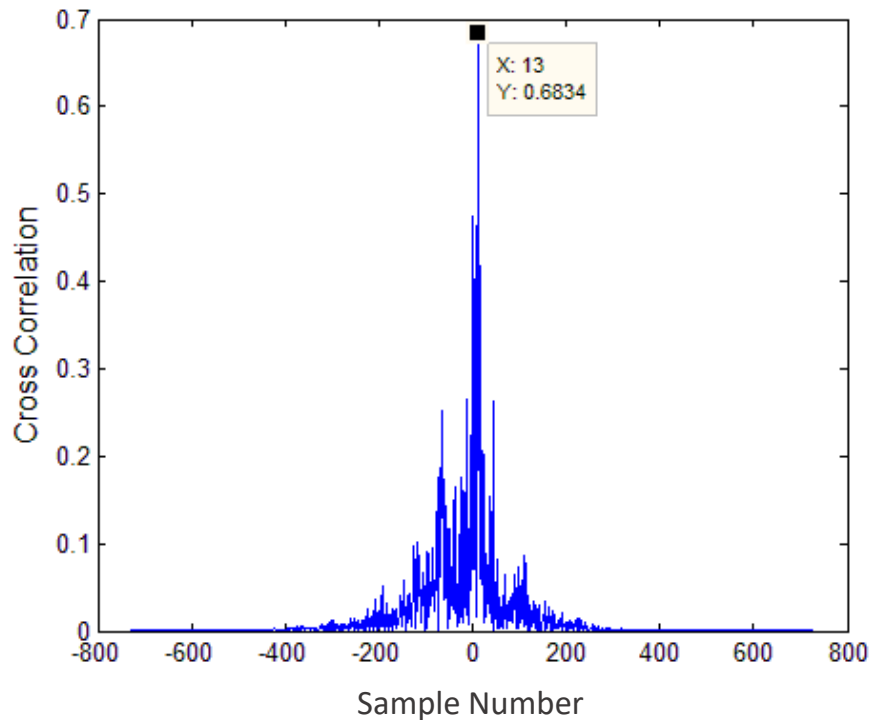


Figure 6- 7: Cross Correlation results for an individual Partial Discharge detected on Rx1 and Rx2 during test in an anechoic water tank.

were not known as the position of cable sample was measured from the topside of the water tank, and the depth plane was not considered. As confirmed in analysis of the through-cable signals, the cross correlation results are considered to be more accurate and consequently Rx1 is considered to be 0.44m further from the fault than Rx2.

Figure 6- 8 presents the frequency spectrum for an individual discharge. This differs from the frequency spectrum of the through-cable propagation results as it is highly broadband, spanning the complete measured 22kHz spectrum. This is partly due to the large attenuation of the higher frequency components over the length of the cable in the through-cable sensing, in comparison to the short propagation range within the anechoic tank. An additional influence is due to sound travelling well through water when compared to sound travelling through changing mediums such as that of the cable construction, as high losses are experienced at each interface.

The spectrogram of the complete 60 second recording can be seen on Figure 6- 9, with a 2D time vs frequency plot shown in (a), and a corresponding 3D plot shown in (b), whereby the magnitude of the signal is also considered. The spectrograms show the complete capture and therefore contain both the EM and AE signals, however the impact of the EM signal is minimal when compared to that detected during through-cable analysis as in this case, the magnitude of the acoustic signal is much greater than the EM signal. The spectrograms

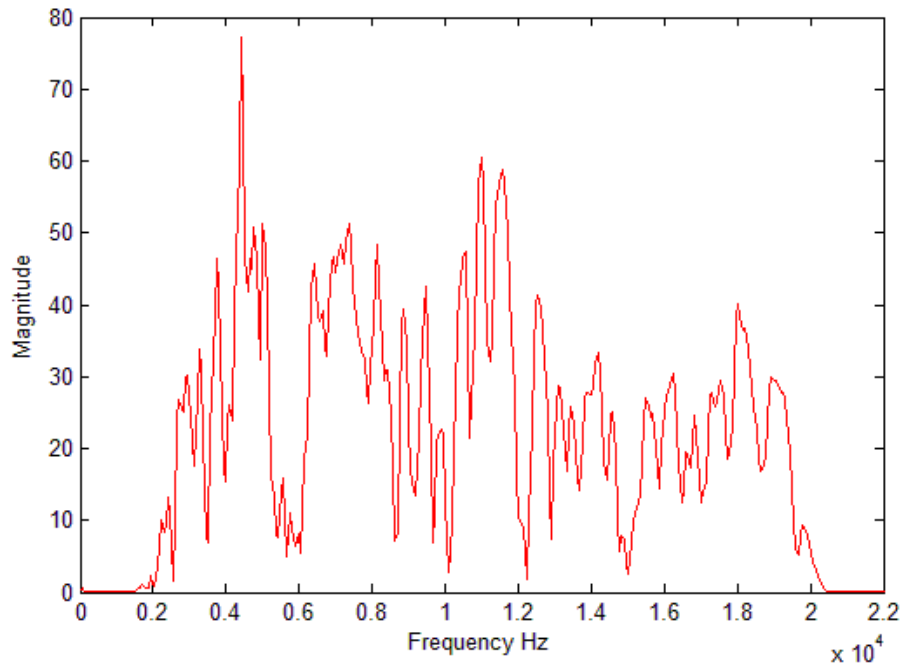


Figure 6- 8: Frequency Spectrum of Individual AE from PD within Power Cable Insulation, detected with Hydrophones via through-water Acoustic Sensing.

focus on the same recording as shown in Figure 6- 4, and it can be seen that the detected discharges are of short duration, highly broadband, with the signals energy remaining relatively consistent across the full 22kHz spectrum. This is further confirmed by the power spectral density presented in Figure 6- 10, which focuses on an individual PD event detected on both Rx1 and Rx2. The signal strength will vary depending on the characteristics of the discharge, however it is clear the signal energy is strong across the 22kHz spectrum. It should be noted that the power spectral density considers only the acoustic signal and not the electrical discharge, therefore shows the true characteristics of the detected acoustic emission.

The analysis presented is based on close range recordings to develop an understanding of the characteristics of the through-water acoustic signals emitted during PD occurrence. It is recognised that the signal will experience attenuation over a greater distance, particularly the higher frequency components, however, there is a large signal energy across the spectrum and thus the focus can be on the lower frequency components when long distance detection is required.

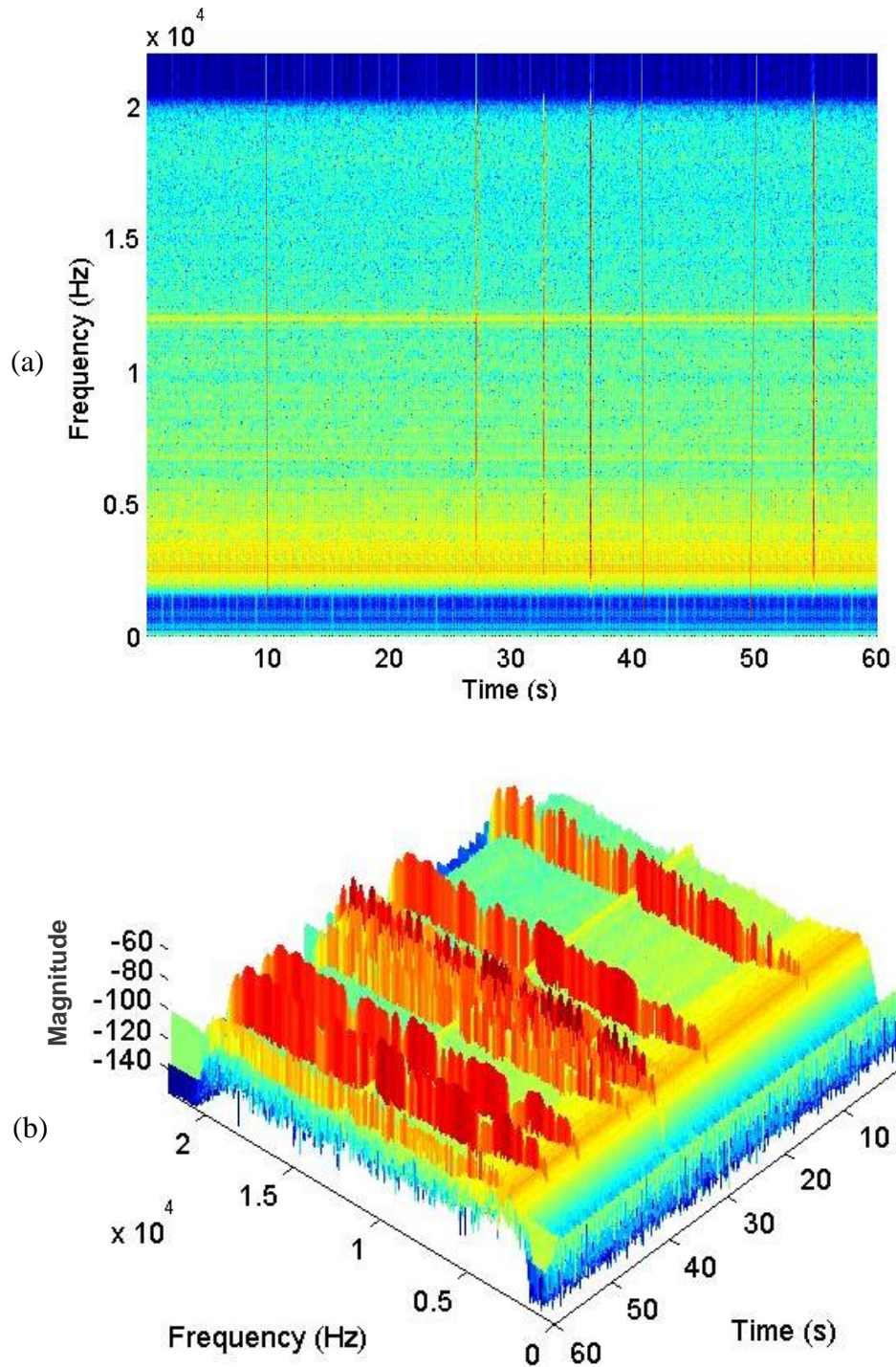


Figure 6- 9: Spectrogram of AE Signals from PD within Power Cable Insulation detected with Hydrophones via through-water Acoustic Sensing: (a) corresponding 2D time vs frequency plot, (b) corresponding 3D plot including signal magnitude

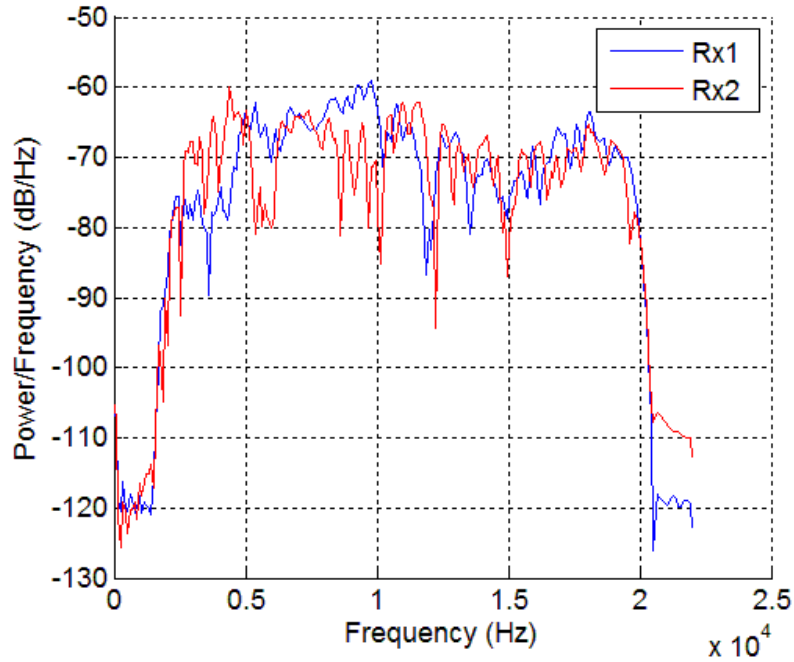


Figure 6- 10: Power Spectral Density of Individual Acoustic Emission from PD within Power Cable Insulation detected with Hydrophones via through-water Sensing

6.3.2 Calibration & Detectability

Following examination of the through-water signal characteristics, an additional trial was performed whereby a transmitter was used to send a known signal to allow the hydrophones to be calibrated in order to get an understanding of the source level of the acoustic emissions from PD within the cable. Knowing the source level would allow for estimation of the detectable distance at varying SNR's and also ensure the recorded AE discharges are sent through the transmitter during the open water trial at a level which replicates the actual PD.

For this trial the hydrophones were moved to approximately 1m from the fault location. The known signal was transmitted at a voltage of 20Vpp and a frequency of 12kHz, with the test setup shown in Figure 6- 11.

The transmitter source level, SL , can be calculated utilising (6.8), where V_{rms} is the RMS voltage of the transmission signal, and the Transmit Voltage Response, TVR , is defined as the output sound intensity level generated by the transducer per 1V of input voltage as a function of frequency, which in this case results in 156dB re 1 μ Pa at 1m based on a TVR of 139dB and a V_{rms} of 7.07.

$$\text{Transmitter } SL(\text{dB}) = 20\log_{10}(V_{\text{rms}}) + TVR \quad (6.8)$$

The recorded signals from both the PD emissions and the known signal transmission can then be evaluated to determine the V_{rms} for each, with the values then input to (6.9) to establish the SL for the acoustic PD events, where TSL relates to the transmitter source level, x to the RMS value of the PD emission and y to the RMS value of the known signal.

$$\text{PD emission } SL(\text{dB}) = TSL + 20\log_{10}\frac{x}{y} \quad (6.9)$$

As each PD event differs depending on the fault itself, an average RMS value was established through analysis of multiple PD events, resulting in a SL of 144dB for the PD acoustic emission.

This value can then be used to estimate the SNR and detectable distances for varying sea states by considering (6.10), where r , is the range, α is the absorption loss, NSL , is the noise spectral density level of the sea and β is the bandwidth. For these calculations, the absorption loss is ignored, particularly as the focus is on the low frequency components and therefore the impact is considered minimal.

$$SNR(\text{db}) = SL - (20\log_{10}(r) + \alpha(r)) - (NSL + 10\log_{10}\beta) \quad (6.10)$$

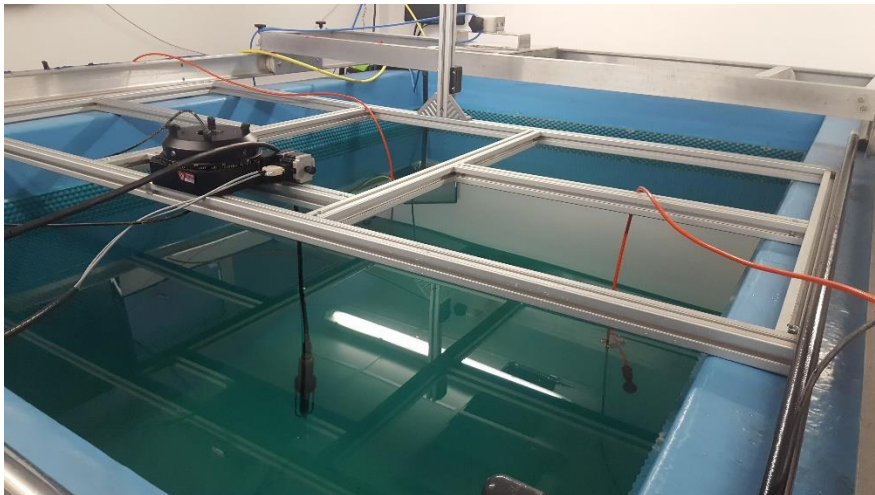


Figure 6- 11: Anechoic Tank Controlled Experimentation

Broadband ambient noise spectrum levels range from 45-60dB in relatively quiet ocean regions with light shipping and calm seas [132]. For areas with heavy shipping traffic and high sea states the noise level increases to around 80dB. Based on these *NSL* values, (6.10) can be utilised to estimate the SNR at varying distances. The dB detection threshold for the through-water sensing system is indicative based on results from the through-cable sensing analysis and therefore, SNR's of both 3dB and -3dB were considered in the estimation of the detectability range.

Firstly, focusing on the lowest *NSL* of 45dB and a bandwidth of 17.6kHz, an SNR between -3dB and 3dB would allow detectability of PD over a calculated range of approximately 500-1000m from the source. Considering a more realistic *NSL* value of 60dB, the detectability range drops to around 100-200m from the source. Finally, considering a heavy noise ocean environment of around 80dB, the detectability range reduces greatly to around 10-20m from the source of PD. This illustrates the effect of the environmental noise on the capability of the system, although the detectability distance could be greatly improved through the use of directional sensing, as opposed to the omnidirectional hydrophones used within the trials. Furthermore, for deepwater conditions with a high level of ambient ocean noise, there is also the potential option to position AE sensors within closer proximity to the power umbilical through the use of underwater vehicles as this would again offer a retrofit option. This, however, would be a more costly method than deploying hydrophones from the surface of the water and consequently would only be considered if the operating depths or environmental noise was considered too great for the systems capability.

6.3.3 Open Water Test Configuration and Initial Findings

The open water trial was performed at North Shields Marina in Newcastle upon Tyne. An image of the marina can be seen in **Error! Reference source not found.** This allowed for testing in an open water environment, where hydrophones could be positioned at differing locations to allow for position estimation and at a suitable range from the transmitter. Unlike the through-cable sensing, a minimum of three hydrophones were required for localisation of the fault as the area of sensing was no longer performed on a linear axis. Only two sensors are required for linear positioning, whereas three or more are required when considering additional axes. Having the PD occurrences pre-recorded for transmission allowed multiple trials to be performed without needing to repair the cable between insulation breakdowns. The position of the three hydrophones, Rx1, Rx2, Rx3, remained constant throughout all of the trials, with the transmitter, Tx1, being moved to varying locations within the marina for each trial performed.

The test was performed with the three hydrophones and transmitter located between jetty's labelled 1 and 2 in Figure 6- 12. Figure 6- 13 focuses on this area and presents the fixed positions of the hydrophones, along with the position of the transmitter for one of the trials. A total of sixteen trials were performed across eight locations, with the furthest being

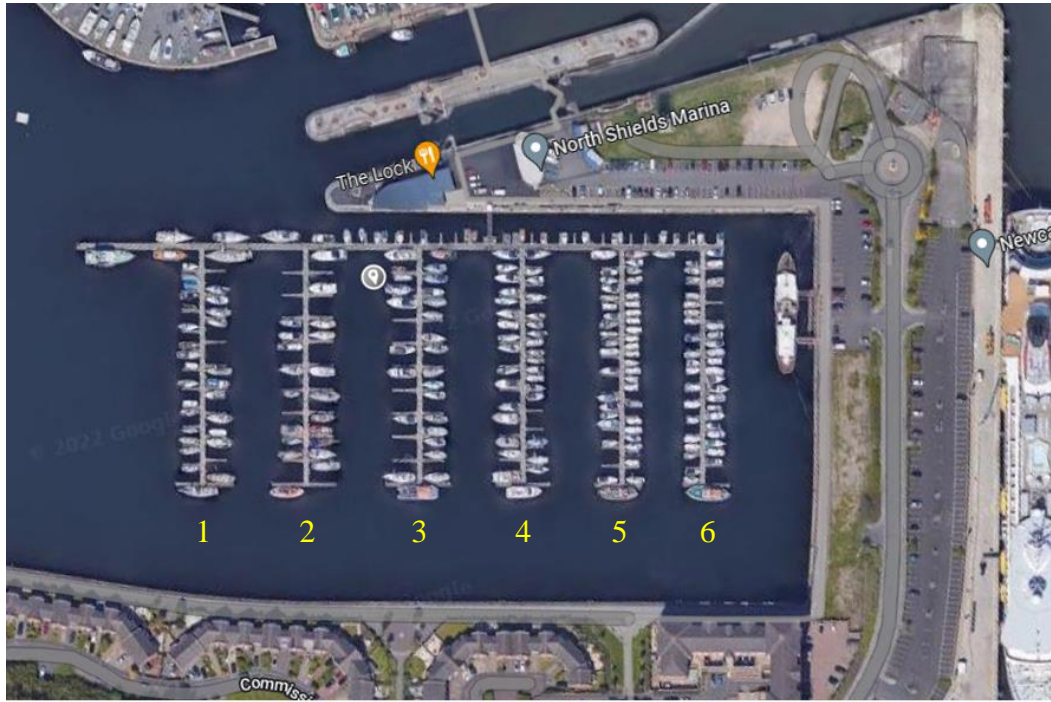


Figure 6- 12: North Shields Marina

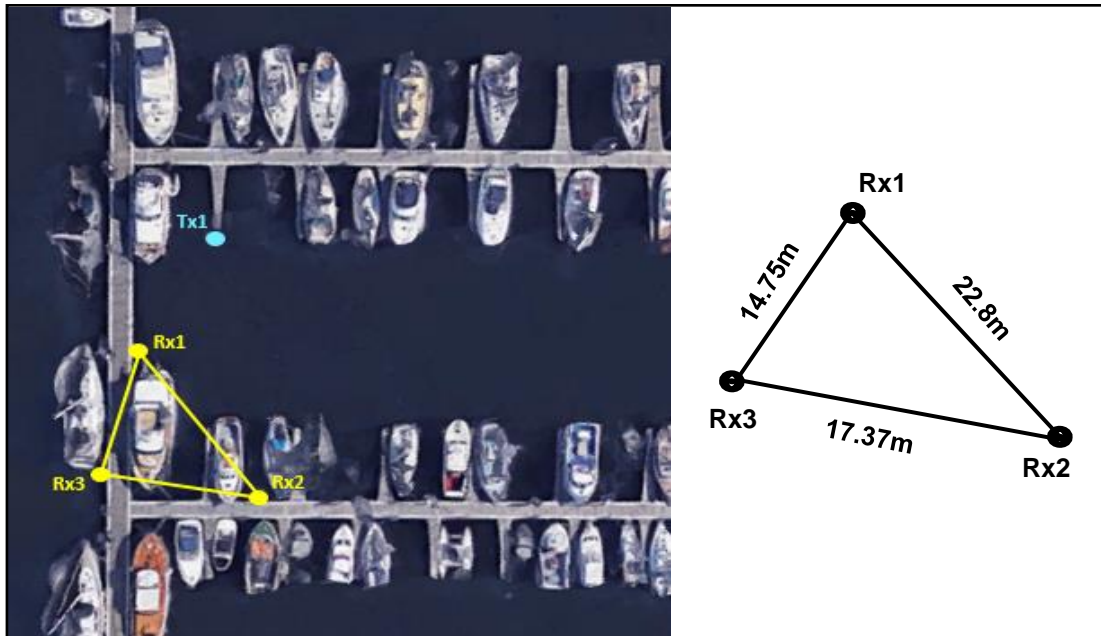


Figure 6- 13: Open Water Trial – Receiver Positions

approximately 85m from the fault. Each of the eight locations consisted of two recordings, the first with the transmitter positioned at 1m water depth and the second at 3m water depth. The depth of the receivers remained constant at 1m throughout all trials. Positioning the receivers at a greater depth would have reduced the likelihood for multipath due to reflected signals from the surface and surrounding boats, however the receiver cables were length limited. The change in transmitter depth was recorded to allow the z-plane to also be considered in 3D localisation of the PD source. Four of the transmitter locations were within the receiver triangle and the other four were outside of this area. For each trial, the transmitter position is known and recorded to allow the accuracy of the localisation system to be assessed. Table 6- 1 presents the measured distances from transmitter to receiver for each of the sixteen trials.

The data acquisition setup remained the same as that shown in Figure 4- 3, however with the power cable replaced by the transmitter and an additional hydrophone fed into the same system, thus allowing clock synchronisation of the received signals for TDoA estimation. The files were recorded with a sampling frequency of 48kHz and an array gain of 0dB for the hydrophones. The marina was regarded as a quiet sea state, when considering the expected SNR of the detected emissions.

Figure 6- 14 displays an 80 second recording taken during the first trial, with signals detected on all three hydrophones, Rx1, Rx2 and Rx3. The previously recorded PD signals were transmitted on a loop during each trial performed therefore the signals will repeat

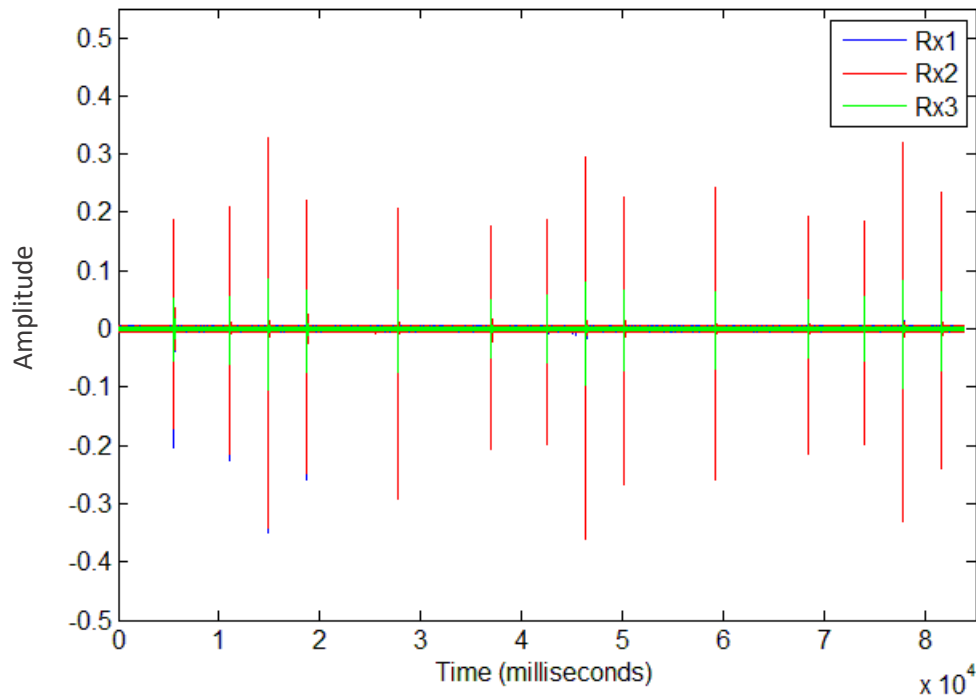


Figure 6- 14: Open Water Trial 1a, PD emission captures on receivers Rx1, Rx2 and Rx3.

<i>Trial Number</i>	<i>Transmitter Depth (m)</i>	<i>Rx1 Distance from Fault (m)</i>	<i>Rx2 Distance from Fault (m)</i>	<i>Rx3 Distance from Fault (m)</i>
<i>1a</i>	1	12.04	10.82	12.27
<i>1b</i>	3	12.20	11.00	12.43
<i>2a</i>	1	19.70	6.00	11.56
<i>2b</i>	3	19.80	6.32	11.73
<i>3a</i>	1	5.00	19.10	9.91
<i>3b</i>	3	5.39	19.20	10.11
<i>4a</i>	1	14.00	14.56	3.03
<i>4b</i>	3	14.14	14.70	3.63
<i>5a</i>	1	38.08	24.70	40.37
<i>5b</i>	3	38.13	24.78	40.42
<i>6a</i>	1	16.12	32.56	30.49
<i>6b</i>	3	16.24	32.62	30.56
<i>7a</i>	1	40.03	39.70	49.49
<i>7b</i>	3	40.08	39.75	49.53
<i>8a</i>	1	78.72	71.11	85.38
<i>8b</i>	3	78.75	71.14	85.40

Table 6- 1: Transmitter to Receivers Distances for all Sixteen Trials at Locations 1 through to 8.

after 60 seconds. The PD occurrences can be clearly seen throughout the recording, with the signal amplitude remaining well above the noise level. The position of the transmitter remained in close proximity to the receiver triangle for the initial trial, with the actual positions shown in Figure 6- 15. An individual discharge from the same trial is presented in Figure 6- 16, whereby the occurrence of each captured discharge is as expected, with the signal detected first on Rx2, then on Rx1, shortly followed by Rx3.

Signals detected during trial 1a remained highly detectable and visibly clear, however the transmitter position was relatively close to the receivers at a maximum distance of approximately 12.3m, and so, an individual discharge from trial 8a is shown in Figure 6- 17, where the receivers were positioned at a maximum distance of approximately 85.4m from the transmitter, as illustrated in Figure 6- 18. Again, the signals are clearly visible above the noise level and remain detectable throughout the complete recording. A greater time delay can be seen between each detected signal as each receiver is approximately 7m further from the fault than the previous. The detectability at a distance of 85m was confirmed, providing confidence in the feasibility of a localisation system as the signals remained distinct above the noise.

For the localisation system, the speed of sound is key and varies with environmental aspects such as, temperature, salinity and water depth. Consequently, an additional trial was performed with a fourth channel recording the transmitted signal to allow time of transmission (ToT) to be known and in turn the speed of sound to be calculated. In reality,

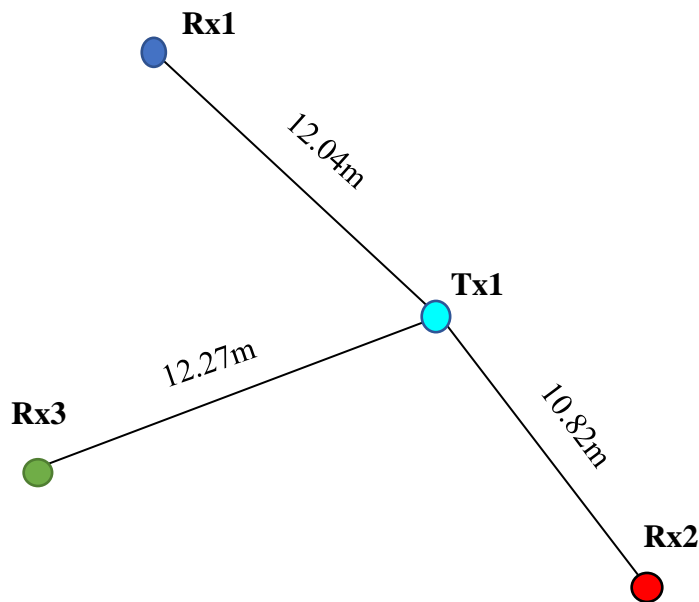


Figure 6- 15: Transmitter Position – Trial 1a

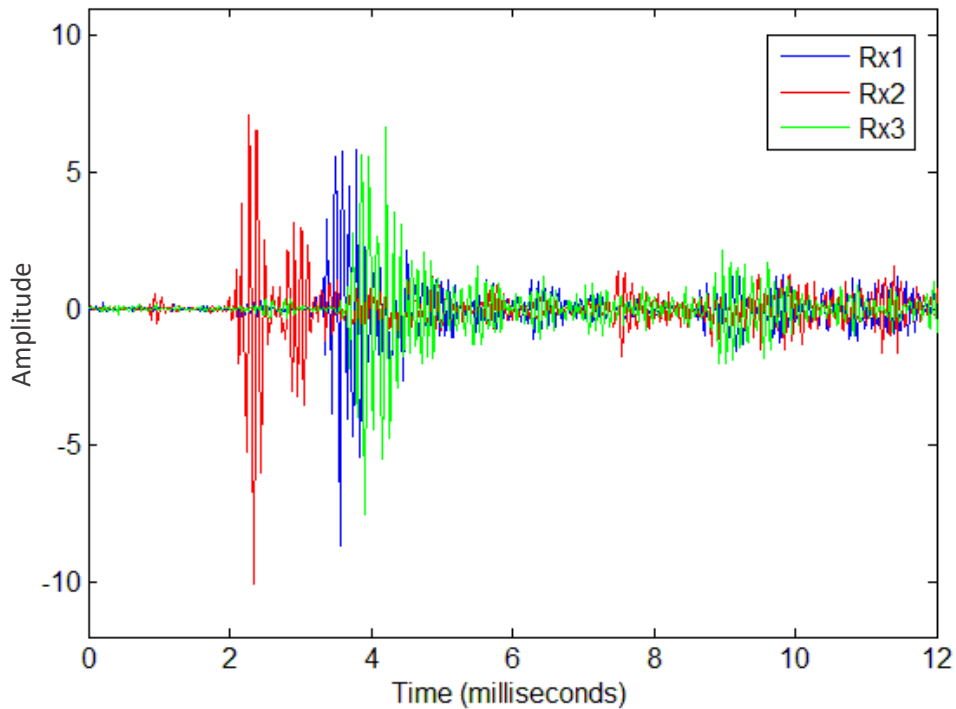


Figure 6- 16: Open Water Trial 1a, Individual Partial Discharge

ToT would not be known as PD occurrences are non-periodic, however, using the transmitter to broadcast the PD signals enables this and subsequently allows an accurate signal speed to be determined without knowledge of the water properties through TDoA calculations. Figure 6- 19 presents an individual discharge from this additional trial, displaying both the transmitted and received signals, along with the resultant normalised signal envelopes. As the transmitted signal relates to the signal ToT, the envelope peaks can be used to calculate the speed of sound propagation through the water. The distance of receivers to transmitter were in line with those stated in trial 1 and shown in Figure 6- 15. Considering these distances, along with the time delay between envelope peaks, the propagation speed was calculated to be between 1458m/s and 1480m/s, providing an average value of 1465m/s from the evaluation of multiple PD occurrences recorded throughout the trial. Using the transmitted signal as ToT allows an accurate assessment to be made of on the signal propagation speed without the need of detailed evaluation of the water properties and thus a speed of 1465m/s will be utilised in the localisation algorithm for PD source estimation.

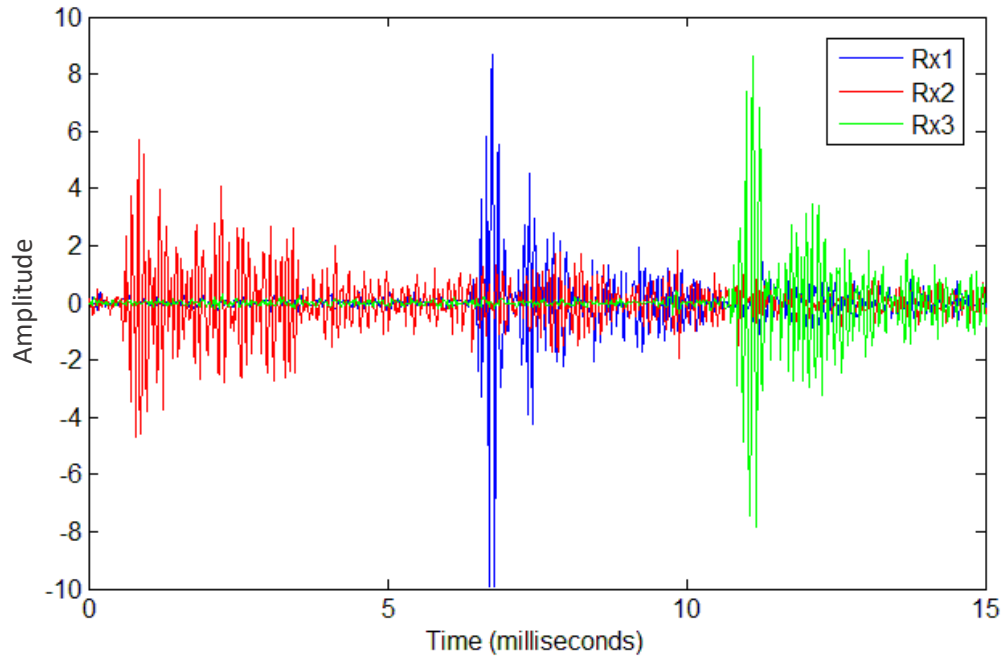


Figure 6- 17: Open Water Trial 8a, Individual Partial Discharge

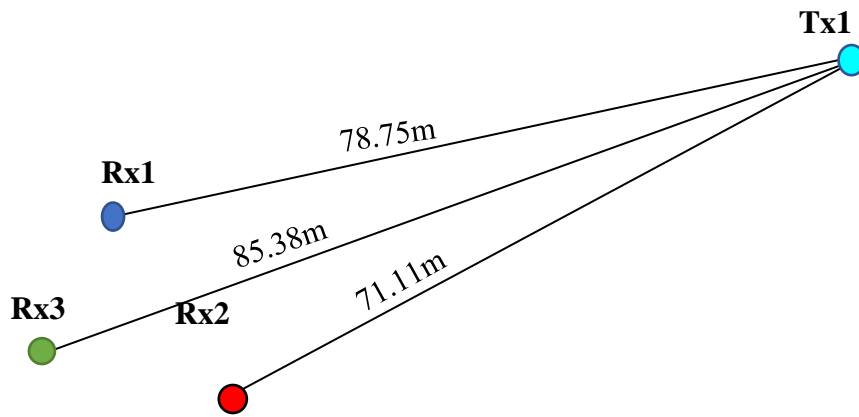


Figure 6- 18: Transmitter Positions, Trial 8a

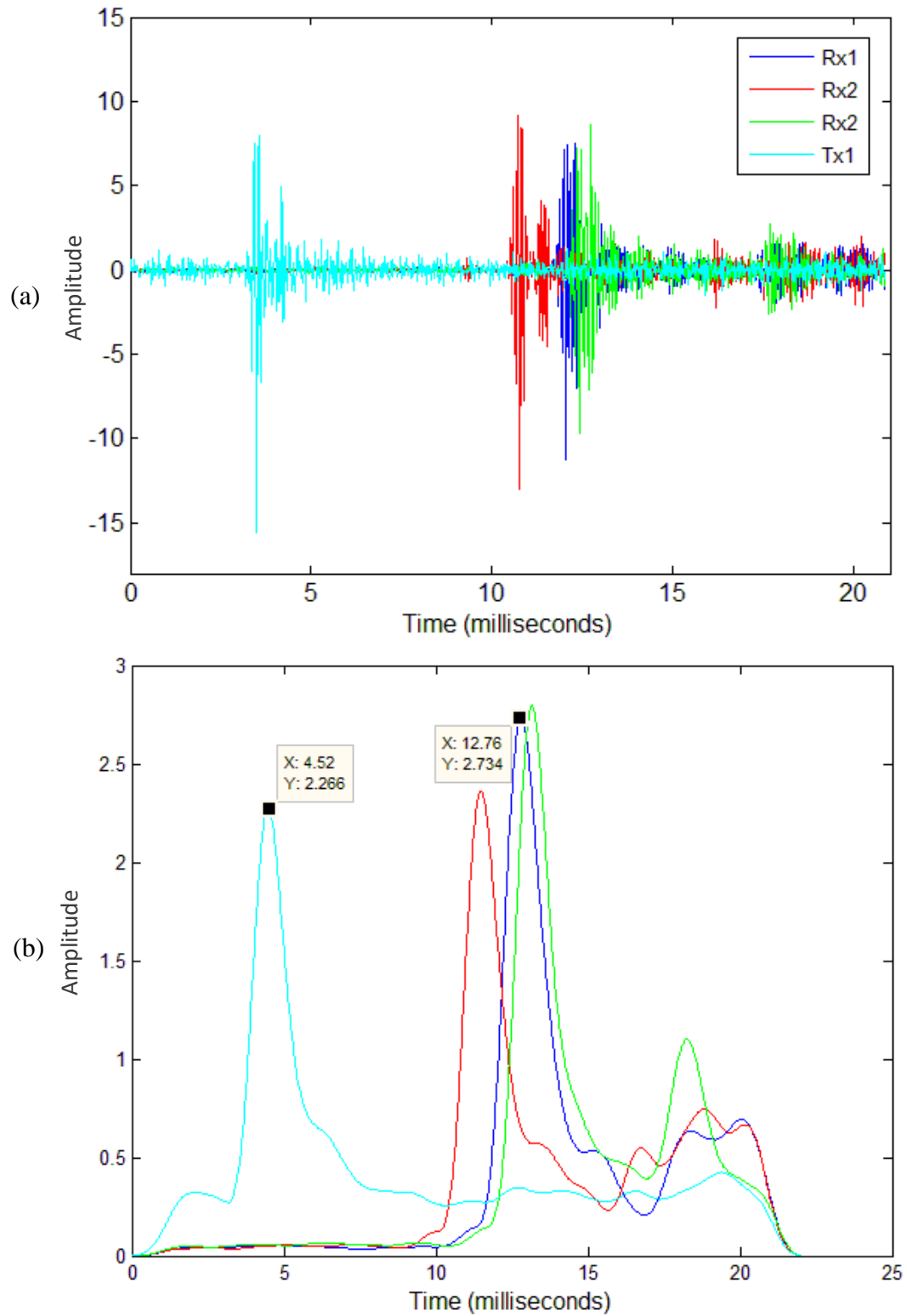


Figure 6- 19: Open Water Trial Pre-test including transmitted signal for ToT Measurements, (a) Individual Partial Discharge in Time Domain, (b) Signal Envelopes

6.4 Summary

The focus of this chapter was on the through-water propagation of the acoustic signals emitted during PD occurrence within the subsea power cable. A review of the underwater acoustic channel was performed to develop a good understanding of the aspects which affect the transmitted signal to ensure these are considered within the localisation algorithm. The power cables will be installed in varying environments and thus it is important to understand the impacts this may have on the propagated signal. The speed of sound is key within the localisation algorithm and is influenced by the conditions of the water such as pressure, temperature and salinity, although salinity has less of an effect. The average speed of sound in water is approximately 1500m/s, however it is extremely difficult to calculate the exact speed based on the complexities of the water conditions, although the discussed aspects can be taken into account to get as close to the actual speed as possible, based on the body of water in which the system shall be utilised.

In addition, the characteristics of the emitted signal changes before reaching the hydrophones due to transmission loss and multipath and so these aspects were investigated. Transmission loss is due spreading loss and absorption, whereby the signal strength is reduced with distance and thus has a direct impact on the received SNR. Multipath is a phenomena where both directly transmitted and reverberated signal may be received due to the propagation path and surrounding media causing reflections. It is less likely to be an issue in the water depths where the power cable will be installed due to the probability of the signal attenuating greatly before reaching the hydrophone, however floating structures and equipment within the subsea field may cause this issue and so it should be considered within the localisation system. Environmental noise and interference have also been reviewed as again, they directly influence the SNR and consequently impact the capability of the localisation system. Some aspects of noise can be predictable based on the geographical location and therefore can be accounted for within the system, however, there will also be less predictable noise present and knowledge of the potential sounds and their corresponding frequencies is highly beneficial.

Prior to performing an open water trial, an initial lab based test was performed where a cable sample was tested within an anechoic chamber and PD occurrences recorded with hydrophones to examine the characteristics of the through-water emitted PD signal. The detected acoustic signals were easily visible, however the EM signal was much weaker than that detected during through-cable analysis due to high attenuation of electrical signals in seawater. The shape of the emitted pulse also differs from that detected during through-cable analysis, however the duration remained at approximately 4ms. Analysis of the frequency spectrum concluded that the signal is highly broadband, showing strong signal energy across the complete 22kHz spectrum. This trial also allowed recording of the AE signals to enable the discharges to be replayed through a transmitter during the open water trial to minimise complexities at the Marina.

To ensure the hydrophones were calibrated and understand the detectability lengths further testing was performed where a known signal was sent through the transmitter and recorded on the hydrophones. Calculations were performed to determine the source level of the PD emissions, which in turn allowed for detectability range estimations based on the SNR, whilst considering varying sea states. Considering a low *NSL*, the detectability range was calculated to be around 500-1000m from the source, whereas a more realistic *NSL* was around 100-200m from the source and a high *NSL* was around 10-20m from the source, thus highlighting the large impact of environmental noise on the system's capabilities.

The open water test performed at the Marina consisted of three hydrophones positioned at fixed locations and a transmitter moved to varying locations for a number of trials. Sixteen trials were performed in total with the transmitter position recorded to allow for assessment of position estimation accuracy in later analysis. Evaluation of the recorded signals showed clear detectable PD occurrences throughout all trials, with distances ranging as far as 85m from the transmission source. Sending the PD signal through the transmitter also allowed the propagation speed to be established without detailed evaluation of the seawater properties as the ToT was known and could therefore be used to calculate the signal velocity through TDoA calculations. The propagation speed was calculated to be an average of 1465m/s and so this provides a value to be utilised in forthcoming localisation analysis which will improve the system's accuracy from using the 1500m/s generic value.

Chapter 7

Through-water Source Localisation

This chapter focuses on localisation of the PD source through analysis and processing of the recorded acoustic signals from open water trials. A review of positioning techniques is performed to firstly understand the applicable methods, deciding which is most suitable for use within the localisation system.

A localisation algorithm is developed utilising hyperbolic positioning and applied to previous open water trial data in order to estimate the location of the PD source. The accuracy of the system is assessed through comparison of the estimated PD location against the known location recorded during the trial. A fourth receiver is simulated to establish if any further improvements can be made to the system, along with an evaluation of the implications of receiver positions.

A second open water trial was performed whereby a real cable sample was used to create the PD emissions, as opposed to the transmitter, and hydrophones individually positioned with clocks synchronised through Global Positioning System (GPS) techniques, allowing more realistic conditions to be assessed to further confirm the capability of the system.

The potential of a combined electro-acoustic sensing method is discussed, followed by an overview of 3D localisation methodologies. The chapter concludes with a review of the systems application and usage.

7.1 Motivation

Having the ability to determine the location of PD occurrence is highly beneficial as this provides an understanding of the potential fault area thus allowing for planned intervention of the specific area prior to complete breakdown, or in some cases, allowing the potential fault region to be bypassed and operation continue.

Many other applications use acoustic sensing for position estimation however the complexity of the system is increased as the ToT of the PD emissions is unknown and there is no clock synchronisation between the source and the receiver, therefore many time of arrival (ToA) techniques cannot be applied. Hyperbolic positioning techniques are used in navigation systems where synchronisation between source and receiver is not possible and therefore this technique is investigated. The use of hydrophones would allow both detection

and localisation of the PD source, whilst providing a non-intrusive, retro-fit system which could be used whilst the power cable remains in operation.

Localisation provides the ability to have an understanding of not only the overall PD occurrence, but also if this is from one or more events to understand if one particular area is worsening and reaching a critical state, or if multiple minor fault areas are present. A system which offers both detection and position estimation of the PD source would provide useful information to consider the cable's condition as a whole.

7.2 Survey of Localisation Techniques

Within the through-water localisation system, cross correlation and envelope techniques can again be applied to determine the TDoA between the signals detected across the three hydrophones, however, unlike the through-cable detection, the propagation axis is no longer linear and thus the position cannot be calculated utilising the time delay and ratio between the two sensors. The area of interest is now omnidirectional, therefore, the time delay between detected signals can be used to determine how much further from the fault one receiver is compared to the other, however the direction of the fault is unknown and so a different localisation method is required to establish its location. The complexity of the positioning system is further increased with the PD signal's ToT being unknown unless an additional method of EM sensing is also utilised. Though acoustic only methods would be the preferred option due to costs and achievable distances, localisation techniques applicable to both methods are considered as a combined sensing option may suit some short-range applications, or on systems where an HFCT may already be in use.

With initial consideration of the combined EM and AE sensing method, trilateration, received signal strength localisation and triangulation are discussed, followed by a review of angle of arrival and multilateration techniques for the acoustic only sensing method.

Trilateration is commonly used in GPS where the signals ToT is known [133]. Three or more clock synchronised receivers are used to determine the location of the transmitting source. The time of flight (ToF) is calculated considering the ToT, the velocity of the signal and the signals ToA, then a sphere is drawn around the receiver with a radius equating to the resultant distance. The process is repeated at each receiver and the position at which the sphere's intersect relates to the estimated source location. This technique could be applied to the combined sensing method to estimate the position of the PD source as ToF would be known, along with the signals propagation speed.

Received signal strength localisation methods use knowledge of the transmitted signal strength and the propagation path losses, along with the received signal strength to estimate the distance from transmitter to receiver [134]. This method cannot be utilised within the discussed systems as the emitted acoustic signal is inconsistent and varies in strength depending on the severity of the fault.

Triangulation is a commonly used method amongst surveyors whereby angles are measured rather than distance. The distance between two fixed points is known and referred to as the baseline. Line of sight to the source is required and an optical tool is typically used to measure the angles from each point to the source, therefore allowing a triangle to be constructed with one known length (the baseline), and two measured angles, thus allowing calculation of the distance to the source. For the proposed application there is no line of sight to the source and angle measurement between the source and baseline cannot be performed, therefore triangulation cannot be used alone to determine the PD location within this system.

Angle of arrival utilises hydrophone arrays whereby the direction is determined through a process referred to as beamforming, where phase differences of the detected array signals are analysed to determine the estimated angle. At least two angle of arrival measurements are required to allow for source localisation based on intersection of the line of bearing and triangulation calculations, however the method is susceptible to multipath and so more arrays are generally required [135]. Angle of arrival techniques do not require clock synchronisation, however accurate measurements may require directional arrays, multiple-element arrays, and often complex processing algorithms. Complex hydrophone arrays will not be utilised within the proposed localisation system and as a result, this method cannot be implemented.

Multilateration, also known as hyperbolic positioning, utilises similar methodology to trilateration, however circles and spheres are replaced with hyperbolas and hyperboloids. Hyperbolic positioning is considered when the ToT is unknown, and thus the ToF cannot be calculated. Instead, TDoA between signals detected at each receiver are calculated and through non-linear regression, TDoA equations can be converted to the form of a hyperbola. This would be repeated for each TDoA between three or more receivers and the area of intersection of the hyperbolas relates to the location of the source transmission. Each calculated hyperbola will have two branches, which could increase the complexity of source localisation as two intersection points would be present, however, for the required application, the approximate location of the subsea cable would be known, therefore allowing one of the branches of each hyperbola to be discarded. For hyperbolic positioning, receivers need to be synchronised to allow for accurate TDoA measurement, with a minimum of three receivers required for 2D positioning and four for accurate 3D positioning [133]. The use of hyperbolic positioning within the proposed localisation system would offer a suitable localisation technique based on the discussed methodology.

In summary, an evaluation of source localisation techniques highlights trilateration as the most suitable method for the combined EM and AE sensing method, whereas hyperbolic positioning was identified as the most appropriate method for inclusion within the acoustic only method, which is the main focus of the proposed localisation system.

7.3 Open Water Trial – Localisation

The localisation system requires an algorithm capable of estimating the position of the PD source from the detected acoustic emissions. The acoustic only sensing method, whereby hydrophones are deployed near the surface of the water, has been highlighted as the main focus of the through-water detection of PD and the most suited positioning technique to include within the localisation algorithm was identified as hyperbolic positioning. Signals recorded during the open water trial performed in Section 6.3.3 can be utilised to assess the capabilities of the localisation algorithm, with comparison being made to the actual PD source position, hence also allowing for an assessment of the system's accuracy.

7.3.1 Hyperbolic Positioning

A hyperbola has two pieces, referred to as branches, which are mirror image curves that are infinite in length. In analytic geometry, a hyperbola is a conic section formed by intersecting a right circular cone with a plane at an angle such that both halves of the cone are intersected. This intersection produces two separate unbounded curves that are mirror images of each other [136]. Figure 7- 1 presents the characteristics of a hyperbola, where each key parameter is labelled. A hyperbola has two axes of symmetry known as the

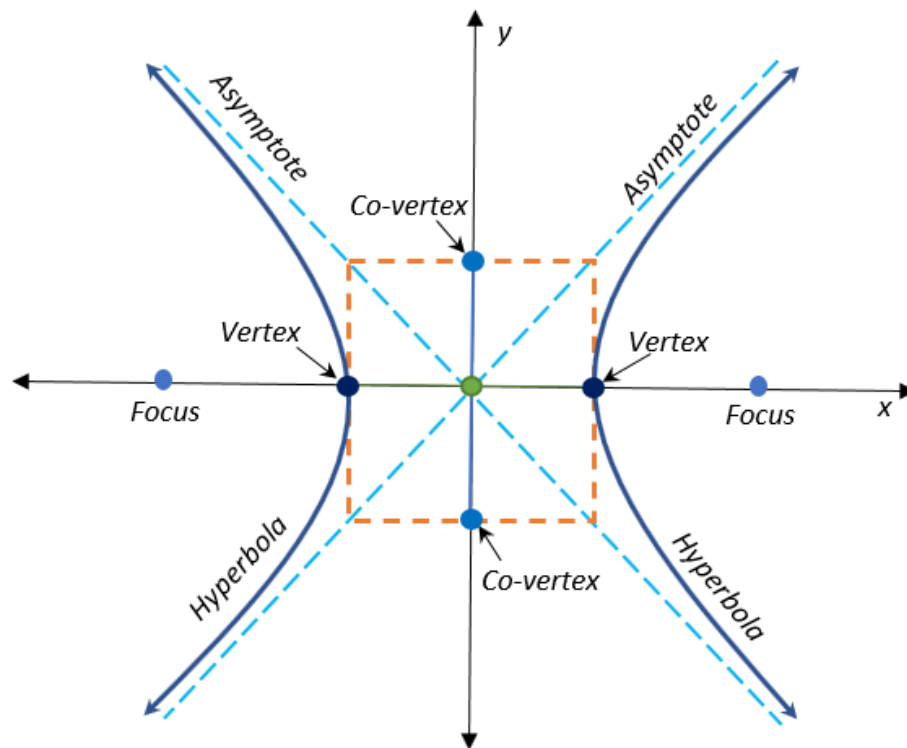


Figure 7- 1: Characteristics of a Hyperbola

transverse axis and the conjugate axis. The transverse axis is a line which passes through the centre of the hyperbola and has vertices at each end, in the case of Figure 7- 1, this falls on the x-axis. The conjugate axis falls on the axis 90° from the transverse, which in this case is on the y-axis. The conjugate axis has co-vertices at each end. There are two foci which can be found on the transverse axis. The latus rectum of a hyperbola is a line drawn perpendicular to the transverse axis which passes through the foci. Hyperbolas have two asymptotes which run through the centre and a rectangle which runs through each vertex and co-vertex point. As the hyperbolas branches curve back from the vertices, they approach the asymptotes. The image shown depicts the transverse axis on the x-axis presenting a horizontal hyperbola, however, the hyperbola can also centre on the y-axis as a vertical hyperbola, and in this case, all presented parameters will rotate 90° .

Figure 7- 2 again presents a horizontal hyperbola, but this time shows some key parameters relating to the standard hyperbolic equation (7.1). The vertices of the hyperbola are located at $(a,0)$, $(-a,0)$ and the major axis is $2a$ units. The minor axis is $2b$ units and the foci are at $(c,0)$ and $(-c,0)$.

$$\frac{x^2}{a^2} - \frac{y^2}{b^2} = 1 \quad (7.1)$$

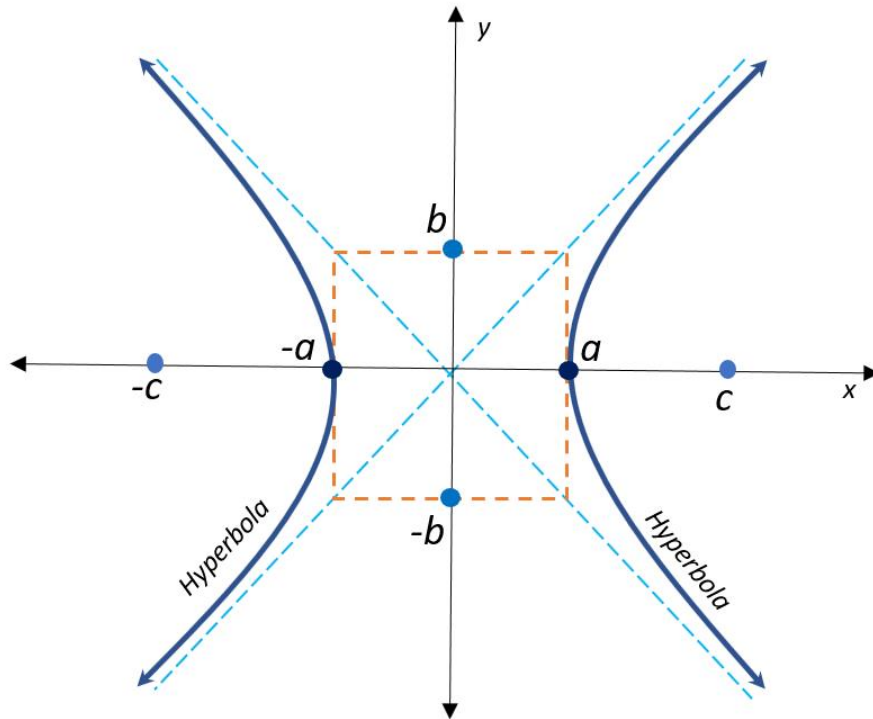


Figure 7- 2: Hyperbola with Centre as Origin

When considering the system application, the distance between foci, $2c$, relates to the distance between receivers, the distance between vertices, $2a$, relates the distance equivalent to the calculated TDoA and the distance between co-vertices, $2b$, can then be calculated utilising (7.2).

$$b^2 = c^2 - a^2 \quad (7.2)$$

A hyperbola is a set of all points x,y whereby the difference of distances from x,y to the foci is a constant value. Consider Figure 7- 3, $d2$ minus $d1$ is a constant for any point on x,y . As the distance between vertices is known to be $2a$, equation (7.3) presents the relationship.

$$|d_2 - d_1| = 2a \quad (7.3)$$

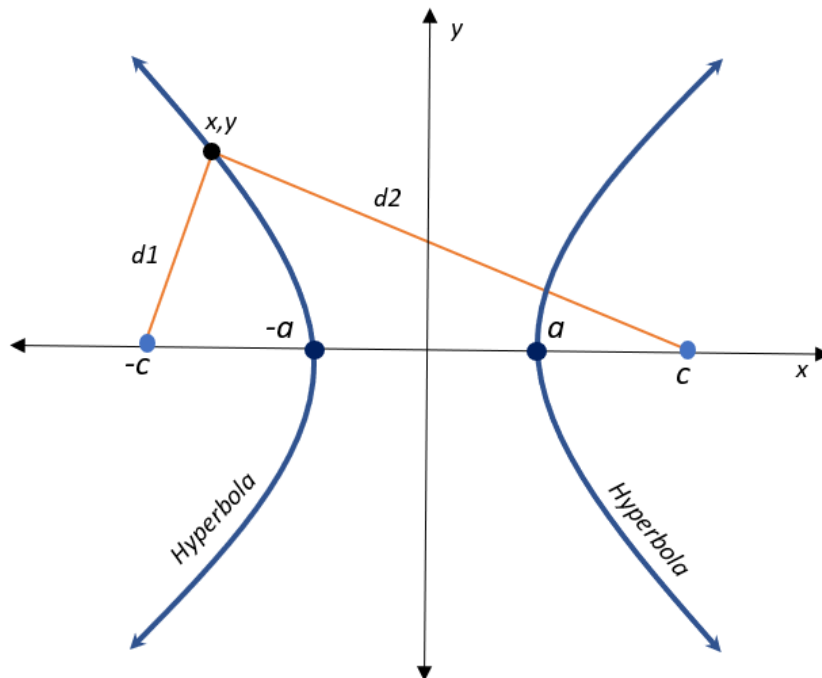


Figure 7- 3: Distance relationship of Hyperbolic Curves

Considering coordinates x, y and equation (7.3), the standard hyperbolic equation (7.1) can be derived as follows;

$$\sqrt{(x+c)^2 + y^2} - \sqrt{(x-c)^2 + y^2} = 2a \quad (7.4)$$

$$\sqrt{(x+c)^2 + y^2} = 2a + \sqrt{(x-c)^2 + y^2} \quad (7.5)$$

Now squaring on both sides provides;

$$(x+c)^2 + y^2 = 4a^2 + (x-c)^2 + y^2 + 4a\sqrt{(x-c)^2 + y^2} \quad (7.6)$$

$$x^2 + c^2 + 2cx + y^2 = 4a^2 + x^2 + c^2 - 2cx + y^2 + 4a\sqrt{(x-c)^2 + y^2} \quad (7.7)$$

$$4cx - 4a^2 = 4a\sqrt{(x-c)^2 + y^2} \quad (7.8)$$

$$cx - a^2 = a\sqrt{(x-c)^2 + y^2} \quad (7.9)$$

Simplifying and squaring on both sides gives;

$$\frac{x^2}{a^2} - \frac{y^2}{c^2 - a^2} = 1 \quad (7.10)$$

And from (7.2) it is known that $a^2 + b^2 = c^2$ therefore arriving at the standard hyperbola equation stated in (7.1).

To include this in the localisation algorithm, the right branch of the hyperbola can then be parametrised by (7.11) and the left branch by (7.12).

$$x = a \cosh t, \quad y = b \sinh t, \quad t \in (-\infty, \infty) \quad (7.11)$$

$$x = -a \cosh t, \quad y = b \sinh t, \quad t \in (-\infty, \infty) \quad (7.12)$$

It should also be noted that when considering a vertical hyperbola, with the transverse axis on the y-axis, (7.13) should instead be considered.

$$\frac{y^2}{a^2} - \frac{x^2}{b^2} = 1 \quad (7.13)$$

7.3.2 System Evaluation

The proposed through-water sensing system will be used for both detection and localisation of the acoustic PD emissions, through signals received on hydrophones deployed near the water's surface. The system itself will comprise of three or more hydrophones, a data acquisition system, and an algorithm developed in Matlab capable of detecting and processing the relevant acoustic signals to establish TDoA's and calculate the estimated PD locations through hyperbolic positioning.

Figure 7- 4 provides a high level overview of the system's processes. The hydrophones and data acquisition unit enable the continuous monitoring of acoustic signals until a set amplitude threshold is met. Once met, the developed algorithm in Matlab triggers a looped processing sequence where a section of the signal, both before and after the threshold trigger, is analysed to determine the TDoA through envelope or cross correlation techniques. The TDoA between each receiver is established and fed into the hyperbolic positioning equation, with each hyperbola then plotted and the area of intersection determined through identification of the crossing point of all hyperbolic curves within the algorithm. The intersection of the hyperbolic curves is identified within the Matlab coding at the point where the coordinates of each curve are equal. The system has been developed to automatically plot a marker at each point of intersection of all of the hyperbolic curves and output the position to a data table to provide an average estimated source location. This process is automatically repeated each time the amplitude threshold is met, continuously updating the average estimated PD location with each iteration and taking into account all previous position estimations.

Recordings from the open water trial performed in Section 6.3.3 were utilised within the discussed localisation algorithm to assess its capability in detecting the PD source. Only trials performed with the transmitter positioned at 1m water depth were considered within this analysis as the initial concentration was on proof of the hyperbolic positioning concept and localisation system which could be further adapted to consider hyperboloids. The receiver position was known and therefore the distance between receivers was input to the hyperbolic calculations, along with the established TDoA between received signals. Through consideration of the discharges amplitude against the noise level, a threshold of 0.1 was implemented to ensure all discharges are detected whilst minimising the chances

of false alarms due to noise. The duration of the signal is analysed once the threshold was met varied between 20 to 30ms depending on the trial performed and distances travelled. This was to ensure the emitted signal was captured on all receivers within the timeframe, whilst also reducing the likelihood of including the next PD emission within the analysed section.

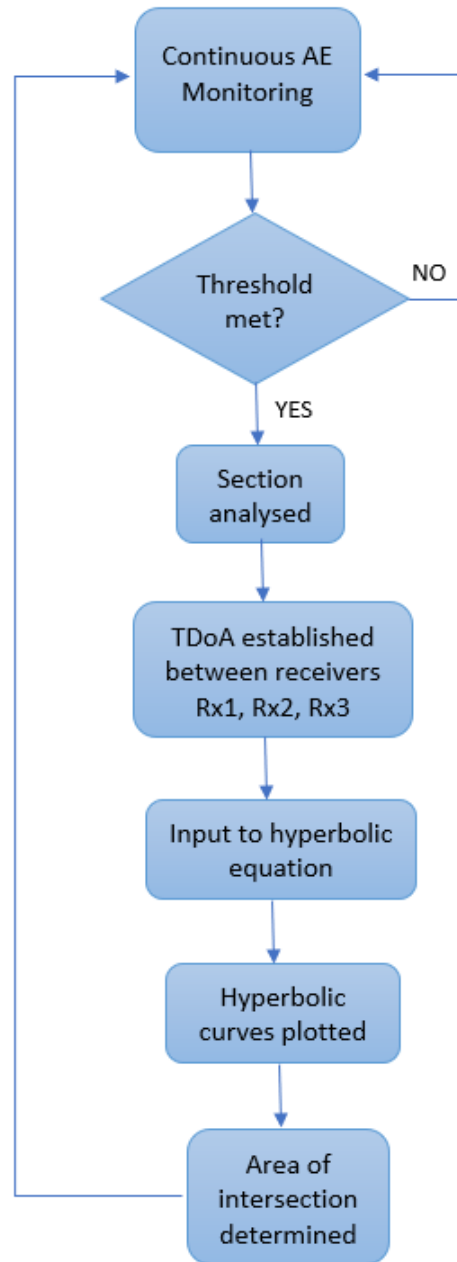


Figure 7- 4: Localisation System Overview

Figure 7- 5 presents the plotted hyperbolas, along with the known receiver positions and estimated fault location relating to trial 1a. The hyperbolas with foci relating to Rx1 and Rx2 are shown in blue, Rx2 and Rx3 are shown in green and Rx1 and Rx3 are shown in red. A degree of rotation was added to the hyperbolas within the algorithm to ensure the transverse axis lies perpendicular to the plane of the two receivers being analysed. The angle of rotation varied between each pairing of receivers as it is based on the receiver positions. The actual transmitter location, Tx, is illustrated at coordinates (13,11), whereby all receiver and transmitter positions have been plotted to equate to the relevant distances experienced during the open water trial to ensure all results are comparable to the actual events. As a hyperbola is plotted each time a discharge is detected, multiple curves can be seen between each sensor pair. The plotted curves between receivers Rx1 to Rx2 and Rx2 to Rx3 remain fairly consistent, however a second set of curves with a more noticeable difference can be seen on the hyperbolas plotted between receiver Rx1 and Rx3. Although a more noticeable variation can be seen, the estimated PD location based on the average hyperbola intersections remained highly accurate at (13.6,11.2), presenting an MSE of 0.29. The process was repeated for all 8 trials with positioning results presented in Figure 7- 6 through to Figure 7- 13, whereby both envelope and cross correlation methods have been applied.

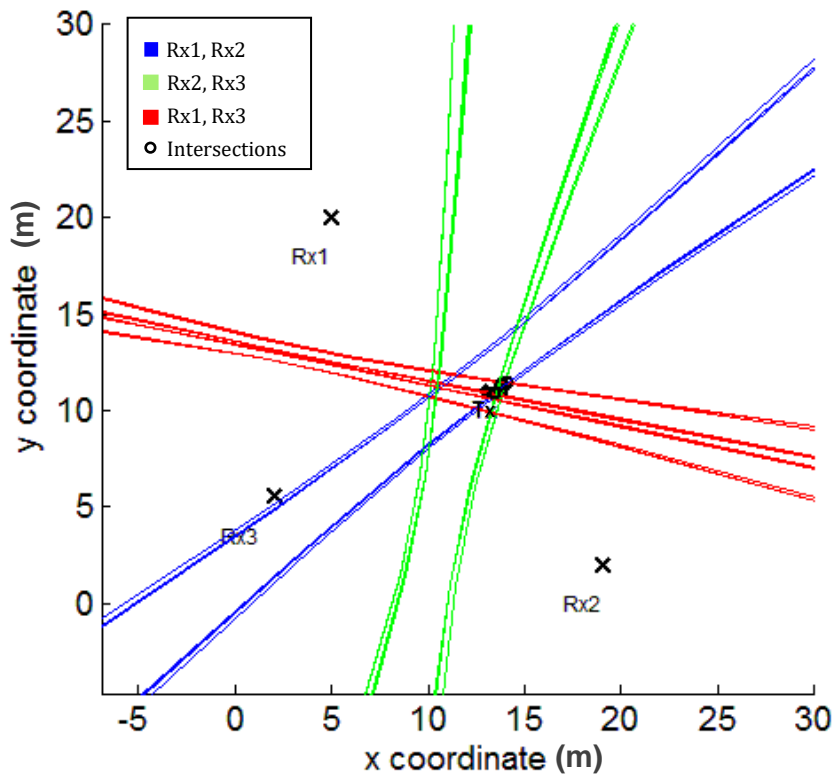


Figure 7- 5: Source Localisation utilising Hyperbolic Positioning and Cross Correlation Techniques – Trial 1a

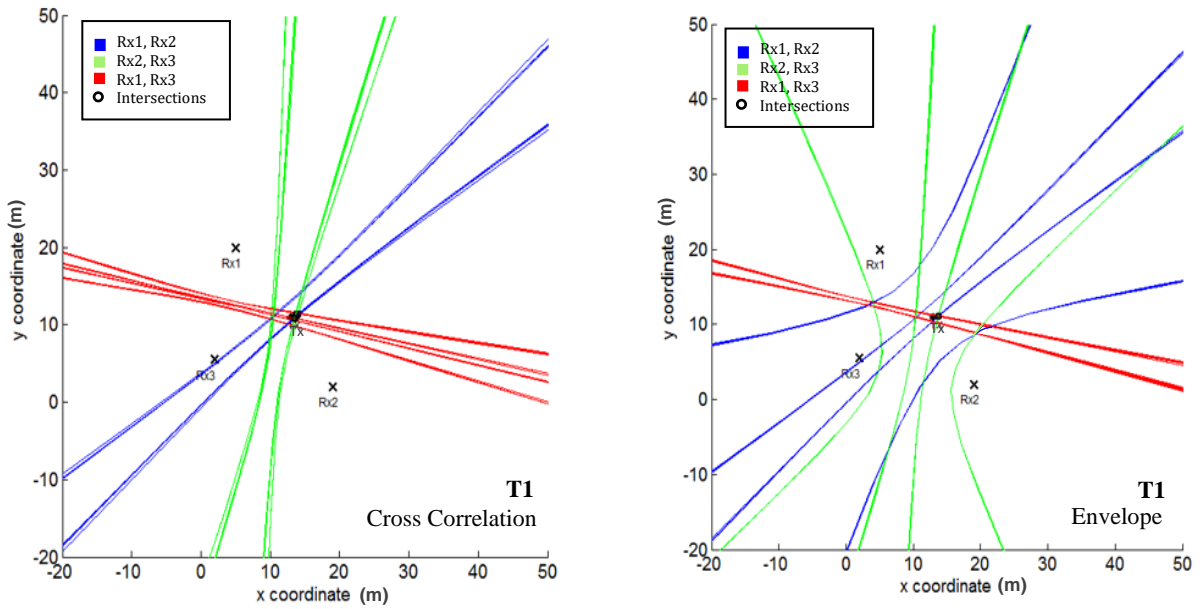


Figure 7- 6: Open Water Trial 1a – Source Localisation utilising Cross Correlation and Envelope Techniques

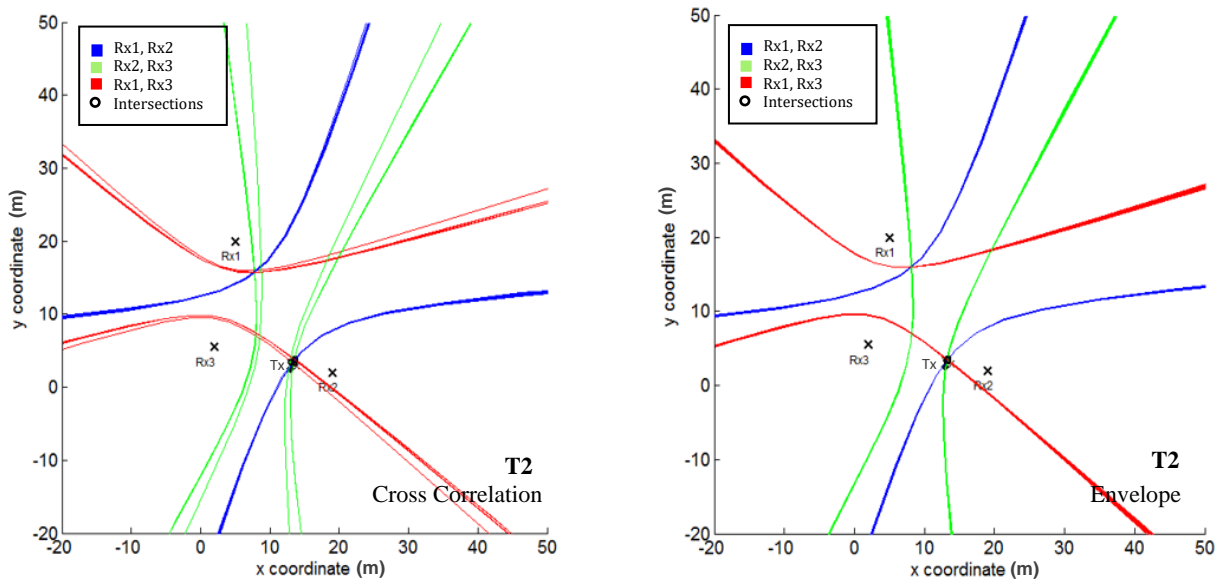


Figure 7- 7: Open Water Trial 2a – Source Localisation utilising Cross Correlation and Envelope Techniques

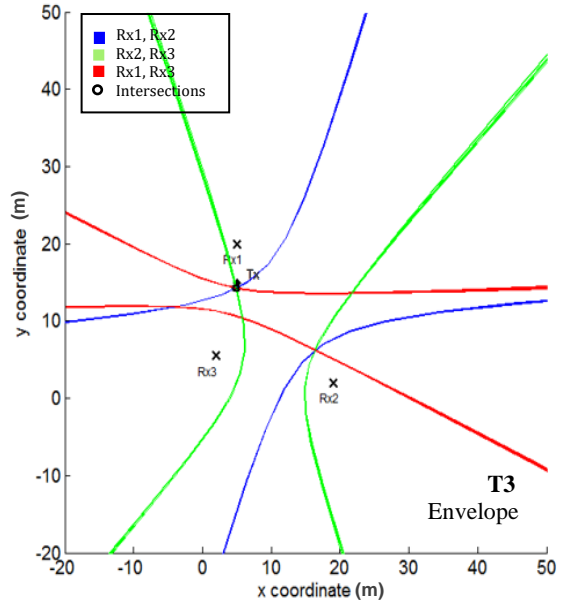
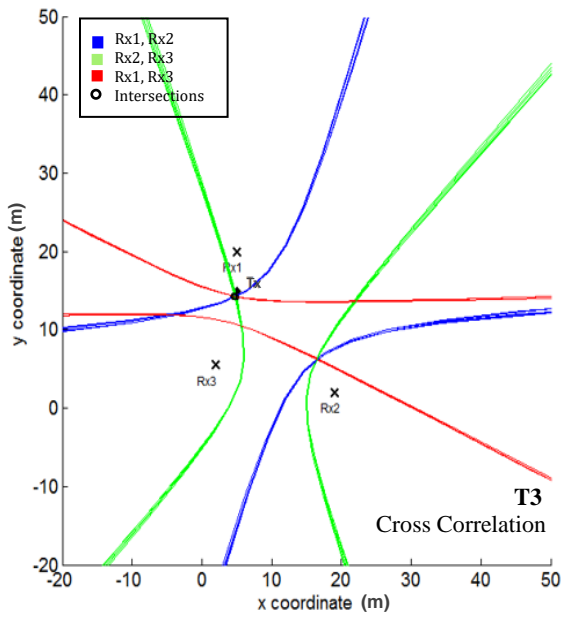


Figure 7- 8: Open Water Trial 3a – Source Localisation utilising Cross Correlation and Envelope Techniques

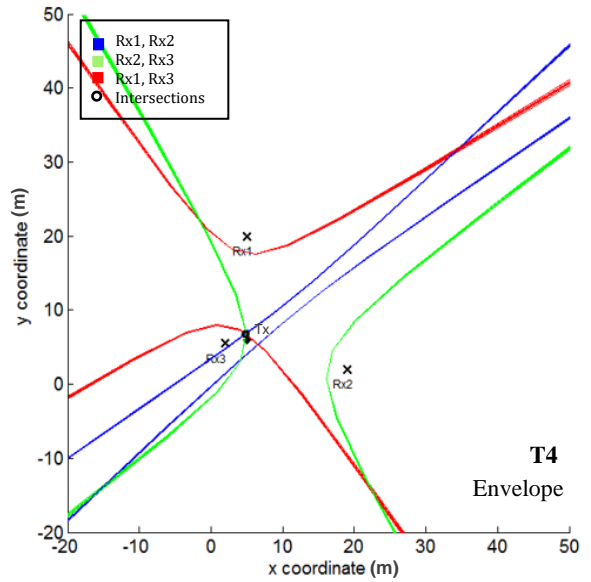
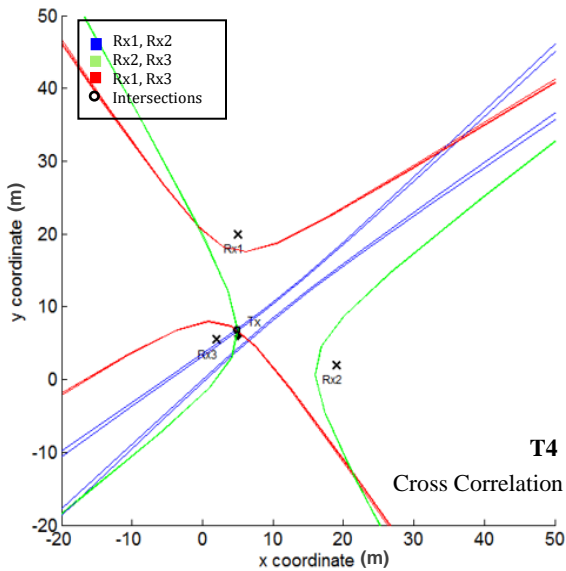


Figure 7- 9: Open Water Trial 4a – Source Localisation utilising Cross Correlation and Envelope Techniques

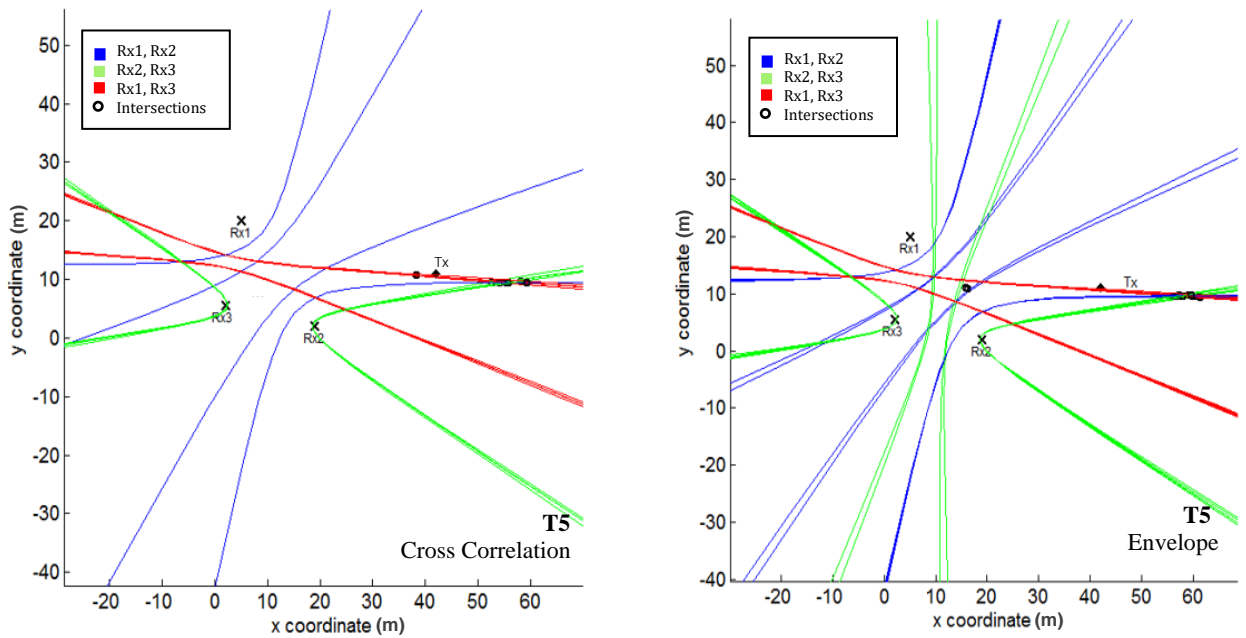


Figure 7- 10: Open Water Trial 5a – Source Localisation utilising Cross Correlation and Envelope Techniques

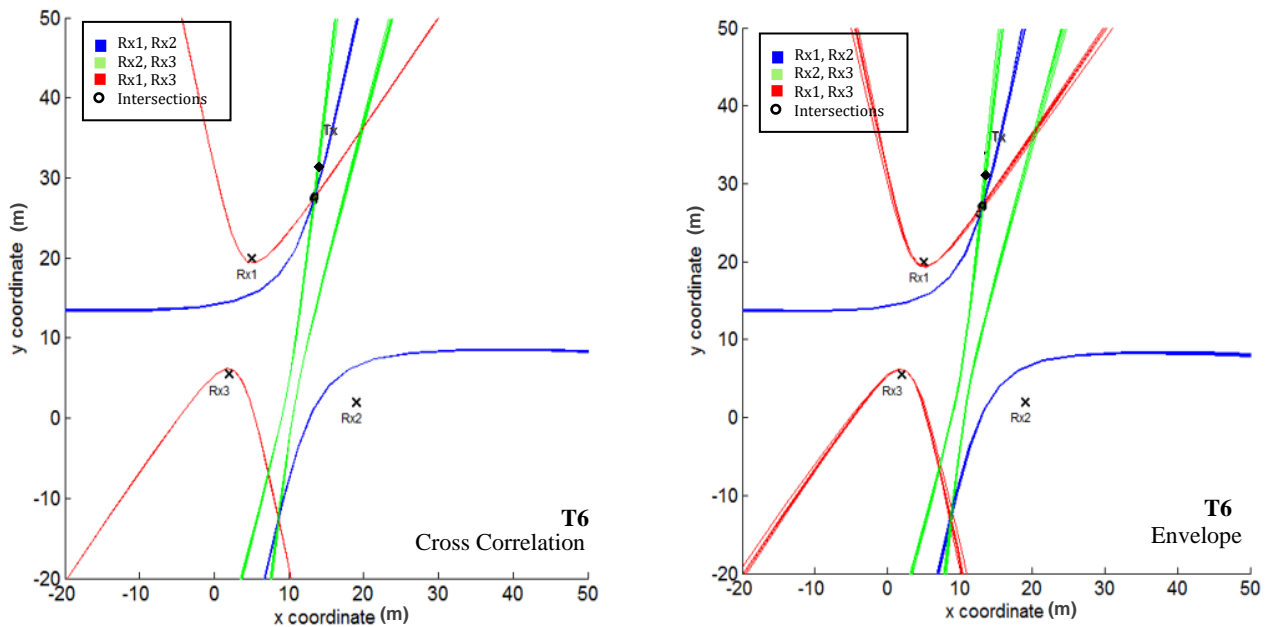


Figure 7- 11: Open Water Trial 6a – Source Localisation utilising Cross Correlation and Envelope Techniques

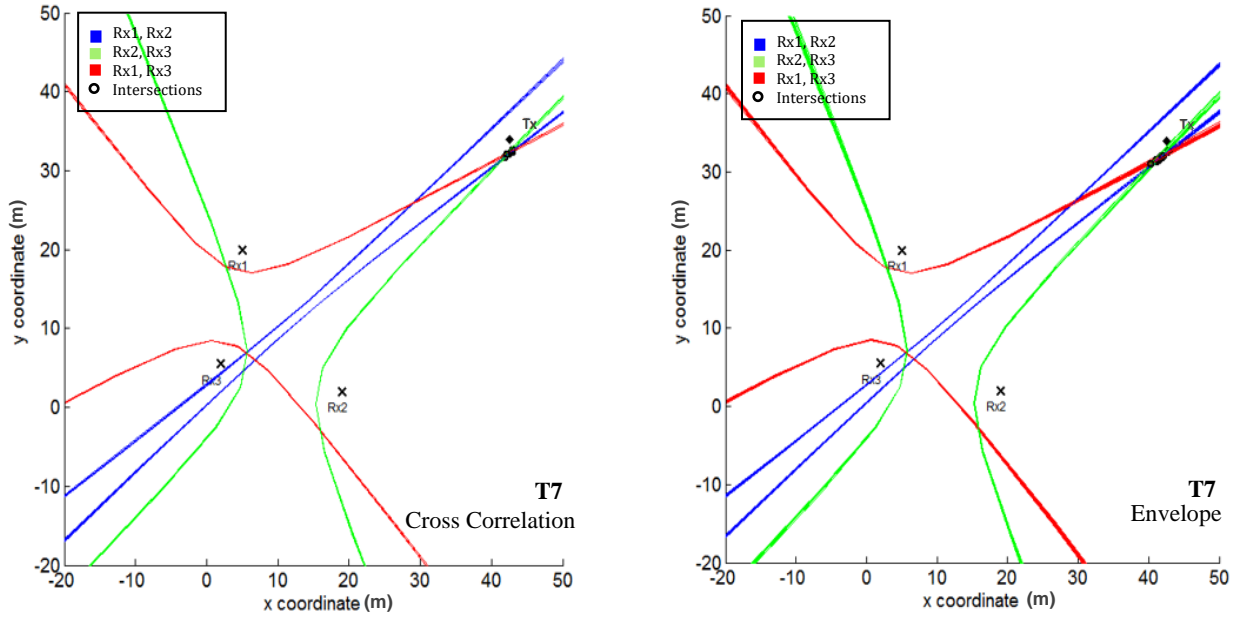


Figure 7- 12: Open Water Trial 7a – Source Localisation utilising Cross Correlation and Envelope Techniques

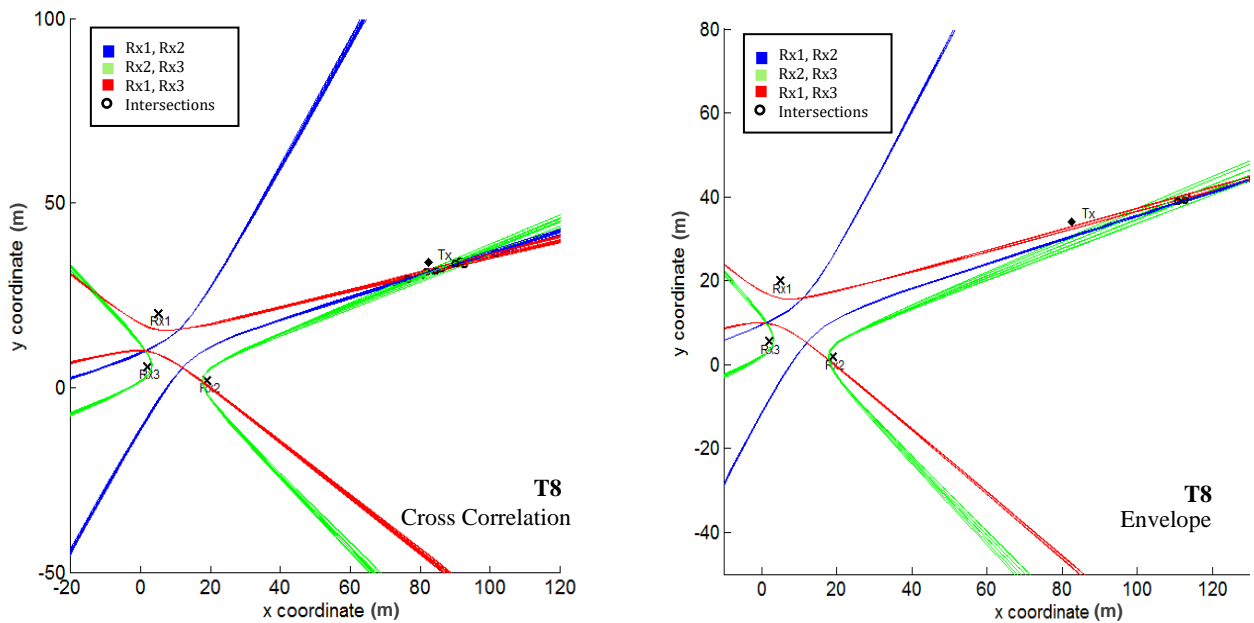


Figure 7- 13: Open Water Trial 8a – Source Localisation utilising Cross Correlation and Envelope Techniques

The average MSE for each trial was determined based on the estimated PD location compared with the actual known transmitter location, with results presented in Table 7- 1. Following a review of the results, along with the hyperbolic positioning figures, it can be seen that the system provides the most accurate results when the transmitting source lies within the receiver triangle. With the exception of one, trials 1-4 provide MSE results <1 for both envelope and cross correlation techniques. Focusing on the exception, the envelope results presented in Figure 7- 6 illustrate two varying sets of hyperbolic curves between receivers Rx1 to Rx2 and Rx2 to Rx3, thus leading to two sets of position estimations. A potential cause for this error could be due to the irregularity and unpredictability of the occurrence of PD events, as there is a potential for more than one discharge to fall within the time window analysed for TDoA. This may affect the signal being analysed if two or more discharges are too close together, thus creating new peaks at incorrect delay locations, resulting in an error in the plotted hyperbolas and in turn, an error in source localisation. Trials 5a through to 8a have the transmitting source positioned outside of the receiver triangle and findings present a higher error rate, particularly for Trials 5a and 6a. Figure 7- 10 illustrates hyperbolic curves in multiple locations for both the envelope and cross correlation results, with envelope showing greater errors. With certain errors being present on both plots it suggests that an error was present from the TDoA analysis, potentially due to two PD events occurring in close timings or due to other causes such as multipath propagation. Trial 6a, however, differs as there are no unexpected hyperbolic curves displayed in Figure 7- 11. This instead indicates that the error is more likely related

<i>Trial Number</i>	<i>Cross Correlation MSE</i>	<i>Envelope MSE</i>	<i>Most Accurate Method</i>
<i>1a</i>	0.299	6.207	Cross Correlation
<i>2a</i>	0.683	0.474	Envelope
<i>3a</i>	0.282	0.261	Envelope
<i>4a</i>	0.292	0.330	Cross Correlation
<i>5a</i>	92.261	170.066	Cross Correlation
<i>6a</i>	16.191	24.040	Cross Correlation
<i>7a</i>	1.932	2.950	Cross Correlation
<i>8a</i>	3.134	22.163	Cross Correlation

Table 7- 1: Hyperbolic Positioning System Accuracy Evaluation

to the positioning of the transmitter in relation to the receivers as the transmitter is almost positioned behind receiver Rx1. The sensors are omni-directional, however, the hyperbolas extend between receiver pairs and thus the curves retreat back towards the transmitter position, away from the preferred receiver range, indicating an influence in receiver positioning to the overall system accuracy. Trials 7a and 8a had receivers positioned furthest from the transmitter location, however results show a higher level of accuracy than the previous two trials, further emphasising the likelihood of receiver positioning having an effect on the system outcome. With focus on Figure 7- 12 and Figure 7- 13 , the position of the transmitter in relation to the receiver triangle is similar within both trials, with one trial being of longer range than the other, thus suggesting a preferred transmitter region when compared to trial 6a. The envelope results from trial 8a, present a higher MSE, consequently providing further confidence in the cross correlation methodology. Table 7- 1 displays the most accurate method for each trial performed, with cross correlation showing favorable results in most instances. Envelope analysis did show marginally improved results for trials 2a and 3a, where the transmitter was located within the receiver circle, however the differences were minor and consequently cross correlation is again considered the superior technique to be used within the localisation system. It should also be noted that there is a chance of human error when measuring the exact transmitter location during the open water trial which may also have a slight effect on the evaluated results. Through review of the results, the localisation algorithm has shown to provide effective position estimation of the PD source, whereby in most cases, a high level of accuracy was maintained. Further review of the implications of receiver positioning would enable optimisation of the overall system.

7.3.3 Receiver Positioning

To develop an understanding of the potential errors caused within the localisation system due to the positions of the receivers in relation to the source location, a simulation was developed, considering the same receiver positions as those within the trial, with a changing transmitter location to establish the MSE at a large range of positions. This was done based on a perfect system, whereby no acoustic signals were input, and instead the input to the hyperbolic equation was the calculated differences in distance from transmission source to each receiver. Figure 7- 14 presents the results from this simulation in both graphical and colourmap formats. The MSE for each transmitter position was calculated and colour coded based on the resultant value, with green illustrating an MSE below 10, yellow between 10 and 29, amber between 30 and 99 and red for MSE values greater than 100. When looking at the colourmap, it is apparent that the ideal system setup would be to ensure the PD source lies within the receiver configuration as this provides the highest level of accuracy. Reviewing the sections outside of this area, it can be seen that there is a low MSE range propagating out from each side of the triangle, showing most favourable results to the upper right region due to the sensor spacings. As expected, the errors increase with

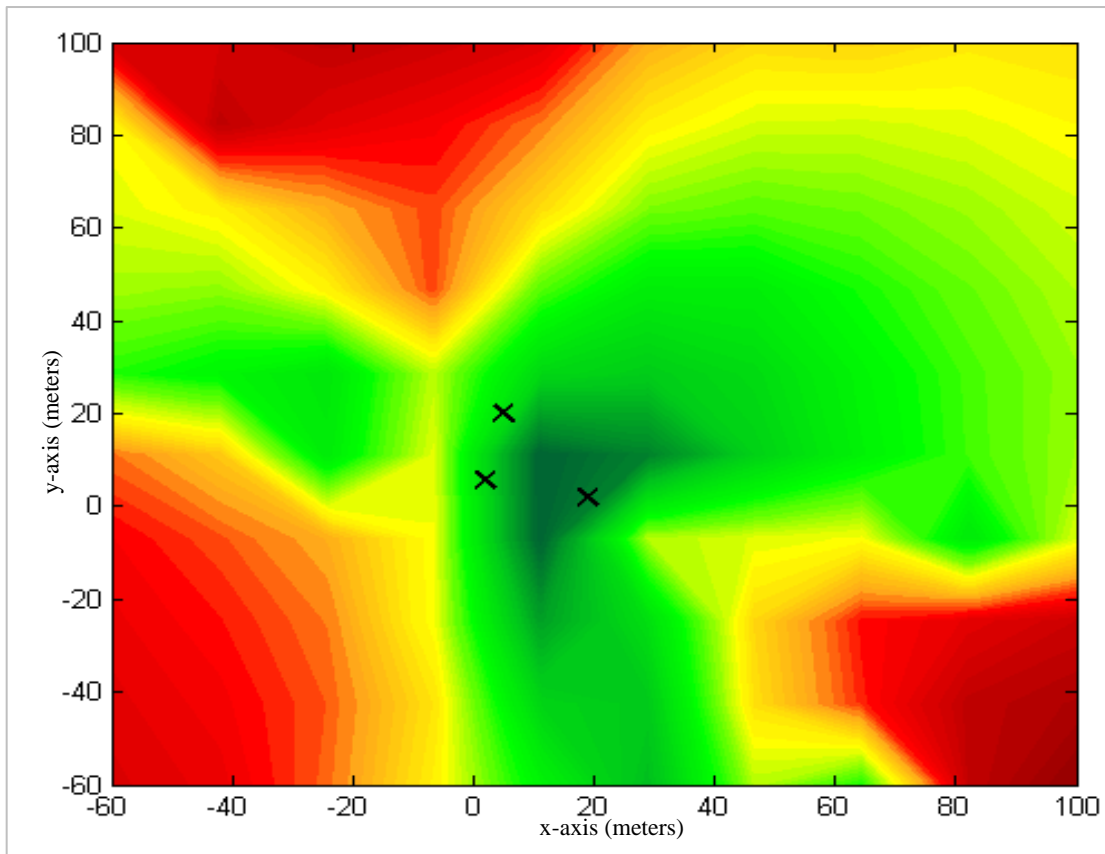
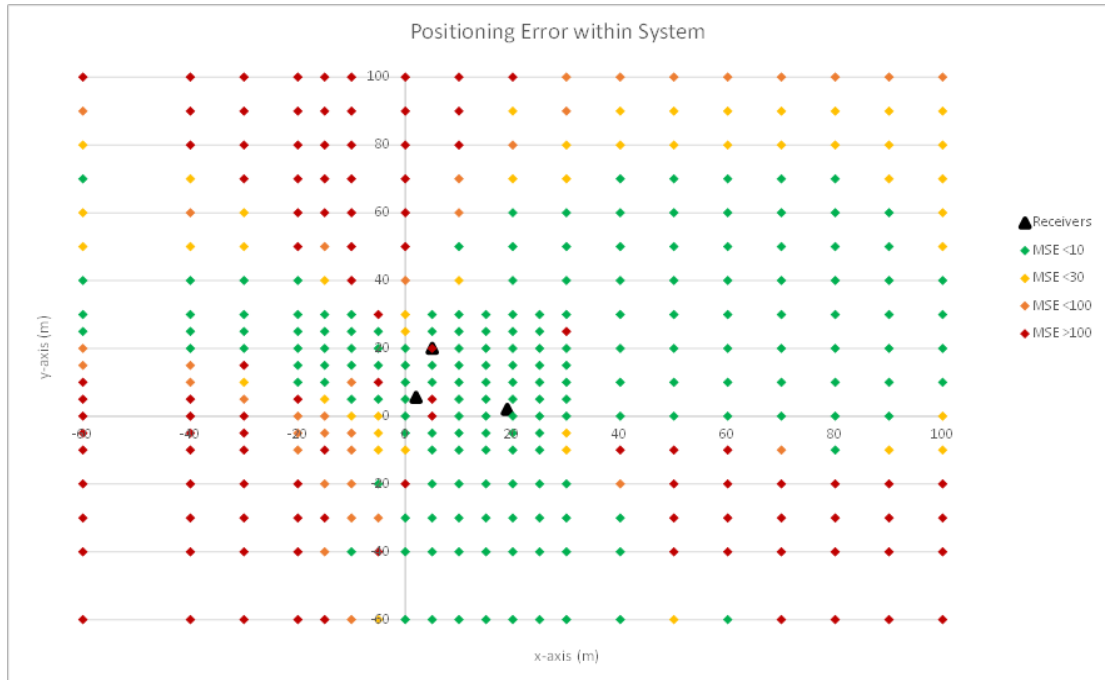


Figure 7- 14: System Simulation to Identify Influence of Receiver Positions

distance as the hyperbolic curves will run more in line with each other, increasing the range of intersection points. The position of the amber and red sections coincides with the results found in the localisation system evaluation whereby having the source transmission positioned behind the receivers, in relation to the hyperbolic curve axis, results in greater positioning errors within the system. To explain this further, the hyperbolic curves were plotted for one of the simulated transmitter positions located in one of the red regions, as illustrated in Figure 7- 15. Only one branch of each hyperbola is shown to ease viewing of the intersections as only one branch is relevant to the source localisation. It is evident from the figure that the hyperbolic curves intersect at two areas where the red curve recedes back from Rx3, consequently resulting in an average position far from the actual transmitter location. For this simulation, the transmitter position was at coordinates (-40,-40), however the average position estimation was plotted at (-18.8, -19.6), as shown with a magenta marker, due to the two points of intersection. Other high MSE simulations were evaluated, each showing similar results with one of the hyperbolic curves creating two areas of intersection due to the location of the transmitter in relation to the receivers and thus this should be taken into consideration during system setup and deployment of the hydrophone receivers.

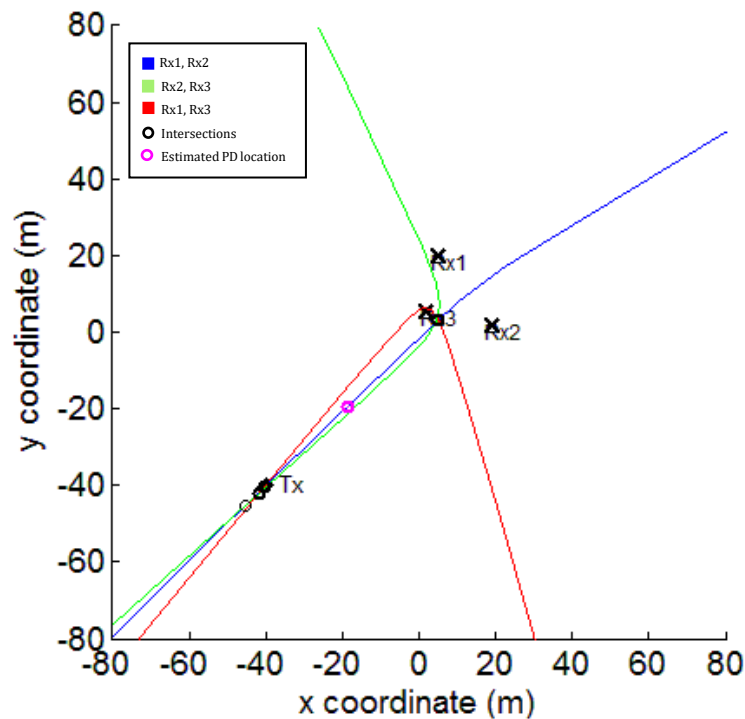


Figure 7- 15: Hyperbolic Positioning Simulation – Transmitter in Red Zone

7.3.4 Impacts of Additional Receiver

Along with receiver positions, a potential improvement to the system's accuracy could come from the use of an additional receiver. The open water trial was performed utilising three receivers, therefore a fourth was added to the simulation plot to evaluate any improvements. The original three hydrophones remained in the same positions as in the trial and previous simulation in order to make results comparable and the fourth hydrophone was added at coordinates (22,14). The addition of a fourth hydrophone results in an additional three hyperbolas with axis between Rx1 to Rx4, Rx2 to Rx4 and Rx3 to Rx4. The simulation was run with the transmitter positioned at multiple locations within the green, amber and red areas of the plotted region.

Review of the result presented no real improvement when the transmitter was located within the receiver boundaries, and for that reason was considered an unnecessary complexity in these instances due to the additional processing and assessment of the many intersections of the hyperbolic curves, along with the additional equipment required relating to the fourth hydrophone and acquisition system.

Results in amber and red regions did, however, present an improvement. To allow comparison, Figure 7- 16 presents results for both three and four receiver options, with the transmitter positioned in the amber region at coordinates (-15,-40). Again, only one side of each hyperbolic curve is displayed for ease of assessment. It is apparent from the three receiver plot that the estimated source location will be inaccurate as there are two points at which all three hyperbolic curves cross. Without knowledge of the source position, it is therefore unclear as to which is the correct position and thus an average is calculated and displayed with a magenta marker. In comparison, the plot illustrating the four receiver setup again shows intersections at the region where the red hyperbolic curve recedes back from receiver Rx2, however there is only one area where all hyperbolic curves intersect, consequently ruling out the other area of intersection closest to Rx2 and resulting in a more accurate source estimation. For further evaluation, Figure 7- 17 presents results for both three and four receiver options, with the transmitter positioned in the red region at coordinates (-35,80). Again, there are two areas of intersection displayed on the three receiver plot, resulting in a high MSE, however, it is clear from the four receiver plot that there is only one area where all of the six hyperbolic curves intersect, thus eliminating the second area shown in the three receiver results.

This concludes that an additional hydrophone should be considered to improve the systems accuracy when the transmitting source is located outside of the receiver boundaries, particularly in the highlighted amber and red regions. The added complexity and potential costs of an additional hydrophone may outweigh the benefits in green regions and thus should be considered depending on the system requirements. The receiver setup assessed was that used within the trial and consequently the regions will differ depending on the actual positions, however, a similar approach can be taken whereby a simulation plot is run to assess potential errors within the system itself to establish the most suitable setup.

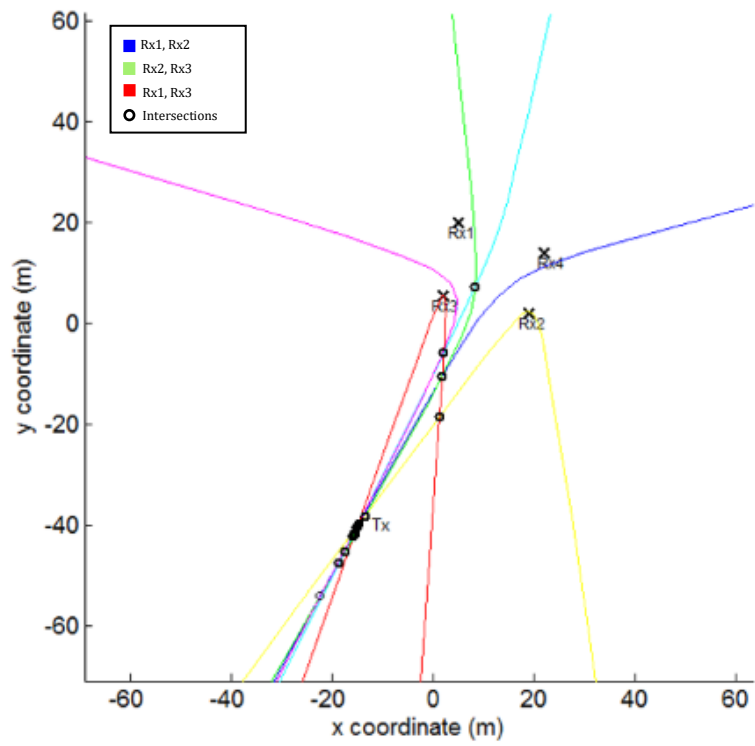
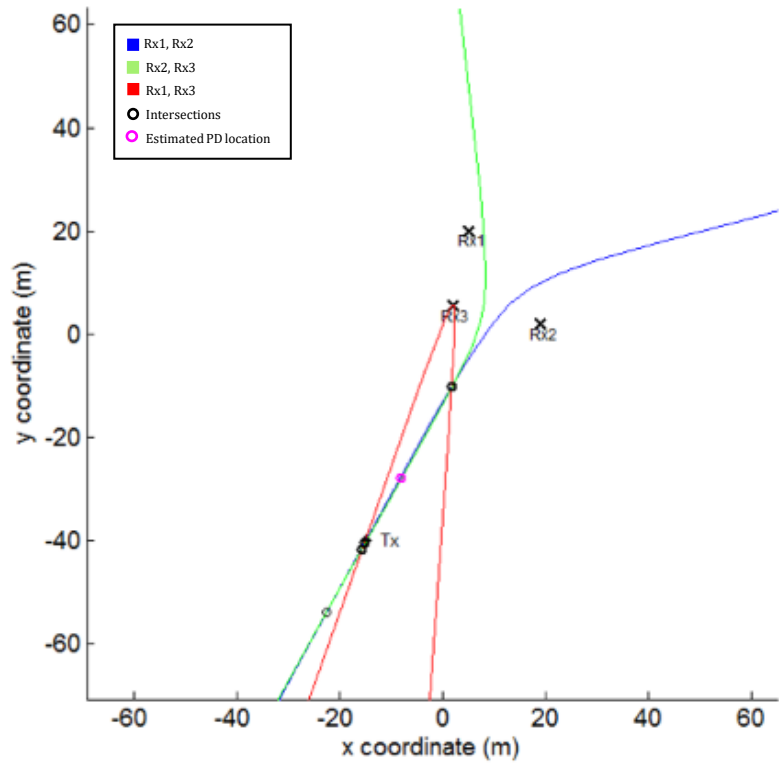


Figure 7- 16: Additional Receiver Simulation – Transmitter in Amber Zone

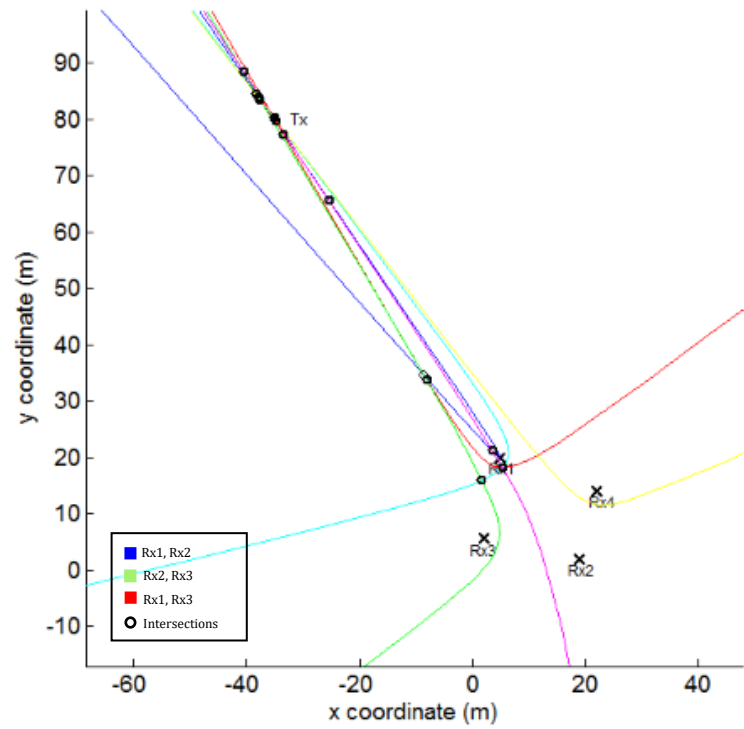
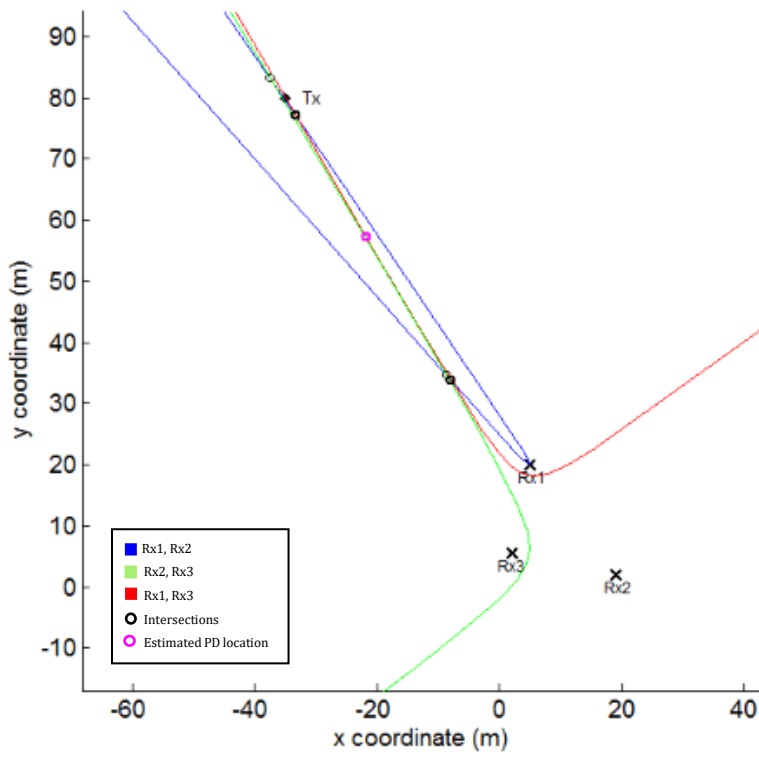


Figure 7- 17: Additional Receiver Simulation – Transmitter in Red Zone

7.3.5 Additional Trial

The open water trial was performed with a transmitter and pre-recorded acoustic emissions from PD occurrences which were obtained during controlled testing in an anechoic tank. This provided many benefits including; the ability to perform many tests at varying locations without the need to strip and repair the cable following each insulation breakdown, the transmitted signal could also be recorded to allow ToT to be known in order to establish the signal propagation speed, the transmitted discharges were the same for each trial and therefore comparable in amplitude, and the complexity of the test setup was reduced by the removal of the HV test equipment required to create the PD events. In particular, the use of HV equipment brought health and safety concerns as each area of test would need to be cordoned off with barriers at a sufficient distance to ensure public safety, and thus it was concluded to be too complex for the many trials required to assess the localisation system, hence the use of the transmitter during that trial. The trials performed with the transmitter were based on the calibrated transmission of the discharge signals at the correct source level, however, an additional trial performed with actual cable samples would provide further confidence in the detection system in more realistic conditions, whilst also presenting a different severity of fault as no two discharges are the same, and therefore an additional trial was performed at the marina including live cable samples.

Due to the discussed complications around the use of HV equipment, only one area of transmission was performed, and so the focus of the trial was on detection and localisation of the acoustic emissions from genuine PD occurrence, rather than localisation at multiple positions. Figure 7- 18 presents the setup of the cable sample and HV power supply. As with previous testing, a man made fault was introduced to the cable sample to ensure PD occurrence, and the fault region was sealed to prevent water ingress. The cable sample was fixed to one of the platforms of the marina, ensuring the exposed cable end was far enough from the water or any earthing points. The cable was then connected to the HV transformer and back to the HV test kit, to allow control of the voltage increments. The complete area was then barriered to prevent any pedestrian access, ensuring safe operating conditions.

A supplementary aspect of the test was to evaluate the feasibility of using GPS within the system to allow clock synchronisation of the receivers, therefore extending the range at which they can be positioned from each other by allowing separate acquisition systems to be utilised. To do this GPS antennas and receivers were included within the system setup and the output signal fed into the data acquisition unit, along with the received signals from the hydrophone. A high level overview of the system can be seen in Figure 7- 19. As well as its use for navigation systems, GPS can be applied to enable clock synchronisation through absolute time or pulse-per-second synchronising techniques. For this trial, pulse-per-second methods were utilised, where the GPS receiver outputs a repetitive pulsed signal every second, which is time synced across all GPS receiver units due to the atomic clocks onboard the GPS satellites. An individual acoustic discharge will all arrive at each



Figure 7- 18: Open Water Trial Test Setup – Live PD Occurrence through Cable Sample Testing

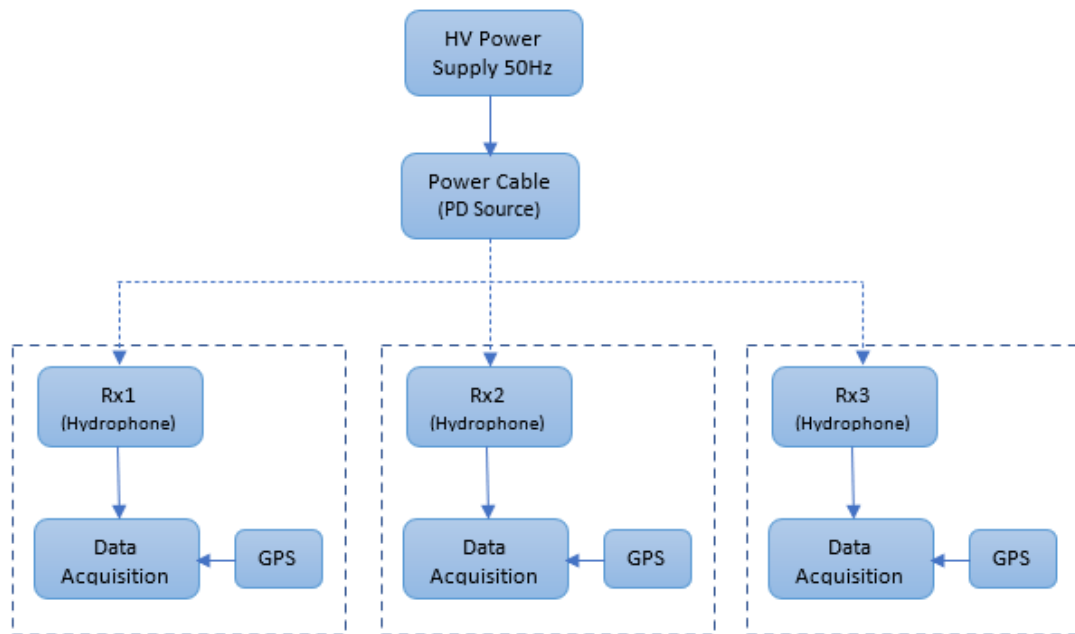


Figure 7- 19: Sensing System complete with GPS Synchronisation

hydrophone between one set of pulses as the 1 second delay between each pulse equates to a distance of approximately 1465m, which is much greater than that of the distances between receivers. Through post processing of the data and alignment of the GPS pulses, the TDoA between receivers can be established as the hydrophones will be clock synchronised, which in turn allows the PD source location to be determined.

Figure 7- 20 illustrates the positions of the hydrophones, Rx1, Rx2 and Rx3, along with the cable sample creating the partial discharges, Tx1. The range of the receiver triangle has been greatly extended in comparison to that performed in Section 6.3.3, however the position of the PD source is located within the receiver boundaries, with the maximum distance from source to receiver being approximately 60m from Tx1 to Rx2. Again, the voltage was increased in incremental stages to ensure PD occurrence with the aim of maintaining the insulation integrity for as long as possible as the fault area could not be easily repaired.

The initial concentration was on detection of the acoustic PD emissions at the hydrophones to confirm the ability for monitoring of genuine live PD occurrences. Figure 7- 21 presents an individual acoustic emission recorded on Rx2, which is positioned approximately 60m from the PD source. The overall recorded trace presented more noise than the previous open water trial, showing characteristics of a high frequency acoustic device such as an

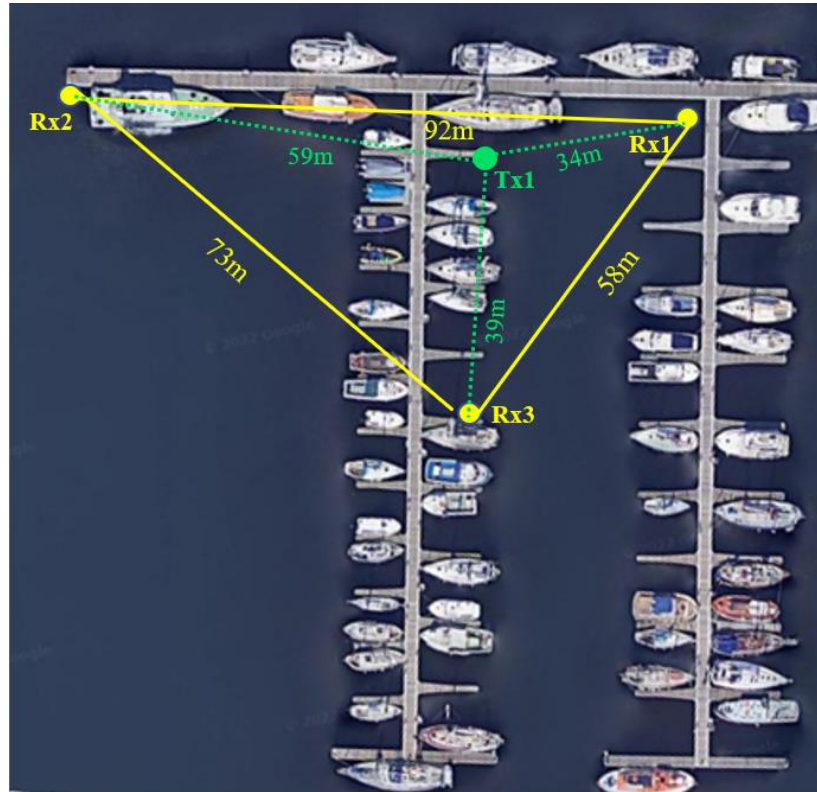


Figure 7- 20: Open Water Trial – Live PD, Receiver Positions

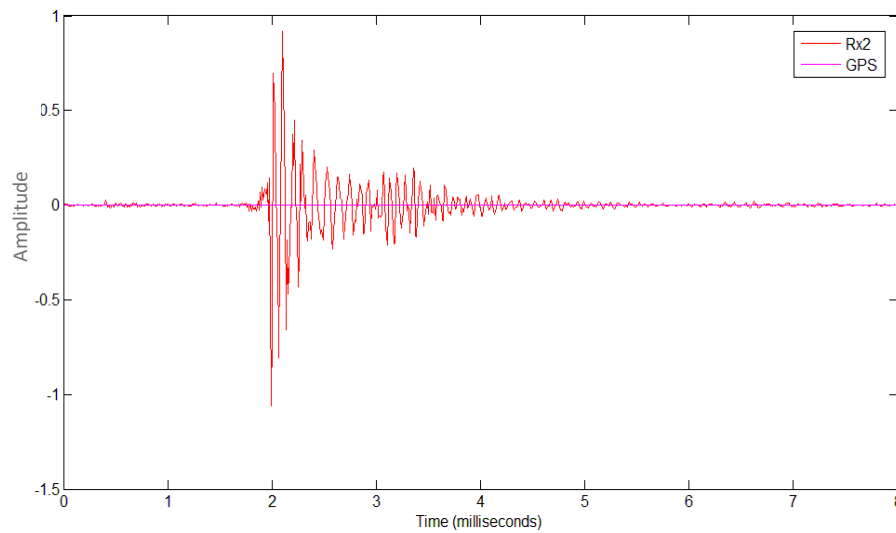


Figure 7- 21: Open Water Trial - Individual Acoustic Discharge detected at Hydrophone Rx2

antifouling system used on boats to reduce biofouling. Additional filtering was therefore required to remove the unnecessary high frequency signals and focus in on the PD events. A low pass filter was applied with as cutoff of 15kHz as the signals of interest are below this value. The signal presented in Figure 7- 21 displays comparable characteristics to those detected during the previous open water trial, showing a similar profile and duration of approximately 2ms, thus confirming that it is the detected PD signal.

Figure 7- 22 presents the overall trace recorded on Rx1, along with the GPS pulse signal. The discussed interference is not necessarily noticeable on this trace, however when assessing some of the peaks it was found that not all of the emissions displayed the same characteristics as the PD signals and therefore relate to the nearby acoustic transmitting source. The pulse width, signal profile and frequency content differ from that of PD and therefore can be ruled out during analysis. With focus on the GPS signal, it can be seen that the pulse occurs periodically every second throughout the complete recording, which can then be used to align the recordings between receivers. Figure 7- 23 centers on an individual PD emission, where the traces have been aligned based on the common GPS pulse-per-second signal. The output signal from the GPS receiver can be seen in magenta, where two pulses occur, and repeat every second. As noted, the distance equivalent to the 1 second time difference results in emitted acoustic signal being present on all receivers between one set of GPS pulses. As expected, the AE signal is first detected on Rx1, then Rx3 and finally on Rx2 due positions of the receivers. The amplitude of the detected signal can also be seen to be reducing with distance, through the anticipated attenuation of the signals.

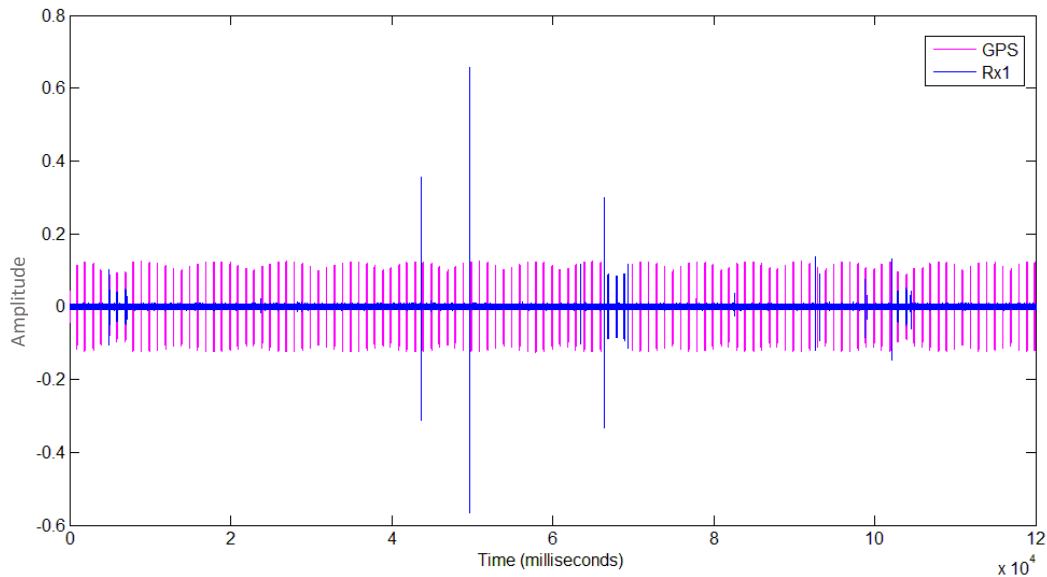


Figure 7- 22: Open Water Trial – Rx1 and GPS Signals

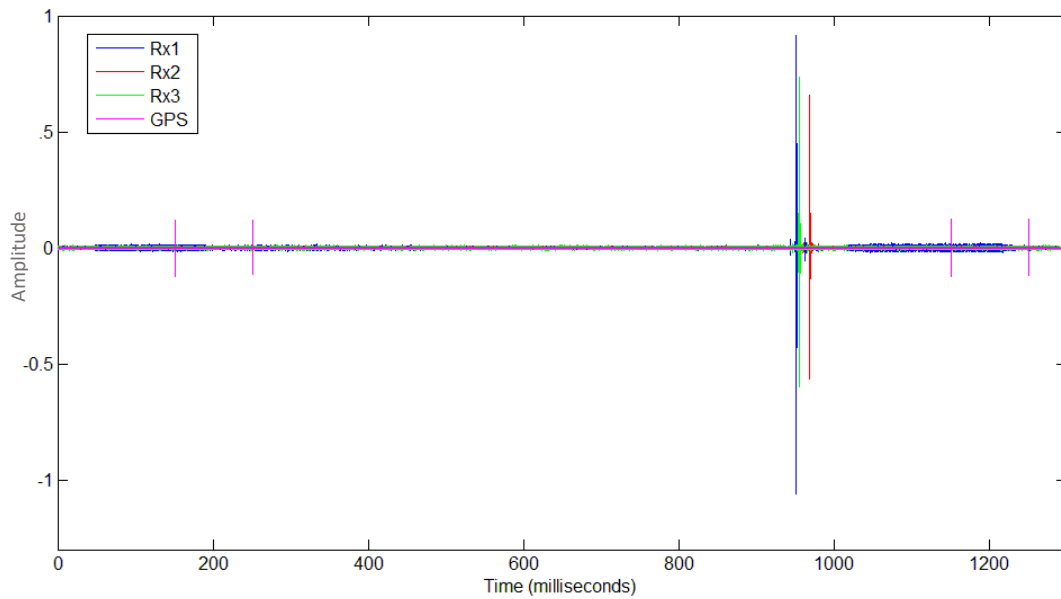


Figure 7- 23:Open Water Trial, Acoustic Discharge and GPS Signal Clock Synchronised on Rx1, Rx2 and Rx3

To further assess the signals, Figure 7- 24 and Figure 7- 25 present the individual emission detected on all hydrophones, along with the resultant signal envelopes. Considering (4.13) and a signal speed on 1465m/s, the distance equivalent to the TDoA between each receiver can be calculated, equating to how much further each hydrophone is positioned away from the PD source. A time difference of 3.2ms can be seen between hydrophones Rx1 and Rx3, and a difference of 16.8ms between Rx1 and Rx2, therefore resulting in a distance of 4.7m and 24.6m respectively. Figure 7- 20 shows the measured distances whereby Rx3 can be seen to be approximately 5m further from the PD source than Rx1, and Rx2 can be seen to be approximately 25m further from the PD source, therefore coinciding with the results from the envelope analysis.

The recorded signals were again input to the developed localisation algorithm to establish the location of the PD source. Figure 7- 26 illustrates the resultant hyperbolic curves along with the positions of the receivers and known PD location. A magenta marker is plotted at the intersecting hyperbolic curves, relating to the estimated position of PD. This estimated location falls within 1.5m of the known source location and presents an MSE of 0.625.

Multiple signals were evaluated in this way showing similar results and consequently providing confidence in both the ability to detect genuine PD acoustic emissions, along with the potential for utilising GPS pulse-per-second techniques to enable clock synchronisation of the receivers, thus allowing a greater range of positioning with the use of individual data acquisition units.

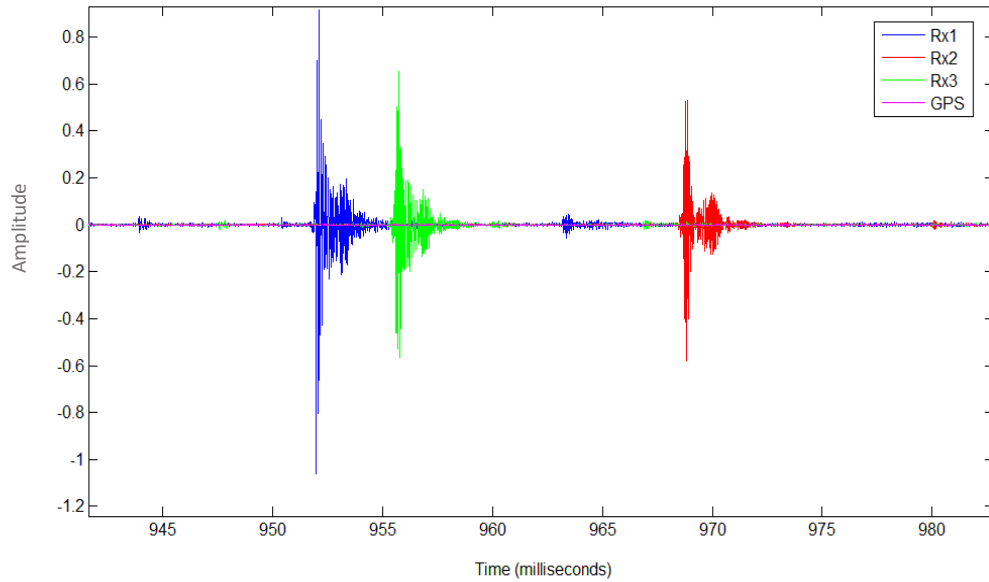


Figure 7- 24: Individual Acoustic Discharge Clock Synchronised on Rx1, Rx2 and Rx3

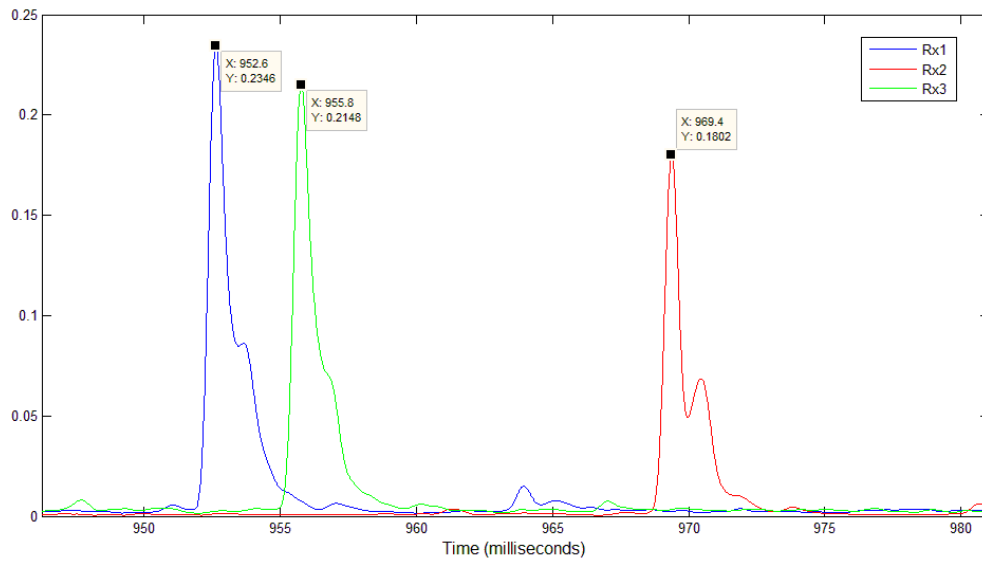


Figure 7- 25: Envelopes of Individual Acoustic Discharge Clock Synchronised on Rx1, Rx2 and Rx3

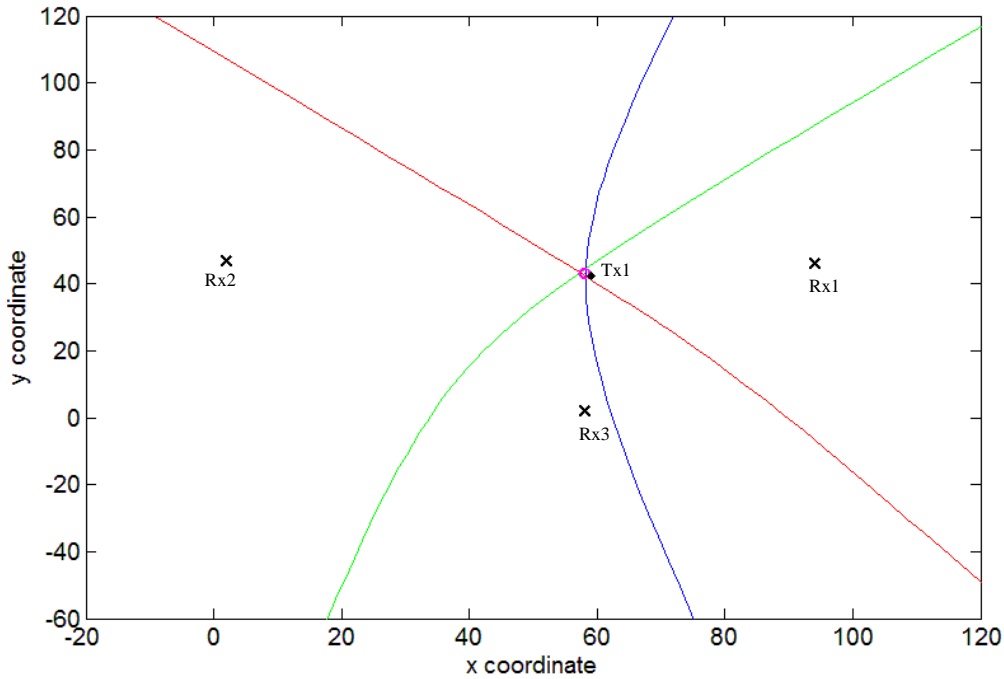


Figure 7- 26: Open Water Trial – Source Localisation of Genuine PD AE c/w GPS clock Synchronisation

7.4 Electro-acoustic Combined Method

For systems with preinstalled HFCT or other electrical PD detection devices, the potential of a combined electro-acoustic method is proposed. The use of an electrical PD detection device would allow for known ToT, however this would need to be clock synchronised with the hydrophone receivers to enable the use of trilateration within the localisation algorithm.

Figure 7- 27 illustrates the trilateration technique for source localisation, whereby the distances $d1$, $d2$ and $d3$ are calculated based on the signals ToF. In this application the process involves the ToF being established from the signals ToT, taken from the electrical detection methods, and the ToA of the acoustic signal at the systems hydrophones. This time delay can then be utilised to calculate the distances $d1$, $d2$ and $d3$, as shown in (7.14), where c is the signals velocity.

$$d = (ToA - ToT) * c \quad (7.14)$$

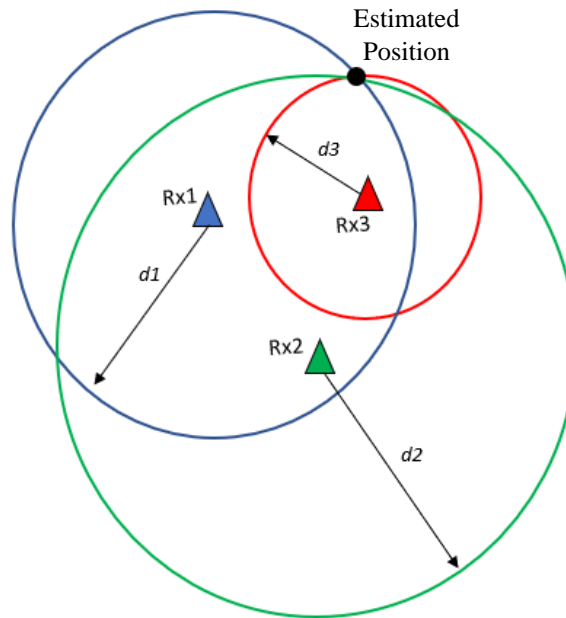


Figure 7- 27: Trilateration for Source Localisation

These calculated distances equate to the radius of the circles drawn around each hydrophone location. The area at which all of the circles intersect is the estimated location of the PD source. As with hyperbolic positioning, a minimum of three hydrophones are required to allow source estimation due to the two crossing points evident in Figure 7- 27 when only considering two intersecting circles. For 3D localisation, a fourth hydrophone would again be required to provide highly accurate results.

7.5 3D Source Localisation

The assessment of the localisation system considered both the transmitting source and the receivers to be on the same plane, hence the use of hyperbolas. This enabled the localisation system to be reviewed with a reduced complexity and the aid of visual intersection points, in comparison to the use of hyperboloids, whereby it is difficult to visually see the area of intersection. To ensure accurate results, the use of hyperboloids would be required in instances where the PD source and hydrophones are no longer on the same plane. The majority of the localisation algorithm remains the same, however the equations utilised to plot the hyperbolic curves are changed with those required to instead plot hyperboloids.

A hyperboloid is a quadratic surface generated by rotating a hyperbola about either of its axis. A revolution of a hyperbola about its conjugate axis produces a one-sheeted hyperboloid, whereas a revolution about the transverse axis produces a two-sheeted hyperboloid. The two-sheeted hyperboloid is of interest for use within the localisation system and is illustrated in Figure 7- 28.

The basic hyperboloid of two-sheets is given by the equation (7.15).

$$-\frac{x^2}{a^2} - \frac{y^2}{b^2} + \frac{z^2}{c^2} = 1 \quad (7.15)$$

The parametric equations of the top sheet to be considered in the localisation algorithm are shown in (7.16).

$$\begin{aligned} x &= \alpha \sinh u \cos v \\ y &= \alpha \sinh u \sin v \\ z &= c \cosh u \end{aligned} \quad (7.16)$$

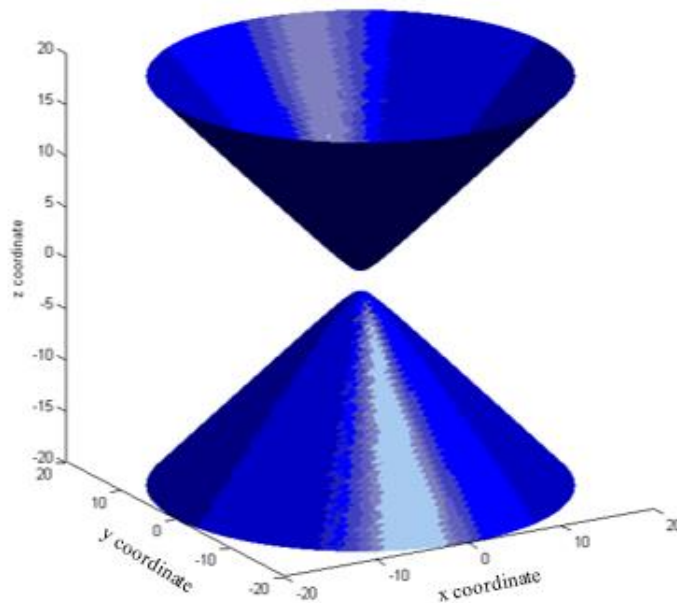


Figure 7- 28: Hyperboloid of two-sheets

The localisation algorithm was modified to plot hyperboloids instead of hyperbolas, with the parameters again based on the established TDoA, sound propagation speed and the distance between receivers. The recordings from section 6.3.3 were utilised, with the concentration this time being on the trials performed with the transmitter located at 3m water depth to provide a 3D plane for analysis. Figure 7- 29 presents the plotted results from trial 1b. The receivers are positioned at distances which replicate the trial, with the aim of the intersecting hyperboloids providing a PD source estimation. The figures displays results in the x,y axis only to illustrate the plot in comparison to the previous hyperbola results. Figure 7- 30 presents the same results, however also displays the z-axis. A volume of intersection can be seen between the three hyperboloids, however it is not a distinct intersection point as it was with the 2D hyperbola curves. Based on the plotted receiver coordinates and the distances from transmitter to receivers during the trial, the actual coordinates for the transmitter should be (13,11,3), however a precise location is not determined and instead a small volume highlighted. It is difficult to see on the figure, however magenta markers are presented in the volume of intersection. The process was repeated on other 3m water depth recordings from Section 6.3.3 to analyse the intersecting hyperboloids. Each time an area of intersection was highlighted rather than a specific location, with results varying by approximately 4m per axis. With consideration of the system usage, this level of accuracy may be acceptable depending on the application, however the use of an additional hydrophone would generate another three hyperboloids, and therefore further limit the area of intersection, as confirmed in section 7.3.4. Though

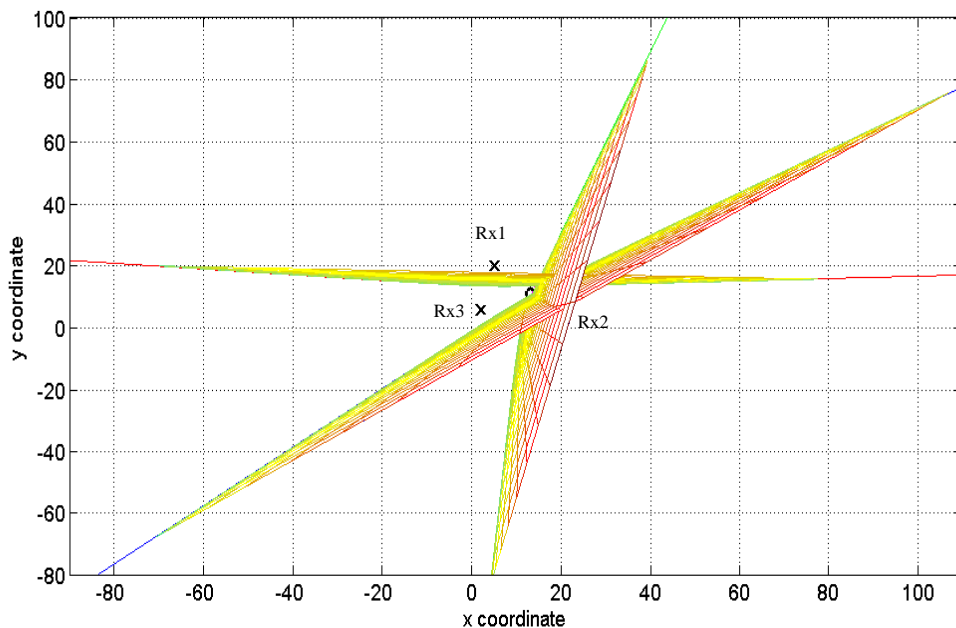


Figure 7- 29: Trial 1b – 3D Localisation utilising Hyperboloid Positioning, (x,y) axis

confirmation is presented in the implementation of hyperboloids within the positioning algorithm to allow for 3D positioning, it is recommended that a fourth hydrophone should be included within the system for improved levels of accuracy for PD source localisation.

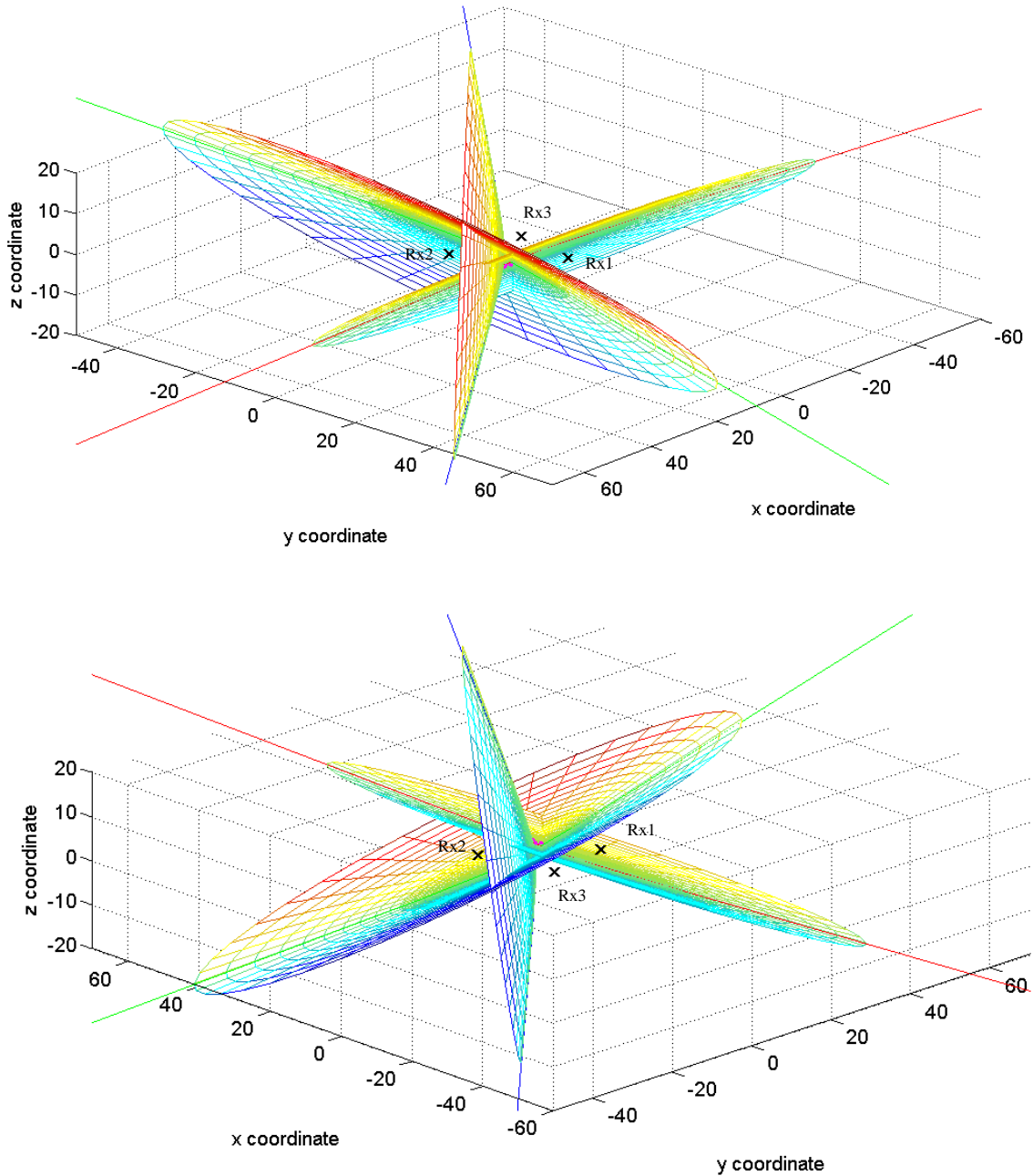


Figure 7- 30: Trial 1b – 3D Localisation utilising Hyperboloid Positioning, (x,y,z) axis

7.6 Practical Implementation

The through-water detection system requires the deployment of four or more hydrophones within the body of water surrounding the installed subsea power cable to listen for PD occurrence. This could be applied as a continuous method of detection over a set period of time in order to make an assessment on the condition of the cable, or it could be implemented when a known fault is present and highlighted through other electrical means of detection, with the system's aim being to localise the position of the potential fault. As the method is non-intrusive, the operation of the power cable can proceed, causing no issues to planned production. The preferred option is a system involving acoustic only sensing as this offers the most minimalistic approach for use in a variety of subsea environments.

Evaluation of the receiver positions has highlighted that the ideal system would involve the hydrophones being deployed to ensure that the potential fault region sits within the receiver boundaries. In most instances, the approximate location of the installed subsea power cable will be known, however, the lengths of the cables would make it difficult to ensure the complete cable was positioned within these boundaries, without going to unfeasible distances between each hydrophone. Knowledge of the power cable's position would however be beneficial as the hydrophones could be positioned to ensure the length remains outside of the red regions found behind the receivers, ensuring that a section of the cable runs through the receiver boundaries. The distance between each hydrophone should be kept as great as possible, whilst ensuring good accuracy is maintained, as this will increase the green regions previously illustrated, which provide the lowest error rates from inaccuracies within the system itself. As the geographical location and installed environment changes with each application, a simulation could be run to ensure suitable hydrophone locations prior to system deployment.

Depending on the underwater noise levels within the area of implementation, along with the overall power cable length, the detectability range may be too short and therefore a number of hydrophone arrays positioned every so many meters to increase the overall range may be a requirement. This would lead to an increased system cost and consequently, depending on the reason for implementation, it may be preferred to record at one position for a certain length of time and then move to another position toward the end of the detectability range. As well as cable length, water depth also impacts the detectability range as a power cable installed in deep waters would greatly increase the required distance. If the water depth is greater than the detectable range with the hydrophones deployed at their maximum water depth, another option to reach the subsea power cable would be to utilise underwater vehicles complete with acoustic sensors, thus allowing detection at a much closer range. This, however, would be considered as a worst case option due to the heavy costs associated with the use of underwater vehicles.

In addition, it was proven that the implementation of an additional hydrophone provides improved accuracy in high error regions, and thus this should be considered for each potential application, though the complexity and the costs of an additional hydrophone and acquisition system may outweigh the potential benefits.

In the alternative combined sensing method, an HFCT or other electrical PD detection equipment would be installed on the cable topside, above water level. Again, hydrophones would be deployed utilising the same methodology as discussed previously, however the complexity of the localisation algorithm would be reduced and accuracy improved as the detected EM signal allows ToT to be known, thus enabling the use of trilateration, as opposed to hyperbolic positioning. The HFCT's would need to be clock synchronised with the hydrophone receivers to calculate ToF between transmitted and received signals. Typical maximum detection lengths for HFCT's are around 1km due to the attenuation and dispersion effects of EM PD signals in power cables before reaching the HFCT [54]. Unlike the discussed acoustic only localisation methods, the detectable EM distance cannot be extended by positioning additional sensors along the installed length or in closer proximity to the umbilical, due to the need for HFCT's to be positioned above water level and requiring a physical clamped connection around the cable itself. As previously mentioned, the use of HFCT's would also bring about a large additional cost as they are required on each individual cable, along with monitoring equipment, and therefore they would only be utilised within the localisation system if they were already fitted to the power cable installation.

7.7 Summary

This chapter has discussed and evaluated the through-water acoustic system for PD source localisation. An initial review was performed on various localisation techniques to establish the most suitable for both the acoustic only and the combined electro-acoustic localisation techniques. With focus on the acoustic only method, hyperbolic positioning was identified as the most suited option as it is commonly used in applications where the signals ToT is unknown. Angle of arrival also presented an option capable of doing this, however this was ruled out due to the need for complex array structures and processing algorithms. Trilateration was highlighted as the preferred option for the combine electro-acoustic method as the EM signal could be considered as ToT of the resultant emissions from PD occurrence, thus allowing ToF calculations between ToT and the ToA at each receivers.

Hyperbolic positioning was then reviewed in more detail to understand how it can be utilised within the localisation algorithm. The key parameters of the hyperbola were discussed, where it was identified that the distance between foci relates to the distance between receivers and the distance between vertices relates the distance equivalent to the calculated TDoA, consequently allowing the hyperbolic calculations to be input to the

localisation system to produce intersecting hyperbolic curves, thus providing a position estimation.

The hyperbolic calculations were then included within the localisation system and the recordings from the previous open water trial were input to assess the ability to locate the transmitting source. The position of the transmitter was recorded during each trial, subsequently allowing the accuracy to be assessed. Hyperbolic plots were shown for each trial performed at 1m water depth, where in most cases position estimations were found to be highly accurate. Results again concluded that cross correlation techniques provide more accurate results than with envelope analysis. Results also highlighted that the position of the transmitter in relation to the receivers had an effect on the accuracy of the estimated source location, and so this was investigated further.

A simulation was performed based on the perfect system, where the transmitting source was positioned at multiple locations and the receivers positioned to match the trial. The plotted hyperbolic curves showed areas where errors could be present even in a perfect system based on actual distances from transmitter to receiver. Multiple intersection points of the hyperbolic curves were present when the transmitter was positioned in certain areas causing errors in the average estimated source positions. The areas with the highest error rate were found behind the receivers, when considering the hyperbolic axis, as this led to two areas where all three hyperbolas intersected. The locations with the highest accuracy were found when the transmitter was positioned within the receiver boundaries. The addition of a fourth receiver was also investigated, with results showing improved accuracy in high error regions, as there was only one area where all six hyperbolas intersected.

An additional open water trial was performed with actual cable samples to produce genuine PD events. This was to further confirm the capabilities of the system through more realistic conditions than the use of the transmitter for pre-recorded signals. The acoustic PD signals were able to be detected at the tested range of up to 60m, validating the ability to detect the acoustic emissions from live PD events. In addition, the initial open water test was performed with all receivers tying back to the same acquisition system, however this limits the allowable distance between receivers and as a result the methodology of using GPS to clock synchronise the receivers was assessed and proven to be feasible.

Although the aim was to use an acoustic only system, it was noted that the complexity of the localisation algorithm would be greatly reduced and the accuracy improved through the use of trilateration. This is possible if EM PD detection equipment is already installed and could be incorporated within the system to allow known time of PD occurrence. This combined electro-acoustic method was therefore discussed, detailing how it would be applied to the localisation system.

The progression of the system for 3D localisation was examined through the use of hyperboloids instead of hyperbolas. Recordings from the open water trial performed in Section 6.3.3 were considered, with the transmitter placed at 3m water depth and as such sits on a different axis to the receivers. Results presented the ability for 3D positioning

within the system, however, confirmed that a fourth hydrophone was needed to provide more accurate intersection results.

The chapter concluded with a discussion around the practical implementation of the system, where the various methods of hydrophone deployment are considered to suit varying applications and environments.

Chapter 8

Conclusion

The final chapter begins with an initial summary of the key technical contributions of this thesis, as presented in Table 8- 1.

<i>Chapter</i>	<i>Key Contributions</i>
4	<p>Acoustic PD characteristics examined – broadband signal, pulse duration $\approx 3\text{ms}$, main signal energy below 5kHz</p> <p>Through-cable signal propagation speed varies with distance, stabilising at around 25m at $\approx 2442\text{m/s}$ showing properties of a longitudinal wave propagating through high density polyethylene.</p> <p>Comparative electrical PD testing to establish the severity of detected AE from PD confirmed levels of around 25.5pC peak PD and 837pc/cycle of PD activity, allowing assessment of criticality of the fault.</p>
5	<p>Developed Cross correlation methods provide a high level of accuracy for source localisation when considering low SNR environments down to -7dB.</p> <p>System detectability lengths calculated to be between 70m to 85m for SNR's between 3dB to -11dB.</p>
6	<p>Through-water acoustic PD signals analysed - broadband signal spanning 22kHz spectrum, pulse width $\approx 4\text{ms}$.</p> <p>Controlled testing confirmed an acoustic PD emission source level of 144dB.</p> <p>Detectability distance calculated as follows; $\approx 500\text{-}1000\text{m}$ for sea NSL levels of 45dB, $\approx 100\text{-}200\text{m}$ for NSL levels of 60dB and $\approx 10\text{-}20\text{m}$ for NSL levels of 80dB.</p>
7	<p>Development of localisation algorithm utilising hyperbolic positioning and TDoA between receivers able to detect & locate transmitted PD.</p> <p>Developed system utilised on genuine live PD in an open water environment, providing highly accurate localisation results, whilst also implementing GPS clock synchronisation techniques.</p>

Table 8- 1: Key Technical Contributions

The chapter goes on to summarise the findings and conclusions from the preceding chapters, with focus on the contributions towards the development of an online system able to detect and locate PD occurrences within subsea power cables. Suggestions for future work are also identified, highlighting potential areas to progress the contributions further.

Chapter 2 - The background research carried out in Chapter 2 identified the increasing need for more subsea power cables following changes in both the oil and gas and the offshore renewable sectors. Progression within the oil and gas industry around subsea processing, all-electric control, and heated pipelines has led to MV/HV power cables becoming a key component within subsea umbilicals and therefore highlighting the criticality of the cables condition. The global drive to tackle climate change and reduce greenhouse gases has brought on the floating offshore wind market, which results in the need for increased quantities of highly dynamic power cables. Not only has the quantity of cables increased but the technology has developed, resulting in more dynamic applications, higher voltages and in turn, higher levels of electrical and mechanical stress. In both applications, the integrity of the power cable is vital to allow power transfer to take place and thus a technology capable of assessing the component condition, whilst the cables remain operational, was identified as a necessary area for research and development.

A review of common failure modes within subsea cables recognised a method for detection and localisation of partial discharge events to be the most beneficial area for study as it could be applied as a means of preventative cable failure, showing potential to provide large cost savings from unplanned production downtime. The amplitude and frequency of PD occurrence provides an indication of the condition of the cable and having the ability to locate the potential fault allows for planned intervention of the specific area, if necessary.

Chapter 3 – This chapter explored the potential techniques to be used for PD detection, along with the main challenges associated with the subsea cable environment including; long distance detection, the challenging and varying subsea environment, the bespoke nature of each umbilical design and the need for a non-intrusive retro-fit option which can be used whilst the cable remains online. Acoustic sensing was determined the most suitable method to address the challenges highlighted. Acoustic techniques can be applied to listen for both through-cable and through-water signals propagating from the discharge location, whilst offering the significant advantage of not requiring a physical connection to the conductor, consequently allowing the system to be used online. This non-intrusive option also allows the sensing system to be retrofitted to pre-installed cables. Acoustic waves propagate well within seawater, particularly the lower frequency components and therefore, to allow the maximum detectability range, the focus is on the lower frequency range. For through-water detection, hydrophones are the preferable option as they are designed for underwater detection of acoustic waves, whilst also allowing localisation of the PD source through TDoA techniques, based on the received signals. As a result, hydrophones are the chosen acoustic sensing method utilised during experimental trials.

Chapter 4 - With focus on the through-cable detection of the acoustic signals emitted during PD, Chapter 4 explores the characteristics of the detected signal. Experimental

testing showed clear PD signals could be detected, with the acoustic signals displaying a short pulse duration of around 3.0ms. An EM signal was also present on the recorded events, preceding the acoustic emissions and occurring instantaneously across both sensors. Analysis of the frequency content of the signals demonstrates that the spectrum is dominated by the frequency response of the channel rather than the emission itself as different channels for the same PD event show a different spectrum, whereas different PD events on the same channel display a very similar spectrum. Evaluation of the signal spectrogram and power spectral density show the main signal energy to be below 5kHz.

A review of differing wave types and mediums highlighted the complexity of the through-cable propagation path as the signal can travel a multitude of ways, which in turn causes variations to the signal velocity. Testing concludes that the signals propagation speed varies with the through-cable distance travelled, showing a gradual increase in speed until around 25m from the fault where the velocity begins to stabilise at an average speed of 2442m/s. This indicates that the signal is propagating out from the fault region, through varying mediums and stabilising once at the outer polymer sheath as the resultant velocity is in line with that of a longitudinal wave propagating through high density polyethylene, which has a value of approximately 2430m/s. When considering the changes in the signals amplitude with distance, the nature of the test makes it difficult to make a true comparison as the amplitude is dependent on the mechanical energy released in each individual discharge, however the test does confirm an overall reduction in amplitude as the propagation distance increases.

Chapter 4 concludes with a comparative test to assess the severity of PD detected acoustically, through the inclusion of conventional electrical PD detection equipment within the test setup. Results showed that at time of acoustic emission detection, the average pC readings were around 25.5pC peak PD and 837pC/cycle of PD activity. This provides an indication to the magnitude of the PD events which can be detected utilising these acoustic techniques, which, based on previous literature, puts the cable into the ‘potential risk’ category.

Chapter 5 - The methodologies of both distributed acoustic sensors and combined EM and AE sensing were investigated, with a main focus on the acoustic only technique. Through analysis and processing of previous test data and through utilisation of cross correlation and envelope analysis techniques, highly accurate position estimates were made for tests with the receiver positioned 5m from the fault, through to 55m. In both methods, the application of a cut-off of one SD from the mean vastly improved the accuracy of the position estimation as the results were then based on the main body of data, without influence from outliers. With outliers removed, results from envelope analysis provided an MSE of 0.24, an MAE of 0.39m, a percentage error of 1.9% and a position estimation falling within 1m of the true PD location. Cross correlation results provided an MSE of 0.29, an MAE of 0.43m, a percentage error of 0.91% and a position estimation located within 0.5m from the actual PD location. Review of the combined AE and EM sensing method resulted in a high level of accuracy, presenting an MSE of 0.31, an MAE of 0.43m,

a percentage error of 1.99% and a position estimation within 1m of the true location. This method however, is not suitable for long length power cables as the HFCT capabilities are length limited due to the attenuation and dispersion effects of the high frequency EM signals through the cable.

To assess the systems ability to operate in varying environments, noise was added to the system to produce SNR's between 10dB and -7dB. Cross correlation and envelope analysis methods both provide a good levels of accuracy within the system for SNR's down to -3dB, with results falling within 2m of the position estimation from the original signal. Below this value, the accuracy of the results from envelope analysis decreased rapidly, unlike cross correlation results which maintained high levels of accuracy through to an SNR of -7dB, whereby an average position estimation of 1m from the original signal estimation continued, with a percentage error of 4.98%, in comparison to 14.63% from the use of envelope techniques. The lowest SNR at which a PD localisation remained achievable was found to be -11dB, whereby anything below this value caused too many errors within the estimation algorithm due to the noise levels reaching the threshold of the signal.

The results also include the EM signal within the localisation algorithm which acts as a trigger due to its amplitude being larger than the acoustic signals, however, in reality this will not be present without the additional use of EM detection equipment. From the findings presented, an SNR of 3dB or above would be preferred for accurate localisation results where no EM signal is present.

SNR analysis confirmed the preferable use of cross correlation TDoA techniques within the through-cable localisation algorithm as this method consistently showed more accurate results attributable to the process of comparing the similarity of two signals as a function of displacement, instead of the analysis of the signal envelope peaks, which is far more likely to be influenced by noise.

The attenuation rate was established, allowing estimation of distances past those recorded during the tests, consequently enabling estimation of the propagation distances at which varying SNR's will be reached. Following on from the SNR findings, SNR's of 3dB, -7dB and -11dB were evaluated, resulting in detectability distances of approximately 70m, 80m and 85m, respectively. It was noted that improvements could be made to increase the detectability range with changes to both the acoustic sensor type, position and coupling method, as benefits were discussed with sensors being coupled directly to semi-conductive or insulating layers, or alternatively, sensors being fully bonded to the sheath to minimise signal losses. The practical implementation of the sensor setup is discussed, with options of multiple sensors, or topside only systems, however differing environments may suit different setups and thus no universal method was confirmed.

Chapter 6 – The chapter begins with an investigation of the properties of the underwater acoustic channel to develop an understanding of the complexities and influences varying environments would have on the received acoustic signal.

Controlled testing was initially performed in an anechoic water tank to develop an understanding of the signals through-water characteristics. Analysis showed clear detection of the acoustic signals emitted during PD occurrence, with the shape of the individual AE pulse differing from that detected during through-cable sensing, although the pulse duration remained similar at around 4ms. The EM signal was also detected, however the amplitude was much smaller than that detected during through-cable sensing due to the conductivity of seawater causing high levels of attenuation. Evaluation of the signals in the frequency spectrum again showed results which differed from those analysed during the through-cable analysis as the signal spanned the measured 22kHz spectrum, with the power spectral density showing consistent signal energy across this frequency range. This variation is partially attributable to the test being of short range, therefore reducing the higher frequency attenuation in comparison to that shown in through-cable sensing, and also the efficient propagation of sound through water, when compared against the losses experienced at each changing medium of the through-cable propagation path.

Further testing allowed calibration of the hydrophones to determine the source level of the detected PD acoustic emissions, which in turn allows calculation of the estimated detectability range based on varying levels of ocean noise. Through analysis of multiple PD events, a source level of 144dB was calculated for the detected PD acoustic emission. Based on previous findings, SNR's of both 3dB and -3dB were considered in the estimation of the detectability range, along with sea noise spectral levels of 45dB, 60dB and 80dB, based on typical values from literature. Detectability distances were calculated to be approximately 500-1000m for quiet sea states, 100-200m considering more realistic levels of ocean noise, and 10-20m for areas experiencing high levels of ocean noise. As the system is designed for use in many geographical locations, improvements such as directional sensing should be investigated when areas present high noise levels, whilst requiring long range detection. Alternatively, in areas exhibiting very high noise levels, sensors could be positioned closer to the cable through use of underwater vehicles, though this would be a more costly option and thus the use of directional hydrophones deployed near the surface of the water would be the first consideration for improved detectability distances.

Signals recorded during the controlled testing were then utilised in a large scale open water trial with the aim of testing the through-water system in more realistic conditions, whilst considering varying transmitter positions. Detailed analysis of the recorded files showed that the AE signals remained highly detectable and visibly clear throughout each trial, whereby the greatest distance from PD source to receiver was approximately 85m, thus providing confidence in the feasibility of the localisation system. As a transmitter was used to broadcast the recorded PD emissions, an additional test was performed where ToT was known, therefore allowing the propagation speed to be calculated through TDoA measurements, consequently providing a highly accurate speed without detailed knowledge of the water properties. Results provided an average value of 1465m/s and so this value was utilised within the localisation algorithm.

Chapter 7 - The final technical chapter focuses on localisation of the PD source in an open water environment. Hyperbolic positioning was identified as the most suitable positioning technique to be utilised within the localisation algorithm when considering the acoustic only sensing system, whereas trilateration was highlighted as the preferable option for the method of combined EM and AE sensing. Hyperbolic positioning calculations were then discussed and included within the algorithm to allow position estimation. Recordings from the previous open water trial were utilised to evaluate the systems performance and ability to estimate the transmitter position. Recordings were input to the localisation algorithm to analyse the accuracy of the results against the known transmitter locations. The resultant hyperbolic plots were presented for each trial and the accuracy assessed through MSE calculations, with the highest level of accuracy found when the transmitter was positioned within the receiver boundaries. A high level of accuracy was also achieved in areas outside of receiver triangle, however the results indicated that the transmitter position in relation to the receivers had an effect on the overall system error. This influence was therefore assessed through simulation of the transmitter at multiple locations, considering an ideal system with no input signal, based only on actual difference in distances from transmitter to receivers. The MSE was calculated for each position, highlighting areas susceptible to higher error rates. Results confirmed that the highest accuracy is found when the transmitter sits within the receiver boundaries and the area with the greatest errors is when the transmitter is positioned behind the receivers, in relation to the hyperbolic axis. A further assessment was carried out with the addition of a fourth hydrophone to the simulated hyperbolic plots. Results demonstrate an improvement for transmitter locations within amber and red regions as the use of an additional hydrophone results in more hyperbolic curves which all intersect at one distinct area, in comparison to the results for three hydrophones which show two areas of intersection.

An additional open water trial was performed with focus on the through-water detection of genuine PD events and utilisation of GPS techniques for clock synchronisation of the hydrophone receivers. Results confirmed the ability to detect acoustic emissions from PD occurrence at tested distances of up to 60m. The method of utilising a GPS receiver within the system providing a pulse-per-second output was also confirmed as feasible through alignment of the pulses to determine the TDoA between signals received at each receiver.

The option of a combined electro-acoustic method involves the implementation of the trilateration technique, as opposed to hyperbolic positioning, and thus the methodology was discussed to provide an overview of how this would be applied to the localisation system if EM detection means were also in use.

To further progress the system to allow for 3D source localisation, the implementation of hyperboloids was investigated. The localisation algorithm was modified to plot hyperboloids based on the TDoA results and receiver positions from previous open water trials. Results confirmed the methodology of utilising hyperboloid positioning techniques for 3D localisation, however they presented an area of intersection, as opposed to a specific

location, and therefore it was recommended that a fourth hydrophone be included within the overall system to provide more accurate results due to more intersecting hyperboloids.

The chapter concluded with a discussion around the practical implementation of the proposed localisation system, whereby the preferred method would be the deployment of four hydrophones positioned at as great a distance from each other as practicable, with the power cable running through the receiver boundaries, which in turn minimises the system errors associated with the geometry of the receivers and hyperbolic curve intersections. Should the detectability range and SNR require it, additional hydrophone arrays could be positioned along the length of the installed subsea power cable, or to minimise costs, the same hydrophones could be deployed at multiple positions for a set period of time. The use of hydrophones for acoustic PD monitoring provides a non-intrusive retrofit option at a relatively low cost.

8.1 Concluding Remarks

The results and findings presented in this thesis show technical feasibility for both through-cable and through-water detection and localisation of acoustic emissions from PD occurrence. The proposed systems allow for non-intrusive monitoring of operational cables within a subsea environment, with the aim of preventing high costs associated with unplanned downtime and allowing for planned intervention of a known fault location. With future work on directional sensing and receiver optimisation, detectability ranges could be further increased.

8.2 Future Work

Based on the findings and results of the presented thesis, further areas of work are proposed to progress and build on this research;

Considering the through-cable sensing, the cable layer at which the sensor is coupled could be investigated as testing was performed with the sensor positioned on the cable outersheath, however literature has shown improvements in results where sensor placement was on the semi-conducting or insulating layer. A key aspect of the system is to remain a retro-fit non-intrusive option, however this could be applied if sufficient benefits are found as the topside of the cable may be accessible.

Furthermore, investigation into other acoustic coupling mediums could be performed, whereby a fixed bonded solution could be applied in order to minimise losses through potential airgaps. Similar through-cable tests could be repeated with suitable materials to evaluate possible improvements.

Focusing on the through-water sensing, omnidirectional hydrophones were used during the open water trials due to the nature of the test and the changing transmitter position, however, in reality the location of the subsea cable will often be approximately known and

consequently directional sensing could be utilised to provide improved results, leading to a greater detectability range. Open water testing with directional sensing could be repeated and benchmarked against the results presented within this thesis.

As with through-cable sensing, the addition of existing electrical PD detection equipment within through-water trials would allow the magnitude of the PD events to be compared against existing pC recommendations, consequently providing additional knowledge around the presented findings.

In both instances, testing was performed at a component level only, considering an individual single-phase power cable, as opposed to the complete three-phase power cable or umbilical structure. The influence of the additional components and sheathing layers on the propagation of the acoustic signal from the PD location is therefore unknown and as a result further testing is recommended on an umbilical sample containing a PD fault to understand these effects.

References

- [1] O. E. Gouda, “Electrical and Water Treeing of Cable Insulation,” in *Environmental Impacts on Underground Power Distribution*, 2016, pp. 318–333.
- [2] TechnipFMC, “Technip Umbilicals - Engineering and Technologies.” TechnipFMC, p. 6, 2014.
- [3] C. Hardee and for Technip, “Longer life for deepwater umbilicals,” *Offshore*, vol. 70, no. 8, 2010.
- [4] R. Ellwanger, B. Sawatzky, and K. Zmitrowicz, “Factors Behind the 2014 Oil Price Decline,” *Bank Canada Rev.*, pp. 1–13, 2017.
- [5] J. B. and D. V. Marc Stocker, “Special Focus 1: With the Benefit of Hindsight: The Impact of the 2014-16 Oil Price Collapse,” *Glob. Econ. Prospect.*, pp. 49–71, 2018.
- [6] J. Baffes, M. Ayhan Kose, F. Ohnsorge, and M. Stocker, “Down the Slide,” *Financ. Dev.*, vol. December, pp. 20–23, 2015.
- [7] K. R. D. Trigg, S. Rado, C. Milterberger, “The oil and gas downturn and its impact on commercial real estate,” *Ernst Young LLP Trans.*, no. December, 2016.
- [8] M. Adeosun, “Falling oil prices - How will they impact the deepwater market?,” *Offshore*, vol. 75, no. 5, 2015.
- [9] J. F. Muller, “Down but not out,” *Offshore Eng.*, vol. 52, no. 43, pp. 36–39, 2016.
- [10] A. Deighton and A. Dobson, “Design Challenges of the Next Generation of All Electric Umbilical Systems,” in *International Conference on Ocean, Offshore and Arctic Engineering, OMAE*, 2017.
- [11] R. M. Ramberg, S. R. h Davies, H. Rognoe, and O. Oekland, “Steps to the Subsea Factory,” in *Offshore Technology Conference*, 2014.
- [12] S. R. H. Davies, W. Bakke, R. M. Ramberg, and R. O. Jensen, “Experience to date and future opportunities for subsea processing in StatoilHydro.” *Offshore Technology Conference*.
- [13] O. T. McClimans and R. Fantoft, “Status and New Developments in Subsea Processing,” in *Offshore Technology Conference*, 2006.
- [14] T. Ruud, A. Idrac, L. J. McKenzie, and S. H. Høy, “All Subsea: A Vision for the Future of Subsea Processing,” in *Offshore Technology Conference*, 2015.
- [15] R. Marjohan, “How to Increase Recovery of Hydrocarbons Utilizing Subsea Processing Technology,” in *Offshore Technology Conference*, 2014.
- [16] F. A. Albuquerque *et al.*, “Subsea Processing Systems: Future Vision,” in *Offshore Technology Conference*, 2013.

-
- [17] T. Myhvoid and P. Lovegrove, “Subsea all electric is here to stay,” *Technol. Outlook* 2030.
- [18] A. Nysveen, H. Kulbotten, J. K. Lervik, A. H. Børnes, M. Høyer-hansen, and J. J. Bremnes, “Direct Electrical Heating of Subsea Pipelines — Technology Development and Operating Experience,” *IEEE Trans. Ind. Appl.*, vol. 43, no. May 2007, pp. 118–129, 2007.
- [19] Y. Bai and Q. Bai, “Chapter 20 - Hydrates,” in *Subsea Pipelines and Risers*, Y. Bai and Q. B. T.-S. P. and R. Bai, Eds. 2005, pp. 357–382.
- [20] M. Gainville, C. Cassar, A. Sinquin, and C. Tzotzi, “Hydrate Plug Management using Electrically Trace Heating Pipe in Pipe-A Full Scale Experimental Study Hydrate Plug Management using Electrically Trace Heating Pipe in Pipe,” in *9th North American Conference on Multiphase Technology*, 2014.
- [21] Energy and climate Intelligence Unit, “The science of ‘carbon budgets,’” *Energy Clim. Intell. Unit*, no. September 2018, pp. 1–3, 2018.
- [22] Controller of Her Majesty’s Stationery Office and Queen’s Printer of Acts of Parliament, “Climate Change Act 2008,” *Parliamentary Affairs*, vol. Chapter 27. 2008.
- [23] S. Dray, “Climate Change targets: the road to net zero,” *House of Lords Library*, 2021. [Online]. Available: <https://lordslibrary.parliament.uk/climate-change-targets-the-road-to-net-zero/>.
- [24] A. Samuel, “UKCS Energy Integration Final report.” Oil and Gas Authority, pp. 1–35, 2020.
- [25] OGA, BEIS, Crown Estate, and Ofgem, “UKCS Energy Integration: Final Report,” *Oil Gas Auth.*, no. August, pp. 1–27, 2020.
- [26] D. Paterson, “Electrification is Key to Decarbonizing the North Sea,” *Offshore Eng.*, 2022.
- [27] J. Warnock, D. McMillan, J. A. Pilgrim, and S. Shenton, “Review of offshore cable reliability metrics,” *IET Conf. Publ.*, vol. 2017, no. CP709, pp. 1–6, 2017.
- [28] M. Froese, “How the wind industry is reducing cable failures,” *Wind. Eng.*, 2018.
- [29] C. Strang-Moran, “Subsea cable management: Failure trending for offshore wind,” *Wind Energy Sci. Discuss.*, no. March, pp. 1–11, 2020.
- [30] D. Young, “Predicting Dynamic Subsea Cable Failure for Floating Offshore Wind David Young | September 2018 | AP-0016,” *Catapuly Offshore Renew. Energy*, pp. 1–8, 2018.
- [31] F. Dinmohammadi *et al.*, “Predicting damage and life expectancy of subsea power cables in offshore renewable energy applications,” *IEEE Access*, vol. 7, pp. 54658–54669, 2019.
- [32] T. Schlemmer and L. Greedy, “TENNET, NL OFFSHORE WIND FARM TRANSMISSION SYSTEMS: 66 kV Systems for Offshore Wind Farms,” 2015.
- [33] A. Ferguson, P. De Villiers, B. Fitzgerald, and J. Matthiesen, “Benefits in moving
-

- the inter-array voltage from 33 kV to 66 kV AC for large offshore wind farms,” *Eur. Wind Energy Conf. Exhib. 2012, EWEC 2012*, vol. 2, no. 1, pp. 902–909, 2012.
- [34] International Standard, “IEC 60502-2:2014 - Power cables with extruded insulation and their accessories, for rated voltages from 1kV ($U_m = 1,2\text{kV}$) up to 30kV ($U_m = 36\text{kV}$) - Part 2: Cables for rated voltages from 6kV ($U_m = 7,2\text{kV}$) up to 30kV ($U_m = 36\text{kV}$).” 2014.
- [35] International Standard, “IEC 60270 - High-voltage test techniques - Partial discharge measurements (Third Edition).” IEC.
- [36] E. Gockenbach, “Partial discharge measuring technique,” in *High Voltage Engineering and Testing*, 2nd Editio., H. M. Ryan, Ed. Institute of Engineering and Technology, 2001, pp. 533–548.
- [37] A. El-faraskoury and O. E. Gouda, “Partial Discharge Measurements with Internal Artificial Cavities Defects for Underground Cables,” in *16th International Middle-East Power Systems Conference -MEPCON*, 2014.
- [38] H. S. and K. A. and T. T. Okamoto, “Complex behaviour of a simple partial-discharge model,” *EPL (Europhysics Lett.)*, vol. 66, no. 1, p. 28, 2004.
- [39] International Standard, “C37.301 - IEEE Standard for High-Voltage Switchgear (Above 1000 V) Test Techniques - Partial Discharge Measurements,” *IEEE Std C37.301-2009*. IEEE, 2009.
- [40] J. C. Hernandez-Mejia and J. Perkel, *Partial Discharge (PD) HV and EHV Power Cable Systems*, no. February. National Electric Energy Testing, Research and Applications Center, 2016.
- [41] International Standard, “400.3 - IEEE Guide for Partial Discharge Testing of Shielded Power Cable Systems in a Field Environment.” *IEEE Std 400.3-2006*. IEEE, 2006.
- [42] H. Orton and R. Hartlein, “Predicting Long-term Behavior,” in *Long-life XLPE-insulated power cables*, 2006, p. 121.
- [43] C. N. Sanniyati *et al.*, “Water tree in polymeric cables: a review,” *Malaysian J. Fundam. Appl. Sci.*, vol. 12, 2017.
- [44] J. C. Fothergill, “A critical review of water treeing mechanisms,” in *IEE Colloquium on Recent Advances in the Understanding of Water Trees*, 1993, pp. 4/1-412.
- [45] Malik, “Treeing in Cables,” in *Electrical Insulation in Power Systems*, p. 408.
- [46] J. Ceovic and M. Sirola, “Medium Voltage and Low Voltage Cable Measurements,” *J. Energy*, vol. 65, no. 12, pp. 24–37, 2016.
- [47] G. E. Brown, “Operational considerations for underwater-mateable connectors,” *Ocean. 2003 Celebr. Past... Teaming Towar. Futur.*, vol. 4, pp. 1843–1848, 2003.
- [48] Det Norske Veritas (DNV), “DNV-RP-A203 Qualification of New Technology,” *DNV Recomm. Pract.*, no. July, p. 78, 2011.
- [49] G. C. Stone, “Partial Discharge - Part VII: Practical Techniques for Measuring PD in Operating Equipment,” *IEEE Electr. Insul. Mag.*, vol. 7, no. 4, pp. 9–19, 1991.

-
- [50] M. Wu, H. Cao, J. Cao, H. L. Nguyen, J. B. Gomes, and S. P. Krishnaswamy, "An overview of state-of-the-art partial discharge analysis techniques for condition monitoring," *IEEE Electr. Insul. Mag.*, vol. 31, no. 6, pp. 22–35, 2015.
- [51] M. M. Yaacob, M. A. Alsaedi, J. R. Rashed, A. M. Dakhil, and S. F. Atyah, "Review on partial discharge detection techniques related to high voltage power equipment using different sensors," *Photonic Sensors*, vol. 4, no. 4, pp. 325–337, 2014.
- [52] International Standard, "IEEE Std. 1434 - Guide for the Measurement of Partial Discharges in AC Electric Machinery." 2014.
- [53] Omicron, "Partial Discharge Measurement Coupling Methods." Omicron Energy, pp. 1–2, 2020.
- [54] F. Álvarez, F. Garnacho, J. Ortego, and M. Á. Sánchez-Urán, "Application of HFCT and UHF sensors in on-line partial discharge measurements for insulation diagnosis of high voltage equipment," *Sensors (Switzerland)*, vol. 15, no. 4, pp. 7360–7387, 2015.
- [55] C. T. F. D1.02.05, "Practical aspects of the detection and location of partial discharges in power cables," *Tech. Broch. CIGRE*, no. 297, pp. 1–24, 2006.
- [56] R. Sarathi, A. Nandini, and M. G. Danikas, "Understanding electrical treeing phenomena in XLPE cable insulation adopting UHF technique," *J. Electr. Eng.*, vol. 62, no. 2, pp. 73–79, 2011.
- [57] G. Chen, J. Tao, Y. Ma, H. U. I. Fu, Y. Liu, and Z. Zhou, "On-site Portable Partial Discharge Detection Applied to Power Cables Using HFCT and UHF methods 3 Portable PD Monitoring Device," *On-site Portable Partial Disch. Detect. Appl. to Power Cables Using HFCT UHF methods*, vol. 15, pp. 83–90, 2016.
- [58] H. Chai, B. T. Phung, and S. Mitchell, "Application of UHF sensors in power system equipment for partial discharge detection: A review," *Sensors (Switzerland)*, vol. 19, no. 5, 2019.
- [59] G. Luo and D. Zhang, "Study on performance of HFCT and UHF sensors in partial discharge detection," *2010 9th Int. Power Energy Conf. IPEC 2010*, pp. 630–635, 2010.
- [60] A. Kraetge, S. Hoek, M. Koch, and W. Koltunowicz, "Robust measurement, monitoring and analysis of partial discharges in transformers and other HV apparatus," *IEEE Trans. Dielectr. Electr. Insul.*, vol. 20, no. 6, pp. 2043–2051, 2013.
- [61] M. D. Judd, "Experience with UHF partial discharge detection and location in power transformers," *2011 Electr. Insul. Conf. EIC 2011*, no. June, pp. 201–205, 2011.
- [62] P. Drexler *et al.*, "A sensor system for detecting and localizing partial discharges in power transformers with improved immunity to interferences," *Sensors (Switzerland)*, vol. 19, no. 4, 2019.
- [63] R. Sarathi and P. G. Raju, "Diagnostic study of electrical treeing in underground XLPE cables using acoustic emission technique," *Polym. Test.*, vol. 23, no. 8, pp. 863–869, 2004.
-

-
- [64] M. Muhr and R. Schwarz, "Experience With Optical Partial Discharge Detection," *Mater. Sci.*, vol. 27, pp. 1139–1146, 2009.
- [65] L. E. Lundgaard and N. Electric, "Partial Discharge - Part XIII: Acoustic Partial Discharge Detection -Fundamental Considerations," *IEEE Electr. Insul. Mag.*, vol. 8, no. August, pp. 25–31, 1992.
- [66] R. T. Harrold, "Acoustic Theory Applied to the Physics of Electrical Breakdown in Dielectrics," *IEEE Trans. Electr. Insul.*, vol. EI-21, no. 5, pp. 781–792, 1986.
- [67] P. Casals-Torrens, A. González-Parada, and R. Bosch-Tous, "Online PD detection on high voltage underground power cables by acoustic emission," *Procedia Eng.*, vol. 35, pp. 22–30, 2012.
- [68] A. E. W. Austen and W. Hackett, "Internal discharges in dielectrics: their observation and analysis," *J. Inst. Electr. Eng. - Part I Gen.*, vol. 91, no. 44, pp. 298–312, 1944.
- [69] T. Czaszejko and J. Sookun, "Acoustic emission from partial discharges in solid dielectrics," *EIC 2014 - Proc. 32nd Electr. Insul. Conf.*, no. June, pp. 119–123, 2014.
- [70] R. T. Harrold, "Acoustic Techniques for Detecting and Locating Electrical Discharges," in *Engineering Dielectrics Volume i*, Bartnikas R., Ed. American Society for Testing and Materials, pp. 327–405.
- [71] P. Arnold and J. F. Kment Attila, Pipa Marek, "On-site Partial Discharges Measurement of XLPE," vol. 1, no. 4, pp. 107–110, 2012.
- [72] W. Higinbotham, N. Davies, and V. Chan, "On-line Partial Discharge Assessment and Monitoring of MV to EHV Cables," 2015.
- [73] L. E. Lundgaard, "Partial discharge Part XIV Acoustic partial discharge detection practical Application," *IEEE Electr. Insul. Mag.*, vol. 8, no. 5, pp. 34–43, 1992.
- [74] International Standard, "C57.127 - IEEE Guide for the Detection and Location of Acoustic Emissions from Partial Discharges in Oil-Immersed Power Transformers and Reactors," *IEEE Std PC57.127/D8.0*, vol. 2007, no. August. 2006.
- [75] L. A. Renforth, R. Giussani, M. T. Mendiola, and L. Dodd, "Online partial discharge insulation condition monitoring of complete high-voltage networks," in *IEEE Transactions on Industry Applications*, 2019, vol. 55, no. 1, pp. 1021–1029.
- [76] R. Cselkó, Z. Á. Tamus, A. Szabó, and I. Berta, "Comparison of acoustic and electrical partial discharge measurements on cable terminations," *Conf. Rec. IEEE Int. Symp. Electr. Insul.*, 2010.
- [77] T. Czaszejko and J. A. D. Stephens, "Toward acoustic detection of partial discharges in high voltage cables," in *9th International Conference on Insulated Power Cables*, 2015.
- [78] Q. Che, H. Wen, X. Li, Z. Peng, and K. P. Chen, "Partial Discharge Recognition Based on Optical Fiber Distributed Acoustic Sensing and a Convolutional Neural Network," *IEEE Access*, vol. 7, pp. 101758–101764, 2019.
- [79] E. Rowen, A. Motil, and E. Inbar, "Novel Classification Of Leak Detection And
-

- Third-Party Intrusion Enabling Best-In-Class False Alarm Rate,” *Pipeline Technol. J.*, vol. 2, 2020.
- [80] K. Li, H. Javed, G. Zhang, and A. T. Plesca, “Analysis of air decomposition by-products under four kinds of partial discharge defects,” *IEEE Trans. Dielectr. Electr. Insul.*, vol. 24, no. 6, pp. 3713–3721, 2017.
- [81] G. C. Montanari, “Partial discharge detection in medium voltage and high voltage cables: Maximum distance for detection, length of cable, and some answers,” *IEEE Electr. Insul. Mag.*, vol. 32, no. 5, pp. 41–46, Sep. 2016.
- [82] G. C. Stone and S. A. Boggs, “Propagation of partial discharge pulses in shielded power cable,” *Conf. Electr. Insul. Dielectr. Phenom. - Annu. Rep. 1982*, pp. 275–280, 1982.
- [83] B. Sheng *et al.*, “Partial discharge pulse propagation in power cable and partial discharge monitoring system,” *IEEE Trans. Dielectr. Electr. Insul.*, vol. 21, no. 3, pp. 948–956, 2014.
- [84] A. Cavallini, G. C. Montanari, and F. Puletti, “A novel method to locate PD in polymeric cable systems based on amplitude-frequency (AF) map,” *IEEE Trans. Dielectr. Electr. Insul.*, vol. 14, no. 3, pp. 726–734, 2007.
- [85] S. Boggs, A. Pathak, and P. Walker, “Partial discharge. XXII. High frequency attenuation in shielded solid dielectric power cable and implications thereof for PD location,” *IEEE Electr. Insul. Mag.*, vol. 12, no. 1, pp. 9–16, 1996.
- [86] M. Seltzer-grant, L. Renforth, and R. Mackinlay, “On-line partial discharge detection , location and monitoring on MV networks,” in *MNC-CIGRE/CIREDA MALAYSIA*, 2010, no. December, pp. 8–12.
- [87] M. Wild, S. Tenbohlen, E. Gulski, R. Jongen, and F. De Vries, “Practical aspects of PD localization for long length power cables,” *2013 IEEE Electr. Insul. Conf. EIC 2013*, no. June, pp. 499–503, 2013.
- [88] K. M. Awan, P. A. Shah, K. Iqbal, S. Gillani, W. Ahmad, and Y. Nam, “Underwater Wireless Sensor Networks: A Review of Recent Issues and Challenges,” *Wirel. Commun. Mob. Comput.*, vol. 2019, 2019.
- [89] Z. Jiang, “Underwater Acoustic Networks – Issues and Solutions,” *Int. J. Intell. Control Syst.*, vol. 13, no. 3, pp. 152–161, 2008.
- [90] J. M. Hovem, “Underwater acoustics: Propagation, devices and systems,” *J. Electroceramics*, vol. 19, no. 4, pp. 339–347, 2007.
- [91] L. Lanbo, S. Zhou, and J.-H. Cui, “Prospects and problems of wireless communication for underwater sensor networks,” *Wiley Intersci. - Wirel. Commun. Mob. Comput.*, no. July 2008, pp. 977–994, 2008.
- [92] S. Al-Dharrab, M. Uysal, and T. Duman, “Cooperative underwater acoustic communications,” *IEEE Commun. Mag.*, vol. 51, no. 7, pp. 146–153, 2013.
- [93] J. P. Steiner, P. H. Reynolds, and L. Weeks, “Estimating the Location Discharge in Cables,” *IEEE Trans. Electr. Insul.*, vol. 27, no. 1, pp. 44–59, 1992.

-
- [94] J. Singsathien *et al.*, “Partial discharge detection and localization of defected power cable using HFCT and UHF sensors,” *ECTI-CON 2017 - 2017 14th Int. Conf. Electr. Eng. Comput. Telecommun. Inf. Technol.*, no. June, pp. 505–508, 2017.
- [95] S. H. Lee, C. K. Lee, J. B. Park, and K. S. Kwak, “Impedance change localization for live underground cable using time-frequency domain reflectometry,” *IEICE Electron. Express*, vol. 9, no. 5, pp. 359–364, 2012.
- [96] P. F. Fantoni, “Condition monitoring of electrical cables using line resonance analysis (LIRA),” in *International Conference on Nuclear Engineering, Proceedings, ICONE*, 2009, vol. 1, no. January 2009, pp. 171–178.
- [97] P. F. Fantoni, D. Beverly, B. Shumaker, and C. Campbell, “Condition Monitoring of Electrical Cables Using TDR and Line Resonance Analysis (LIRA),” *Plant Oper. Maintenance, Eng. Modif. Life Cycle; Compon. Reliab. Mater. Issues; Next Gener. Syst.*, vol. 1, no. November, pp. 171–178, 2010.
- [98] P. Stajanca, S. Chruscicki, T. Homann, S. Seifert, D. Schmidt, and A. Habib, “Detection of leak-induced pipeline vibrations using fiber—Optic distributed acoustic sensing,” *Sensors (Switzerland)*, vol. 18, no. 9, 2018.
- [99] S. Cherukupalli and G. J. Anders, “Use of Distributed Sensing for Strain Measurement and Acoustic Monitoring in Power Cables,” *Distrib. Fiber Sens. Dyn. Rat. Power Cables*, pp. 185–209, 2019.
- [100] Bandweaver, “Real time thermal rating monitoring system.” Bandweaver Technology Limited, pp. 1–8, 2017.
- [101] Optasense, “Case Study - Reducing Costs in Real Time with Smart Sensing DAS Technology Condition monitoring of power cables for offshore windfarm in Scotland.”
- [102] K. Sing, “Online Power Cables Condition Monitoring using Integrated SMART-SENSING Fibre Optic DAS Technology,” in *Wind Europe Summit*, 2016, p. PO.078f.
- [103] K. Hicke and K. Krebber, “Towards efficient real-time submarine power cable monitoring using distributed fibre optic acoustic sensors,” in *25th International Conference on Optical Fiber Sensors*, 2017.
- [104] I. B. V. da Costa *et al.*, “Electric discharge detection and localization using a distributed optical fiber vibration sensor,” *Opt. Fiber Technol.*, vol. 58, no. May, p. 102266, 2020.
- [105] Y. Tian, P. L. Lewin, A. E. Davies, S. G. Swingler, S. J. Sutton, and G. M. Hathaway, “Comparison of on-line partial discharge detection methods for HV cable joints,” *IEEE Trans. Dielectr. Electr. Insul.*, vol. 9, no. 4, pp. 604–615, 2002.
- [106] A. Stacey, M. Birkinshaw, and J. Sharp, “Life Extension Issues for Ageing Offshore Installations,” in *International Conference on Offshore Mechanics and Arctic Engineering*, 2008.
- [107] J. Perkel and J. C. Hernandez-mejia, “Chapter 7 - Medium Voltage Cable System Partial Discharge,” in *Cable Diagnostic Initiative, Phase II.*, no. February, Georgia
-

- Tech - National Electric Energy Testing, Research and Applications Centre, 2016, pp. 1–114.
- [108] Y. Han and Y. H. Song, “Condition monitoring techniques for electrical equipment - A literature survey,” *IEEE Trans. Power Deliv.*, vol. 18, no. 1, pp. 4–13, 2003.
- [109] R. W. Meggs and K. Daffey, “Partial Discharge Monitoring in Marine HV Systems,” in *Institute of Marine Engineering, Science and Technology Conference*, 2011.
- [110] Z. Nazarchuk, V. Skalskyi, and O. Serhiyenko, *Acoustic emission: Methodology and Application*, vol. i. 2017.
- [111] L. Piche, S. Pelissou, and J.-P. Crine, “Cable Insulation Density Profile Determined from Ultrasonic Velocity Measurements,” *IEEE Electr. Insul. Mag.*, vol. 8, no. June, pp. 33–36, 1992.
- [112] Y. Luo and Y. Guo, “Envelope Analysis Scheme for Multi-Faults Vibration of Gearbox Based on Self-Adaptive Noise Cancellation,” *Proc. - 2018 Progn. Syst. Heal. Manag. Conf. PHM-Chongqing 2018*, pp. 1188–1193, 2019.
- [113] W. Touti, M. Salah, S. Ben Salem, K. Bacha, and A. Chaari, “Spur gearbox mixed fault detection using vibration envelope and motor stator current signatures analysis,” *2016 17th Int. Conf. Sci. Tech. Autom. Control Comput. Eng. STA 2016 - Proc.*, pp. 193–198, 2017.
- [114] P. Nguyen, M. Kang, J. M. Kim, B. H. Ahn, J. M. Ha, and B. K. Choi, “Robust condition monitoring of rolling element bearings using de-noising and envelope analysis with signal decomposition techniques,” *Expert Syst. Appl.*, vol. 42, no. 22, pp. 9024–9032, 2015.
- [115] Y. Yang, “A Signal Theoretic Approach for Envelope Analysis of Real-Valued Signals,” *IEEE Access*, vol. 5, no. 2, pp. 5623–5630, 2017.
- [116] N. Thrane, J. Wisner, H. Konstantin-Hansen, S. Gade, and B. & Kjaer, “Practical use of the Hilbert Transform,” *Microprocess. Microsyst.*, vol. 16, no. 8, p. 446, 1992.
- [117] S. Adrián-Martínez *et al.*, “Acoustic signal detection through the cross-correlation method in experiments with different signal to noise ratio and reverberation conditions,” *Lect. Notes Comput. Sci. (including Subser. Lect. Notes Artif. Intell. Lect. Notes Bioinformatics)*, vol. 8629, pp. 66–79, 2015.
- [118] H. Illias, Teo Soon Yuan, A. H. A. Bakar, H. Mokhlis, G. Chen, and P. L. Lewin, “Partial discharge patterns in high voltage insulation,” *PECon 2012 - 2012 IEEE Int. Conf. Power Energy*, no. December, pp. 750–755, 2012.
- [119] C. Zhou, M. Michel, D. M. Hepburn, and X. Song, “On-line partial discharge monitoring in medium voltage underground cables,” *IET Sci. Meas. Technol.*, vol. 3, no. 5, pp. 354–363, 2009.
- [120] J. Liu, W. H. Siew, J. J. Soraghan, and E. A. Morris, “A Novel Wavelet Selection Scheme for Partial Discharge Signal Detection under Low SNR Condition,” *Annu. Rep. - Conf. Electr. Insul. Dielectr. Phenomena, CEIDP*, vol. 2018-October, pp. 498–501, 2018.

-
- [121] A. Babaei and S. M. Shahrtash, "On-line partial discharge source location in single-core cables with multi sheath-ground connections," *IEEE Trans. Dielectr. Electr. Insul.*, vol. 22, no. 2, pp. 1031–1041, 2015.
- [122] O. Le Bot, C. Gervaise, and J. I. Mars, "Time-difference-of-arrival estimation based on cross recurrence plots, with application to underwater acoustic signals," *Springer Proc. Phys.*, vol. 180, pp. 265–288, 2016.
- [123] N. El Gemayel, H. Jäkel, and F. K. Jondral, "Error analysis of a low cost TDoA sensor network," *Rec. - IEEE PLANS, Position Locat. Navig. Symp.*, pp. 1040–1045, 2014.
- [124] T. Callaghan, N. Czink, F. Mani, A. Paulraj, and G. Papanicolaou, "Correlation-based radio localization in an indoor environment," *Eurasip J. Wirel. Commun. Netw.*, vol. 2011, pp. 1–15, 2011.
- [125] R. Mardiana and C. Su, "Partial discharge location in power cables using a phase difference method," *IEEE Trans. Dielectr. Electr. Insul.*, vol. 17, no. 6, pp. 1738–1746, 2010.
- [126] M. Stojanovic, "Underwater Acoustic Communications: Design Considerations on the Physical Layer," *Wirel. Demand Netw. Syst. Serv.*, vol. 1, no. 2, 2008.
- [127] F. Jensen, W. Kuperman, M. Porter, and H. Schmidt, *Computational Ocean Acoustics*, Second Edi. 2011.
- [128] P. Webb, "Physical Oceanography," in *Introduction to Oceanography*, 2017, pp. 130–135.
- [129] X. Lurton and D. R. Jackson, *An Introduction to Underwater Acoustics*, vol. 115, no. 2. 2004.
- [130] OSPAR Commission, "Underwater Noise Pollution," 2014. [Online]. Available: <http://www.oceanmammalinst.org/underwaternoise.html>.
- [131] J. Hildebrand, "Sources of Anthropogenic Sound in the Marine Environment," *Mar. Pollut.*, vol. 50, no. 2, pp. 226–235, 2005.
- [132] J. Polglaze and M. Wright, "Marine Noise Assessment." URS Ltd - prepared for Northern Territory Department of Lands and Planning, pp. 33–37, 2011.
- [133] F. J. Á. Franco, "Fundamentals of Airborne Acoustic Positioning Systems," in *Geographical and Fingerprinting Data to Create Systems for Indoor Positioning and Indoor/Outdoor Navigation*, J. Conesa, A. Perez-Navarro, and R. Montoliu, Eds. Academic Press, 2019, pp. 335–351.
- [134] D. Munoz, F. Bouchereau, C. Vargas, and R. Enriquez, "Signal Parameter Estimation for the Localization Problem," in *Position Location Techniques and Applications*, Elsevier, 2009, pp. 23–65.
- [135] D. Munoz, F. Bouchereau, C. Vargas, and R. Enriquez, "Location Information Processing," in *Position Location Techniques and Applications*, Elsevier, 2009, pp. 67–102.
- [136] J. Abramson, "Algebra and Trigonometry.," *Arizona State University OER*
-

LibreTexts. pp. 1000–1002, 2021.